



MONASH University

**Microgel-Functionalised Hollow Fibre Membrane for
Dialysis**

LAI LING WONG

A thesis submitted for the degree of Doctor of Philosophy at
Monash University in 2019
School of Engineering (Chemical)

COPYRIGHT NOTICE

© Lai Ling Wong (2019).

ABSTRACT

Treatment for kidney disease comes at a tremendous economic cost. Dialyser-reuse was designed to manage material more efficiently, however current dialysis membranes are brittle and prone to rupturing during dialysis, which limits their reusability. Membrane fouling is also the key factor that hinders the reusability of the membrane, hence the need for reprocessing after each clinical application to maintain membrane performance. Nevertheless, existing reprocessing procedures are time-consuming and involve a substantial amount of cleaning and disinfectant agents, both of which contribute to rising reprocessing and medical waste disposal costs. With that in mind, the aim of this thesis is to propose and develop an innovative approach to account for current limitations that will aid the patient financially, reduce the cost of processing medical waste, and protect the environment. In order to overcome current limitations, two main issues have to be addressed: (1) the mechanical strength of the hollow fibre membranes must be improved, and (2) a functionalised hollow fibre membrane using adjustable-size additive is proposed that will facilitate reprocessing and eliminate the use of chemical agents.

A hybrid of polyvinylidene fluoride (PVDF) and polysulfone (PSF) polymers was used as the membrane material. The ductile and high modulus behaviours of the blended polymers enhance the mechanical strength of the hollow fibres, especially their tensile strength. In the search for a suitable adjustable-size additive, a temperature-responsive poly(2-dimethylamino) ethyl methacrylate (PDMAEMA) was chosen and synthesised into microgel particles using free radical dispersion polymerisation. Then, the fabricated PVDF/PSF hollow fibres were functionalised with PDMAEMA microgel particles through a two-step hydrophilization process using dynamic adsorption and interfacial polymerisation, which resulted in uniform deposits. Chemical-bonding based mechanisms provide a more durable embedment of the microgel particles on the membrane surface.

The findings show that the polymer dope concentration, viscosity, and internal coagulant concentration determine the membrane's morphology and mechanical strength, which is essential for fabricating PVDF/PSF hollow fibres with desirable properties. The effect of cross-linker concentration on the microgel dispersion revealed that, as the *N,N'*-methylene bisacrylamide (MBAA) content increases, the core of the PDMAEMA microgel particles were highly cross-linked and, as a result, smaller microgel particles were formed. The dispersion stability of PDMAEMA improved with the addition of ethanol, which induced electrostatic repulsion and prevented aggregation, which is beneficial for mass production. The use of two-step hydrophilization in microgel embedment leads to excellent stability with respect to permeability testing and backwashing. The proposed innovative approach was examined in the context of practical applications by mimicking dialysis and reprocessing processes. The functionalised membranes exhibited good hemofiltration performance, experienced minimal fouling and had a protein retention flux above 80%. Membrane cleaning using temperature-regulated microgel particles for hemofiltration tested membranes can lead to the recovery of their original pure water permeability (PWP), molecular weight cut-off (MWCO), and protein retention flux behaviours.

Cleaning using microgel-functionalised membranes is a straightforward and efficient process. The results imply that functionalised membranes using temperature-responsive PDMAEMA microgel particles are potentially desirable and promising for the regeneration process. The regeneration outcomes showed that microgel-functionalised membranes could replace the use of chemical agents with water, and promote self-cleaning through temperature regulation.

DECLARATION

This thesis contains no material which has been accepted for the award of any other degree or diploma at any university or equivalent institution and that, to the best of my knowledge and belief, this thesis contains no material previously published or written by another person, except where due reference is made in the text of the thesis.

Signature:

Print Name: LAI LING WONG

Date: November 2019

PUBLICATION

Conference presentation:

1. **Lai Ling Wong**, Siek Ting Yong, Chien Wei Ooi, Abdul Wahab Mohammad, Effect of Spinning Parameters on Morphology of Polyvinylidene Fluoride Hollow Fiber, *Materials, Methods & Technologies*, 2017, 11, 254-265.

ACKNOWLEDGEMENTS

My sincerest gratitude to Monash University Malaysia for giving me the opportunity of being in this PhD program. The completion of this doctoral thesis is not possible without the continuous support from numerous people throughout this research period. I would particularly like to express my appreciation to my principal supervisor Dr Estee Yong Siek Ting and associate supervisor, Associate Professor Dr Ooi Chien Wei. I am extremely grateful for their invaluable guidance and professional advice provided throughout my doctoral studies. I am also indebted to Monash University's scholarships for financial support in diverse ways. This research would not have been possible without financial support from Monash.

I extend my appreciation to my colleagues and friends for academic-related discussions and their support during the past four years. I want to express my heartfelt gratitude to my beloved family and also my family in Christ. Thank you for your unconditional support and encouragement that have helped make this journey possible.

Most importantly, I am grateful for the countless blessings that God has empowered my life with. I am grateful for all the circumstances and achievements I have been blessed with. I truly appreciate the wonders of nature that captivate my contemplation, for the guidance and light in my way, and for the great minds that have continued to inspire me. It has been an incredible journey of self-discovery, thank you, Yahweh!

I would also like to thank you all the readers for spending time to read through my acknowledgements as well as the thesis. Thank you again for your precious time!

Lai Ling Wong
2019

TABLE OF CONTENTS

COPYRIGHT NOTICE	ii
ABSTRACT	iii
DECLARATION.....	v
PUBLICATION.....	vi
ACKNOWLEDGEMENTS.....	vii
TABLE OF CONTENTS	viii
LIST OF FIGURES.....	xiii
LIST OF TABLES.....	xviii
LIST OF SYMBOLS	xx
LIST OF ABBREVIATIONS	xxiii
Chapter 1: INTRODUCTION.....	25
1.1 Background.....	25
1.2 Problem Statement and Justification.....	29
1.2.1 Current dialysis membrane	29
1.2.2 Reprocessing	30
1.2.3 Membrane Surface Modification.....	31
1.3 Research Objectives	32
1.4 Organisation of Thesis	32
Chapter 2: LITERATURE REVIEW.....	36
2.1 Hollow Fibre Membrane Material.....	36
2.1.1 Polyvinylidene fluoride.....	36
2.1.2 Polysulfone.....	39
2.2 Membrane Fabrication Parameters	40
2.2.1 Polymer dope concentration.....	40
2.2.2 Coagulation concentration.....	42
2.3 Membrane Hydrophilization Material	43
2.4 Parameters of Microgel Particles Synthesis	49
2.5 Dispersion stability	52

2.6 Polymeric Surface Modification	54
2.6.1 Surface coating.....	55
2.6.2 Polymerisation.....	56
Chapter 3: PREPARATION AND CHARACTERISATION OF POLYVINYLIDENE FLUORIDE/POLYSULFONE BLEND HOLLOW FIBRE MEMBRANES	60
3.1 Overview.....	60
3.2 Experimental	60
3.2.1 Materials.....	60
3.2.2 Preparation of a PVDF/PSF blend for the polymer dope solutions	61
3.2.3 Fabrication of hollow fibre membranes	62
3.2.4 Membrane module preparation for filtration experiments.....	63
3.2.5 Characterisation of PVDF/PSF hollow fibre membranes	63
3.2.5.1 Cloud point analysis of PVDF/DMAc and PSF/DMAc systems.....	63
3.2.5.2 Thermal properties and crystallinity of PVDF/PSF/DMAc systems	64
3.2.5.3 Analysis of rheological behaviour of polymer dope solutions	65
3.2.5.4 Morphology study of the hollow fibre membranes.....	65
3.2.5.5 Pore size and pore-size distribution of hollow fibre membranes.....	66
3.2.5.6 Mechanical properties of hollow fibre membranes	69
3.3 Results and discussion.....	70
3.3.1 Cloud point of PSF and PVDF systems.....	70
3.3.2 Effect of the dope polymer concentrations.....	71
3.3.2.1 Viscosity of polymer dope solutions.....	71
3.3.2.2 Morphology study of the hollow fibre membranes.....	74
3.3.2.3 Thermal properties and crystallinity of the hollow fibre membrane.....	80
3.3.2.4 Mechanical properties of the hollow fibre membranes.....	83
3.3.2.5 Pure water permeability and solute rejection performance of the hollow fibre membranes	84
3.3.3 Effect of the internal coagulant concentrations.....	87
3.3.3.1 Morphology study of the hollow fibre membranes.....	87
3.3.3.2 Surface topography of hollow fibre membranes.....	93
3.3.3.3 Mechanical properties of the hollow fibre membranes.....	99

3.3.3.4 Pure water permeability and solute rejection performance for the hollow fibre membranes.....	100
3.4 Conclusion	103
Chapter 4: SYNTHESIS AND CHARACTERISATION OF STABILISED TEMPERATURE-RESPONSIVE POLY(2-DIMETHYLAMINO) ETHYL METHACRYLATE MICROGEL PARTICLES.....	104
4.1 Overview.....	104
4.2 Experimental	104
4.2.1 Materials	104
4.2.2 Preparation of PDMAEMA microgel particles	105
4.2.3 Purification of PDMAEMA microgel particles	107
4.2.4 Characterisation of PDMAEMA microgel particles.....	107
4.2.4.1 Morphology studies of PDMAEMA microgel particle dispersion.....	107
4.2.4.2 Stimuli-response of PDMAEMA microgel particle dispersion.....	108
4.2.5 Zeta potential of PDMAEMA microgel particles	108
4.2.6 Stability of PDMAEMA microgel particles	108
4.3 Results and discussion	109
4.3.1 Effect of polymerisation parameters on the hydrodynamic diameter and size distribution of PDMAEMA microgel particles	109
4.3.1.1 Effect of PVP and ethanol as a stabiliser	109
4.3.1.2 Effect of cross-linker concentrations	112
4.3.1.3 Effect of monomer concentrations	114
4.3.2 Effect of ethanol on the zeta potential of PDMAEMA microgel dispersions	117
4.3.3 Dispersion stability of PDMAEMA microgel particles.....	121
4.4 Conclusion	125
Chapter 5: DEVELOPMENT OF A MICROGEL-FUNCTIONALISED HOLLOW FIBRE MEMBRANE VIA HYDROPHILIZATION BY EMBEDDING PDMAEMA MICROGEL PARTICLES ON PVDF/PSF HOLLOW FIBRE MEMBRANE.....	126
5.1 Overview.....	126
5.2 Experimental	126

5.2.1 Materials	126
5.2.2 Fabrication of PVDF/PSF-PDMAEMA functionalised hollow fibre membranes	127
5.2.2.1 Preparation of PVDF/PSF hollow fibre membranes	127
5.2.2.2 PDMAEMA microgel synthesis.....	127
5.2.2.3 Membrane embedment techniques.....	127
5.2.3 Characterisation of PVDF/PSF-PDMAEMA functionalised hollow fibre membranes	129
5.2.3.1 Functionalised hollow fibre membrane morphologies	129
5.2.3.2 Hydrophilicity measurements.....	129
5.2.3.3 Protein compatibility.....	130
5.2.3.4 Stability of the functionalised hollow fibre membranes	130
5.3 Results and discussion	131
5.3.1 Effect of embedment techniques on hollow fibre membranes	131
5.3.2 Effect of embedment parameter on membrane permeability	135
5.3.3 Characterisation of PDMAEMA microgel layer on PVDF/PSF membrane surface	138
5.3.3.1 Surface topography and surface roughness	138
5.3.3.2 Water contact angle measurement	139
5.3.3.3 Protein compatibility of the functionalised hollow fibre membranes .	141
5.3.3.5 Stability of the functionalised hollow fibre membranes	144
5.4 Conclusion	146
Chapter 6: MEMBRANE PERMEABILITY AND REGENERATION OF MICROGEL-FUNCTIONALISED HOLLOW FIBRE MEMBRANES FOR DIALYSIS	147
6.1 Overview	147
6.2 Experimental	147
6.2.1 Membrane module preparation for filtration experiments.....	147
6.2.2 Preparation of PDMAEMA-PVDF/PSF functionalised hollow fibre membranes	148
6.2.3 Characterisation of functionalised hollow fibre membranes.....	148
6.2.3.1 Ultrafiltration experiments.....	148

6.2.3.2 Hemofiltration tests using a blood model solution	149
6.2.3.3 Membrane cleaning tests	150
6.2.3.4 AFM characterisation of the functionalised hollow fibre membranes.....	151
6.3 Results and discussion	151
6.3.1 Pure water permeability and molecular weight cut-off measurements.....	151
6.3.2 Hemofiltration tests	153
6.3.3 Regeneration process of the functionalised hollow fibre membranes.....	156
6.4 Conclusion	164
Chapter 7: CONCLUSION AND RECOMMENDATION FOR FUTURE RESEARCH	
.....	165
7.1 Conclusion	165
7.2 Future recommendations.....	167
REFERENCES	169

LIST OF FIGURES

- Figure 1.1. Schematic diagram illustrated dialysis machine (left), dialyser (centre) and a cross-section of the dialyser showing the hollow fibres (right). (Modified from [3])
- Figure 2.1. Chemical structure of PVDF.
- Figure 2.2. Chemical structure of (a) HFP; (b) PTFE.
- Figure 2.3. Chemical structure of PSF.
- Figure 2.4. Chemical structure of (a) PNIPAAm; (b) PVCL.
- Figure 2.5. Chemical structure of PDMAEMA.
- Figure 2.6. Schematic diagram of a particle surrounding in a liquid layer. Modified from [136]
- Figure 3.1. A schematic diagram presented the set-up of a pure water permeability experiment using ultrapure water at room temperature.
- Figure 3.2. The critical concentration of PVDF/DMAc dope solution at 25°C.
- Figure 3.3. Shear rates and viscosities for PVDF/PSF dope solutions with different PSF weight ratios.
- Figure 3.4. FE-SEM micrographs of PVDF membranes with a polymer concentration of 20 wt% spun with different PSF weight ratios and pure PSF membrane with 20 wt% polymer concentration, using 100 wt% water as the internal coagulant. (a) S0; (b) S5; (c) S10; (d) S15; (e) S100. CS, OS, and IS are cross-section, outer surface, and inner surface, respectively.
- Figure 3.5. Cross-section morphology of hollow fibres prepared using water as an internal coagulant. (a) S0; (b) S100. CS-I and CS-O represent cross-section near the inner surface and cross-section near the outer surface, respectively.
- Figure 3.6. FE-SEM coupled with EDX analysis of cross-section of hollow fibre membrane (S15): (a) FE-SEM micrograph, 10.0 kV 17.9 mm x 3.00 k SE (L); (b) EDX spectrum of membrane matrix and “big spherical crystalline particle” of S15; (c) fluorine mapping from the micrograph (a); (d) sulphur mapping from the micrograph (a).
- Figure 3.7. Schematic diagram of “big spherical crystalline particle” structure for the PVDF/PSF hollow fibre membrane (S15).

Figure 3.8. DSC curves of hollow fibres spun with different PSF weight ratio annealed at 250 °C for 10 min. (a) Heating curves; (b) cooling curves.

Figure 3.9. (a) Solute rejection curves and (b) probability density function curves of PVDF/PSF hollow fibre membranes prepared with different PSF weight ratios.

Figure 3.10. FE-SEM micrographs for the cross-sections of PVDF membranes with polymer concentration of 20 wt% spun with different PSF weight ratios and DMAc/water mixture of different DMAc concentrations as internal coagulant. (a) S5; (b) S10; (c) S15.

Figure 3.11. FE-SEM micrographs for the outer surfaces of PVDF membranes with polymer concentration of 20 wt% spun with different PSF weight ratios and DMAc/water mixture of different DMAc concentrations as internal coagulant. (a) S5; (b) S10; (c) S15.

Figure 3.12. FE-SEM micrographs for the inner surfaces of PVDF membranes with polymer concentration of 20 wt% spun with different PSF weight ratios and DMAc/water mixture of different DMAc concentrations as internal coagulant. (a) S5; (b) S10; (c) S15.

Figure 3.13. AFM micrographs and 3-D images of PVDF membrane with polymer concentration of 20 wt% spun with different PSF weight ratio and DMAc/water mixture of different DMAc concentrations as internal coagulant. (a) S0; (b) S5; (c) S10; (d) S15. IS and OS are inner surface and outer surface, respectively.

Figure 3.14. (a) Solute rejection curves and (b) probability density function curves of PVDF/PSF (S15) hollow fibre membranes prepared from DMAc/water mixture of different DMAc concentrations as internal coagulant.

Figure 4.1. A schematic diagram for PDMAEMA microgel synthesis. Reaction mixture consists of DMAEMA, MBAA, APS, ethanol/PVP, and DI water.

Figure 4.2. Effect of stabilisers on the hydrodynamic diameters of the PDMAEMA microgel dispersion prepared with 0.5 wt% of MBAA at a temperature ranging from 25 to 60 °C at pH 7.45. (a) PDMAEMA-PVP dispersion, (b) PDMAEMA-EtOH dispersion.

Figure 4.3. Effect of the cross-linker on the hydrodynamic diameters of the PDMAEMA microgel particles prepared in ethanol/water mixture at a temperature ranging from 25 to 60 °C at pH 7.45. (■) 0.4 wt% of MBAA; (●) 0.5 wt% of MBAA; (▲) 0.6 wt% of MBAA; and (▼) 0.7 wt% of MBAA.

Figure 4.4. Schematic diagram of a cross-linked PDMAEMA using free radical dispersion polymerization at 65 °C, 500 rpm.

- Figure 4.5. Swelling ratio of the PDMAEMA microgel particles with different cross-linker concentrations was calculated from D_h (37 °C)/ D_h (60 °C) at pH 7.45.
- Figure 4.6. Effect of monomer concentration on the hydrodynamic diameters of the PDMAEMA microgel particles prepared with 0.5 wt% MBAA based on the weight of DMAEMA in ethanol/water mixture at a temperature ranging from 25 to 60 °C at pH 7.45. (■) 0.4 wt% of DMAEMA; (●) 0.5 wt% of DMAEMA; (▲) 0.6 wt% of DMAEMA; and (▼) 0.7 wt% of DMAEMA.
- Figure 4.7. Swelling ratio of the PDMAEMA microgel particles with different monomer concentrations was calculated from D_h (37 °C)/ D_h (60 °C) at pH 7.45.
- Figure 4.8. Zeta potential of the stimuli-responsive of the PDMAEMA microgel dispersion (M0.5) prepared with 0.5 wt% MBAA and 0.5 wt% DMAEMA in ethanol/water mixture. (■) pH-responsive of the microgel particles at 37 °C from pH 4-10; (●) Temperature-responsive of the microgel particles with a 1 to 5 ratio of ethanol to microgel dispersion, from 25 to 60 °C at pH 7.45.
- Figure 4.9. Schematic diagram of a protonated and deprotonated PDMAEMA microgel particle.
- Figure 4.10. FE-SEM micrographs of PDMAEMA microgel dispersions (M0.5) at pH, (a) 7.45; (b) 10.
- Figure 4.11. Effect of the ratios of ethanol to microgel dispersion at 37 °C, pH 7.45.
- Figure 4.12. (a) FE-SEM and (b) AFM micrographs of freshly polymerised PDMAEMA microgel dispersion (M0.5) which acted as a control.
- Figure 4.13. FE-SEM micrographs of PDMAEMA microgel dispersion (M0.5) incubated over a period of time (i) with (M0.5-EtOH) and (ii) without (M0.5-C) 1:5 ethanol to microgel dispersion ratio. (a) 30-days, (b) 180-days.
- Figure 4.14. The hydrodynamic diameters of the PDMAEMA microgel particles after 180-days incubation at a temperature ranging from 25 to 60 °C at pH 7.45. (■) M0.5-C; (●) M0.5-EtOH.
- Figure 5.1. FE-SEM micrographs of the techniques applied to embed PDMAEMA microgel dispersion (M0.5) on PVDF/PSF (S15-15) hollow fibres at room temperature. 10 g/L XDC-ethanol was used to undergo interfacial polymerisation for 10 min. All membranes were rinsed with fresh DI water by stirring at 100 rpm for 30 min. (a) Uncoated-bare PVDF/PSF membrane; (b) dip-coating, inset: before rinsing; (c) interfacial polymerisation; and (d) dynamic-interfacial polymerisation.
- Figure 5.2. A schematic representation of the preparation of the PDMAEMA-PVDF/PSF membrane and formation of the quaternary ammonium salt (red bonds) when PDMAEMA was cross-linked with XDC.

- Figure 5.3. Effect of the coating time of the microgel dispersion (M0.5) on the pure water permeation of the functionalised hollow fibre prepared using dynamic-interfacial polymerization at a constant suction of 0.33 mL/min, and 10 g/L XDC for 10 min.
- Figure 5.4. FE-SEM micrographs of the outer surface and cross-section of the functionalised hollow fibre membranes with M0.5 solution using dynamic-interfacial polymerisation. Constant suction at 0.33 mL/min for (a) 30 min; (b) 60 min. OS and CS are outer surface and cross-section, respectively.
- Figure 5.5. AFM micrographs of the outer surface of the S15-15 hollow fibre membranes with M0.5 dispersion using dynamic-interfacial polymerisation: (a) non-functionalised membrane; (b) functionalised membrane.
- Figure 5.6. Time-dependency associated with water contact angles of the non-functionalised and functionalised hollow fibre membrane at room temperature. The inset images show the water contact angle of the functionalised membrane at different angles: (a) 75°; (b) 70°; (c) 61°; (d) 53°.
- Figure 5.7. The amount of BSA adsorption on the non-functionalised and functionalised membranes determined using UV-Vis scanning at a wavelength of 280 nm. BSA solution with 1 mg/mL BSA in phosphate-buffered solution at pH 7.4 and incubated at 37 °C for 1 hour. Values were expressed as mean \pm SD, n = 5.
- Figure 5.8. FE-SEM micrographs of the outer surface of a hollow fibre membrane coated with 1 g/L BSA in phosphate-buffered solution at pH 7.4 and incubated at 37 °C for 1 hour. All membranes were rinsed with fresh DI water. (a) Non-functionalised membrane; (b) functionalised membrane.
- Figure 5.9. Pure water permeation of a functionalised hollow fibre membrane using dynamic-interfacial polymerization over a period of 10 days at room temperature.
- Figure 5.10. Stability of a functionalised hollow fibre using dynamic-interfacial polymerization for backwash cycles against pure water permeation conducted at 3 bar each for 1 min at room temperature.
- Figure 6.1. A schematic diagram of a hemofiltration experiment using blood model solution at 37 °C. (a) Standard permeation rig; (b) Membrane module with heating tape attached to maintain the temperature of the experiments.
- Figure 6.2. A schematic diagram of a regeneration experiment using ultrapure water at 60 °C. (a) Standard permeation rig; (b) Membrane module with heating tape attached to maintain the temperature of the experiments.
- Figure 6.3. BSA rejection and PEG (12,000 Da) sieving performance for functionalised hollow fibre membrane (S15-15-Aft) during 4 hours hemofiltration tests.

Figure 6.4. Pure water permeability of S15-15 hollow fibre membranes: S15-15-Aft refers to functionalised membrane; S15-15-Aft-H1 refers to the functionalised membrane after the first hemofiltration; S15-15-Aft-R regenerated-functionalised membrane.

Figure 6.5. AFM micrographs of the functionalised (S15-15-Aft), after first hemofiltration (S15-15-Aft-H1), and regenerated (S15-15-Aft-R) membranes.

Figure 6.6. Probability density function curves of S15-15 hollow fibre membranes: (■) S15-15-Bef is a non-functionalised membrane; (●) S15-15-Aft is a functionalised membrane; (▲) S15-15-Aft-R is a regenerated-functionalised membrane after hemofiltration.

Figure 6.7. BSA rejection and PEG (12,000 Da) sieving performance before (H1) and after (H2) regeneration for functionalised hollow fibre membrane (S15-15-Aft) during 4 hours hemofiltration tests.

Figure 6.8. Schematic diagrams of (a) non-functionalised hollow fibre membrane and (b) microgel-responsive functionalised hollow fibre membrane (S15-15-Aft): (i) during dialysis treatment; (ii) completion of dialysis; and (iii) reprocessing-cleaning.

LIST OF TABLES

- Table 3.1. Compositions of polymer dope and internal coagulant for hollow fibre membranes preparation.
- Table 3.2. Experimental parameters for hollow fibre membrane fabrication.
- Table 3.3. Characteristics of PVDF hollow fibre membranes with different PSF weight ratios.
- Table 3.4. Enthalpy and degree of crystallinity of the hollow fibres spun with different PSF weight ratio.
- Table 3.5. Mechanical properties of PVDF/PSF membranes fabricated from different PSF weight ratios.
- Table 3.6. Mean pore size, MWCO, and pure water permeability of membranes with different polymer dope concentrations.
- Table 3.7. Characteristics of PVDF/PSF hollow fibre membranes prepared from DMAc/water mixture of different DMAc concentrations as internal coagulant.
- Table 3.8. Solubility parameters of polymers, solvent, and non-solvents for hollow fibre fabrication [186].
- Table 3.9. Roughness parameters of the hollow fibre membranes spun from different polymer dope solutions and internal coagulant concentrations.
- Table 3.10. Mechanical properties of PVDF/PSF hollow fibre membranes fabricated from DMAc/water mixture of different DMAc concentrations as internal coagulant.
- Table 3.11. Mean pore size, MWCO, and pure water permeability of S15 membranes obtained from solute transport technique.
- Table 4.1. Standard composition of microgel particles synthesis
- Table 5.1. Surface roughness of the non-functionalised and functionalised S15-15 hollow fibre membranes.
- Table 5.2. Protein adsorption compared with references.
- Table 6.1. Reference measurements of the commercial membranes obtained from *in vitro* characterization.

Table 6.2. Results of the ultrafiltration experiments of S15-15 hollow fibre membranes.

Table 6.3. Comparison of various parameters of S15-15 hollow fibre membranes calculated from the solute rejection experiments.

LIST OF SYMBOLS

Symbols	Units	Definitions
C_0	mg	protein concentrations of before adsorption
d_p	nm	pore diameter
m_{PSF}	g	the weight of PSF blends
m_{PVDF}	g	the weight of the PVDF
W_{PVDF}	g	fractional weight of PVDF
μ_p	nm	mean pore size
σ_p	-	geometric standard deviation (deviation ratio of r_{84}/μ_p)
~	%	tensile strain
~	%	porosity
~	°	degree of water contact angle
~	°C/min	cooling/ heating speed per minute
~	dynes/cm	surface tension
~	h	hour(s)
~	min	minute(s)
~	mL/min	dope/bore solution flow rate
~	mm	air gap
~	mm/min	testing speed used for mechanical strength testing
~	MPa	tensile strength
~	MPa	Young's modulus
~	MPa ^{1/2}	solubility parameter
~	mV	Zeta potential
~	nm	wavelength
~	nm ⁻¹	Probability density function
~	ppm	parts per million
~	rpm	revolutions per minute
~	s	second(s)
~	s ⁻¹	shear rate
~	v/v%	volume concentration, volume per volume
~	wt%	weight percentage

~	wt/wt	weight per weight ratio
~	$\mu\text{g}/\text{cm}^2$	amount of protein adsorption
ΔH_m	J/g	100% crystalline PVDF
ΔH	J/g	fusion enthalpy of the membrane
ΔP	atm	pressure difference between the feed side and the permeation side of the membrane
A	m^2	effective membrane surface area
C	mg	protein concentrations of after adsorption
C_b	ppm	solute concentration of the blood model solution
C_f	ppm	solute concentrations in the feed
cP	mPa^s	centipoise
C_p	ppm	solute concentration of the permeate
D	m	outer diameter of hollow fibre
D_h	nm	hydrodynamic diameter
d_s	nm	solute diameter
J	$\text{L}/\text{m}^2 \text{ h atm}$	specific flux of the hollow fibre membrane
l	m	effective length of the hollow fibre
LCST	$^\circ\text{C}$	lower critical solution temperature
M	mol/L	Molar
Mw	Da or g/mol	molecular weight
MWCO	Da	molecular weight cut-off
P_{inlet}	bar	feed side inlet pressure
P_{outlet}	bar	feed side outlet pressure
P_{permeate}	bar	permeate pressure at permeate side
Q	L/h	difference in water flux before and after the lumen
r	nm	Stokes radius of solute
$R(d_p)$	%	solute rejection
R_a	nm	average roughness
R_{max}	nm	maximum roughness
R_q	nm	root mean square roughness
S	cm^2	area of the membrane (protein adsorption)
SC_0	-	sieving coefficient
SD	-	standard deviation

TMP	bar	transmembrane pressure
UCST	°C	upper critical solution temperature
V	μg	volume
VPTT	°C	volume phase transition temperature
X_c	%	crystallinity degree
δ_d	MPa ^{1/2}	dispersive parameter
δ_h	MPa ^{1/2}	hydrogen bonding parameter
δ_p	MPa ^{1/2}	polar parameter
δ_t	MPa ^{1/2}	total solubility parameter
φ	g	PVDF fractional weight in the blended membrane

Note : "-" indicates dimensionless and "~" means symbol was not use in the context.

LIST OF ABBREVIATIONS

Abbreviations	Definitions
3-D	three-dimensional
AA	acrylic acid
AAm	acrylamide
AAMI	Association for the Advancement of Medical Instrumentation
ABMs	aquaporin-based biomimetic membranes
AFM	Atomic force microscopy
alb	albumin
APS	ammonium persulfate
AR	analytical reagent
BSA	bovine serum albumin
CKD	chronic kidney disease
CS	cross-section
DI	deionised water
DMAc	dimethylacetamide
DMAEMA	2-dimethylamino ethyl methacrylate
DSC	differential scanning calorimeter
EDX	energy dispersive X-ray analyser
EGDMA	ethylene glycol dimethacrylate
ESRD	end-stage renal disease
FE-SEM	field emission scanning electron microscopy
GPC	gel permeation chromatography
HCl	hydrochloric acid
HFP	hexafluoropropylene
ID	inner diameter
IS	inner surface
LbL	layer-by-layer
LCN	lignocellulose nanofibrils
MAA	methacrylic acid
MBAA	<i>N,N'</i> -methylene bisacrylamide
MIP	mercury intrusion porosimetry
MPC	2-methacryloyloxyethyl phosphorylcholine

M-PDA	<i>m</i> -phenylene-diamine
NaOH	sodium hydroxide
NIPAAm	N-isopropylacrylamide
OD	outer diameter
OS	outer surface
PAES	Polyarylethersulfone
PAN	lignocellulose nanofibrils
PDMAEMA	poly(2-dimethylamino) ethyl methacrylate
PEG	polyethylene glycol
PEI	polyethyleneimine
PEO	polyethylene oxide
PES	polyethersulfone
PLA	poly(lactic acid)
PNIPAAm	poly(N-isopropylacrylamide)
P-PDA	<i>p</i> -phenylene-diamine
PSBMA	poly(sulfobetaine methacrylate)
PSF	Polysulfone
Pt	platinum
PTFE	Polytetrafluoroethylene
PVCL	poly-N-vinylcaprolactam
PVDF	polyvinylidene fluoride
PVDF-a	PVDF-amorphous
PVDF-c	PVDF-crystalline
PVP	polyvinylpyrrolidone
PWP	pure water permeability
SG	Sigma-Aldrich
SPEEK	sulfonated poly(ether ether ketone)
SPSf	PES/sulfonated polysulfone
ST	solute transport
TFC	thin-film-composite
TiO ₂	titanium oxide
TMC	trimesoyl chloride
TOC	total organic carbon analyser
UV-Vis	ultraviolet-visible

Chapter 1: INTRODUCTION

1.1 Background

The progression of chronic kidney disease (CKD) raises concerns about the capacity to cope with its economic burden to patients, caregivers and society. According to the 2018 *Global Burden of Kidney Disease* report, 2.62 million people received dialysis universally, and this is expected to double by 2030 [1]. In Malaysia, Ismail, *et al.* [2] reported that, despite 9.07% of the total population being affected with CKD, only 0.36% have been diagnosed with end-stage renal disease (ESRD). Even though such a small population have been diagnosed with ESRD, total expenditure increased by 94% between 2010 and 2016, from 572 million to 1.12 billion Malaysian ringgit. It has been reported that only 6% of the ESRD expenditure was used on renal transplantation, with the remaining being used to pay for dialysis [2]. The result reflects the fact that the chances of finding compatibles kidneys are unquestionably slim. Therefore, besides advocating kidney health and prevention, the advancement of dialysis processes is likewise crucial to efficiently reducing the global burden.

The continuous emergence of novel techniques and innovations to dialysis machines is intended to reduce the overall mortality rate amongst the ESRD population [3]. In seeking to reduce ESRD mortality, each component of the dialysis machine plays a crucial role. The major components are the dialysis machine, the dialysate, and the dialyser, as shown in Figure 1.1. A dialysis machine mixes and monitors the dialysate and blood flow during treatment. The dialyser is often referred to as an artificial kidney; it mimics the form of the nephron of the which is also kidney and consists of as many as 20,000 extremely thin fibres, known as hollow fibres. They are encased in plastic tubes that are approximately 30 centimetres long. It is designed to provide a controllable channelling of solutes and water across a semipermeable membrane, thereby separating blood and dialysate. Dialysate consists of waste products that leave the dialyser, whereas the clean blood will circulate back into the body. The purpose of the dialysate is to withdraw salts, excess water, and metabolic wastes without eliminating too many other nutrients from the bloodstream, such as electrolytes and minerals. This is designed not

just to rid of the waste from the body, but more importantly, to maintain an individual's homeostasis.

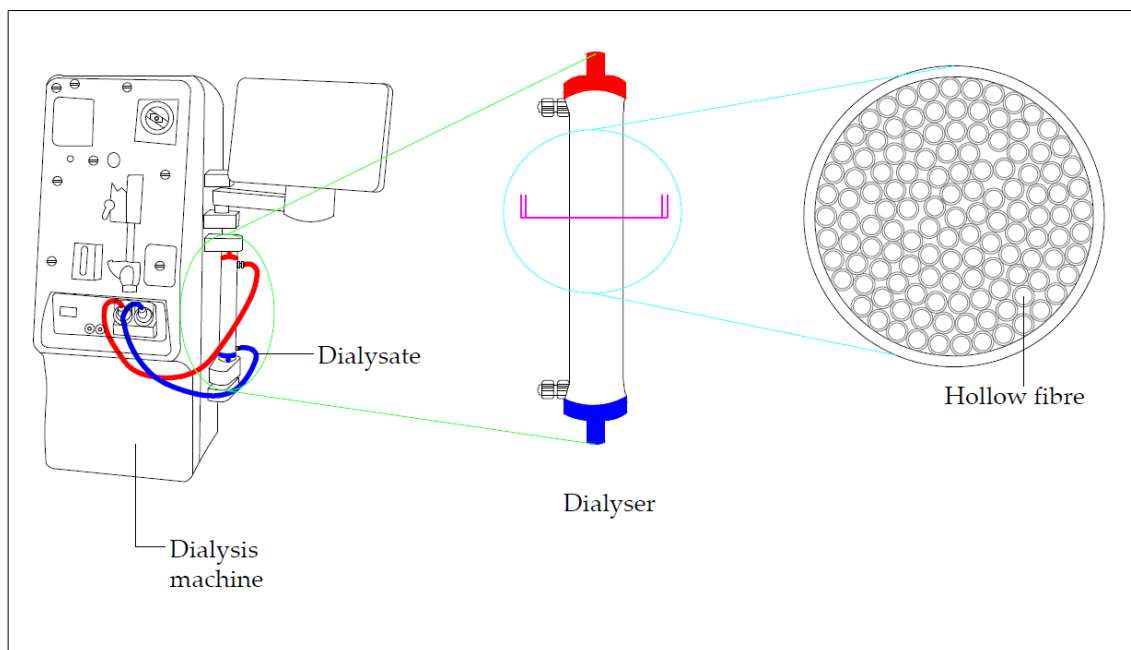


Figure 1.1. Schematic diagram illustrated dialysis machine (left), dialyser (centre) and a cross-section of the dialyser showing the hollow fibres (right). (Modified from [3])

There has been a shift from using natural to synthetic polymers in the hemofilter-mimicking hollow fibre membrane in the dialyser. Natural polymer membranes aren't reusable, due to their poor chemical resistance and mechanical strength. Therefore, synthetic polymers appear to be a potential candidate for extending the lifespan of the hollow fibre, meaning that the dialyser can be used repetitively. The primary motivation behind dialyser-reuse is the desire to improve cost efficiency. The emergence of dialyser-reuse has not only reduced the cost of processing the solid waste by at least half, but has also eased the burden that dialysis has on the patient.

The hollow fibre membranes made for current dialysis membrane are synthetic polymers and mostly a mixture of hydrophobic base polymers and hydrophilic copolymers, as they have better membrane biocompatibility and membrane permeability. Membrane biocompatibility refers to the effects of the biological responses on the membrane, whereas membrane permeability refers to the solute transport capabilities of the membranes. The hydrophilic copolymers are incorporated to improve the transmembrane solute passage [4] and reduce hydrophobic interaction. This is

because the hydrophobic base polymer has a greater interaction with biological substances such as proteins and microorganisms [5], which triggers a complex series of biological responses, including protein adsorption, platelet adhesion, and complement activation. These responses ultimately lead to membrane fouling [6,7]. The biological interaction is caused by a lack of hydrogen bonding interactions between the hydrophobic membrane interface and water. The repulsion of water molecules away from the hydrophobic polymer surface is an involuntary process with increasing entropy, and thus protein molecules are inclined to adsorb on the membrane surface [8]. The occurrence of fouling is liable to pore narrowing, pore caking, and pore plugging, which severely limits the long-term use of the membrane in many filtration systems. Hence, a reprocessing technique is developed to facilitate multiple applications.

Dialyser-reuse that is designed for multiple treatments has to strictly follow the reprocessing standards outlined by the Association for the Advancement of Medical Instrumentation (AAMI). These AAMI standards and guidance are provided to ensure that if dialysers are reused, they are done so in a safe and effective way. Reprocessing undergoes a series of steps, including rinsing, cleaning, membrane performance testing, disinfection, and sterilisation until the next use. Rinsing is performed immediately to minimise clotting of the hollow fibres after a clinical application. Next, cleaning of the dialyser is completed using cleaning agents, such as bleach or peracetic acid, to remove deposited proteins on the membrane. After cleaning, the performance of the dialyser is examined – for example, a pressure test is carried out to spot leakages, and the blood compartment volume is measured, as is water permeability and clinical confirmation. Then, the dialyser undergoes a chemical and physical process that uses germicides and heat respectively, to destroy all living organisms. At the end of the reprocessing procedure, a thorough visual inspection of the dialyser is carried out before it is labelled and stored ready for use [9].

Despite the fact that the hydrophobicity of the membrane provides excellent chemical and mechanical strength, wetting and fouling of the membrane are yet to be enhanced by membrane hydrophilization. Various methods of hydrophilic modification can enhance the lifespan and reduce the operation costs of the dialyser. Two common

methods are used to improve the hydrophilicity and fouling resistance of the membranes, which include blending and surface modification. The addition of functional properties on a membrane through polymer blending is achieved in a single step, and allows the membrane surfaces and cross-sectional pores of the membrane to be modified simultaneously during the preparation and modification process. Surface modification is accomplished by coating a functional layer on the prepared membrane surface, where the modified sites are located, either on the top or bottom surface of the membrane. The pores inside the membrane are usually excluded because of the inadequate diffusion ability of the modifying compounds within them.

The refinement of the pore dimensions is also important. Membranes with narrow pore sizes are preferable, because the distribution of pore size affects the removal spectrum of the molecular weights and the membrane's performance. Although membranes with larger pore sizes not only lead to higher performance and better removal of uremic solutes, such as β_2 -microglobulin (Mw: 11,800 Da), they also increase albumin loss (Mw: 67,000 Da) in clinical applications [10,11]. Therefore, an upper membrane pore size limit is established to ensure that the essential proteins are retained during dialysis. The molecular weight cut-off (MWCO) for better separation between uremic solutes and albumin ranges from 15,000 Da up to approximately 50,000 Da [12,13]. Unfortunately, most of the dialysis membranes with additives are incompatible for this separation purpose [12].

One of the innovative approaches to overcoming both limitations described by Boschetti-de-Fierro, *et al.* [12] is the use of swellable or adjustable-size additives. This method uses a membrane that is modified such that it consists of a water-swelling, biocompatible polymer, in addition to the base polymer membrane. The addition of the adjustable-size additives alters the membrane pore size and increases the membrane permeability, as the water and water-soluble molecules can diffuse through the membrane with the aid of the additive matrix. These additives can be added either by being blended or through surface modification. The exploration of adjustable-size additives that are stimuli-responsive polymers will bring greater advantages for preparing functionalised membranes for dialysis.

1.2 Problem Statement and Justification

The fundamental goal of existing dialyser is to manage material more efficiently by reducing, reusing, and recycling. The intention is to aid the patient financially, to reduce the cost of processing medical waste, and to protect the environment. Hence, hollow fibre membranes based on synthetic polymers are developed.

1.2.1 Current dialysis membrane

At the current point in time, polysulfone (PSF)-based polymeric membranes have been globally available because they provide high permeability for low-molecular-weight proteins and have a high resistance to sterilisation. However, PSF membranes are brittle, meaning they are prone to rupturing in the dialysis process, which consequently limits their reusability. A further modification is mandatory to conserve the efficiency and sustainability of a dialysis membrane. Inasmuch as PSF requires membrane hydrophilization, the use of polyvinylidene fluoride (PVDF), which is a hydrophobic polymer, as an alternative base polymer becomes more attractive for use in dialysis membranes. This is for several reasons. PVDF has been used as a biomaterial in tissue engineering applications [14,15], specifically in medical implants and devices, because it provides excellent biocompatibility and is subject to minimal tissue reaction. PVDF possesses better ductility and lower tensile strength. Theoretically, according to the mechanical properties of PVDF, it would have higher reusability than PSF polymer. Studies reported that, when similar dimensions of PVDF and PSF membrane were compared, the tensile strength of the PVDF membrane was close to that of the PSF membrane [16,17]. In order to preserve the ductility of PVDF and simultaneously increase tensile strength, the blending of PVDF and PSF polymers will result in enhanced mechanical strength and membrane performance. Aside from that, the manipulation of the coagulant concentration was studied to regulate the pore formation of the membrane.

1.2.2 Reprocessing

It is necessary to perform reprocessing after each clinical application to maintain membrane performance. It is undeniable that the existing reprocessing standards are comprised of thorough and efficient steps; however, these steps are time-consuming and use a substantial amount of cleaning and disinfectant agents, which contributes to rising reprocessing and medical waste disposal costs. Furthermore, the majority of the commercial dialysis membranes suffer from membrane deformation. For example, the deformation of the membrane pore size affects the polarity of the membrane [18]. This is due to the chemical agents involved in the reprocessing standards outlined by AAMI, which cause the modified sites to leach from the membrane surfaces and pores. The hydrophilicity properties of the membrane eventually diminish, leading to membrane fouling and albumin loss.

In order to improve the hydrophilicity of the membrane and simplifying the reprocessing steps, it is proposed that an adjustable-size additive is deposited on the membrane if it is to achieve its maximum performance. Theoretically, the size of an adjustable-size additive can be changed according to the stimulus-responsive, such as an externally induced temperature change. Poly(2-dimethylamino) ethyl methacrylate (PDMAEMA) that is responsive to temperature and pH was chosen as an adjustable-size additive. As the aim of this research is to minimise the consumption of chemical agents, the pH-responsive of PDMAEMA is excluded. PDMAEMA is superior to other stimulus-responsive polymers because it has been proven to be non-toxic and anti-bacterial, and possesses a higher lower critical solution temperature (LCST). When the temperature is below the LCST, the bonds between the water and microgel particles attract strongly, meaning the microgel particles swell with water molecules. When the temperature is above the LCST, the bonds between the water and polymer molecules within the microgel particles break, causing the microgel particles to shrink. In short, the pore dimension of the modified membrane can be controlled by manipulating the temperature of the surrounding water. The alteration of the size of the microgel particles during reprocessing could induce self-cleaning using thermo-regulated microgel coating.

1.2.3 Membrane Surface Modification

Conventional surface coatings stand out as an attractive technique due to their simplicity and ease of use. However, the configuration of their hollow fibres would limit the ability of the microgel particles to coat the membrane surfaces. Furthermore, the microgel particles possess a lower density, which restricts their ability to uniformly settle down on the membrane surface. Lastly, the operational life of functionalised hollow fibres with respect to the number of dialysis-regeneration cycles remains an open question as little work has been done in quantifying the effectiveness of conventional embedding techniques for long-term usage. Therefore, it is proposed that surface membrane modification is accomplished in two steps. Surface coating via dynamic adsorption was performed as the first step of the modification to embed the microgel particles uniformly on the membrane surface. Then, a chemical bonding using interfacial polymerisation reinforced the microgel particles. These steps are adopted to ensure that little or no microgel particles escape to the bloodstream during dialysis.

The present work seeks to enhance the functionalities and responsive behaviour of the membrane materials for the use of dialysis and reprocessing. The changes in the dialysis membrane will increase the reusability of the membrane by enhancing its mechanical strength. The inclusion of the adjustable-size additive will improve protein retention by tailoring the pore dimensions of the dialysis membrane, and eliminate the need to use chemical agents during the reprocessing procedure. Finally, and importantly, it will reduce costs and environmental impacts by reducing the amount of harmful and persistent waste produced.

1.3 Research Objectives

The objective of this research is to fabricate a functionalised PVDF/PSF hollow fibre membrane through surface modification using PDMAEMA microgel for hemofiltration. The specific objectives of the research as follows:

1. To examine the effect of PSF weight ratio and internal coagulant concentration on the membrane formation of the PVDF/PSF hollow fibre membrane.
2. To investigate the effect of stabilisers, and cross-linker and monomer concentrations on the temperature-responsiveness of PDMAEMA microgel particles.
3. To develop and examine functionalised membranes by embedding PDMAEMA microgel particles on PVDF/PSF hollow fibre membranes via hydrophilization.
4. To investigate the membrane permeability and regeneration of the functionalised PVDF/PSF hollow fibre membrane.

1.4 Organisation of Thesis

The core aim of this thesis is the fabrication and characterisation of a functionalised PVDF/PSF hollow fibre membrane through surface modification using temperature-responsive PDMAEMA microgel particles for hemofiltration. This study ultimately seeks to provide a fundamental picture of novel polymer blending and embedment techniques, potentially for liquid separations and membrane reprocessing. This thesis consists of seven chapters; the objectives and contributions of each chapter are briefly presented:

Chapter 1: Introduction

This chapter briefly introduces the fundamental mechanisms involved in the dialysis process. It follows the emergence of the dialyser-reuse to manage costs. It will show that current commercial membranes and standard reprocessing techniques have

several limitations, which are time-consuming and restrict their reusability, respectively. These shortcomings have encouraged researchers to opt for an alternative approach, which is also briefly discussed.

Chapter 2: Literature review

This chapter presents a review of the current base material used for hollow fibres fabrication, followed by fabrication parameters, and the use of membrane hydrophilization to minimise membrane fouling. Current polymers that have been synthesised for microgel particles are briefly discussed. As the membrane modification plays a vital role in determining the anti-fouling performance of the membrane, a comprehensive review of the techniques used also features in this chapter.

Chapter 3: Preparation and characterisation of polyvinylidene fluoride/polysulfone blend hollow fibre membranes

Relevant fabrication parameters for the preparation of PVDF/PSF hollow fibre membranes are established in this chapter. The weight ratios of PVDF to a diluent, dimethylacetamide (DMAc), were 20 to 80 at a fabrication temperature of 25 °C, and used a dry-wet spinning method based on diffusion induced phase separation. Subsequently, a study on the effect of PSF weight ratios on the blending of the membranes was performed to achieve ideal fabrication conditions for the formation of a PVDF/PSF membrane. DMAc, as a diluent for membrane fabrication, was incorporated into the internal coagulant at controlled weight ratios to regulate the structural properties of the membrane. The aim was to improve the selectivity of the polymer blend. In the presence of DMAc, the phase separation of PVDF in conjunction with crystallisation was delayed. Inspection through field emission scanning electron microscopy (FE-SEM) of the retarded formation of the membrane revealed a decrease in pore size across the polymer blends. These findings indicated that the modification of a membrane structure could be attained by manipulating the fabrication parameters.

Chapter 4: Synthesis and characterisation of stabilised temperature-responsive poly(2-dimethylamino) ethyl methacrylate microgel particles

This chapter demonstrated the effect of using ethanol and polyvinylpyrrolidone (PVP) as a stabiliser on PDMAEMA microgel particles with respect to temperature-responsive behaviours. The PDMAEMA microgel particles were synthesised by free radical polymerisation using 2-dimethylamino ethyl methacrylate (DMAEMA) as the monomer, and *N,N'*-methylene bisacrylamide (MBAA) as the cross-linker. The addition of PVP in the PDMAEMA synthesis was excluded because the temperature behaviour of PDMAEMA did not correspond to the proposed outcome required for the reprocessing process of an existing dialyser. The effects of polymerisation parameters on ethanol as a stabiliser, the concentration of cross-linker, and the concentration of monomer were systematically investigated. The effect of ethanol in the microgel particle dispersion on the aggregation behaviour was studied through the zeta potential, which showed that the application of a tailored ratio of ethanol into a microgel dispersion at pH 7.45 (human blood's pH) was able to prevent the aggregation between particles without altering the swelling behaviour of the PDMAEMA microgel particles.

Chapter 5: Development of a microgel-functionalised hollow fibre membrane via hydrophilization by embedding PDMAEMA microgel particles on PVDF/PSF hollow fibre membrane

This chapter focuses on the embedment techniques of PDMAEMA microgel particles on PVDF/PSF hollow fibre membranes into a single functionalised membrane. A comparison between dip-coating, dynamic adsorption, and interfacial polymerisation was investigated. A two-step hydrophilization was used for microgel particle embedment. The uniformity of embedment was provided by dynamic adsorption and the benefits of chemically bonding two materials. The hollow fibre membrane that was successfully embedded with the microgel particles was then renamed a microgel-functionalised hollow fibre membrane. This embedment method serves as an interesting approach, wherein both materials are interconnected into a single functionalised membrane to improve membrane fouling.

Chapter 6: Membrane permeability and regeneration of microgel-functionalised hollow fibre membranes for dialysis

This chapter demonstrates the anti-fouling performance of microgel-functionalised hollow fibre by performing a series of filtration experiments. Initially, pure water permeation was determined, followed by hemofiltration using a blood model solution. The blood model solution composed of 1 g/L bovine serum albumin (BSA) and the polyethylene glycol (PEG) with an average molecular weight of 12,000 Da. The addition of 12,000 Da PEG is to mimic β_2 -microglobulin (Mw: 11,800 Da), which is the largest toxin molecule to be removed from the blood. After the hemofiltration tests, a cleaning process was undertaken as the final stage. Atomic force microscopy (AFM) will be used to examine the surfaces of the membrane before and after cleaning.

Chapter 7: Conclusion and recommendation for future research

This chapter summarises the main conclusions and findings, as well as the limitations of the study. A number of recommendations are proposed for the future development of this approach.

Chapter 2: LITERATURE REVIEW

2.1 Hollow Fibre Membrane Material

Synthetic polymers have been used as a base material in many industrial and medical sectors due to its mechanical robustness when compared to natural polymers. Polymers that have been widely available in the market for dialysis are PSF and polyethersulfone (PES) [4,19]. In consideration of environmental and economic interests, sustainable and degradable biomaterials have been established but are emerging to broader applications. For example, poly(lactic acid) (PLA) is one the most widely researched; it used in biomedical applications due to its excellent biodegradability [20-22], biocompatibility [20,22] and low cost [21]. However, several studies have been reported that the degradation tests showed a significant mass loss over a period of time [22,23]. The results indicated that PLA is impossible for long-term application such as haemodialysis, whereas there is a high potential for applications where degradation plays a crucial role, such as medical sutures which can be reabsorbed by the human body [20]. Exploration of the base material continues to take place in order to achieve better dialysis performance relative to existing membranes with regard to biocompatibility, chemical resistance, and mechanical strength.

2.1.1 Polyvinylidene fluoride

Polyvinylidene fluoride (PVDF) is a semi-crystalline fluoropolymer that exhibits outstanding chemical resistance, thermal stability, and mechanical properties. The applications of PVDF membranes in various fields have been widely reported [24-26]. Mackey, *et al.* [27] stated that the excellent resistance of PVDF is closely related to its crystalline structure. It is important to mention that the strong chemical stability of fluoropolymers is directly related to the bonds between the carbon and fluorine atoms within the polymer [26]. The polymer structure of PVDF is shown in Figure 2.1. PVDF membranes have been employed in ultra- and micro-filtration for separation applications, such as carbon dioxide absorption/capture, water reuse, and wastewater treatment [25,26,28].

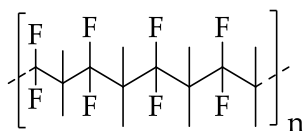


Figure 2.1. Chemical structure of PVDF.

PVDF is bio-inert, and exhibits excellent biocompatibility and non-reactivity, which have led to it being one of the widely used polymers in medical settings. It is mainly used for implants or medical devices [15,29] such as vascular grafts [15,30] and bone fillings [31]. For instance, Laroche, *et al.* [30] used PVDF as a vascular suture to determine biocompatibility in *in vivo* experiments. After one six-month *in vivo* experiment, the biocompatibility of the PVDF was confirmed using histological examination. The results showed no calcification, minimal inflammation, and fibrous tissue development near the PVDF suture.

Extensive studies on fabrication methods and properties of PVDF membranes in either flat sheet or hollow fibre have been reported [25,32-34]. Several techniques have been studied and performed in membrane fabrication, including phase separation, electro-spinning, and stretching. Among these techniques, phase separation is the most frequently employed because of its simplicity and the ease with which it can be dissolved in common organic solvents. Phase separation is sometimes described as a demixing process, which is a controlled process of transforming a homogeneous polymer solution from a liquid to a solid phase. One of the phase separations for preparing membrane is known as diffusion induced phase separation, which involves non-solvent and solvent exchange.

One important fact that has been scarcely addressed is the mechanical strength of the PVDF membrane. A membrane made of PVDF alone has exceptional ductility, but low tensile strength [24,34,35]. Polymer blending is a common and effective method to overcome material deficiencies and improve membrane properties. Therefore, additives are added by blending one or more polymers, whether hydrophilic or hydrophobic materials. The incorporation of polymer blending using PVDF as a base membrane is closely associated with its physical properties.

As mentioned earlier, mechanical strength can be modified by the crystallinity of PVDF, which is attributed to the composition of amorphous and crystalline structures. Several studies have reported on the integration of amorphous polymers to enhance the mechanical strength and minimise the membrane defects of the PVDF membrane [36-39]. For example, Laiarinandrasana, *et al.* [37] demonstrated that the incorporation of an amorphous polymer could modify the fracture behaviour of the polymer blend. They examined the way that an amorphous polymer transitioned from brittle to ductile after the addition of a semi-crystalline polymer. They discovered that, as the degree of crystallinity increased, the fracture energy gradually increased from a lower to higher state, indicating the transition from brittle to ductile fracture behaviour.

In the work of Shi, *et al.* [38], poly(vinylidene fluoride-*co*-hexafluoropropylene) (PVDF-HFP) was used to prepare hollow fibre membranes. The result demonstrated that PVDF-HFP exhibited better mechanical strength than pure PVDF. Hexafluoropropylene (HFP) is a potential polymer because it is an amorphous polymer that possesses outstanding hydrophobicity [40], and chemical and thermal resistance [41]. These properties are attributed to the fluorine content in HFP, as shown in Figure 2.2. (a). Teoh and Chung [39] have shown that the development of macrovoids in the membrane could result in weaker mechanical strength. Hence, they demonstrated the formation of macrovoid-free hollow fibre membrane by integrating Polytetrafluoroethylene (PTFE) particles into a PVDF polymer blend. Figure 2.2. (b) shows the chemical structure of the PTFE. PTFE possesses excellent mechanical strength, chemical, and thermal stability, and it is naturally hydrophobic. Upon increasing the PTFE particles to 50 wt%, the macrovoid formation was successfully suppressed.

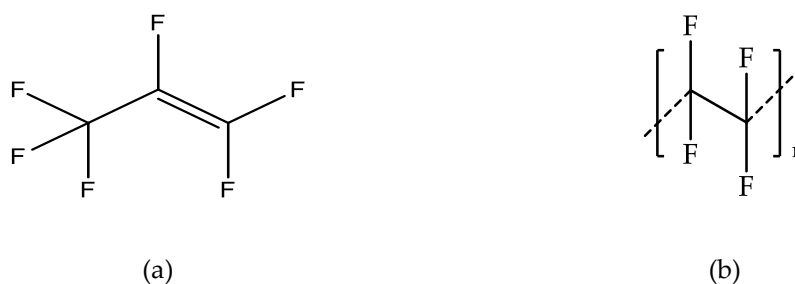


Figure 2.2. Chemical structure of (a) HFP; (b) PTFE.

2.1.2 Polysulfone

Polysulfone (PSF) is an amorphous polymer. PSF was widely available on the market as a membrane material before PVDF emerged as a preferred polymer for hollow fibre fabrication. Figure 2.3. shows the chemical structure of PSF. One of the features is that the pore formation of an amorphous polymer is more superior to semi-crystalline polymers, such as PVDF. This is because an amorphous polymer does not undergo crystallisation as a semi-crystalline polymer to fully reach its solid phase. Therefore, PSF possesses a faster solidification rate, resulting in high surface porosity and a thin skin layer in the membrane [26].

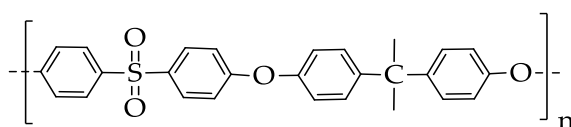


Figure 2.3. Chemical structure of PSF.

Both PSF and PVDF exhibit comparable hydrophobicity, good mechanical strength, and stability against harsh conditions. PSF has been generally used because of its excellent chemical and mechanical properties, but the durability of PSF is slightly different from PVDF [42]. PSF possesses brittle (high modulus) behaviour, which results in better impact resistance. However, because of its brittleness, the membrane is prone to stress cracking [43] and has weak fatigue resistance [44]. According to the manufacturer's guidelines, the application duration of the Fresenius Polysulfone[®], which is made of PSF, is limited to 72 hours [45]. Zhang, *et al.* [46] compared the mechanical strength of a commercial PSF, Fresenius F60S membrane and a fabricated PVDF membrane. The overall mechanical properties of the fabricated PVDF were higher than the commercial PSF hollow fibre [46,47]. Specifically, the tensile strain of PVDF was six times higher than that of the PSF membrane.

In addition, because of its hydrophobic properties, pure PSF is subject to membrane fouling, which is one of its drawbacks. Therefore, membrane modification is a necessary procedure to improve the biocompatibility of the membrane. PSF-modified membranes have been widely reported. For instance, Ding, *et al.* [48] introduced lignocellulose

nanofibrils (LCN) into PSF blends to fabricate ultrafiltration membranes through immersion precipitation. LCN is a naturally hydrophilic material because of the cellulose chain segment. The resulting membrane demonstrated significant improvement on the hydrophilicity in comparison with pure PSF via contact angle measurement and membrane permeation.

Kim, *et al.* [49] performed oxygen plasma treatment to modulate PSF's ultrafiltration membrane properties from a hydrophobic to a hydrophilic membrane. The hydrophilicity and membrane fouling of the treated membrane was examined by introducing hydrophobic gelatin molecules. After the oxygen plasma treatment, the results showed that polar functional groups were introduced to the treated membrane, resulting in hydrophobic gelatin molecules being repelled from the membrane surface. This was because of the charge repulsion between the membrane and gelatin molecules. Therefore, the deposition of the gelatin molecules was also lower than the untreated membrane, indicating that the fouling resistance of the treated membrane had increased.

2.2 Membrane Fabrication Parameters

The parameters of the membrane fabrication are essential factors that affect the membrane's morphology and, subsequently, its mechanical strength and performance. These parameters are polymer dope concentration, solvents for dissolving the polymer, additives, internal and external coagulants, air-gaps, dope extrusions and internal coagulant flow rates, and temperature.

2.2.1 Polymer dope concentration

One of the crucial aspects of formulating optimum polymer dope concentration is by exploring the dope rheology, which is associated with the viscosity of the polymer dope. Hollow fibre membrane prepared with low polymer dope concentration often suffers from excessive macrovoid formation and broad pore distribution [50], which has an adverse effect on the mechanical strength.

Bakeri, *et al.* [51] determined the effect of different polyetherimide dope concentration on hollow fibre membrane structure. The fibres were fabricated from a 10

to 15 wt% polymer dope concentration using a wet phase separation method. A subtle difference at the inner skin was observed, though the range of polymer dope concentration possessed relatively low viscosity, and all of the fabricated membranes developed similar finger-like macrovoids. At higher polymer dope concentrations, the inner skin layer of the membrane became thicker, which contributed to the delayed solvent-non-solvent exchange. Moreover, upon increasing the polymer dope concentration, the membrane density of the resulted membrane increased, whereby the mean pore size, effective porosity, and pore fraction decreased.

Tang, *et al.* [52] investigated the effect of PVDF hollow fibre fabrication using the phase separation method on different polymer dope concentrations. Hollow fibres were prepared that were 13, 15, and 17 wt% of PVDF, with an added constant weight ratio of additives. With an increase in polymer dope concentration, they discovered that the inner and outer layers of fibre developed a higher proportion of the sponge-like structure and better tensile force than a finger-like structure. This was attributed to the increase in the viscosity of the polymer dope, which delayed solvent exchange during the phase separation [53]. A similar observation was presented by Wei, *et al.* [54]. They discussed the impacts on membrane morphology when the polymer dope concentration increased. The results showed that the pores of the membrane decreased and suppressed macrovoid formation. Moreover, the thickness of the membrane increased as the polymer dope concentration increased.

Ismail and Mansourizadeh [26] demonstrated the effect of additives on the PVDF and PSF membrane structure. It was found that changes to polymer dope viscosity were attributed to the addition of the additives in the polymer dope solution. The exchange diffusion between the solvent and non-solvent decreased with the increase in the viscosity. As a result, the enlarged finger-like macrovoid was not seen, as it was with pure PVDF; instead a more sponge-like structure was presented on the membrane structure of PVDF and PSF. Moreover, the effective surface porosity reduced when the additive was added, resulting in lower membrane performance.

2.2.2 Coagulation concentration

Aside from controlling the polymer dope concentration, the manipulation of internal and external coagulant can also reduce or diminish the membrane defects. The application of solvent and non-solvent mixture as internal or external coagulants can be used to delay the demixing process and subsequently change the membrane morphology.

For instance, Sukitpaneent and Chung [32] discovered that the different solubility parameters between the polymers and non-solvents have an impact on the demixing process. The larger the contrast in solubility parameters, the faster the demixing process [55]. When water, as a strong non-solvent, was used in the external coagulant, the demixing happened instantaneously and formed a thin skin layer with large, finger-like macrovoids at the outer membrane surface. Nevertheless, when a weak non-solvent such as alcohol was used, the demixing was delayed. The delayed demixing process provided enough time to induce solid-liquid demixing, and hence changed the morphology and the mechanical strength of the membrane.

Young, *et al.* [56] demonstrated the transformation of a typical liquid-liquid demixing to a solid-liquid demixing membrane structure by replacing the non-solvent coagulant from water to 1-octanol. When water was used in the coagulation process, the membrane structure consisted of a dense skin layer and a sponge-like structure accompanied by finger-like macrovoid. On the other hand, when water was replaced with 1-octanol, uniform spherical particles were observed at the cross-section, forming crystalline particles. The former structure represents the liquid-liquid demixing, which occurs rapidly, resulting in an asymmetrical structure. On the contrary, the formation of the latter structure implies that the behaviour of the phase separation was dominated by crystallisation, and hence resulted in a symmetrical structure.

Internal coagulant, sometimes known as bore fluid, is composed of either a mixture of solvent and non-solvent, or solely solvents, and is used to induce a delayed demixing at the inner surface [38,57]. This prolonging allows the macromolecule, to a certain extent relax and re-arrange, such that membrane deformation is reduced. Several studies have

reported the effect of internal coagulant composition on membrane structure. For instance, Tang, *et al.* [52] prepared hollow fibre membranes using water in the internal and external coagulant. The large difference in solubility parameters between solvents and non-solvents led to fast solvent exchange, and hence large macrovoids were formed in the fibre.

Wang, *et al.* [58] found that the use of ethanol can diminish the appearance of large macrovoids at the inner surface, resulting in better permeation flux. Besides the use of alcohol, the same solvent used to dissolve the polymer has also been employed in the internal coagulant to suppress membrane deformation, where a higher solvent ratio was applied to achieve similar membrane structure and properties [59-61].

The fabrication of a hollow fibre membrane with an asymmetric structure with a variety of pore sizes is preferred, as it has better selectivity compared to a symmetrical membrane [34,62,63]. This is because the asymmetric membrane is composed of a dense skin layer and a highly porous support layer. The difference in pore sizes can function as a selective layer and facilitate several applications, for example, a dense skin layer (which is pore-less) can be used for gas separation, and nano-sized and micro-sized pores can be used for liquid separation. However, its hydrophobic nature decreases the water permeability rate and increases membrane fouling.

2.3 Membrane Hydrophilization Material

Aside from the ductility of PVDF, PVDF membranes possess low surface porosity [59] and have large pores [34,64], resulting in poor filtration performance, including albumin loss and membrane fouling. Kajekar, *et al.* [65] mentioned that, although the promotion of pore formation without the use of additives can be achieved by reducing the polymer dope concentration, the membrane's mechanical strength may be weakened. Conversely, an increase in the polymer dope concentration can decrease the mean pore size of the membrane [25].

Therefore, additives (whether as single components or in a mixture) are added to enhance the membrane structure. Hydrophilic polymers that are commonly employed

as additives include PVP [28,65,66], polyacrylonitrile (PAN) [67,68], poly(methyl methacrylate) [69,70], and PEG [41,71]. PVP and PEG aren't only used to modify the membrane properties of a hydrophobic to a hydrophilic polymer blend, but can be used as pore-former. Moreover, inorganic materials are frequently used to enhance membrane hydrophilicity and promote pore formation, including titanium oxide (TiO₂) [68,72], calcium carbonate [24], zirconium dioxide [73] and silica [74]. The integration of these materials increases the hydrophilicity of a membrane, resulting in lower susceptibility to membrane fouling.

For instance, Wongchitphimon, *et al.* [41] demonstrated that PEG with different molecular weight and loading increased, leaving a visible morphological impact on the PVDF-HFP membrane. The change of the membrane structure also increased its water permeation. Kajekar, *et al.* [65] reported that the addition of PVP has significantly increased the membrane porosity and improved the filtration performance. In their work on the use of inorganic materials, Bae and Tak [68] integrated TiO₂ particles into the polymer blend to modify PVDF, PSF, and PAN membranes. The study aimed to produce membranes with anti-fouling properties. The experimental results demonstrated that PVDF-TiO₂ exhibited the highest water permeation and rejection of activated sludge, regardless of polymeric materials. Similar outcomes when TiO₂ was added were also reported by Damodar, *et al.* [75].

The improvement of the fouling resistance between the membranes and protein adsorption is associated with the hydration ability of the hydrophilic membrane. The hydrophilic membrane becomes highly hydrated on contact with water. This is attributed to the formation of the hydrogen-bond network among the water molecules and the membrane, which exhibit anti-fouling properties. Nevertheless, hydrogen bonds are known to break easily and re-form [76]. Therefore, the incorporation of hydrophilic polymer as an additive encounters challenges such as leaching [77,78], which consequently transit from the non-fouling to fouling membrane surface.

Besides incorporating additives, other methods were reported [79-81], such as depositing of polymer on the membrane surface to enhance the hydrophilicity of the

based material. Studies have also focused on membrane surface modification using stimuli-responsive polymers and zwitterions, because of their anti-fouling and hydrophilic effects. For example, Zhao, *et al.* [81] prepared a zwitterionic¹ membrane for wastewater application. The modified membrane was fabricated by coating polydopamine, followed by grafting 2-methacryloyloxyethyl phosphorylcholine (MPC). The zwitterion layer coated on the membrane shows resistance to protein adsorption and bacterial adhesion. Another study by Yue, *et al.* [82] introduced a zwitterionic membrane by grafting poly(sulfobetaine methacrylate) (PSBMA) on the PSF membrane to enhance the biocompatibility. The modified membrane exhibited significant improvements in blood biocompatibility, which might result from the enhanced hydrophilic effect.

The stimuli-responsive polymer has been a promising polymer, because of its ability to undergo a reversible volume change in response to different environmental stimuli, such as temperature, pH, electrical charge, and ion strength. As a result of its high water content and properties, the intelligence of hydrogels opens up a diverse variety of applications in different technological areas, predominantly for biomedical applications. For example, drug delivery systems [83,84], lubricious coating [85,86], scaffold material for tissue engineering [87], sensing [88], and separation and purification technologies [89].

From the viewpoint of medical and sensor applications, the sensitivity of microgel means it reacts more quickly to changing stimuli and is more efficient in an aqueous environment than hydrogel or macro-sized gel. This is because of its higher interfacial area per unit mass, hence it produces a better exchange rate [90]. Three potential stimulus-responsive polymers that are widely used are poly(N-isopropylacrylamide) (PNIPAAm), poly-N-vinylcaprolactam (PVCL), and PDMAEMA.

¹ A zwitterion is a neutrally charged molecule composed of both positive and negative functional groups.

Among these intelligent hydrogels, PNIPAAm is the best-known hydrogel in responding to temperature. Second is PVCL, PVCL has gradually taken over PNIPAAm because it induces cytotoxicity [91,92]. Figure 2.4. shows the chemical structure of PNIPAAm and PVCL. The cross-linked PNIPAAm and PVCL have a unique phase transition, which sees them being able to undergo a reversible phase transition. Both undergo a volume change at an LCST of around 32 °C in an aqueous medium [93,94]. If temperature is applied below the LCST, the cross-linked PNIPAAm and PVCL polymers that are hydrophilic will swell in water. Above the LCST, they are hydrophobic and expel water.



Figure 2.4. Chemical structure of (a) PNIPAAm; (b) PVCL.

Other than the temperature-responsive behaviour of the hydrogel-based on PNIPAAm and PVCL, another type of classical stimulus-response of interest is a pH-responsive hydrogel. The swelling behaviour of a hydrogel would exhibit pH-responsive behaviour because of the protonation and deprotonation of the hydrogen bonding upon external pH changes. In biomedical applications, a hydrogel that is capable of simultaneously responding to two types of stimuli is more favourable, particularly when it comes to temperature and pH responses. Studies have reported on the introduction of acrylic acid monomer on a PNIPAAm chain to achieve copolymers that show temperature-induced phase separation over a broad range of pH values [93,95]. However, the incorporation of an acrylic acid monomer, which is a pH-responsive monomer, could eradicate the temperature-responsive behaviour of the PNIPAAm in a copolymerised hydrogel [96]. This is because of interruptions to the continuous isopropylamide chain [97].

An alternative way to induce pH-responsiveness and simultaneously prevent the destruction of the temperature-responsive hydrogel is to incorporate a novel co-monomer with PNIPAAm without hindering the original continuous hydrogel chains. For example, copolymerisation with any of the following: 2-carboxyisopropylacrylamide [98], N-isopropylmaleamic acid [99] and DMAEMA [97]. Among these monomers, DMAEMA is not only responsive to pH, but also to temperature. The responsive behaviours of PDMAEMA indicate that it exhibits different LCST values at various temperatures and with different pH values. Moreover, PDMAEMA has the ability to exhibit upper critical solution temperature (UCST) if multivalent counter-ions are added [100] or the amine group is quaternized [101]. Figure 2.5. shows the chemical structure of PDMAEMA. Xu, *et al.* [94] stated that the maximum LCST of PDMAEMA was about 45-50 °C at pH 7-8.5, demonstrating the possibility of its use in biomedical applications.

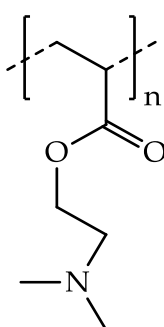


Figure 2.5. Chemical structure of PDMAEMA.

In addition, microbial contamination in food and medical settings, such as food packaging and implanted medical devices respectively, is a major concern which can lead to development of severe infections. In order to hinder the microbial invasions, researchers discovered that the presence of hydrogel synthesised from PDMAEMA on the surface membrane could inhibit microbial activity, thus preventing the growth of microbial cells [102,103]. In the light of the discovery of this unique microbial activity, further studies have been performed to examine the range of antimicrobial activity on PDMAEMA against Gram-positive and Gram-negative bacteria as well as the antimicrobial mode of action [104,105]. Rawlinson, *et al.* [105] reported that the addition of PDMAEMA able to inhibit bacterial growth by direct binding, and disrupt the

cytoplasmic membrane of bacteria, and subsequently caused cell death. Moreover, the incorporation of PDMAEMA with an antimicrobial agent, erythromycin (which used in treating Gram-positive bacteria), it enhanced the efficacy of the agent against Gram-negative bacteria up to 59-fold.

Copolymerisation between DMAEMA and other polymer materials is of emerging interests in the biomedical field [97,106-109]. For instances, Chen, *et al.* [108] synthesised dual-responsive, comb-type grafted hydrogels using N, N-diethylacrylamide and DMAEMA. The prepared hydrogels demonstrated an LCST at about 31°C. The copolymerisation of both monomers exhibited enhanced temperature- and pH-responsive characteristics, including faster de-swelling and re-swelling kinetics and better oscillating de-swelling/swelling behaviour. Wang, *et al.* [97] prepared hydrogels based on NIPAAm and DMAEMA using free radical polymerisation. They discovered that the introduction of DMAEMA not only provided addition pH-responsive, but also retained the temperature-responsive of P(NIPAAm-co-DMAEMA). The thermo-sensitivity of a thermal-responsive monomer, such as NIPAAm often reduced or eliminated when copolymerising with other pH-responsive monomers. A similar study reported by Zhang, *et al.* [107], dual stimuli-responsive poly(NIPAAm-co-DMAEMA) hydrogels were synthesised and exhibited LCST at approximately 34°C. The results showed an improvement in the mobility of the polymers, leading to a rapid response to temperature and pH stimuli.

The unique characteristics of these hydrogels have extended to a broader range of applications by reducing the sizes of the gels, into microgel or nanogel. These include wastewater treatment, the food industry, and drug delivery systems. The term microgel was first established in 1949, and implies that the hydrodynamic diameters range from 100 nm to 1000 nm [110,111]. The popularity of using microgel particles prepared by free radical dispersion polymerisation in organic solvents to produce monodispersed particles in an aqueous phase has risen in recent decades [112]. Free radical polymerisation is a technique extensively used in industrial settings because of the simplicity of its to preparation and reproduction [113]. This preparation is further

categorised based on the particle formation mechanism; it is either formed by heterogeneous nucleation or homogeneous nucleation [114,115].

Heterogeneous nucleation is used in emulsion and suspension processes, and it involves two steps. Firstly a suspension of large aqueous droplets is formed in an oil phase, and secondly, the droplets are polymerized into microgel particles. Homogeneous nucleation refers to the initial composition of the microgel particles in a homogeneous solution, and mainly applies to bulk and solution processes. The mechanisms involved in homogeneous nucleation requires a solution of a soluble monomer, which contains a cross-linking agent to prevent microgel particles from dissolving after the end of the polymerisation. Hence, they are usually copolymerised and cross-linked with one or more polymers to increase the colloidal stability of the microgel particles.

One of the main concerns of free radical polymerisation is the lack of control of the polymer's molecular weight. As a result, the polymerised microgel particles have a wide range of sizes. A conventional practice performed in a single step polymerisation is to agitate the entire synthesis at a constant speed [92,93,111,116,117]. This technique not only allows for spherical microgel particles to be obtained but can also overcome the drawbacks mentioned above. To further address the problem, another technique was used to reduce the size range: a selective purification process.

2.4 Parameters of Microgel Particles Synthesis

The polymeric particles that are prepared by incorporating cross-linkers provide a finite structure through intramolecular cross-links and form a colloidal dispersion. The presence of cross-linkers within the particle network affects the swelling extent of microgel particles. Monomers or co-monomers have been introduced for the preparation of microgel particles, with promising effects. The monomers are methyl methacrylate [118], methacrylic acid (MAA) [119], styrene [120,121], acrylic acid (AA) [104], MBAA [96,111,122] and ethylene glycol dimethacrylate (EGDMA) [123]. The effects of these monomers on polymer particles include improvements to the swelling behaviour,

alterations to the volume phase transition, and influence on the responsive behaviour of the polymer.

For instance, Yuk, *et al.* [124] prepared a copolymer of DMAEMA and acrylamide (AAm) via free radical polymerisation. The copolymers that resulted showed responsiveness to pH and temperature and exhibited LCSTs. Upon increasing the AAm in the DMAEMA mixture, the LCST moves to the lower temperature. When the copolymer was subjected to differing pH level, the LCST decreased dramatically. The study described that the transition resulted from increasing polymer-water and polymer-polymer interactions, which impeded the hydrogen bond between DMAEMA and AAm.

Another study by Goganian, *et al.* [125] also reported on the hydrogel synthesised from copolymer, DMAEMA and AAm using MBAA as a cross-linking agent. With high amounts of cross-linkers, the morphological observations of the hydrogel revealed that pore structure decreases and becomes more regular, as the irradiation time increased. This was attributed to the increasing number of hydrogen bonds in the resultant hydrogel. Moreover, the thermal stability of the hydrogel was higher, which is associated with a higher amount of cross-linker in the hydrogel network. In contrast, the swelling ratio of the hydrogel was lower at higher cross-linker concentrations. This was because, when the concentration of cross-linker increased, the degree of the hydrogel network increased and hence decreased the dipolarity value of the hydrogel.

Ni, *et al.* [126] discovered novel amphoteric microgel particles composed of DMAEMA, AAm, and MAA and cross-linked with MBAA via semicontinuous polymerisation. This polymerisation allowed the particles to produce bigger and polydispersed microspheres. The microspheres with a smaller amount of DMAEMA were formed, when the same starting concentration was utilized, and MAA was continuously added at a higher rate to the polymerisation system. The resulted microgel particles possessed a distinctive pH-volume phase transition. The experimental results demonstrated that, when the pH was neutral, the microgel particles absorbed 75-80% of

the dye. When the environment changed (such that it became either more acidic or basic), the dye was released, 10% and 6% remained in the microgel particles, respectively.

Emileh, *et al.* [111] performed theoretical work on the preparation and characterisation of PDMAEMA microgel particles. The main composition of the mixture consists of DMAEMA and MBAA in an ethanol/water mixture and synthesised via dispersion polymerisation with constant stirring. A similar study was performed by Hu, *et al.* [96] with extensive research on the effects of the synthesis parameters, except that the dispersion polymerisation of PDMAEMA microgel particles was completed without agitation. The microgel particles produced without agitation are relatively large compared to those under constant agitation. The micrographic results reveal that the larger particles were formed from aggregated particles. This phenomenon was attributed to the electrostatic attraction between the particles. In order to suppress the aggregation of the particles, PVP was added to act as a steric stabiliser. Upon increasing the PVP molecular weight, the size of the particles decreases, and hence monodispersal distribution was achieved.

Orakdogan [123] investigated the effect of initial monomer concentration with a constant cross-linker on swelling behaviour with respect to pH-responsive. With a higher initial monomer concentration, the water uptake of PDMAEMA is greater under acidic conditions. This was because the tertiary PDMAEMA group undergoes protonation, resulting in higher charge density and PDMAEMA in the swollen state. In contrast, the water withdrawal was greater at higher initial monomer concentrations under basic conditions, as PDMAEMA underwent deprotonation and shifted to a collapsed state.

Hu, *et al.* [96] demonstrated the effect of initial monomer and cross-linker concentrations on the polymerisation process. Upon increasing the cross-linker concentration, the particles were heavily cross-linked and become hydrogels in place of microgel particles. This suggested that excessive cross-linkers could carry on interacting with the unreacted monomer during the polymerisation process. Instead of forming a hydrogel, aggregation was observed with increasing monomer concentration, resulting

in larger particles [96,127,128]. Similar to the possession of higher monomer concentration, the dispersion became unstable, and the unreacted monomer extended the duration of the polymerisation and led to severe aggregation.

2.5 Dispersion stability

Another way of developing a dispersion polymerisation system with a narrow particle-size distribution, other than nucleation, is through stabilisation. Achieving a stable dispersion is crucial, because newly formed polymer particles rapidly aggregate, as the size of the particles can increase considerably in aqueous media. This phenomenon is due to the mutual attraction of the polymer particles generated by van der Waals forces. Steric stabilisation is a technique frequently used to overcome the aggregation caused by the van der Waals forces. It uses a form of a protective barrier surrounding the polymer particles to interpose between them. Several studies have been reported that employ ethanol, an organic solvent, and aliphatic hydrocarbon in dispersion polymerisation to prevent aggregation, which involves mutual repulsion of electric charges [96,111,112,129].

Another similar stabilisation mechanism is using a barrier of water-soluble polymer to function in aqueous media. The choice and properties of stabiliser played an essential role in conserving the colloidal stability, particle size, size distribution, and morphology under specific conditions. Studies have reported that the application of steric stabilisers during particle synthesis can achieve colloidal stability and controlled particle size, including citrate [130,131], PEG [132] and PVP [96,109,133]. Citrate stabilises a particle's core via charge repulsion and produces particles with a negative surface charge over an environmental pH range from 3–10. Nevertheless, it has been reported that the use of charge repulsion to stabilise the core of a particle was inefficient [130,131].

On the other hand, PEG and PVP are hydrophilic homopolymers and frequently chosen as hydrated steric barriers [134]. The steric stabilisation of both polymers provides stronger bonding to the core compared to citrate. Riley, *et al.* [132] reported that the introduction of these hydrophilic stabilisers could significantly reduce the aggregation in an aqueous dispersion with an increase of the ionic strength of a medium.

Another study reported by Tejamaya, *et al.* [130] demonstrated the effect of different stabiliser coatings, including citrate, PEG, and PVP, on silver nanoparticles. They discovered that PVP-coated particles were the most stable combination, and they were able to withstand all media at different ionic strength over an extended period. The standard media were based on the Organization for Economic Co-operation and Development for *Daphnia* species for acute and chronic studies, which include chloride, nitrate, and sulphate media. In the study, citrate-coated particles were completely lost when they were exposed to the media. Although the PEG-coated particles were more stable than citrate-coated particles, aggregation was seen in the nitrate and sulphate media after a period of time.

The zeta potential is an essential indicator of the stability of a colloidal dispersion. A net charge of a particle affects the distribution of the ions in the liquid layer of the surroundings. Each particle is surrounded by an electrical double layer; the inner and outer regions, which are known as the Stern layer and the diffuse layer respectively. The ions are strongly bound at the Stern layer, and are loosely attached at the diffuse layer. There is an abstract boundary surrounding the Stern layer, which is located in the diffuse layer, where the ions and particles form a stable entity, as shown in Figure 2.6. This abstract boundary is also called a slipping plane. When a particle moves, the ions within this layer move concurrently with it; however, ions beyond this layer do not move with the particle. The potential exhibited at this boundary is known as the zeta potential [135]. When a dispersion exhibits high zeta potential value (either negative or positive), the particles in the dispersion repel each other, and hence flocculation will not take place. Nevertheless, when the dispersion possesses a low zeta potential value, the weakening of the force causes aggregation between particles. In general, a dispersion is considered colloidally stable when the zeta potential value is above + 30 mV or below – 30 mV, and with values in between implying that the dispersion is colloidally unstable [135,136].

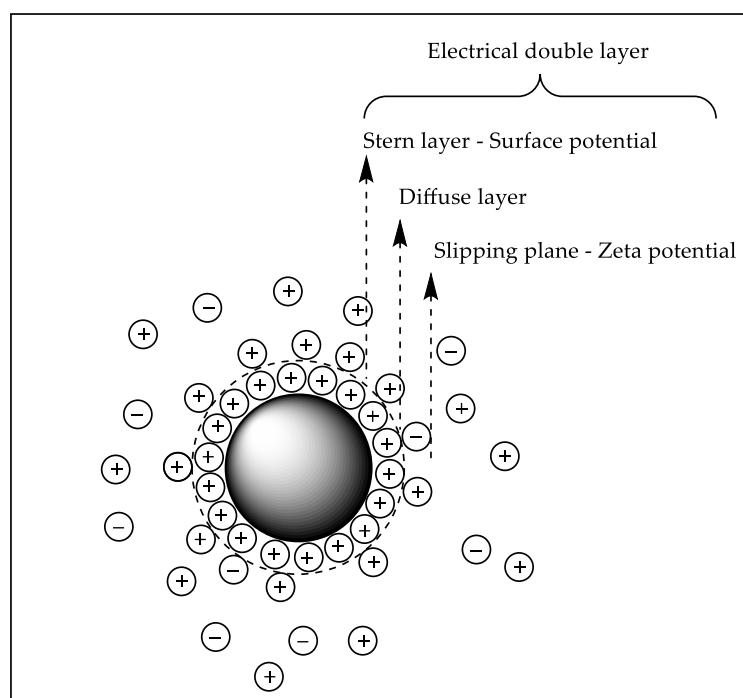


Figure 2.6. Schematic diagram of a particle surrounding in a liquid layer. Modified from [136]

2.6 Polymeric Surface Modification

Membrane surface modification is a method of modifying the original property of a material surface, whether that is the physical, chemical or biological properties. The wettability and biocompatibility of a membrane surface of hydrophobic material is usually the main disadvantage in clinical applications. Therefore, the membrane surface should be modified to enhance its performance. Various surface modification techniques have been developed for preparing a thin layer on the membrane surface, including (1) surface coating via dip-coating or depositing layer-by-layer [8,79], (2) chemically polymerised of polymer/monomer via interfacial polymerisation [137,138], and (3) irradiation and grafting reactions through photo-grafting or oxygen plasma treatment [49,139]. Among these modification techniques, photo-grafting is the most commonly used for flat sheet membranes due to its simplicity, cost, and wide range of potential applications. Unfortunately, using this technique on hollow fibre membranes would be a challenge, as uneven grafting may result. The following sections will focus on surface coating and polymerisation.

2.6.1 Surface coating

Surface coating is the most straightforward approach used to perform surface hydrophilization. The main drawback of this technique is that coating via direct attachment is temporary, as the coated layer is unstable, and could wash away after extensive operations and cleaning. Considerable research has been dedicated to improving the adsorption interaction between the membrane and the coated layer by diligently choosing a specific surface interaction or adopting layer-by-layer (LbL) fabrication [140-142].

He, *et al.* [143] prepared composite nanofiltration membranes for application in dye recovery. The fabrication involved coating sulfonated poly(ether ether ketone) (SPEEK) on the inner membrane surface of the PES substrate. The coating process was accomplished by following the SPEEK solution through the lumen from bottom to top using an air bulb. Immediately after draining the excess SPEEK solution, the membrane was subjected to nitrogen gas. Despite possessing a high MWCO, the resulted membrane exhibited high levels of salt rejection. They also discovered that the increase of coating thickness and SPEEK concentration elevated the rejection performance.

Chanachai, *et al.* [144] investigated the coating effect of chitosan on PVDF hollow fibre membranes for membrane protection against membrane wetting and reducing flavour loss during the osmotic distillation process. The outer membrane surface was coated with and without a cross-linking agent via a dip-coating method. The membrane was submerged in the coating solution and air-dried at room temperature, after which the solvent was further vaporised in the oven. Greater protection against membrane wetting was observed on the coated membrane, and hence membrane permeation was inevitably improved. The coated membrane also showed a decent reduction in flavour loss as compared to the uncoated membrane. However, membrane permeation decreased with the coated membrane that was subject to cross-linking, whereby the reduction of flavour loss was comparable to the coated membrane that was not subject to cross-linking.

Nishigochi, *et al.* [79] reported a simple surface modification on PVDF hollow fibre membranes via dip-coating for use in water treatment processes. The dip-coating of the phosphorylcholine copolymer, which is a hydrophilic polymer, was performed on the outer surface of the membrane via hydrophobic interaction. The outcome was that the one-step coating of the copolymer not only efficiently enhanced the anti-fouling properties of the membrane, but also exhibited relative stability after ultrasonic cleaning with a surfactant. What's more, the water permeability remained relatively constant throughout the test.

The LbL technique is another practical alternative for modifying the surface of a hollow fibre membrane. The functionalised membrane was achieved by sequentially adsorbing positively and negatively charged polyelectrolytes onto the membrane surface. Nevertheless, the conventional LbL technique is time-consuming, because it involves as many as 60 bilayers to have sufficient properties for the preparation for polyelectrolyte multilayer membranes [145]. Therefore, dynamic adsorption was introduced to simplify LbL adsorption. In the study conducted by Menne, *et al.* [141], LbL fabrication was accomplished using dynamic adsorption by using constant flux instead of the conventional static adsorption method. The result showed that the use of dynamic adsorption accelerated the coating layers, which potentially reduced the production effort compared with static adsorption. The LbL functionalised membrane showed excellent stability when it came to backwashing and regeneration capability [140,141].

2.6.2 Polymerisation

Surface modification technique using polymerisation involves chemical cross-linking between a support membrane and the active site of a monomer or polymer [146]. Polymerisation is applied to the membrane that has been physically adsorbed with layers of active sites so that they can be bound firmly to the membrane surface. Interfacial polymerisation has been widely used to create a thin-film coated on the membrane surface for desalination. It is a step-growth polymerisation that involves either two

reactive monomers [147-149] or a polymer with a cross-linker agent [137,150]. The polymerisation occurs at the interface of two immiscible phases [151].

Wang, *et al.* [152] introduced a thin-film-composite (TFC) forward osmosis membrane via interfacial polymerisation to enhance the membrane hydrophilicity. A substrate that was fabricated from PES/sulfonated polysulfone (SPSf) porous membrane was used to undergo interfacial polymerisation between *p*-phenylene-diamine (P-PDA) and trimesoyl chloride (TMC) to form a thin film composite. The polymerisation was performed by contacting one side of the membrane with the PPDA solution first, followed by a TMC solution, to form a thin layer of composite on the substrate. The micrographic observation showed insufficient coverage of the composite on the membrane surface, though an improvement in hydrophilicity and water permeation was observed.

Zhao, *et al.* [153] developed robust TFC aquaporin-based biomimetic membranes (ABMs) for application in desalination processes. ABMs were prepared using interfacial polymerisation techniques by soaking PSF substrate with an M-PDA that consisted of aquaporin-based proteoliposomes. Subsequently, the substrate was contacted with TMC to create a three-dimensional (3-D) cross-linked ABM. The experimental results presented that the surface morphology of ABMs was not significantly affected by the addition of the proteoliposomes, which could be attributed to the small size of proteoliposomes and the fact that it was embedded in the polyamide blend layer. The performance of the fabricated membrane demonstrated that the water permeation was far superior to that of commercial membranes (with a 40% improvement), despite resulting in comparable levels of salt rejection.

In the work of Fang, *et al.* [137], composite nanofiltration hollow fibre was fabricated for water softening applications. A positively charged thin film was produced using the inner surface of the PES substrate through interfacial polymerisation with branched polyethyleneimine (PEI) and TMC. In order to coat the PEI on the inner membrane surface, the substrate was mounted in a membrane module to effectively introduce the PEI solution into the lumen with a syringe. After the removal of the excess PEI solution,

the TMC solution was pumped through the lumen using a peristaltic pump. The composite membrane prepared with optimised preparation parameters exhibited promising hydrophilic properties with decent water permeation and MWCO.

Du, *et al.* [154] prepared a modified membrane by using a hydrophobic membrane interfacial polymerised with PDMAEMA for gas separation. PDMAEMA acted as a reactive polymer to create an active layer on the membrane surface. The substrate membrane and PDMAEMA were separately prepared to avoid incomplete removal of solvent during interfacial polymerisation, which may affect the final polymer product. Therefore, PDMAEMA was prepared via free-radical bulk polymerisation, which involved solvents such as toluene and tetrahydrofuran. The membrane became positively charged after cross-linking, and a thickness of approximately 1 μm of PDMAEMA layer on the composite membrane.

In summary, in order to fabricate feasible and porous hollow fibre membranes, especially those that overcome the weakness of the PVDF membrane, the blending of PVDF with co-polymer is indispensable. PVDF was chosen as the base membrane for hollow fibre fabrication because of its superior chemical resistance and durability, which result from its highly hydrophobic nature and crystalline structure, respectively. Moreover, PVDF is non-toxic, has excellent biocompatibility and leads to minimal cellular inhibition in long-term implantation. In this study, PSF was chosen as the copolymer to reinforce the mechanical strength of the PVDF membrane, as PSF exhibits high modulus, which results in higher tensile strength than that of PVDF polymer. Therefore, PSF may be able to reduce the deformity of PVDF and increase the tensile strength of the polymer blend. The manipulation of the internal coagulant was investigated to overcome the pore formation of the polymer blend.

If seeking to enhance the reprocessing steps after the dialysis process, membrane surface modification with stimuli-responsive microgel particles is superior to polymeric blending with a hydrophilic polymer. Stimuli-responsive PDMAEMA, which consists of pH- and temperature-responsive, is an ideal polymer that aligns with the approach chosen, as it acquires the ability to swell and de-swell according to external stimuli-

responsive. However, instead of incorporating PDMAEMA in the base membrane, it was deposited on the membrane to achieve the greatest benefit, including better biocompatibility, in terms of improving the membrane hydrophilicity, and control of the pore dimensions.

The determination of polymeric embedment techniques is questionable, as controversial studies were reported. A uniform and stable embedding of microgel particles on the membrane is an essential criterion in producing a functionalised membrane. Therefore, the various types of embedment techniques, including dip-coating, interfacial polymerisation, and a combination of dynamic adsorption with interfacial polymerisation are investigated to develop the optimum functionalised membrane.

Chapter 3: PREPARATION AND CHARACTERISATION OF POLYVINYLIDENE FLUORIDE/POLYSULFONE BLEND HOLLOW FIBRE MEMBRANES

3.1 Overview

In this chapter, PVDF/PSF blend hollow fibre membranes were prepared using diffusion induced phase separation and fabricated via a dry-wet spinning technique. DMAc was chosen to be the diluent used to dissolve and homogenise the polymer dope solution. This choice was made due to the high solubility of PVDF in DMAc; hence, a high temperature is not necessary during the preparation process. A fundamental investigation on the hollow fibre membrane made of a PVDF/PSF blend was performed to understand the crystallinity rheological behaviours. The effect of PSF as a copolymer and DMAc concentration as part of the internal coagulant during hollow fibre fabrication were studied. The membrane morphology and the mechanical properties of the hollow fibre membrane were also carefully examined. The effects of these variables on the formation of macrovoids were also systematically investigated.

3.2 Experimental

3.2.1 Materials

PVDF (M_w 534,000 by GPC) and PSF (M_w 35,000) were purchased from Sigma-Aldrich (SG). DMAc (purchased from Merck) was used as an organic solvent in the preparation of the polymer dope solution. Glycerol (AR grade, 92.1 g/mol) was supplied by Merck. The chemicals and polymers were used as received. Distilled water was used as an internal coagulant, and tap water was used as an external coagulant. PEG (Sigma-Aldrich, Germany), with molecular weight ranging from 10,000 Da up to 35,000 Da, and polyethylene oxide (PEO) (Sigma-Aldrich, USA), with a molecular weight of 100,000 Da, were used as model solutes to measure the separation performance of the hollow fibre membranes.

3.2.2 Preparation of a PVDF/PSF blend for the polymer dope solutions

The PVDF hollow fibres were fabricated using diffusion induced phase separation, which involved the extrusion of a polymer dope solution using a spinneret. A spinneret with an inner diameter (ID) and outer diameter (OD) of 0.5 mm and 0.86 mm respectively were used. Similar methods have been reported elsewhere [5,24,26,41]. The PVDF powder and PSF pellets were dried at 110 °C for at least 12 hours (h) to remove any possible moisture trapped during transfer or storage. The measured amount of PVDF powder was stirred at around 200 rpm before DMAc solvent was introduced, to prevent the formation of pockets of PVDF powder. The percentages weights of polymer dope and DMAc were maintained at 20 and 80% respectively. Once the DMAc solvent was added, the PVDF mixture was subjected to continuous stirring at 100 rpm at 25 °C until it was homogenised. PSF pellets were then added to the corresponding PVDF solution to reach the desired amount of polymer dope concentration. Finally, the polymer dope solutions were obtained. The homogenised polymer dope solution was immediately transferred to a stainless-steel syringe to degas at 60 °C for approximately 2 hours, and then it was let to cool at ambient temperature to approximately 25 °C before the spinning process. A series of polymer dope solutions were prepared and examined. The membrane code and the composition of the polymer blends are tabulated in Table 3.1.

Table 3.1. Compositions of polymer dope and internal coagulant for hollow fibre membranes preparation.

Membrane code	Polymer dope composition (wt/wt)	Internal coagulant composition (v/v%)
The effect of polymer dope concentrations		
S0	PVDF/PSF 100/0	DMAc/water 0/100
S5	PVDF/PSF 100/5	
S10	PVDF/PSF 100/10	
S15	PVDF/PSF 100/15	
S100	PVDF/PSF 0/100	
The effect of internal coagulant concentrations		
S5-10	PVDF/PSF 100/5	DMAc/water 10/90

S5-15		DMAc/water 15/85
S5-20		DMAc/water 20/80
S10-10	PVDF/PSF 100/10	DMAc/water 10/90
S10-15		DMAc/water 15/85
S10-20		DMAc/water 20/80
S15-10	PVDF/PSF 100/15	DMAc/water 10/90
S15-15		DMAc/water 15/85
S15-20		DMAc/water 20/80

3.2.3 Fabrication of hollow fibre membranes

The polymer dope solution and internal coagulant were dispensed through the spinneret at a controlled volume rate using syringe pumps (NE-1600 and KD scientific 220 respectively), and the spinning of the hollow fibre membranes would first lead to an air gap prior to the external coagulation bath. The nascent hollow fibre was taken up by a roller at free-fall velocity, before being transferred and stored in a distilled water bath, which was used as a washing bath. In this study, the air gap and the temperature of the polymer dope solution, internal coagulants, the external coagulant, as well as the spinneret, were kept constant during the spinning. The details of the spinning conditions are summarized in Table 3.2.

The remaining solvent in the hollow fibre membranes was thoroughly extracted using distilled water for at least three days, with the water replenished daily. A post-treatment was performed to prevent shrinkage and collapse of the porous structures of the hollow fibre membranes during the drying process at ambient temperature. The hollow fibre membrane was subjected to a 50 v/v% glycerol aqueous solution for 2 hours after a solvent exchange. A desired length and amount of hollow fibre membranes were subsequently air-dried at ambient temperature before any further characterisation and the membrane modules were made. The remaining hollow fibre membranes were kept in distilled water until use.

Table 3.2. Experimental parameters for hollow fibre membrane fabrication.

Spinning conditions	
Dope flow rate (mL/min)	1.0
Internal coagulant	Distilled water ^a
Internal coagulant flow rate (mL/min)	0.15
External coagulant (v/v%)	Tap water: 100
Washing bath (v/v%)	Distilled water: 100
Spinning temperature (°C)	Ambient
Spinneret temperature (°C)	Ambient
Take-up speed	Freefall
Air gap length (mm)	50

^aDistilled water unless stated otherwise (refer to Table 3.1.)

3.2.4 Membrane module preparation for filtration experiments

The lab-scale membrane module consists of a quarter-inch stainless-steel tube of a specific length and two union tees. A piece of hollow fibre was placed into the tube with both ends protruded from the union tee outlets. The space between the hollow fibre and the union tee was sealed using epoxy resin and dried overnight, after which a second application of epoxy was applied to ensure complete sealing. The effective length of the fibre in the module was 20 cm.

3.2.5 Characterisation of PVDF/PSF hollow fibre membranes

3.2.5.1 Cloud point analysis of PVDF/DMAc and PSF/DMAc systems

The cloud point of S0 and S100 systems was measured using a titration method at ambient temperature. Method was adopted from Ismail and Mansourizadeh [26]. The preparation sequence was identical to that used in the hollow fibre fabrication discussed above. Distilled water (which acted as a non-solvent) was gradually added in the polymer dope solutions using constant agitation. When local precipitation was spotted during each addition of the non-solvent, agitation was continued without further

addition until the solution once again became homogeneous. The process was repeated until the solution was permanently turbid, whereby it reached the state in titration known as the cloud point.

3.2.5.2 Thermal properties and crystallinity of PVDF/PSF/DMAc systems

The thermal properties and crystallinity of PVDF/PSF polymer blends were determined using a differential scanning calorimeter (DSC) (DSC 4000, Perkin Elmer). Each sample was prepared by directly quenching the polymer dope solution into liquid nitrogen, which Xiao, *et al.* [34] suggests prevents macroscopic phase separation. A solid sample of 5 mg was hermetically sealed in an aluminium DSC pan. Each sample was heated above the melting temperature of PVDF (approximately 170 °C) using an empty aluminium pan; this served as a reference sample. It was heated from 40 °C to 240 °C at a constant rate of 10 °C/min and isothermally annealed at 240 °C for 10 min, before being subsequently cooled from 240 °C to 40 °C at a cooling rate of 10 °C/min.

DSC analysis was conducted to examine the effect of PSF on the crystallinity degree of the fabricated hollow fibre membranes. The degree of crystallinity of the membranes was based on crystallization (X_c) and calculated according to the following equation from the DSC curve:

$$X_c \% = \frac{\Delta H}{\Delta H_m \varphi} \times 100 \%, \quad \text{Eq. 3.1}$$

Where ΔH and ΔH_m represent the fusion enthalpy of the membrane and 100% crystalline PVDF, respectively. The value of ΔH_m is 104.5 J/g [155]. φ is the PVDF fractional weight in the blended membrane. Due to the amorphous nature of the PSF, the measured enthalpy of fusion can be attributed to the PVDF crystallites in the membranes. The fractional weight of PVDF (W_{PVDF}) in the blended mixture was calculated by:

$$W_{PVDF}(\varphi) = m_{PVDF} / (m_{PVDF} + m_{PSF}), \quad \text{Eq. 3.2}$$

Where m_{PVDF} is the weight of the PVDF, m_{PSF} is the weight of PSF blends and W_{PVDF} is the fractional weight of PVDF. Then equation was substituted into the equation to obtain the crystallinity of PVDF.

3.2.5.3 Analysis of rheological behaviour of polymer dope solutions

The rheological behaviour of the polymer dope solutions was characterised by an RVDV+III rheometer (Brookfield, USA) with a temperature-controlled water bath (TC502, Brookfield, USA). The shear viscosity was carried out using a cone spindle (cp-40) at 25 °C. The shear rate of each measurement was altered based on the torque necessary to overcome the viscous resistance when a cone-shape disc rotates in a fluid.

3.2.5.4 Morphology study of the hollow fibre membranes

The prepared hollow fibre membranes were immersed in liquid nitrogen and fractured to obtain smooth cross-sections. Then, they were sputtered with platinum (Pt) using a sputter coater (Q150RS, Quorum). The cross-section, inner surface, and outer surface of the membrane were observed under the FE-SEM (Ultra-High-Resolution FE-SEM Hitachi SU 8000 series, Japan). At least three locations of each sample were measured. Micrographs were taken at a voltage of at least 10 kV to facilitate the following examination.

The energy dispersive X-ray analyser (EDX) (XMax50 EDX, Oxford-Horiba Inca, UK) coupled with the FE-SEM produced high-resolution images for use in elemental analysis and mapping.

AFM analysis was performed using a digital Instruments Multimode 8 (Bruker, USA) to obtain the surface topography of the membranes. The membrane morphologies of the inner and outer surfaces of the membrane were measured using ScanAsyst mode, which is an automated mode used to optimize image parameters. At least three locations were measured for each sample. Three main parameters were used in AFM to determine the roughness of the membranes. First, the arithmetic average of the absolute values of the surface height deviations measured from the centre plane, is known as the average roughness (R_a) for the image. Second, the root mean square roughness (R_q) is the standard deviation from the mean surface plane. Lastly, the maximum roughness (R_{max}) is defined as the vertical distance between the highest peak and the lowest valleys in the image [24].

3.2.5.5 Pore size and pore-size distribution of hollow fibre membranes

Two complementary techniques were used to characterise the pore size and pore-size distribution of the membranes. Firstly, the membranes were investigated using mercury intrusion porosimetry (MIP) (AutoPore V 9600, m\Micromeritics®, USA). A weighed amount of hollow fibre was introduced in the chamber and filled with mercury. The pressure was gradually increased to fill the mercury into the micropores of the membrane. The pore size and pore-size distribution of the membrane were determined from the volume intruded at each pressure increment. Total porosity was obtained from the total volume intruded.

The second technique was achieved using solute transport (ST) experiments. In order to perform this experiment, the pure water permeability (PWP) and MWCO of the PVDF/PSF membranes were examined sequentially. A schematic diagram of a PWP set-up is shown in Figure 3.1. An extra pressure gauge was included after the pump (blue cap circuit) to monitor any blockages during experiment. The selective membrane layer is the outer layer, hence the feed solution was pumped into the shell side of the fibres and the permeate solution was exited from the lumen side, thus forming a cross-flow filtration approach.

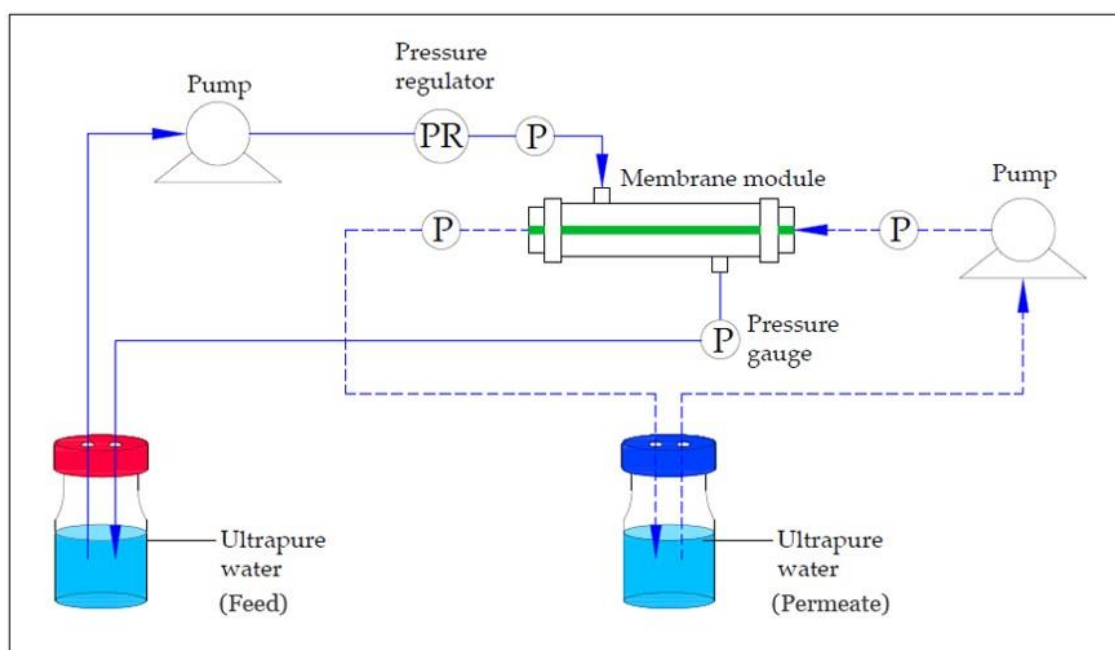


Figure 3.1. A schematic diagram presented the set-up of a pure water permeability experiment using ultrapure water at room temperature.

The prepared hollow fibre membranes were hydrophobic, which increased the difficulty of measuring the pure water permeation. Therefore, the prepared membranes were pre-wetted with pure water for at least 30 min at a transmembrane pressure (TMP) of 2.0 bar prior to collecting the permeated water. Filtration experiments were conducted at constant flow rate at 100 mL/min into the shell side of the fibres using TMP of 0.8 bar and a room temperature of $24\text{ }^{\circ}\text{C} \pm 2\text{ }^{\circ}\text{C}$. The lumen flow rate was manipulated from 10 - 15 mL/min to reach higher TMP for S100. The corresponding Reynolds number greater than 5,000 for all tested conditions to ensure the feed behaviours were within a turbulent range. Then, the pressure regulator was manually controlled while manipulating the flow rate to obtain the desired TMP. The TMP was calculated using the following equation:

$$\text{TMP (bar)} = \frac{P_{\text{inlet}} + P_{\text{outlet}}}{2} - P_{\text{permeate}} \quad \text{Eq. 3.3}$$

Where P_{inlet} and P_{outlet} are the feed side inlet and outlet pressures. P_{permeate} is the pressure of the permeate.

After that, pure water was forced to permeate from the outside to the inside of the hollow fibre membranes for 30 min. The feed and permeate were collected and used for the calculation. At least two modules were tested for each experimental result. The pure water flux calculation was described in Yang, *et al.* [5]. The normalised pure water permeation flux of the membranes was calculated using the following equation:

$$J = \frac{Q}{\Delta P A} = \frac{Q}{\pi D l \Delta P} \quad \text{Eq. 3.4}$$

Where J is the specific flux of the hollow fibre membrane ($\text{L/m}^2\text{ h atm}$), Q is the permeate from the lumen collected at 0.5 hours (L/h), ΔP is the TMP, 0.8 bar (atm), A is the effective membrane surface area (m^2), D is the outer diameter of hollow fibre (m), and l represents the effective length of the hollow fibre, 20 cm (m).

Then, each module was subjected to the pure water permeation experiment, after which the molecular weight of PEG or PEO solutes was gradually increased to perform

the MWCO measurement. The feed concentration of PEG or PEO was 200 ppm and was circulated at the shell side of the membrane. The collected permeate was analysed using a total organic carbon analyser (TOC, Aurora 1030D & 1030S, USA) in order to determine the mean pore size of the membrane. Rejection (R) of PEG or PEO is calculated using the following equation:

$$R \% = \left(1 - \frac{C_p}{C_f}\right) \times 100 \quad \text{Eq. 3.5}$$

Where C_f and C_p are the solute concentrations in the feed and permeate, respectively.

The solute rejection data were further used to estimate the membrane properties, including the mean pore size and the pore size distribution of the selective layer in the hollow fibre membrane. The MWCO for the hollow fibres was obtained from PEG or PEO molecular weight with 90% solute rejection.

The MWCO of membranes were calculated using three consecutive steps:

The mean pore size of the membrane was obtained through the Einstein-Stokes equation [5,156], which describes the radii (r) of PEG and PEO as a function of their molecular weight (Mw) as follows:

$$\text{For PEG, } r = 16.73 \times 10^{-12} \times M^{0.557} \quad \text{Eq. 3.6}$$

$$\text{For PEO, } r = 10.44 \times 10^{-12} \times M^{0.587} \quad \text{Eq. 3.7}$$

A correlation of solute rejections (R) was plotted against the solute diameter of the used solutes ($d_s=2r$), which was obtained using Eq. 3.8.

$$R(d_p) = a + b (\ln d_s) \quad \text{Eq. 3.8}$$

Where R is the solute rejection in %, d_s is the solute diameter in nm, and a and b are the linear coefficients.

The pore size distribution of a membrane can be expressed as the following probability density function [5,156]:

$$\frac{dR(d_p)}{dd_p} = \frac{1}{d_p \ln \sigma_p \sqrt{2\pi}} \exp \left[-\frac{(\ln d_p - \ln \mu_p)^2}{2(\ln \sigma_p)^2} \right] \quad \text{Eq. 3.9}$$

Where $R(d_p)$ is the solute rejection, d_p is the pore diameter, μ_p is the diameter with 50% solute rejection, and σ_p is the geometric standard deviation which is determined from the ratio of diameters with 84.13% and 50% solute rejections.

A linear correlation between the pore diameter of the solutes and their molecular weights was obtained from:

$$\log d_s = a' + b' \log M \quad \text{Eq. 3.10}$$

Where M is the molecular weight of solutes in Dalton, and a' and b' are the linear coefficients. MWCO of membranes is calculated from d_s , which is the diameter with 90% solute rejection.

3.2.5.6 Mechanical properties of hollow fibre membranes

The mechanical properties of the hollow fibre membranes were measured using a texture analyser (TA.XT plus, UK) at ambient temperature. The membranes were pre-measured and air-dried prior to use. The purpose of this test was to determine the tensile stress at break, tensile strain, and Young's modulus strength. They were measured to indicate the mechanical strength of the fibres and the degrees of deformation that could be expected under a given load. Each sample was clamped at both ends with an initial gauge length of 25 mm. A testing speed was kept constant at 50 mm/min. At least five fibre membranes were tested for each membrane code.

3.3 Results and discussion

3.3.1 Cloud point of PSF and PVDF systems

Cloud points were obtained to investigate the precipitation rate of the PSF and PVDF solutions. The precipitation rate of the polymer dope is an essential parameter in the fabrication process because it can affect the pore and mechanical properties of the prepared membranes [26,157-159]. The S0 and S100 polymer dope solutions dissolved in DMAc at the same concentrations were analysed. It was found that the water content required for the precipitation of the S0 and S100 solutions were 2 wt% and 0.7 wt% respectively, indicating that PVDF possesses a slower precipitation rate.

One of the possible factors that affect the rate of precipitation of the polymer dope solutions is the demixing involved during the phase separation. There are three approaches to demixing: liquid-liquid demixing, solid-liquid demixing, and a combination of both, with the subsequent solidification of the polymer [160-164]. In general, once liquid-liquid demixing is initiated, it continues rapidly throughout the phase separation, whereas solid-liquid demixing which is also known as crystallisation, involves nucleation and crystal growth, both of which take place slowly [162]. Moreover, it has been reported that an amorphous polymer, such as PSF, undergoes liquid-liquid demixing [32,56,165,166], whilst a semi-crystalline polymer, such as PVDF, either undergoes solid-liquid demixing or solid-liquid and liquid-liquid demixing [32,34,56,161,166]. Hence, we would expect that S0 possesses a slower precipitation rate than S100. Another factor is the critical surface tension of the polymers; it is a parameter that can be used to differentiate the hydrophobicity and hydrophilicity of a polymer. According to Zisman [167], all polymers that have lower critical surface tension than water (72.8 dynes/cm) are hydrophobic polymers. In this case, PVDF possesses a critical surface tension of 25-28.5 dynes/cm, whereby PSF possesses a critical surface tension of 41 dynes/cm [8]. The lower critical surface tension of PVDF indicates that it is more hydrophobic and hence has a more restrained interaction with water molecules during precipitation. Therefore, a slower precipitation rate was observed for S0. According to previous literature, a slow precipitation rate may enhance the formation of smaller macrovoids and consequently lead to a denser structure with better mechanical strength

[26,159]. Nevertheless, a slower precipitation rate would hinder the development of pores on the membrane surfaces [26]. Therefore, PSF, which has a faster precipitation rate, should be added into PVDF dope solution in a carefully controlled ratio to achieve a membrane with optimum mechanical strength and surface porosity.

3.3.2 Effect of the dope polymer concentrations

The PVDF and PVDF/PSF blended hollow fibre membranes were fabricated using diffusion induced phase separation at a given spinning condition, which is summarized in Table 3.2. The effect of the different weight ratios of PSF in the polymer dopes solutions concerning the viscosity, morphology and mechanical strength of the membrane are also examined.

3.3.2.1 Viscosity of polymer dope solutions

In this study, the viscosity of the polymer dope solutions plays an important role in the precipitation rate of the polymer dope, which subsequently affects the membrane structure. Figure 3.2. shows the viscosity of the polymer dope solution at PVDF/DMAc concentration and a shear rate of 0.75 s^{-1} . The slope of the viscosity shows a rapid change in polymer dope concentration from 10 wt% to 25 wt%. A critical polymer concentration of approximately 18 wt% is obtained by extrapolating the two linear regions at high and low polymer concentrations at their intersection point. Sukitpaneenit and Chung suggested that a polymer at a roughly critical polymer concentration possesses significant chain entanglement, which results in a hollow fibre with an ultra-thin skin layer and minimal defects [9, 32]. In our study, polymer concentration beyond 25 wt% is not practicable, as gelation occurs and complete degassing prior to spinning is impossible under the standard conditions encountered in this study. Therefore, 20 wt% PVDF/DMAc was chosen when preparing the hollow fibres.

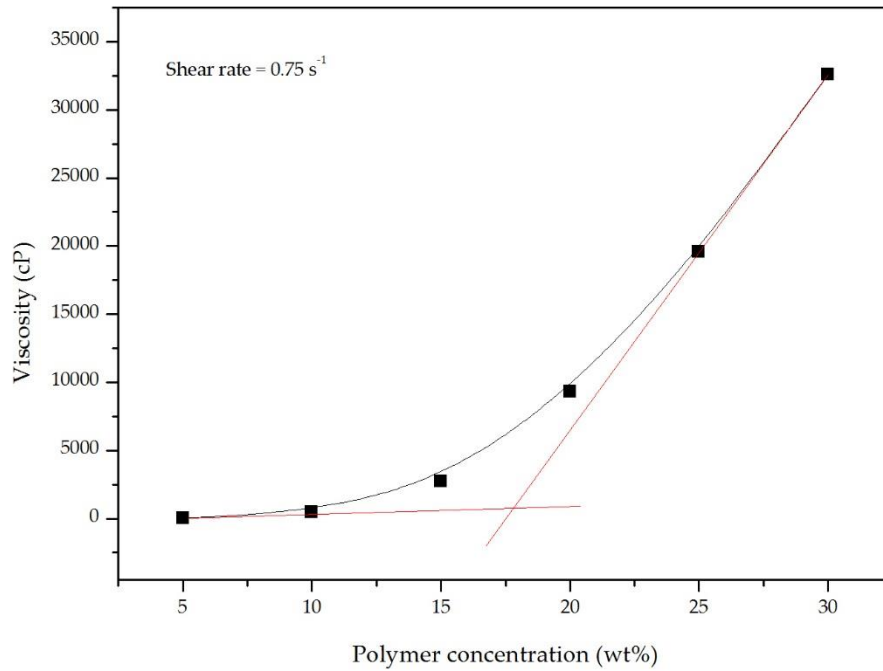


Figure 3.2. The critical concentration of PVDF/DMAc dope solution at 25°C.

The viscosity of S0 is 21 times higher than S100, as shown in Figure 3.3. The sharp distinction in viscosity between S0 and S100 is due to the large difference in the number of repeating units, as indicated by their corresponding molecular weight. The molecular weights of the PVDF and PSF used in this study are 534,000 g/mol and 35,000 g/mol, respectively. The addition of 5, 10, & 15 wt% PSF into the polymer dope caused an increase in its viscosity. The viscosity of polymer dope solution increases from 8,000 cP to as high as 15,000 cP upon addition of PSF. As the PSF concentration in the polymer dope solution increases systematically at 5 wt% intervals, the viscosity increases accordingly, as expected. In addition, S0 shows pure shear thinning behaviour. As the PSF concentration increases, the shape of the graph gradually changes from linear to curved. This is attributed to the increased viscoelastic properties of the polymer dope solution, resulting in a greater degree of chain entanglement, thus develops more resistance to polymer chains stretching and sliding. The greater the polymer dope viscosity, the greater it hinders the penetration of internal and external coagulants via intrusion and diffusion, respectively. As a result, slower precipitation can occur, thus minimising membrane defects.

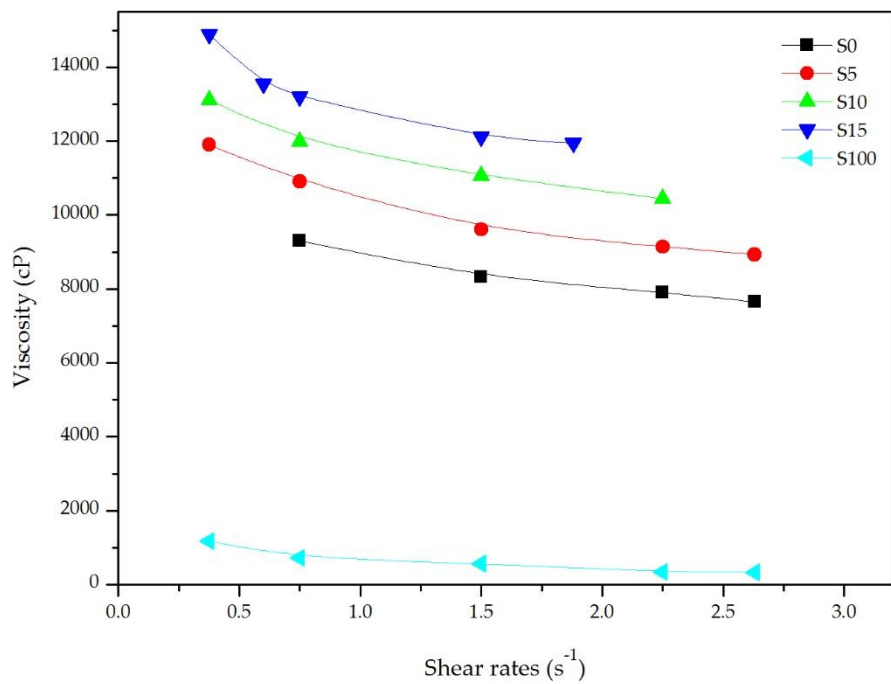
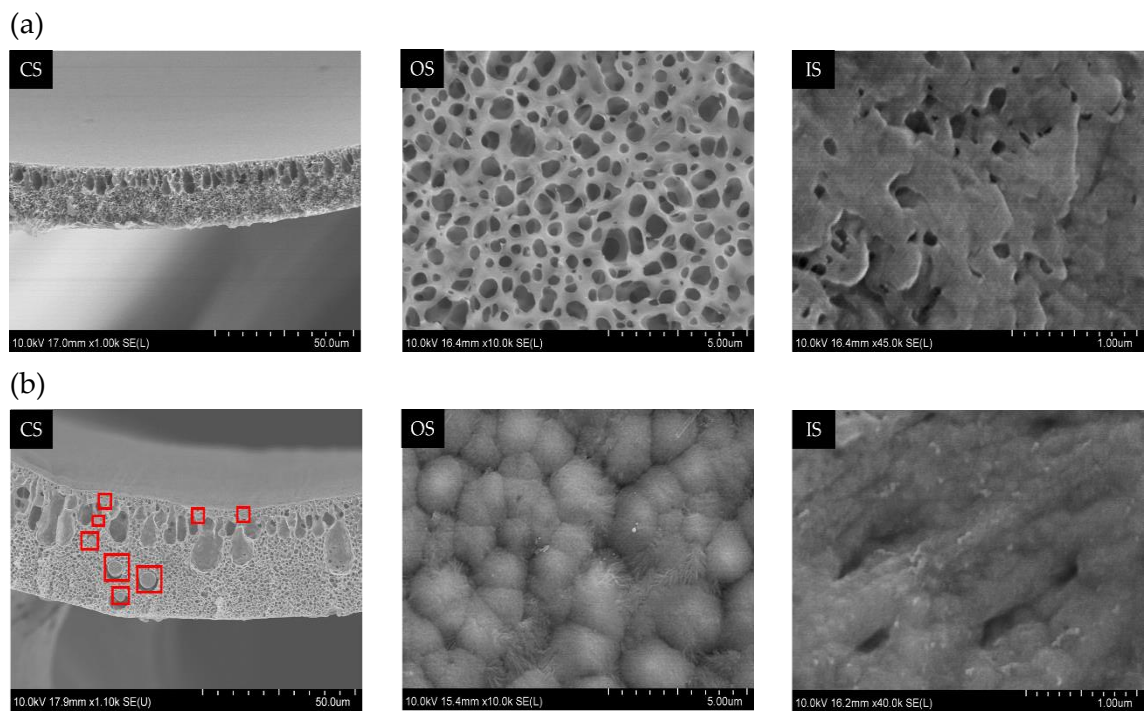


Figure 3.3. Shear rates and viscosities for PVDF/PSF dope solutions with different PSF weight ratios.

3.3.2.2 Morphology study of the hollow fibre membranes

The formation of the membrane using phase separation can be affected by the concentration of the polymer dope solution and the coagulation conditions, which subsequently determine the membrane's morphology [39,55,165,168]. The coagulation condition associated with the solvent–non-solvent interactions will be discussed in Section 3.3.3. Figure 3.4. shows the morphology of the hollow fibre membranes prepared with different PSF weight ratios, with water used as the internal coagulant. All samples achieved asymmetrical membrane structures, consisting of surface skin layers, finger-like macrovoids, and sponge-like structures. The asymmetrical structures seen here were similar to those discussed elsewhere in the literature [55,165,168]. The characteristics of the prepared hollow fibre membranes, including ID/OD, wall thickness, and the average size of macrovoids, are summarised in Table 3.3.



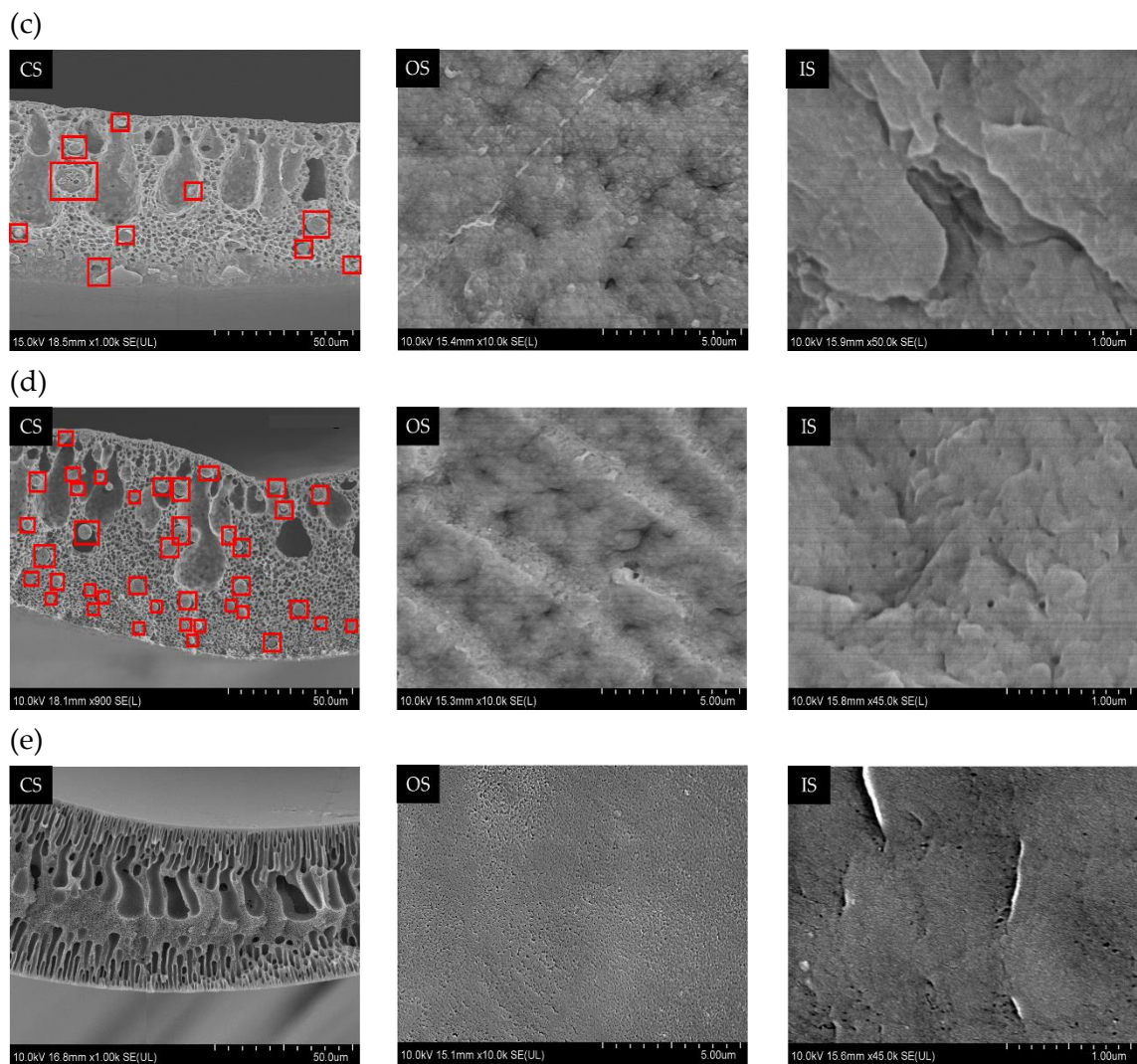


Figure 3.4. FE-SEM micrographs of PVDF membranes with a polymer concentration of 20 wt% spun with different PSF weight ratios and pure PSF membrane with 20 wt% polymer concentration, using 100 wt% water as the internal coagulant. (a) S0; (b) S5; (c) S10; (d) S15; (e) S100. CS, OS, and IS are cross-section, outer surface, and inner surface, respectively.

S100 developed finger-like macrovoids near both the inner and outer surfaces of the membrane, and sponge-like structures were only observed at the centre of the membrane. A set of larger macrovoids extended towards the centre of the membrane, where the macrovoids near the inner surface were larger than those at the outer surface. It is worth noting that these characteristics are typically seen in amorphous membranes. This is due to the low viscosity of S100, which caused the rapid diffusion and penetration of the coagulant. This rapid exchange of solvents and non-solvents allows instantaneous liquid-liquid demixing to occur, immediately forming a thin surface skin. The continuous diffusion of the solvent is then offset by the skin layer, which results in larger

finger-like macrovoids within the membrane. It was found that S0 possesses higher viscosity and a higher proportion of sponge-like structures than S100. Although the solvent–non-solvent exchange is suppressed, the finger-like macrovoids are still present at the cross-section near the inner membrane surface, indicating that S0 also undergoes a liquid-liquid demixing process, but that the process is rather slow.

Table 3.3. Characteristics of PVDF hollow fibre membranes with different PSF weight ratios.

Membrane code	OD/ID (μm)	Wall thickness (μm)	Average macrovoid thickness (μm)
S0	703/663	42.8 \pm 3.0	20.0
S5	762/731	30.7 \pm 0.6	17.2
S10	635/549	79.7 \pm 7.2	54.4
S15	591/533	57.8 \pm 1.1	43.2
S100	647/439	73.5 \pm 1.8	19.55 ^a (both sides)

^a Inner and outer surfaces of the membrane

As mentioned in Section 3.3.1, there are generally three types of demixing processes. In order to determine the demixing process associated with the PVDF membrane, the morphology of the cross-section, and outer and inner surface membranes are examined sequentially. According to a phase diagram of a ternary PVDF/DMAc/water system provided by researchers, a homogenised PVDF/DMAc system is located at the region of gelation [56,169]. This phenomenon indicates that, prior to phase separation, the gelation of the PVDF/DMAc system (which is a crystallisation-induced process) was initiated by the formation of microcrystallites. Generally, these microcrystallites would proceed through solid-liquid demixing to form crystalline particles, also known as spherulites, which appear as interlinked semi-crystalline particle structures. Nevertheless, the formation of spherulites was not seen at the cross-section of the membranes, as shown in Figure 3.4. (a). Aside from spherulites formation, leafy structures surrounding the pores have been reported in literature [164,165]. This morphological feature of solid-liquid demixing was revealed in S0, and shown to be absent in S100, as presented in

Figure 3.5. These observations suggest that the delayed liquid-liquid demixing of S0 has allowed solid-liquid demixing to occur during phase separation.

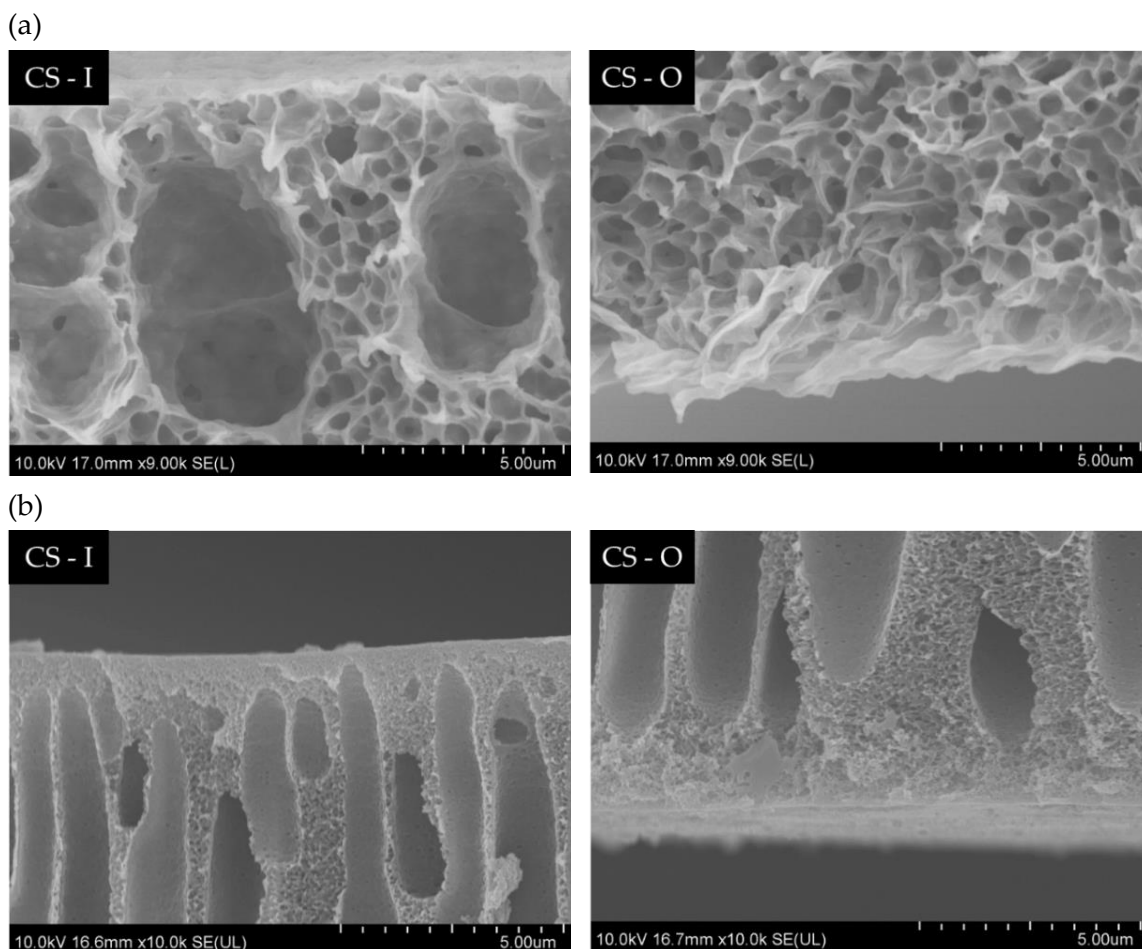


Figure 3.5. Cross-section morphology of hollow fibres prepared using water as an internal coagulant. (a) S0; (b) S100. CS-I and CS-O represent cross-section near the inner surface and cross-section near the outer surface, respectively.

Another typical morphology of a solid-liquid demixing is developed at the outer surface of the membranes, which has also been reported in the literature [63,70,170]. Globular structures with porous regions between the globes are observed most notably at the outer surfaces and, more subtly, at the inner surfaces of the S5 to S15 membranes. The size of the globes at the outer surface decreased, as shown in Figure 3.4. (b) to (d). The possible reason for these observations is the viscosity of the polymer dope solution. The higher the viscosity, the higher the restrictions to mobility within the polymer molecules, and hence the smaller the globular structure.

Because the morphological features of solid-liquid demixing are not witnessed, we can conclude that the phase separation of the resulted membrane structure is governed by liquid-liquid demixing instead of solid-liquid demixing. These observations demonstrate that, the higher the viscosity of the polymer dope solution, the greater the hindrances to solvent and non-solvent exchange during the phase separation. This finding is reported elsewhere in extant literature [32,55,59,74].

As shown in Figure 3.4. (b) to (d), upon the addition of PSF, spherical-shaped globules (boxed in red) are observed. These spherical-shaped globules are referred to as “big spherical crystalline particles” in the proceeding discussion. These “big spherical crystalline particles” are found across the cross-section of the membrane, and presumably result from the macroscopic phase separation of PSF from PVDF bulk. The number of “big spherical crystalline particles” increases as the PSF weight ratio increases. To clarify the component of the “big spherical crystalline particles”, an FE-SEM examination, coupled with EDX analysis, was performed. Additionally, PVDF is a semi-crystalline polymer that consists of two phases. Hence, in the following discussion, PVDF is subcategorised as PVDF-crystalline (PVDF-c) and PVDF-amorphous (PVDF-a).

Figure 3.6. presents the FE-SEM coupled with the EDX analysis of the cross-section for the S15 membrane. The EDX spectrum of the “big spherical crystalline particles” shows that the sulphur element is comparable with the fluorine element. At the membrane matrix, the spectrum shows that the fluorine element is three times higher than the sulphur element. From the element mapping, the fluorine element is dispersed throughout the membrane matrix, whereas, where the “big spherical crystalline particle” is positioned, the fluorine element is insignificant. The sulphur element is exhibited throughout the membrane, but mainly concentrated at the surface of the “big spherical crystalline particle”. This demonstrates that the proportion of the elements throughout the membrane is unequal. The amorphous region of PVDF (PVDF-a) may have separated from the crystalline region (PVDF-c) during phase separation. PVDF-c and PSF may have coalesced to form “big spherical crystalline particles”. The sulphur element was detected strongly in the sulphur mapping, which suggests that PVDF-c may have been surrounded by PSF, as presented in Figure 3.6. (d). A proposed schematic

diagram of the “big spherical crystalline particle” structure in the PVDF/PSF membrane, which includes PVDF-c, PVDF-a and PSF, is shown in Figure 3.7.

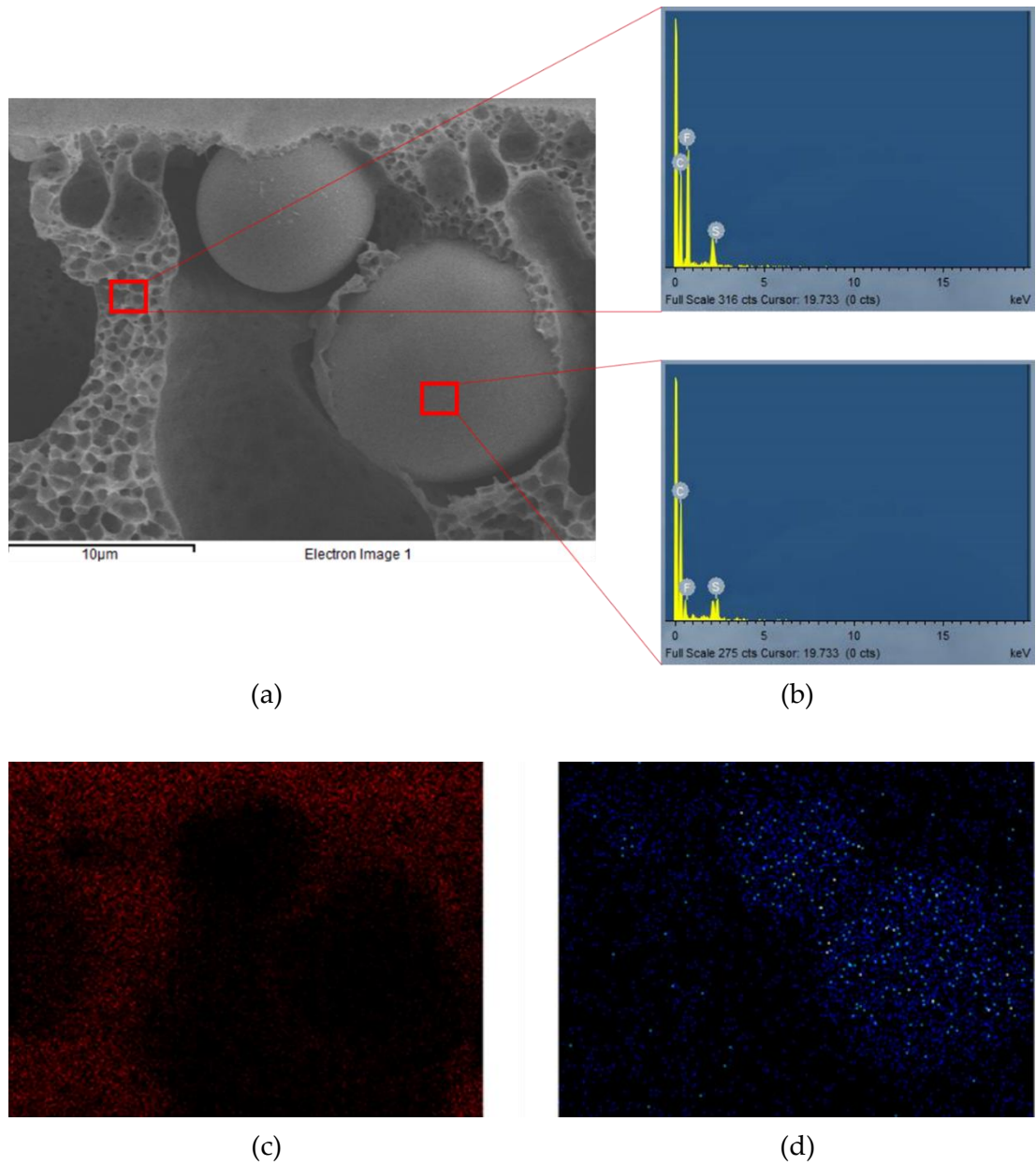


Figure 3.6. FE-SEM coupled with EDX analysis of cross-section of hollow fibre membrane (S15): (a) FE-SEM micrograph, 10.0 kV 17.9 mm x 3.00 k SE (L); (b) EDX spectrum of membrane matrix and “big spherical crystalline particle” of S15; (c) fluorine mapping from the micrograph (a); (d) sulphur mapping from the micrograph (a).

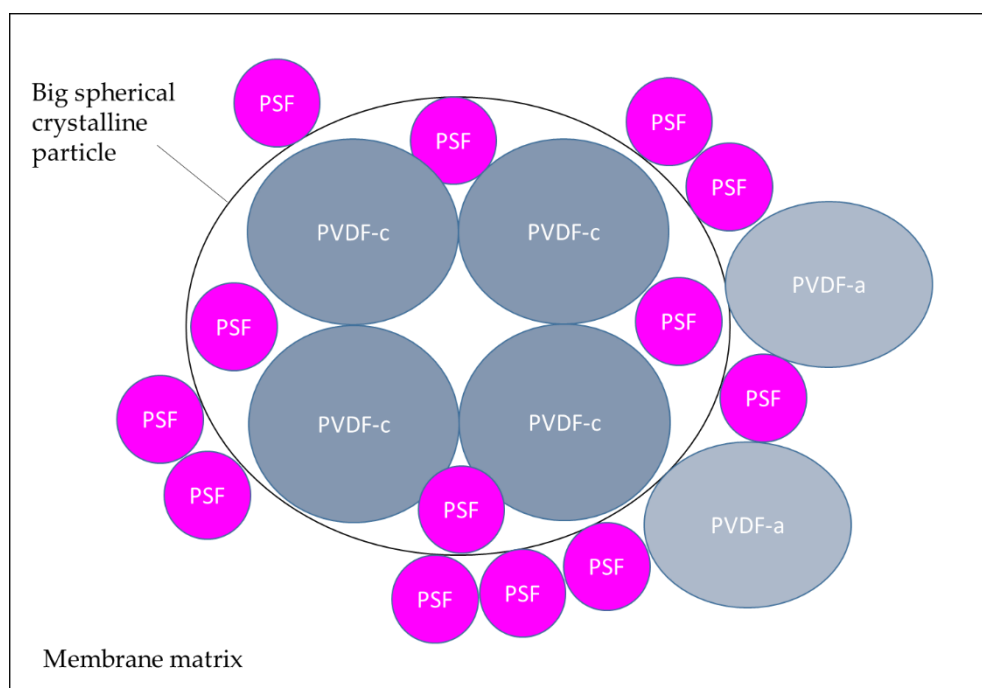


Figure 3.7. Schematic diagram of “big spherical crystalline particle” structure for the PVDF/PSF hollow fibre membrane (S15).

3.3.2.3 Thermal properties and crystallinity of the hollow fibre membrane

Figure 3.8. (a) shows the heating curves obtained from the DSC analysis. S0 and the polymer blends possess a main melting peak of approximately 158 °C and a weak melting peak of approximately 82 °C. These main and weak peaks are associated with the primary and secondary crystallisation of the PVDF chains, respectively [25,171-174]. The primary crystallisation occurs during membrane fabrication, whereas the secondary crystallisation is related to the realignment of the crystal structure during the melting-recrystallisation-remelting process upon DSC heating [171-173,175]. A high temperature melting peak is expected for S100, which is observed at 184 °C. This is due to benzene rings within the backbone of the PSF, which increases the steric hindrance, and consequently the rigidity of the PSF structure.

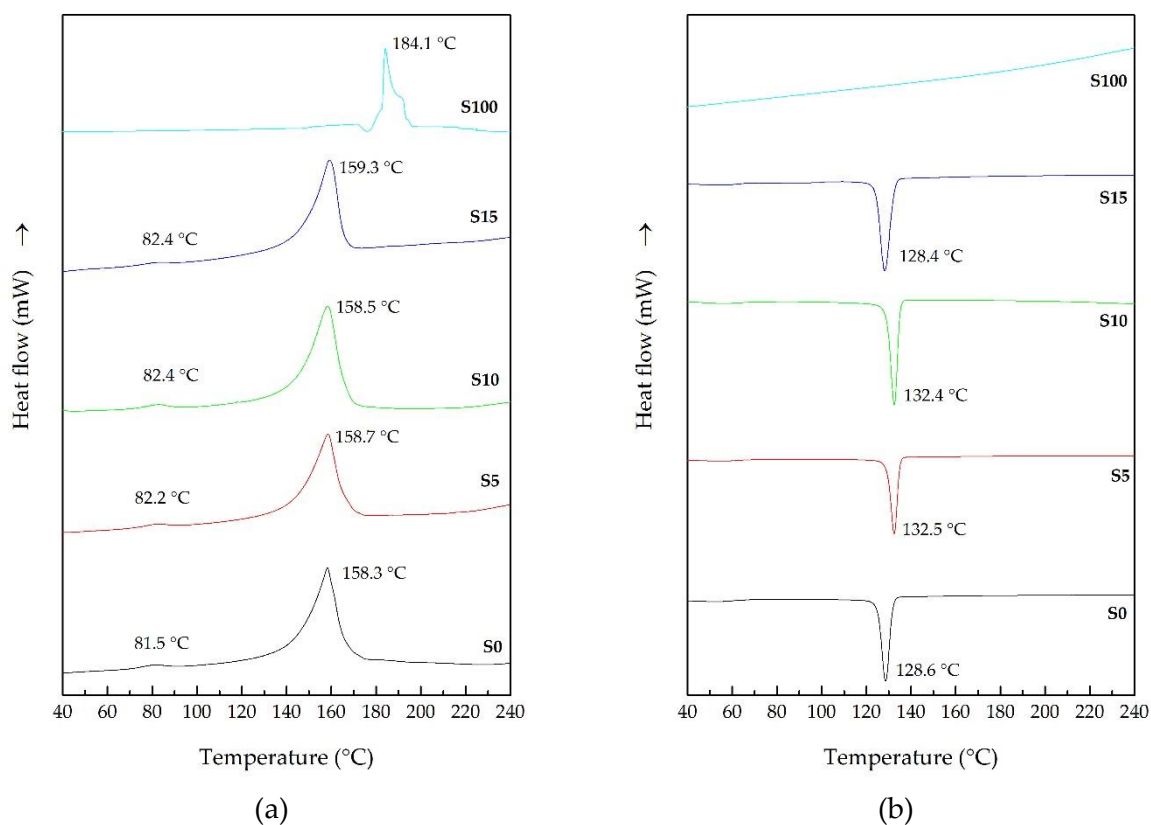


Figure 3.8. DSC curves of hollow fibres spun with different PSF weight ratio annealed at 250 °C for 10 min. (a) Heating curves; (b) cooling curves.

As mentioned in Section 3.3.1, crystallisation involves nucleation and crystal growth. Nucleation can be subcategorised into homogeneous and heterogeneous nucleation. Homogeneous nucleated crystallisation generally occurs at 60-100 °C below the temperature of heterogeneous nucleated crystallisation. Zhong, *et al.* [176] reported concurrent homogeneous and heterogeneous nucleation of PVDF/PSF blends, evident by two distinctive crystallisation temperature ranges. Homogeneous nucleation can only occur in a polymer when a low weight ratio of semi-crystalline polymer is finely dispersed in an immiscible matrix forming an isolated region. This phenomenon is known as fractionated or confined crystallisation [176-178]. The crystallisation peaks observed in Figure 3.8. (b) for S0 to S15 can hence be ascribed to heterogeneous nucleation, as homogeneous nucleation is unlikely due to a high PVDF weight ratio in the present study. PSF is an amorphous polymer; hence, no crystallisation peak was detected for S100, as expected.

As shown in Figure 3.8. (b), the crystallisation temperature for S0 and S5 increases from approximately 128 to 132 °C, and then remains constant for S10. Crystallisation of PVDF polymer involves nucleation kinetics, which is associated with the rate of the formation of nuclei; and crystal growth kinetics, which is associated with the rate of nuclei grow into a macroscopic crystal. Aside from enhancing the mechanical strength of the PVDF hollow fibre, PSF also functions as a nucleating agent in the polymer blends. Upon addition of PSF from S0 to S5, the nucleation kinetics and hence the heterogeneous nucleus density and the crystallisation temperature increased. This effect aligns with findings from elsewhere in the literature [176,179,180]. Nevertheless, the crystallisation temperature becomes stagnant at S10, indicating that PSF has reached its maximum nucleating effect at S5. As shown in Figure 3.3, viscosity increases with the addition of PSF. This results in restricted mobility of polymer segments [181], and consequently suppressed the kinetics of crystal growth. As a result, the crystallinity of the polymer blends decreases steadily from S0 to S10, as evidenced in Table 3.4.

Table 3.4. Enthalpy and degree of crystallinity of the hollow fibres spun with different PSF weight ratio.

Membrane code	ΔH (J/g)	X_c (%)
S0	42.0	40.2
S5	39.6	36.1
S10	37.7	32.8
S15	36.7	30.5

It is interesting to observe that the crystallisation temperature reduces for S15. The outcome suggests that the crystallisation process is governed by nucleation kinetics, though the crystal growth kinetics decreased. This is attributed to the formation of macroscopic phase separation, as proposed previously in Section 3.3.2.2, where majority of the PSF separated from the bulk of the PVDF, resulting in slow nucleation kinetics. Due to the phase separation, the mobility hindrance of the PSF on the kinetics of crystal growth diminished, regardless of the continued increase in viscosity of the polymer blend. As a result, crystallinity decreases less prominently for S15, as shown in Table 3.4.

3.3.2.4 Mechanical properties of the hollow fibre membranes

In view of increasing the reusability in dialysis, it is crucial for the hollow fibre membrane to possess excellent mechanical strength. Moreover, an ideal wall thickness for the dialysis membrane is important to facilitate toxin clearance. Generally, the wall thickness of the synthetic dialysis membranes available on the market is between 30-45 μm [19,182], as a higher wall thickness is attributed to lower diffusive permeability. Therefore, it is important to choose an ideal membrane wall thickness with good mechanical strength.

The effect of PSF weight ratios on the mechanical properties of the membranes is listed in Table 3.5. S0 exhibits ductile behaviour, as proven by the relatively small tensile strength and large tensile strain, which agree with findings in the existing literature [32,34]. S0 and S100 membranes possess comparable tensile strength, whereby the tensile strain of S0 is seven times higher than S100. On the contrary, Young's modulus of S0 is seven times lower than S100, indicating that S100 is stiffer and has greater yield strength to prevent deformation.

Table 3.5. Mechanical properties of PVDF/PSF membranes fabricated from different PSF weight ratios.

Membrane code	Tensile strength (MPa)	Tensile strain (%)	Young's modulus (MPa)
S0	10.53 \pm 0.67	361.18 \pm 2.15	2.49 \pm 0.83
S5	10.89 \pm 0.05	239.44 \pm 0.76	6.20 \pm 0.88
S10	17.83 \pm 0.73	81.44 \pm 4.92	31.78 \pm 3.34
S15	24.61 \pm 3.10	64.29 \pm 0.43	30.16 \pm 1.99
S100	9.17 \pm 0.10	49.83 \pm 1.18	18.42 \pm 0.60

Upon increasing PSF weight ratios, the tensile strength and Young's modulus of the membranes increases. In contrast, the tensile strain decreases dramatically, suggesting that the deformation resistance of S0 to S15 membranes increases, whereas the ductility of the membranes decreases. This outcome is expected; as mentioned in Section 2.1.2.,

PSF is a high modulus material and the stiffness of PSF is attributed to the amorphous structure and the rigid backbone of the polymer. This is because the molecules of the amorphous structure are not organised in a definite lattice pattern. As mentioned in Section 3.3.2.3, upon the addition of PSF that functions as a nucleating agent, resulting in closer packing of the molecules in the polymer blends. The decreased intermolecular distances increase the secondary forces between the chains and thus increases the mechanical properties such as tensile strength and stiffness [183].

In addition to the mechanical outcomes, they may be related to a decrease in crystallinity. Since the ductility of a polymer depends on the formation of crystal structures [184], when it is interrupted, this leads to an increase in the amorphous phase, as evidenced in Table 3.4. In this case, it is worth to note that the mechanical strength of hollow fibres was not entirely governed by the macrovoid, but the inclusion of PSF and the wall thickness of the membrane. Consequently, the addition of PSF in the PVDF dope solution results in better mechanical strength, as proposed previously in Section 3.3.1.

3.3.2.5 Pure water permeability and solute rejection performance of the hollow fibre membranes

Besides acquiring an ideal membrane wall thickness and better mechanical strength, pore size and pore density/porosity are crucial membrane characteristics that affect the membrane performance [13,185]. Moreover, the pore size of the membrane will determine the size range of the microgel particles required for surface hydrophilization.

The effect of polymer dope concentration on the PWP, solute rejection performance and overall porosity of the hollow fibre membranes are summarised in Table 3.6. The mean pore size and pore size distribution of the hollow fibre membranes were characterised using two complementary techniques, MIP and ST. Based on the solute rejection data shown in Figure 3.9., the membrane characteristics (in terms of MWCO and solute diameter) were calculated using the Stokes-Einstein equation. In comparison to S0, S100 has a lower mean pore size and porosity, but high PWP. This is attributed to its finger-like macrovoids (at the cross-section), which promote water transportation as evidenced in Figure 3.4. (e). Similar observations were reported by Yang, *et al.* [5].

Although the MIP technique presents comparable experimental outcomes, the mean pore size is relatively large compared to the ST technique. One possible reason is the broad distribution of pore sizes as shown in Figure 3.9. (b). Upon increasing polymer dope concentration, the mean pore size and MWCO and PWP gradually decrease. However, the porosity for S0 and S5 increases from 75.7 to 88.5% and then drops significantly for S10 and S15. The similarity of porosity between S10 and S15 can be ascribed to the formation of macroscopic phase separation as discussed in Section 3.3.2.2, which was likewise exhibited in the pore size distribution, as shown in Figure 3.9. (b).

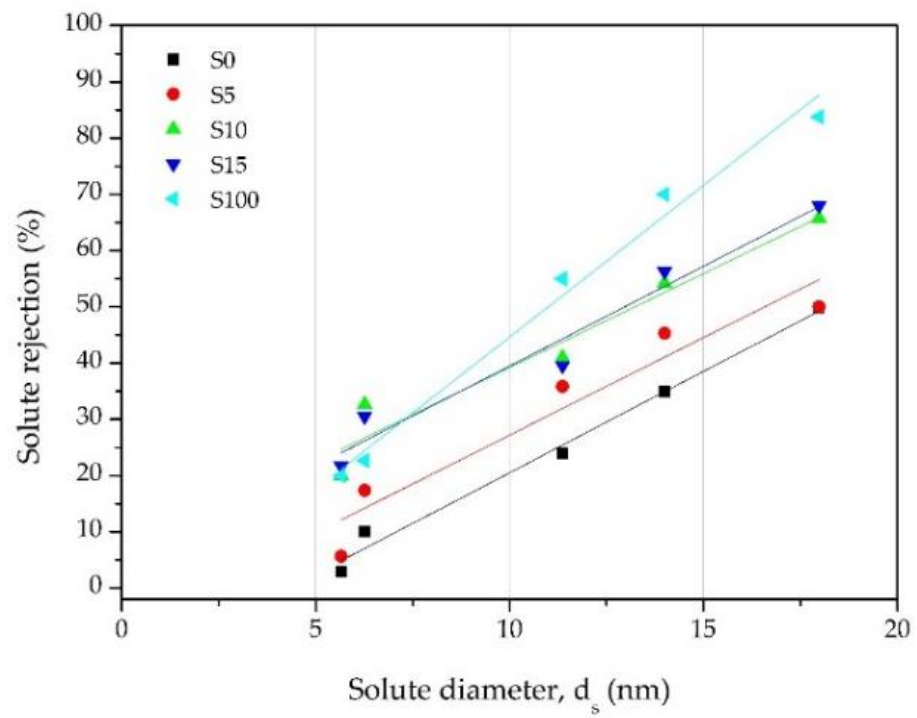
In summary, the PWP and separation performance of a membrane are important assessments to determine the fundamental performance of the membranes. The changes in the membrane characteristics, including membrane wall thickness, pore size, and porosity, are interrelated to each other, which can significantly affect the membrane permeability.

Table 3.6. Mean pore size, MWCO, and pure water permeability of membranes with different polymer dope concentrations.

Membrane Code	Mean pore size, μ_p (nm)		MWCO (Da)	PWP (L/m ² h bar)	Porosity (%)
	MIP	ST			
S0	259.17	6.33	1196 000	225.57	75.7
S5	211.78	5.30	831 000	204.84	88.5
S10	196.73	4.55	522 000	189.79	69.2
S15	195.19	3.97	439 000	152.00	70.1
S100	137.24	0.67	131 000	379.59	72.5

Note: MIP represents mercury intrusion porosimetry; ST represents solute transport. MWCO refers to molecular weight cut-off, the molecular weight of the solute, 90% of which can be rejected by a membrane.

(a)



(b)

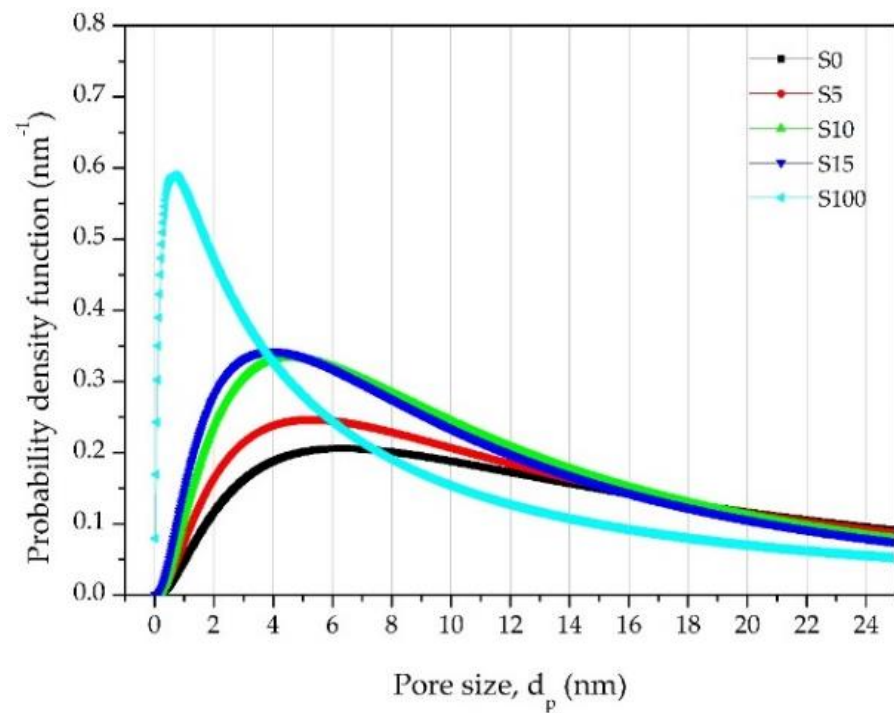


Figure 3.9. (a) Solute rejection curves and (b) probability density function curves of PVDF/PSF hollow fibre membranes prepared with different PSF weight ratios.

3.3.3 Effect of the internal coagulant concentrations

The effect of internal coagulants was considered to improve and regulate the membrane structure, such as pore formation and the thickness of the membrane wall. This is because these membrane characteristics directly affect the mechanical properties and water permeability [46,185]. Therefore, the internal coagulant, which was water, was replaced with a DMAc/water mixture. The different DMAc concentrations were used to examine the membrane structure of the polymer blends prepared from 20 wt% PVDF with different PSF weight ratios.

3.3.3.1 Morphology study of the hollow fibre membranes

Figure 3.10. shows the cross-section morphology of the hollow fibre membrane. The changes to the membrane morphology include the: (1) diameter of the hollow fibre; (2) size of the macrovoids; and (3) wall thickness. Upon increasing the DMAc concentration of the internal coagulant, the ID/OD of the membranes increases and the thickness of the wall membranes becomes thinner. The size of the macrovoids gradually reduced, and some diminished. Internal coagulant with higher DMAc concentrations, such as 30 wt% and 40 wt%, were also tested. However, the ID/OD of the hollow fibre membranes was too large and had very thin walls.

Figure 3.11. shows the effect of the addition of DMAc in the internal coagulant on the outer membrane surface. Upon increasing the DMAc concentration, the pore size decreased. The modification of the membrane surface can be attributed to the delayed demixing process that will be discussed later. It is interesting to discover that the addition of DMAc in the internal coagulant did not significantly affect the overall inner membrane surface, as shown in Figure 3.12. Further membrane examination through AFM examination was performed and will be discussed in Section 3.3.3.2. Table 3.7. summarises the dimensions of the membranes, including ID/OD, wall thickness, and the average size of the macrovoids.

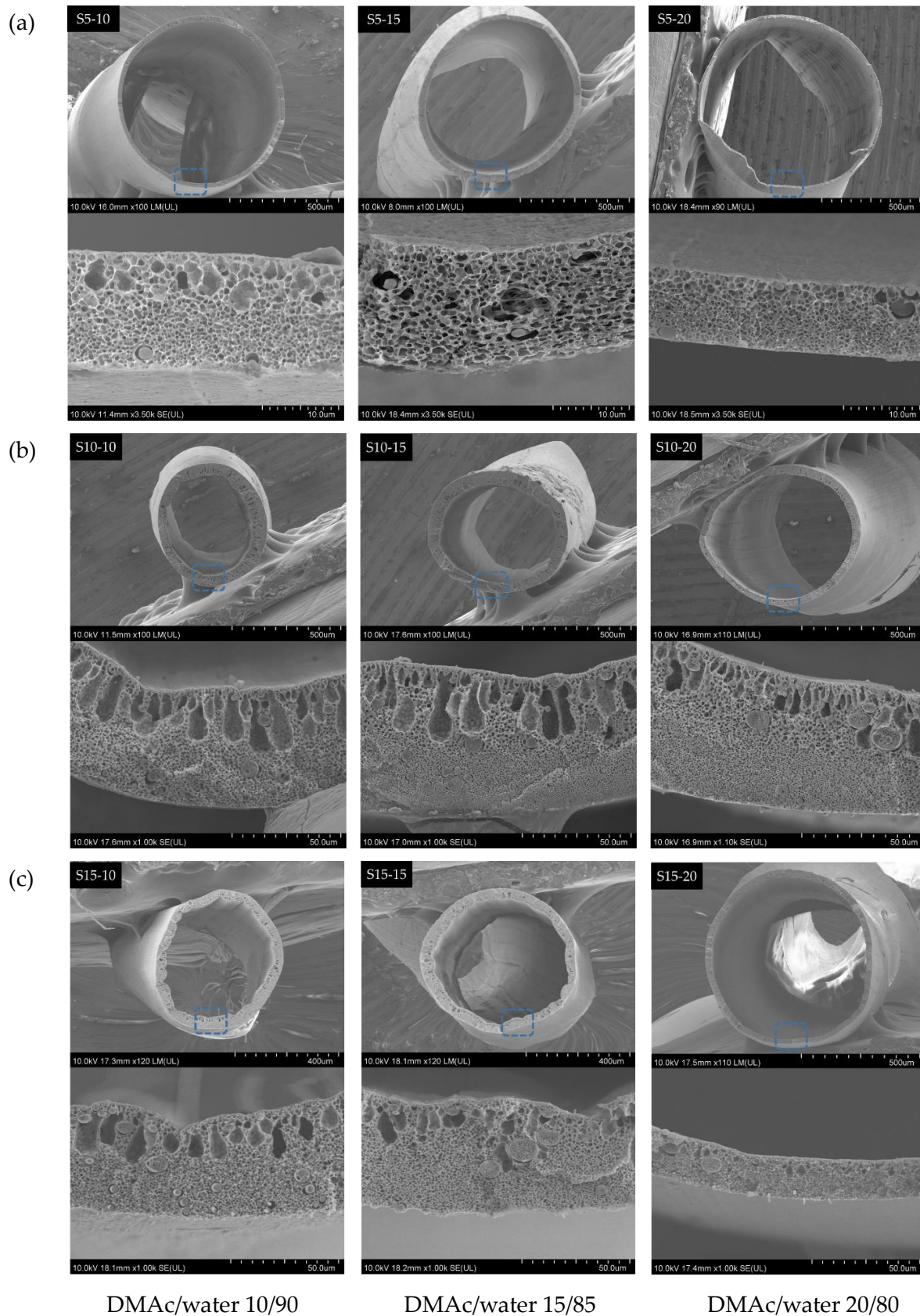


Figure 3.10. FE-SEM micrographs for the cross-sections of PVDF membranes with polymer concentration of 20 wt% spun with different PSF weight ratios and DMAC/water mixture of different DMAC concentrations as internal coagulant. (a) S5; (b) S10; (c) S15.

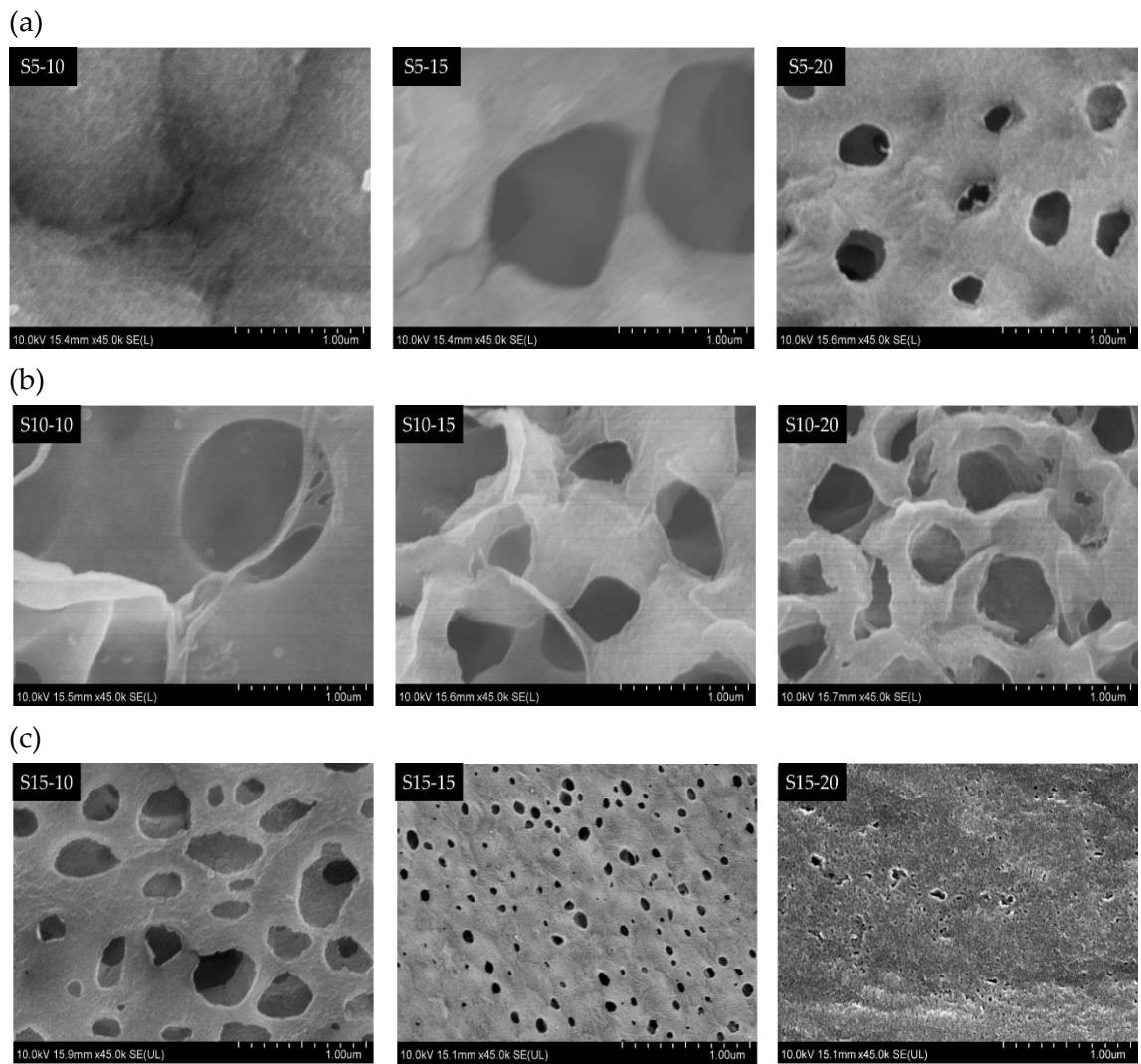


Figure 3.11. FE-SEM micrographs for the outer surfaces of PVDF membranes with polymer concentration of 20 wt% spun with different PSF weight ratios and DMAc/water mixture of different DMAc concentrations as internal coagulant. (a) S5; (b) S10; (c) S15.

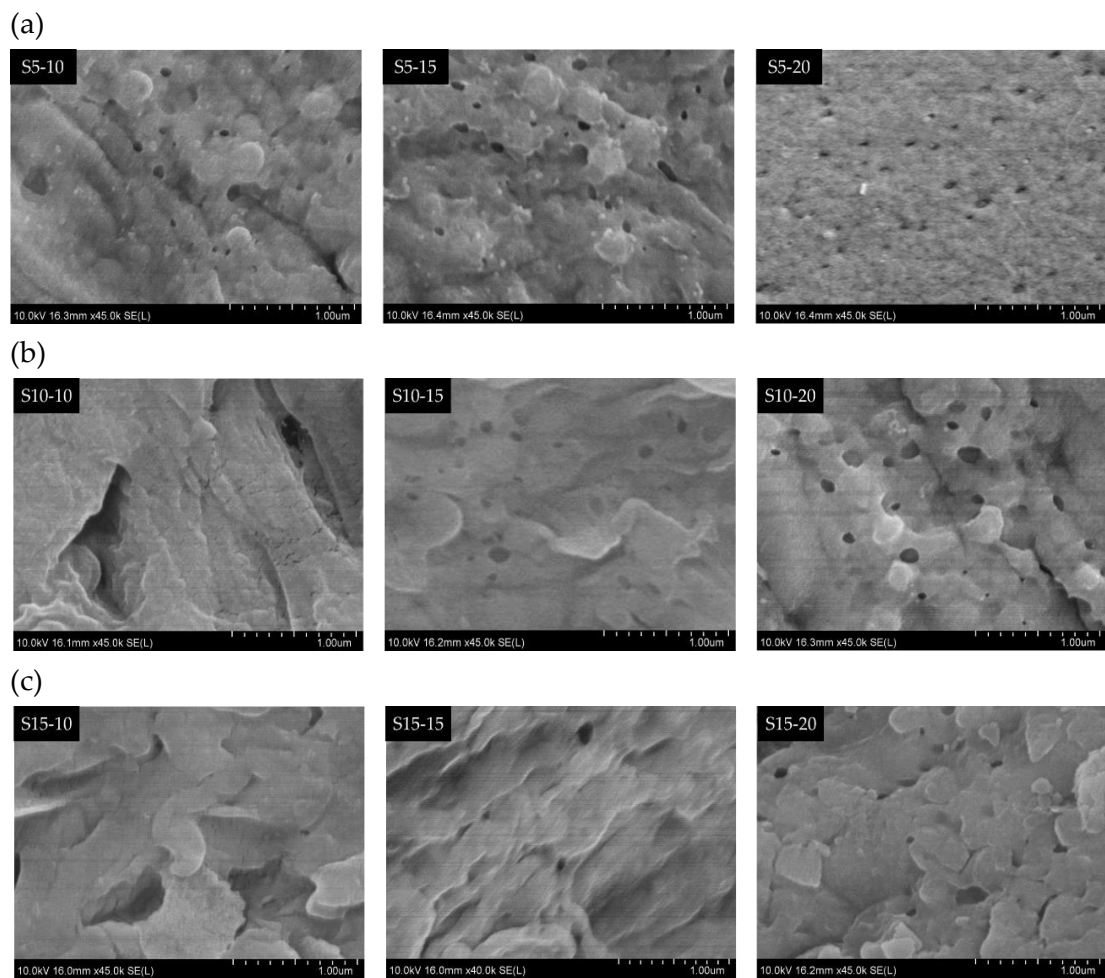


Figure 3.12. FE-SEM micrographs for the inner surfaces of PVDF membranes with polymer concentration of 20 wt% spun with different PSF weight ratios and DMAC/water mixture of different DMAC concentrations as internal coagulant. (a) S5; (b) S10; (c) S15.

Table 3.7. Characteristics of PVDF/PSF hollow fibre membranes prepared from DMAc/water mixture of different DMAc concentrations as internal coagulant.

Membrane code	OD/ID (μm)	Wall thickness (μm)	Average macrovoid thickness (μm)
S5-10	678/652	25.7 \pm 1.5	6.4
S5-15	795/775	19.9 \pm 1.1	3.6
S5-20	922/910	11.8 \pm 0.2	Absent
S10-10	541/452	89.1 \pm 6.8	28.0
S10-15	754/680	28.5 \pm 2.3	25.6
S10-20	821/766	21.3 \pm 0.3	12.7
S15-10	615/559	53.1 \pm 4.5	16.0
S15-15	735/704	31.6 \pm 0.9	7.2
S15-20	753/732	21.8 \pm 0.6	Absent

It has been reported that membrane formation is correlated with the demixing process, which is regulated by the thermodynamics (phase behaviours) and kinetics (mass transfer) of the phase separation [33,41,55,56,161]. In this case, the inclusion of DMAc disrupts the polymer-solvent and solvent-non-solvent interactions, which leads to a complex precipitation phenomenon during phase separation. The order of the demixing process can be deduced based on solubility parameters, as tabulated in Table 3.8. Generally, the greater the difference in the solubility parameter between polymer blends and solvent and non-solvents, the faster the precipitation rate during phase separation [32,161]. The difference in the solubility parameters suggests that the DMAc/water mixtures follow the sequence: 0/100>10/90>15/85>20/80, which corresponds to the order of the precipitation rate of the demixing process.

Table 3.8. Solubility parameters of polymers, solvent, and non-solvents for hollow fibre fabrication [186].

	Solubility parameter (MPa ^{1/2})			
	δ_d	δ_p	δ_h	δ_t
PVDF	17.2	12.5	9.2	23.2
PSF	16.0	6.0	6.6	21.2
DMAc	16.8	11.5	10.2	22.7
Water	15.5	16.0	42.3	47.8
DMAc/water (10/90)				45.3 ^a
DMAc/water (15/85)				44.0 ^a
DMAc/water (20/80)				42.8 ^a

δ_d , dispersive parameter; δ_p , polar parameter; δ_h , hydrogen bonding parameter, δ_t , total solubility parameter.

^a Solubility parameters for mixed solvents were calculated based on mole fraction.

These findings imply that, when water was used as the internal coagulant, the mutual diffusional mass transfer of solvents and non-solvents is undertaken rapidly and surpassed crystallisation. As a result, instantaneous liquid-liquid demixing takes place and subsequently produces an asymmetric membrane with finger-like macrovoids, as illustrated in Figure 3.4. On the contrary, when a DMAc/water mixture was used, the mutual diffusional mass transfer reduces, and the precipitation rate of the membranes is kinetically slowed down, leading to a delay in the overall demixing process. As a result, the appearance of finger-like macrovoids reduced. Although the delayed demixing process gradually diminished the formation of finger-like macrovoids, the deceleration of the precipitation rate caused the hollow fibre to stretch and elongate at the air-gap during membrane fabrication, resulting in a reduction of the wall thickness. Moreover, because of the decrease of the mass transfer, the internal coagulant did not escape effectively to the external coagulation bath, and subsequently expanded the lumen, causing the diameter of the hollow fibre to increase.

In summary, the changes in membrane structure result from the use of DMAc mixture as an internal coagulant, which causes a delay in the demixing process of the polymer blends. From the perspective of thermodynamics and kinetics, it can be deduced that water induced rapid precipitation, while DMAc, a weak solvent, was able to effectively delay the demixing process. Consequently, it takes longer for the polymer blends to stretch and elongate, which results in larger OD/ID, thinner walls, and a reduction in finger-like macrovoids.

3.3.3.2 Surface topography of hollow fibre membranes

Surface topography is an important surface property and it affects the macroscopic behaviour of a material. It is defined by surface orientation and roughness [187]. Surface roughness is a widely used parameter to investigate the effects of the adsorption and wettability of a material [188,189]. In this case, the adsorption/embedment of microgel particles will be correlated with the roughness of the membrane. The modification of the surface property brought about by embedding the microgel particles will be discussed in Chapter 5.

The surface topography of the inner and outer surfaces of S5, S10, and S15 fabricated with different DMAc concentrations are shown in Figure 3.13. The roughness parameters for each membrane sample are summarised in Table 3.9. In terms of statistical approaches, R_q is an important parameter to describe the surface roughness and it is more sensitive than R_a [190]. In comparison to the polymer dope concentration, the surface roughness of the membrane is strongly affected by the internal coagulant concentration. Upon increasing the DMAc concentration from 0 to 20 v/v%, R_q for both the inner and outer membrane surfaces increases, indicating that the surfaces became rougher. Moreover, it can be seen that the pores at the outer surface are larger than the pores at the inner surface, which corresponds to the roughness of the outer surface being higher than that of the inner surface.

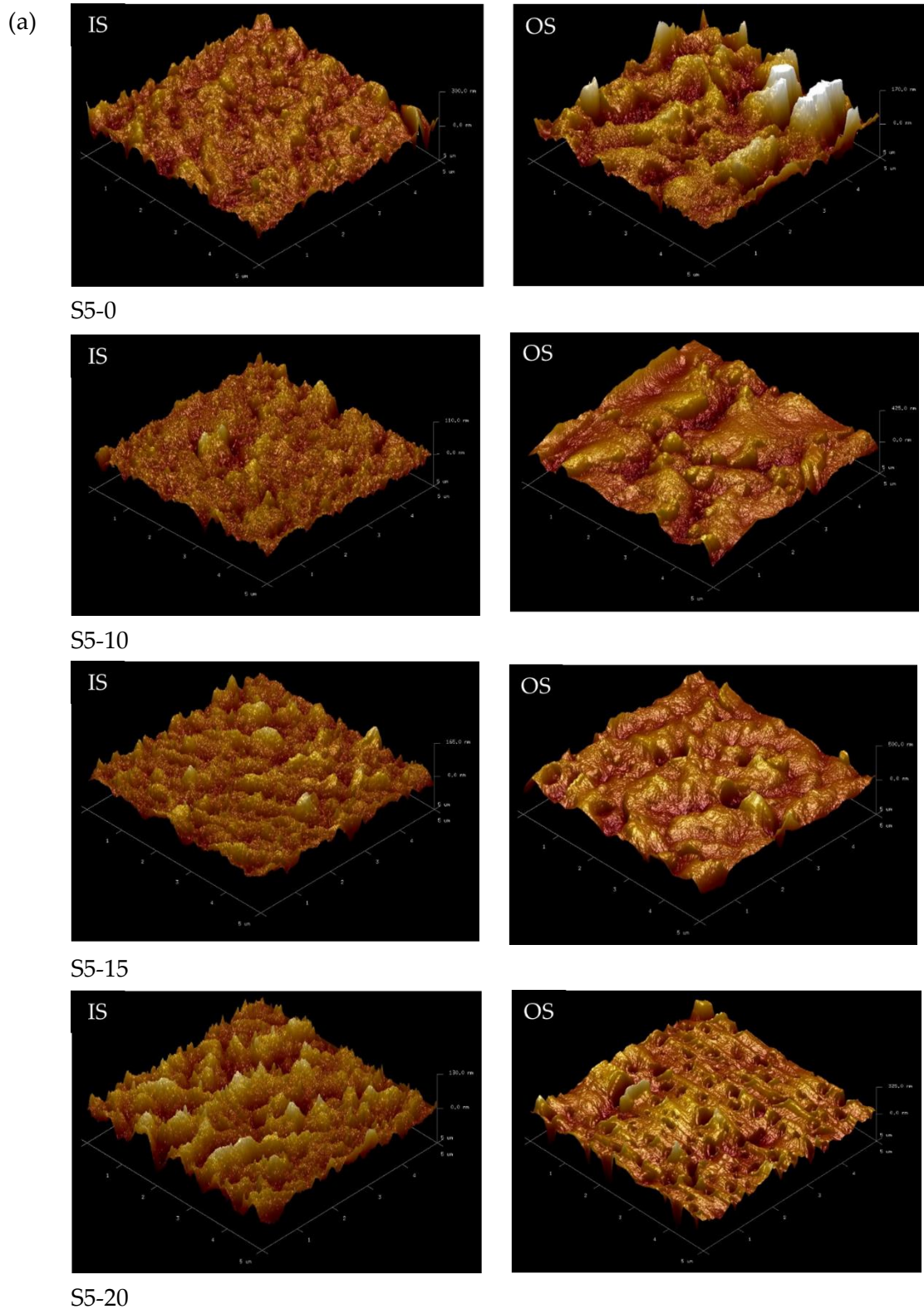
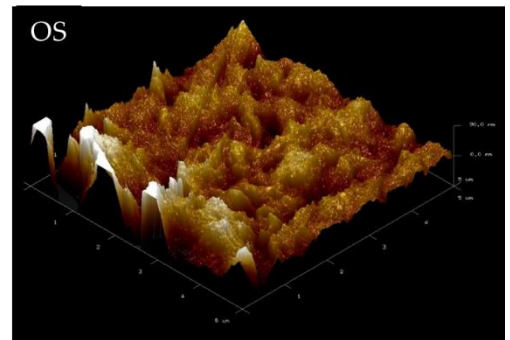
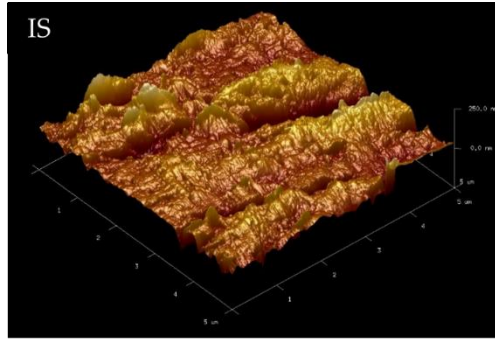
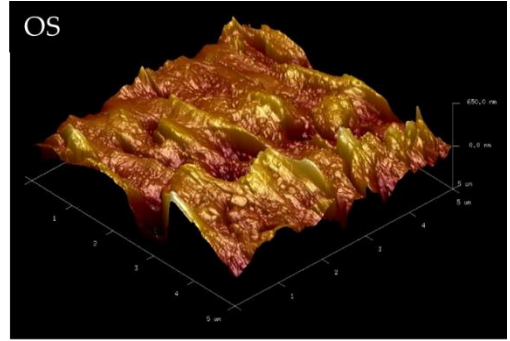
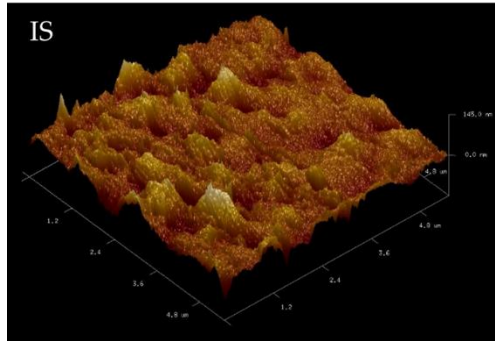


Figure 3.13. AFM micrographs and 3-D images of PVDF membrane with polymer concentration of 20 wt% spun with different PSF weight ratio and DMAc/water mixture of different DMAc concentrations as internal coagulant. (a) S0; (b) S5; (c) S10; (d) S15. IS and OS are inner surface and outer surface, respectively.

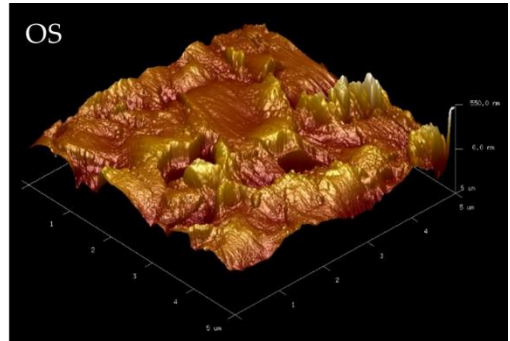
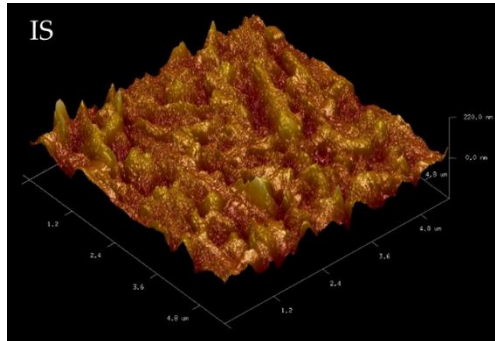
(b)



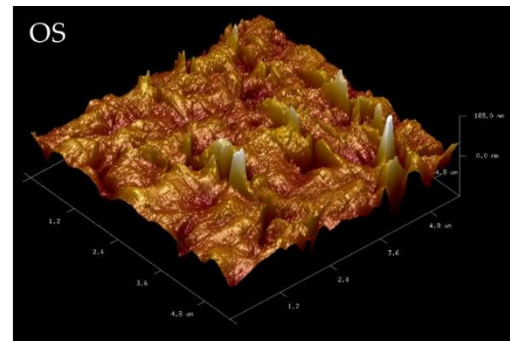
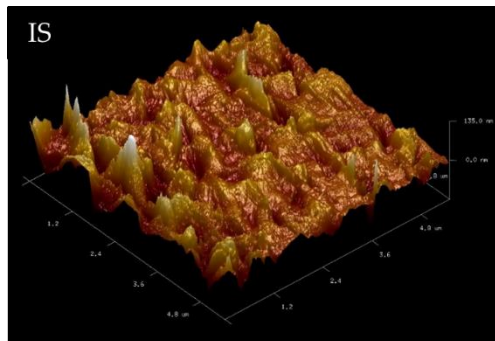
S10-0



S10-10



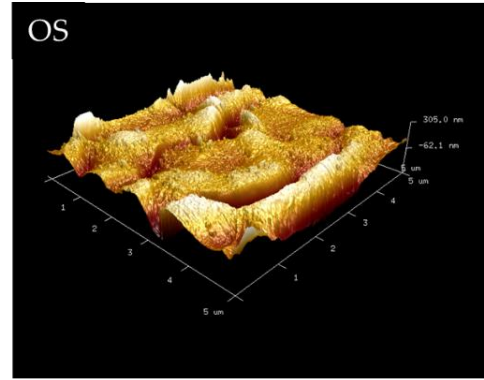
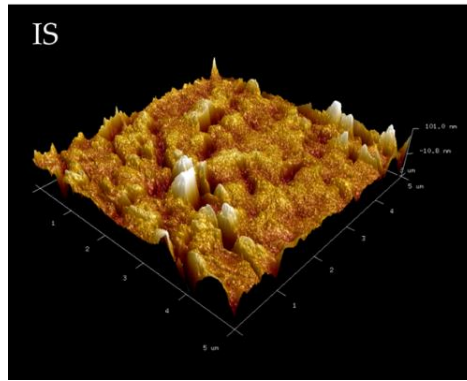
S10-15



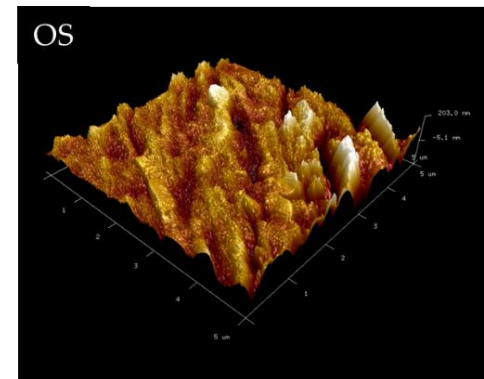
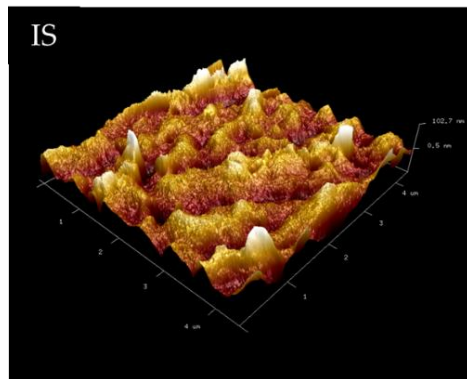
S10-20

Figure 3.13. (Continued);

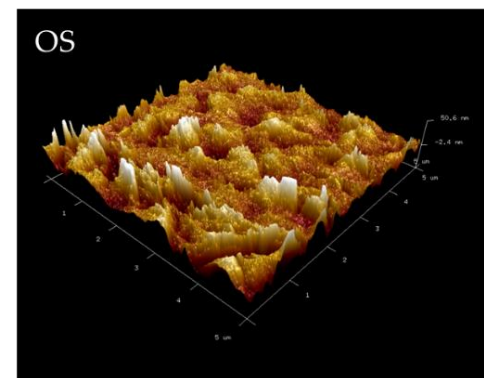
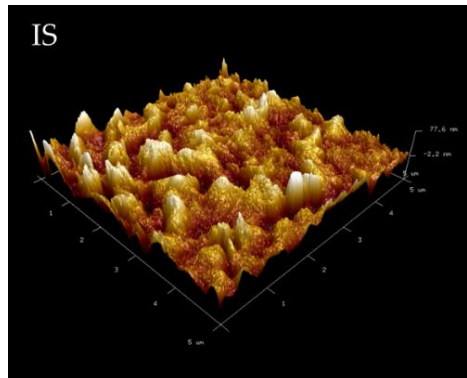
(c)



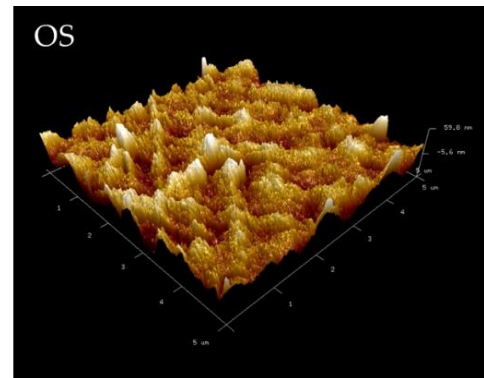
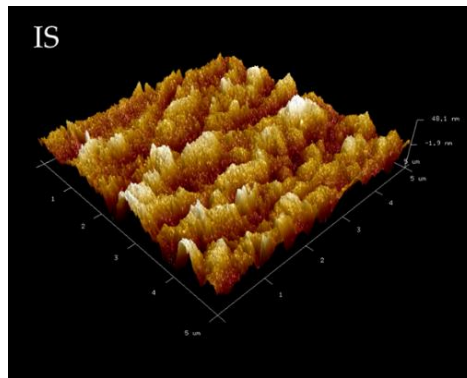
S15-0



S15-10



S15-15



S15-20

Figure 3.13. (Continued).

Table 3.9. Roughness parameters of the hollow fibre membranes spun from different polymer dope solutions and internal coagulant concentrations.

Membrane code	Inner surface			Outer surface		
	R _a (nm)	R _q (nm)	R _{max} (nm)	R _a (nm)	R _q (nm)	R _{max} (nm)
The effect of polymer dope concentrations						
S0	21.6	29.0	350.5	21.7	29.1	242.5
S5	26.2	37.2	464.0	23.7	32.9	361.0
S10	26.2	38.9	424.5	23.0	37.6	635.5
S15	33.3	46.2	389.0	23.4	36.1	541.0
The effect of internal coagulant concentrations						
S5-10	19.1	24.7	199.5	29.15	37.5	299.5
S5-15	19.9	27.4	225.5	32.9	44.3	516.0
S5-20	22.6	28.5	232.0	45.4	60.9	717.5
S10-10	15.7	21.7	281.0	16.8	25.6	402.0
S10-15	15.7	22.1	293.5	63.8	90.3	940.0
S10-20	18.5	25.2	271.5	112.2	151.0	1312.0
S15-10	17.5	23.4	227.7	94.3	129.5	1057.5
S15-15	17.6	24.1	303.0	101.3	131.0	965.5
S15-20	25.5	36.5	599.0	112.8	143.9	1417.0

Note: R_a, average roughness; R_q, root mean square roughness; R_{max}, maximum roughness distance between the highest and the lowest data points.

Two possible factors can account for these observations: (1) the substitution of DMAc mixture affects the mutual diffusion process between the polymer dope solution and internal and external coagulant; (2) the outer membrane surface encountered a 50 mm air gap before interacting with the external coagulation bath. During membrane fabrication, the internal coagulant was directly contacted with the polymer dope solution such that it underwent solvent exchange and phase separation to form a lumen. When water is used as the internal coagulant, the diluent, which is from the polymer dope solution, diffuses rapidly down a concentration gradient, from an area of high DMAc concentration to an area of low DMAc concentration (either to the external coagulation bath or the lumen). However, when the internal coagulant is replaced with DMAc mixture, the diluent and internal coagulant are closer to equilibrium, hence the solvent exchange at the lumen is slower. As a result, smaller pores are formed because the inner membrane surface experienced a delayed demixing process.

On the other hand, the phase separation of the outer membrane surface was sped up when the polymer dope solution experienced an air gap, which led to diluent evaporation [25]. The polymer dope further accelerated its phase separation when it contacted with the external coagulation bath, whereby the internal coagulant remained in the lumen. As a result, the diluent diffused rapidly through the outer part of the membrane, creating larger pores at the outer membrane surface.

In summary, it can be concluded that the composition of the coagulant plays a crucial role in affecting the surface roughness of the membranes. The inclusion of DMAc in the internal coagulant interrupted the diffusion process at the inner membrane surface, and subsequently delayed the demixing process and produced smaller pores. Upon increasing the DMAc concentrations, surface roughness for all membrane samples increased.

3.3.3.3 Mechanical properties of the hollow fibre membranes

Table 3.10. shows the effect of different DMAc concentrations on the mechanical properties of the hollow fibres. The changes in internal coagulant exhibit an inverse relationship as compared to the effect of polymer dope concentration on the mechanical properties. Upon increasing the concentration of DMAc, the tensile strain increases, whereby the tensile strength and Young's modulus decrease. This indicates that the brittleness and stiffness of the hollow fibres declines. Similar observations were reported by Sukitpaneemit and Chung [32], who found that the addition of weak solvent in the external coagulant reduces Young's modulus and tensile strength due to the membrane morphology changes caused by the delayed demixing process. As mention in Section 3.3.3.1, the delayed demixing allows the hollow fibre to stretch and elongate before entering the water bath, which results in a narrowing of the wall thickness and a higher ID/OD. The reduction of the wall thickness (illustrated in Figure 3.10.), which modified the mechanical strength, has caused the hollow fibres to collapse during the drying process at higher DMAc concentrations.

In summary, these results demonstrate that variations in polymer dope and DMAc concentrations significantly impacted on the membrane structure, which eventually modified the mechanical properties of the hollow fibres. In comparison to the mechanical strength and wall thickness of the commercial dialysis membranes (Fresenius F60S membrane: wall thickness 40 μm [46]; tensile strength 7.9 MPa [47]), S15 and its membrane series are membranes that can be potentially employed as a substrate for microgel particle embedment. Further determination on the pore size distribution of the membranes will be discussed in the next section.

Table 3.10. Mechanical properties of PVDF/PSF hollow fibre membranes fabricated from DMAc/water mixture of different DMAc concentrations as internal coagulant.

Membrane code	Tensile strength (MPa)	Tensile strain (%)	Young's modulus (MPa)
S5-10	12.60±0.28	249.74±3.97	8.63±0.77
S5-15	8.92±0.48	330.37±7.81	5.93±0.54
S5-20	6.99±0.30	368.37±1.36	5.79±0.48
S10-10	21.93 ±1.59	106.64±1.56	23.09±0.17
S10-15	20.32±3.60	217.87±1.94	3.21±0.07
S10-20	18.01±0.67	283.58±2.39	3.10±0.51
S15-10	26.66±1.77	195.32±5.04	11.10±2.35
S15-15	18.45±1.15	222.40±8.23	7.94±0.20
S15-20	13.81±0.05	224.75±1.94	7.07±0.10

3.3.3.4 Pure water permeability and solute rejection performance for the hollow fibre membranes

According to the membrane morphology and mechanical strength, S15 and its membrane series are promising membranes for membrane modification. The effect of internal coagulant concentration on the PWP, solute rejection performance and overall porosity of S15 hollow fibre membranes are shown in Table 3.11. It is worth noting that the effect of polymer dope concentration, as shown in Table 3.6., and internal coagulant concentration on the membranes resulted in similar membrane permeability and solute rejection trends. Upon increasing the DMAc concentration, the mean pore size, MWCO and PWP of S15 membranes decreases, which is in agreement with the FE-SEM micrographs of the membranes shown in Figure 3.11. This suggests that the similar trends can be attributed to changes in the demixing processes, which is affected by both the viscosity and solubility parameters. Nevertheless, the porosity of the membranes fluctuated from 70.1 to 67% and then 74.7 to 62.8% for S15 to S15-20, respectively. Despite comparable wall thicknesses for S15 and S15-5, the finger-like macrovoids dramatically reduced in size, which resulted a reduction in porosity.

Table 3.11. Mean pore size, MWCO, and pure water permeability of S15 membranes obtained from solute transport technique.

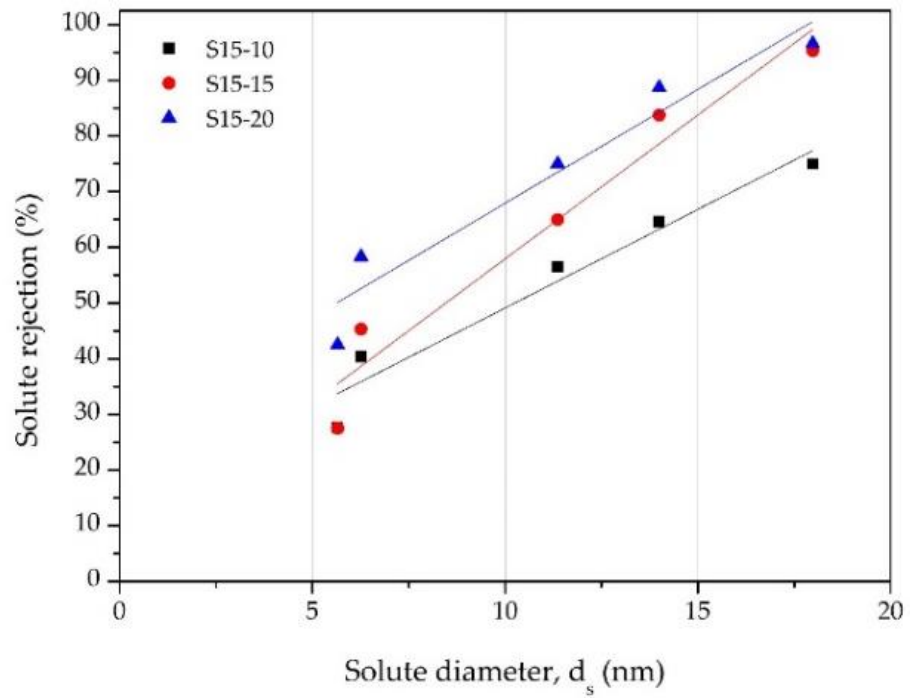
Membrane Code	Mean pore size, μ_p (nm)	MWCO (Da)	PWP (L/m² h bar)	Porosity (%)
S15-0	3.97	439 000	152.0	70.1
S15-10	2.90	241 000	93.8	67.0
S15-15	0.65	85 000	31.2	74.7
S15-20	0.30	72 000	24.5	62.8

Note: MWCO refers to molecular weight cut-off, the molecular weight of the solute, 90% of which can be rejected by a membrane.

It is interesting to observe that the porosity for S15-15 increases, but PWP reduces. The increasing membrane porosity should have resulted in an increase in PWP, as the wall thickness has reduced. However, at S15-15, the permeability test reduces. The outcome suggests that the outer skin surface of the membranes becomes considerably denser and that the pores decrease in size, which is arising from the delayed demixing process. A dense skin layer and further increase in DMAc concentration lead to a drop in membrane porosity for S15-20. This suggests that the membrane structure exhibits a closely packed sponge-like structure containing pores and that possible dead volume has formed under the skin layer, resulting in an increase in permeation resistance, as evidenced in Figure 3.10. (c). Therefore, despite the formation of a porous membrane surface, PWP decreased rather than increased.

The solute rejection and pore size distribution curves of the S15 membranes are shown in Figure 3.14. We can see that, as the DMAc concentration increases, the majority of the pores inclines to a smaller size range, thus resulting in steep probability function curves. The outcome suggests that it is attributed to the dense skin layer and the small pore size forms due to the delayed demixing process, leading to improvements to the selective layer of the membrane. Therefore, the solute rejection curve increases as DMAc concentration increases. According to the MWCO and porosity of the membranes, S15-15 is chosen as the potential hollow fibre membrane to be used as a substrate for membrane hydrophilization. This will be discussed in Chapter 5.

(a)



(b)

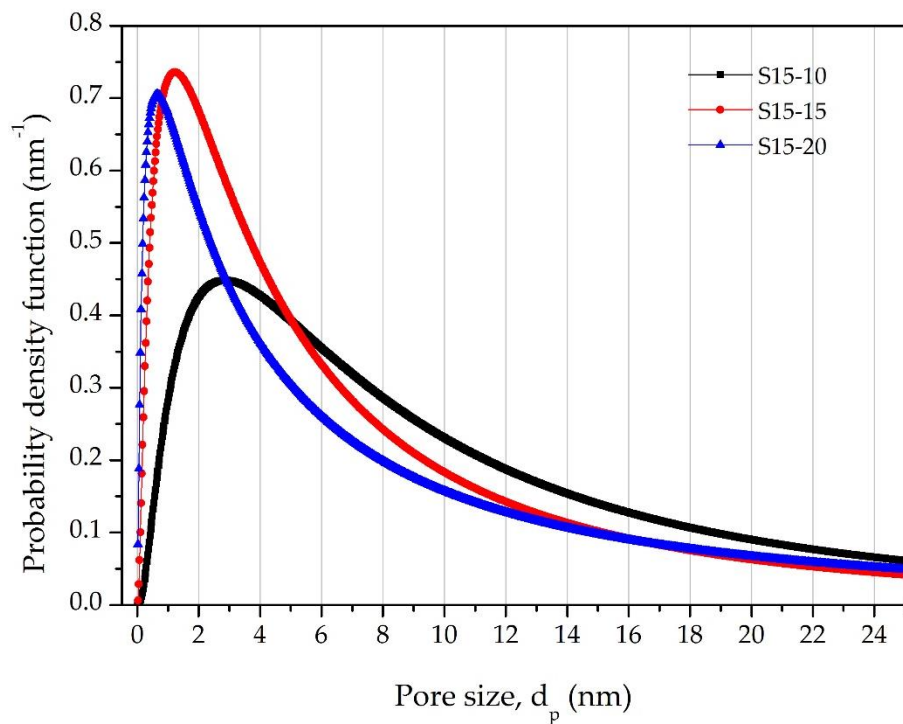


Figure 3.14. (a) Solute rejection curves and (b) probability density function curves of PVDF/PSF (S15) hollow fibre membranes prepared from DMAc/water mixture of different DMAc concentrations as internal coagulant.

3.4 Conclusion

Hollow fibres membranes of PVDF/PSF blends were fabricated via diffusion induced phase separation using DMAc as a solvent. The effect of PSF weight ratios in the PVDF/PSF blends and the effect of internal coagulant concentrations on the morphology, pore size, mechanical strength, and membrane permeability were examined. The addition of PSF in the PVDF dope solutions has significantly altered the crystallinity and rheological behaviour of the polymer dope solution. As the weight ratio of PSF increased, the melting temperature increased, whereas the degree of crystallinity of the polymer blends decreased. These observations were due to the formation of “big spherical crystalline particles” in the membranes. As the PSF weight ratio in the polymer blends increased, the numbers of “big spherical crystalline particles” in the membranes increased dramatically. The membrane morphology studies showed that higher weight ratios of PSF in the polymer blends, led to smaller pores being formed and an increase in the overall surface roughness of the membrane. Upon the increasing PSF, the mechanical strength of the blended hollow fibres was improved, especially their tensile strength. The addition of DMAc in the coagulant had a remarkable effect on the formation of the membrane structure. As the DMAc concentration increased, the wall thickness of the membrane became thinner and denser, and an increase in the membrane diameter was observed. This outcome was because the DMAc in the internal coagulant delayed the solidification of PVDF in conjunction with crystallisation. These findings indicated that the modification of a membrane structure could be attained by manipulating the fabrication parameters prior to spinning.

Chapter 4: SYNTHESIS AND CHARACTERISATION OF STABILISED TEMPERATURE-RESPONSIVE POLY(2-DIMETHYLAMINO) ETHYL METHACRYLATE MICROGEL PARTICLES

4.1 Overview

This chapter aims to prepare PDMAEMA microgel particles by free radical dispersion polymerisation via constant agitation. The weight ratio of the synthesis composition was modified from the method developed by Hu, *et al.* [96]. Several amendments to the standard compositions were made to achieve a desired microgel particle morphology and size. The amendments were (1) constant agitation performed throughout the synthesis process to obtain a smaller hydrodynamic diameter and (2) the initiator being replaced with ammonium persulfate (APS). APS is a water-soluble initiator, and has better reactivity than azobisisobutyronitrile [191,192].

In addition, the effect of the stabiliser PVP and ethanol on the size distribution of PDMAEMA microgel dispersion was studied. This was followed by a study of cross-linker and monomer concentrations on the hydrodynamic diameters with respect to the temperature-responsiveness of the microgel particles. The zeta potential of the microgel dispersion was methodically examined. The effect of the microgel dispersion to ethanol on the stability and aggregation behaviour over a defined period was studied. The morphology characterisation of the microgel particles was determined using FE-SEM and AFM. The hydrodynamic diameters and monodispersity of the microgel particles were determined using dynamic light scattering. Lastly, zeta potentials of the microgel particles, calculated from electrophoretic mobilities, were also measured.

4.2 Experimental

4.2.1 Materials

The monomer DMAEMA (99.0%) was obtained from Merck, China. DMAEMA was stabilised with hydroquinone monomethyl ether (700-900 ppm) and the stabiliser was removed by passing it through an aluminium oxide column (Acros Organics). PVP K90 (Mw = 360,000 Da) was purchased from Fluka® Analytical (Sigma-Aldrich, USA). APS (Friendemann Schmidt Chemical Pty. Ltd., Australia), MBAA (98%, Merck, USA), and

ethanol (99.96%, VMR Chemicals, France) were selected as the initiator, cross-linking agent, and organic solvent respectively. They were used as received. The pH adjustment of the microgel particles dispersions was accomplished by using sodium hydroxide (NaOH) and hydrochloric acid (HCl) 37%, which were obtained from Friendemann Schmidt Chemical Pty. Ltd., Australia and Merck, Germany, respectively. Deionised (DI) water was used in all microgel preparations and purification processes.

4.2.2 Preparation of PDMAEMA microgel particles

PDMAEMA microgel particles were prepared by free radical dispersion polymerisation. The polymerisations were conducted in a 250 mL round-bottomed four-necked flask. The reaction flask was equipped with a mechanical stirrer, a condenser, a thermometer (temperature sensor) and nitrogen inlet and outlet. A schematic diagram of the microgel synthesis set-up is shown in Figure 4.1. The synthesis was performed in a single step preparation employing a conventional stirring technique at 500 rpm. A measured amount of DMAEMA, MBAA, ethanol, and DI water were added into a reaction vessel. The standard composition of the reaction mixture is listed in Table 4.1.

For the PVP study, the polymerisation was repeated with the addition of PVP. PVP was pre-dissolved in DI water and added into the reaction vessel with the DMAEMA, MBAA, and ethanol. The level of DI water was topped-up to the required amount. The reaction mixture was heated to 65 °C in an oil bath and continuously purged with nitrogen gas to exclude oxygen. In the meantime, the initiator solution, composed of APS and DI water, was prepared. Once the reaction mixture reached a constant temperature, the initiator solution, which was purged with nitrogen gas, was introduced to start the polymerisation. Instantly, the colour of the reaction mixture changed from clear to opalescent. The polymerisation process was continued for up to 3 hours while nitrogen gas was purged throughout the polymerisation process. Thereafter, the synthesised microgel dispersion was slowly cooled down to ambient temperature whilst also being continuously stirred prior to purification process taking place.

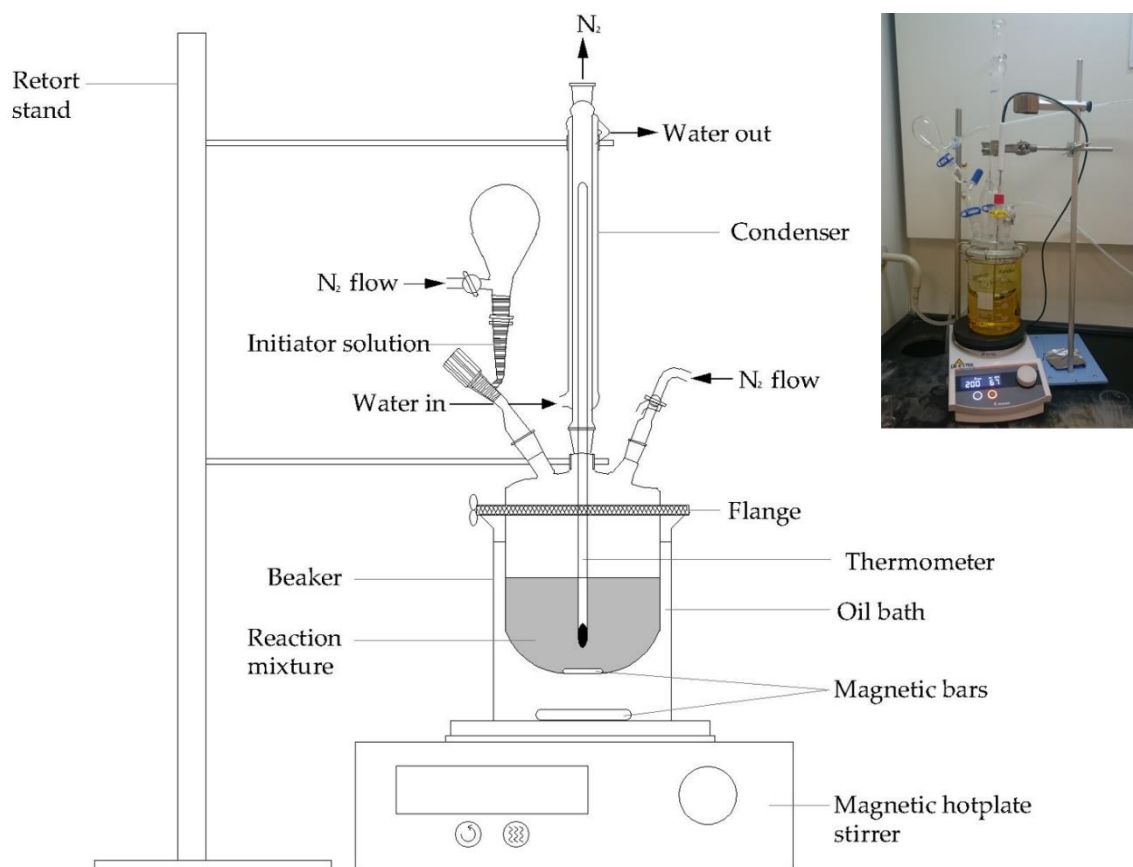


Figure 4.1. A schematic diagram for PDMAEMA microgel synthesis. Reaction mixture consists of DMAEMA, MBAA, APS, ethanol/PVP, and DI water.

Table 4.1. Standard composition of microgel particles synthesis

Ingredient		Standard recipe
DMAEMA ^a	(mol/L)	0.50
Ethanol/water	(vol/vol)	1/9
MBAA ^b	(wt%)	0.50
Initiator, APS ^b	(wt%)	0.35
PVP, K90 ^b	(wt%)	10

^a Based on the total volume of the ethanol/water mixture

^b Based on the weight of DMAEMA

4.2.3 Purification of PDMAEMA microgel particles

The purpose of purification is to remove any traces of unreacted monomer, initiator, and cross-linker. The purification process was completed using a vacuum filtration technique. The synthesised microgel dispersion was filtered consecutively through two different sizes of membrane filters. Before undergoing an intensive purification process, the microgel dispersion was first filtered through a cellulose membrane filter with an 11 μm pore size to remove large and/or aggregated particles. Then, the microgel dispersion was washed with DI water using a hydrophilic PTFE membrane filter with 0.2 μm pore size for at least ten cycles. The microgel dispersion was constantly stirred at 500 rpm using an overhead stirrer to reduce the concentration polarisation of the dispersion. In each cycle, 100 mL of DI water was replaced when the volume of the microgel dispersion was close to the 100 mL mark. This process was continued until a specific ultraviolet-visible (UV-Vis) absorption curve of the filtrate was close to the baseline of 100 nm. The total volume of the purified microgel dispersion was then concentrated to 10 mL in order to compensate for the concentration required for zeta potential analysis.

4.2.4 Characterisation of PDMAEMA microgel particles

4.2.4.1 Morphology studies of PDMAEMA microgel particle dispersion

Scanning electron micrographs were taken with an Ultra-High-Resolution FE-SEM Hitachi SU 8000 series microscope. Diluted microgel dispersions were placed onto a cleaned microscopic slide, which was cut into 5 x 5 mm cube and air-dried at ambient temperature. The samples were coated with Pt using a sputter coater (Q150RS, Quorum) to increase the contrast and quality of the images prior to imaging. Micrographs were taken at a voltage of 10 kV.

AFM analysis was performed using a digital Instruments Multimode 8 (Bruker, USA) to obtain the surface topography of the microgel. Diluted microgel dispersions were placed onto a cleaned microscopic slide that was cut into 5 x 5 mm cube and air-dried at ambient temperature. The microgel particles were measured using the ScanAsyst mode, which is an automated mode used to optimise the image parameters. At least three locations were measured for each sample.

4.2.4.2 Stimuli-response of PDMAEMA microgel particle dispersion

Hydrodynamic diameter and zeta potentials of PDMAEMA microgel dispersion were measured using a Zetasizer Nano series (Malvern Zen 3600 Zetasizer) from Malvern Instruments, which was operated according to standard operating procedure. (Refractive index of the microgel particles dispersion: 1.345). The microgel dispersion was measured using a folded capillary cell at 25 °C, unless otherwise stated.

The temperature-dependent hydrodynamic diameters of the particle were measured at various temperature ranging from 25 °C to 60 °C, at 2 °C increments. The samples were left to equilibrate for 5 min at each temperature interval. Each measurement for the PDMAEMA microgel dispersion was performed in triplicate with pH adjustment to $\text{pH } 7.45 \pm 0.05$ to mimic biological conditions. The swelling ratios of the particles were calculated from the following equation:

$$\text{Swelling ratio} = \frac{D_h(37\text{ }^\circ\text{C})}{D_h(60\text{ }^\circ\text{C})} \quad \text{Eq. 4.1}$$

Where D_h is the hydrodynamic diameter of the microgel particle. The microgel dispersion was measured using a quartz cuvette.

4.2.5 Zeta potential of PDMAEMA microgel particles

The zeta potential is an indicator of the stability of colloidal dispersions. The measurement of the microgel dispersion concerning pH and temperature was adjusted automatically by the instrument through the addition of 0.25 M NaOH, 0.25 M HCl, and 0.01 M HCl and without pH adjustment. An average value of at least three measurements of the hydrodynamic diameters and zeta potentials of the microgel particle dispersion were collected to minimise experimental error.

4.2.6 Stability of PDMAEMA microgel particles

The stability of the PDMAEMA microgel particles dispersion with ethanol in DI water medium was studied. HPLC glass vials were used for incubation. During the incubation, the dispersion was not agitated at ambient temperature. The pH of the media was maintained at a pH of 7.45 ± 0.05 . Two points of incubation were used (30 and 180

days). At the end of the incubation duration, FE-SEM micrographs were captured to compare the size and shape of the microgel particles.

4.3 Results and discussion

4.3.1 Effect of polymerisation parameters on the hydrodynamic diameter and size distribution of PDMAEMA microgel particles

The parameters of the dispersion polymerisation are essential factors that affect the end result of the microgel particles, such as their size and size distribution. The parameters that are taken into account are the inclusion of a stabiliser, and the concentration of both cross-linkers and monomers.

4.3.1.1 Effect of PVP and ethanol as a stabiliser

The PDMAEMA microgel particles stabilised with PVP and ethanol were synthesised and characterised. Figure 4.2. shows the temperature-responsiveness of the PDMAEMA microgel particles stabilised with PVP and ethanol. In the following discussion, they are referred to as PDMAEMA-PVP and PDMAEMA-EtOH, respectively.

A major difference between PDMAEMA-PVP and -EtOH dispersions is the transition temperature. It is interesting to observe that the PDMAEMA-PVP dispersion shows a totally different trend from PDMAEMA-EtOH dispersion. PDMAEMA-PVP dispersion exhibited UCST behaviour, as shown in Figure 4.2. (a). When the temperature gradually increased, the interaction between polymer and water molecules steadily increased. Until the microgel particles attained its water uptake limit, achieving what is known as a swollen state, the hydrodynamic diameter of the microgel particles becomes relatively constant when the temperature reaches 50 °C at pH 7.45.

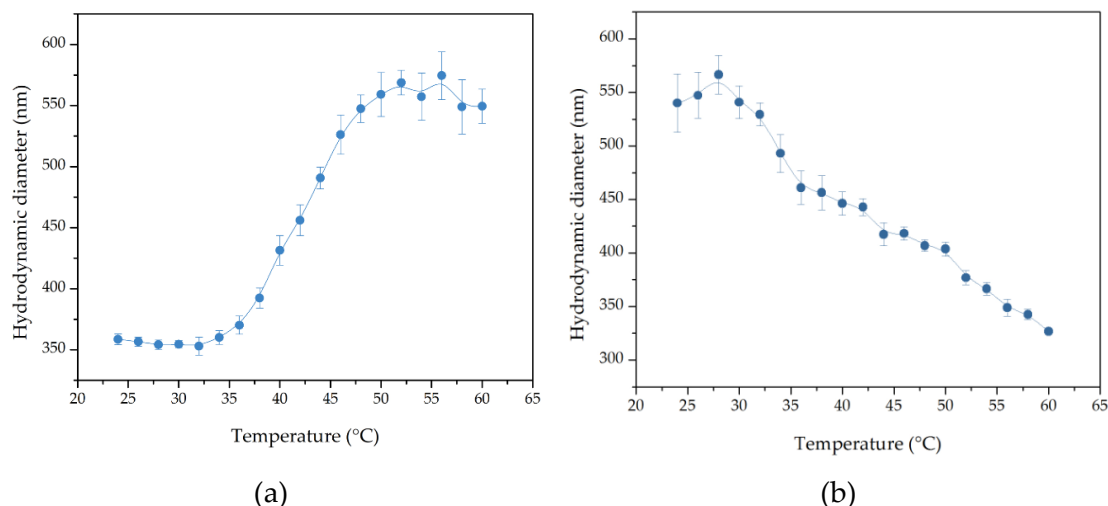


Figure 4.2. Effect of stabilisers on the hydrodynamic diameters of the PDMAEMA microgel dispersion prepared with 0.5 wt% of MBAA at a temperature ranging from 25 to 60 °C at pH 7.45. (a) PDMAEMA-PVP dispersion, (b) PDMAEMA-EtOH dispersion.

One possible reason can explain this outcome. The carbonyl groups and surface hydroxyls of PVP may have bound to PDMAEMA, forming a PVP coating surrounding the particle instead of solely acting as a steric stabiliser in the medium during the polymerisation. This finding is reported elsewhere in literature [130,133,193,194]. When the hydrophobic chains of PDMAEMA-PVP extend into the solvent (water) and interact with each other, they create repulsive forces, which is known as the steric hindrance effect [195]. On the other hand, PVP, which is also known to have hygroscopic and hydrophilic properties, is ready to absorb water, thus leading to an increase in the size of the polymer matrix [196,197]. The trend suggests that, at lower temperatures, the PDMAEMA-PVP dispersion dominates hydrophobic interactions, meaning that hydrogen's ability to bind with water is hindered. It is this strong steric hindrance that prevented the microgel particles from aggregating. As the temperature increased, the repulsive forces gradually weakened and increased the interaction of the hydrophilic component (pyrrolidone moiety) of PVP and water. The viscosity of the microgel dispersion then increased and eventually achieved steric stabilisation [96], but the steric barrier was rather weak. Therefore, a higher standard deviation resulted as the temperature increased.

In contrast, the PDMAEMA-EtOH dispersion exhibits LCST at approximately 30 °C at pH 7.45, as seen in Figure 4.2. (b). When polymer molecules are cross-linked in a

polymer network, the responsivity is referred to as a volume collapse, and results from the exclusion of water. This transition temperature is known as the volume phase transition temperature (VPTT) [110,127,198,199], which is generally adjacent to the LCST of the corresponding linear polymer. This trend demonstrates that, at lower temperatures, PDMAEMA becomes soluble, because extensive hydrogen bonding interactions with the surrounding water molecules are formed, and simultaneously, intra- and intermolecular hydrogen bonding between polymer molecules is inhibited. Therefore, upon heating, the conformation of the particles progressively collapsed and simultaneously became hydrophobic and insoluble once the temperature went beyond the VPTT [200,201].

As shown in Figure 4.2. (b), the hydrodynamic diameter of the microgel dispersion decreased at a fairly stable rate when ethanol, an organic solvent, was used as a stabiliser. The stabilisation of PDMAEMA-EtOH is comparable to PDMAEMA-PVP. When the microgel particles were swollen, the deviation of the hydrodynamic diameter was considerably higher. This outcome could be attributed to the disruption and reformation of the hydrogen bonding interactions between PDMAEMA and ethanol. Therefore, the aggregation of the microgel particles in the dispersion is prevented through the mutual repulsion of electric charges between ethanol and other particles [111,112]. One important benefit is that the addition of ethanol did not interfere with the temperature-responsiveness of PDMAEMA. Similar results have been reported elsewhere in the literature [103,202].

In summary, PVP was excluded as a stabiliser in this study for the following reasons. The inclusion of PVP into PDMAEMA not only acted as a steric stabiliser but also copolymerized, forming a layer of PVP coating during polymerisation that altered the chemical structure of PDMAEMA. Although PVP demonstrated better steric stabilisation, the unique transition temperature of PDMAEMA-PVP dispersion does not align with the proposed innovation mentioned in Section 1.1, meaning it is unsuitable for dialysis and steps involved in reprocessing. Hence, ethanol was chosen as a steric stabiliser for the following experiments.

4.3.1.2 Effect of cross-linker concentrations

Figure 4.3. shows the effect of the cross-linker, MBAA concentrations on the hydrodynamic diameters with respect to the temperature-responsiveness of the PDMAEMA microgel particles. The microgel dispersion that corresponded to gradual increases in the concentration of MBAA from 0.4 to 0.7 wt% were coded as C0.4, C0.5, C0.6 and C0.7, respectively. We can see that, as the temperature increased, the size of the microgel particles decreased linearly, regardless of the concentration of MBAA.

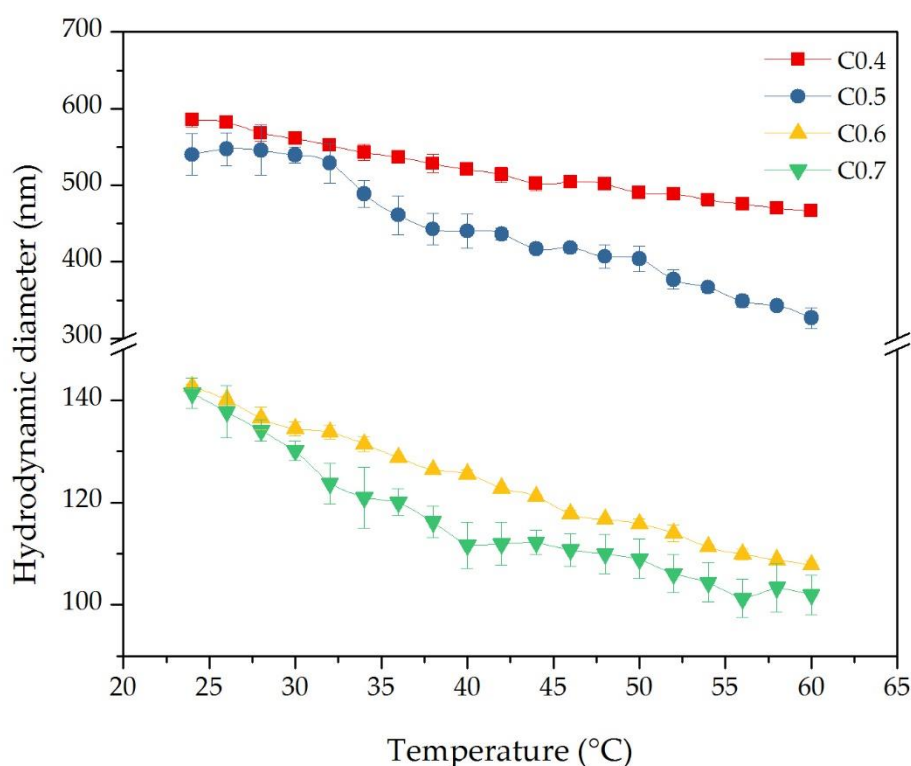


Figure 4.3. Effect of the cross-linker on the hydrodynamic diameters of the PDMAEMA microgel particles prepared in ethanol/water mixture at a temperature ranging from 25 to 60 °C at pH 7.45. (■) 0.4 wt% of MBAA; (●) 0.5 wt% of MBAA; (▲) 0.6 wt% of MBAA; and (▼) 0.7 wt% of MBAA.

As the MBAA concentration increased, two distinct hydrodynamic diameters ranges for the microgel particles were observed. The hydrodynamic diameters for C0.4 and C0.5 had a higher range (between 585 nm and 327 nm), whereas C0.6 and C0.7 had a lower range (between 142 nm and 102 nm). The lower range suggests that, when higher MBAA concentrations were used, highly cross-linked microgel particles were

synthesised [96,117,203,204]. As a result, the core of the microgel particles became compacted and yielded smaller dimensions [198]. A schematic presentation of the highly cross-linked PDMAEMA and low cross-linked PDMAEMA microgel particles is shown in Figure 4.4. Nevertheless, there was no significant effect on the swelling behaviour of the microgel particles, as seen in Figure 4.5.

An exceptional outcome resulted from C0.4, where the swelling ratio was comparable to C0.6 and C0.7, although it possessed a higher hydrodynamic diameter range. This outcome may be due to the low MBAA content, which would lead to weakly cross-linked microgel particles being formed, resulting in a lower swelling ratio [117]. In view of the hydrodynamic diameter and swelling ratio of the PDMAEMA microgel particles, 0.5 wt% MBAA was chosen for the following experiments.

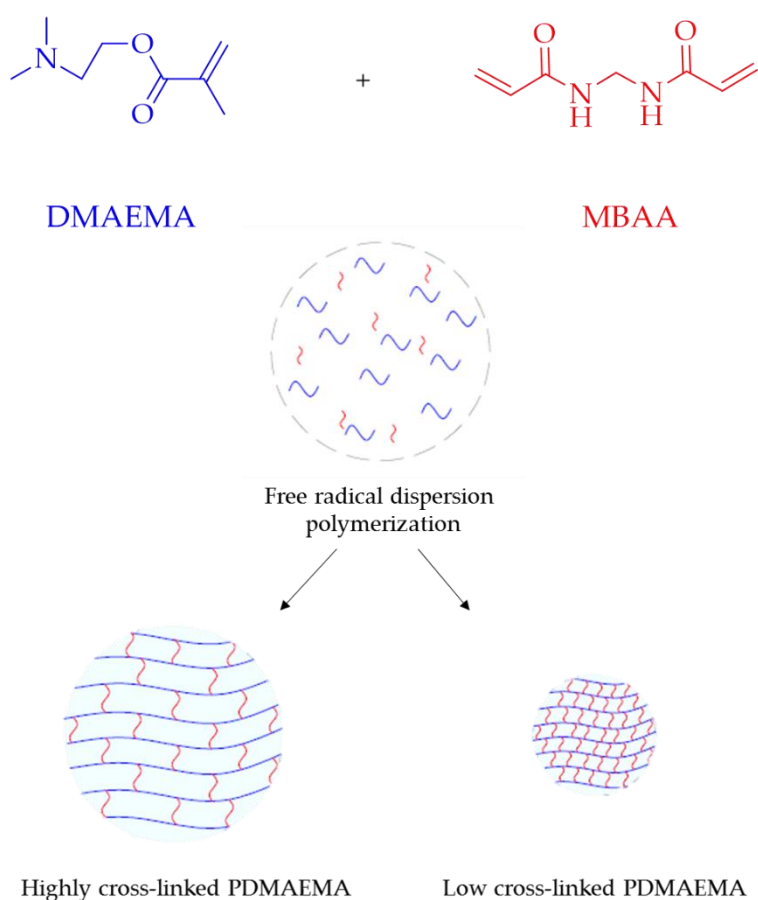


Figure 4.4. Schematic diagram of a cross-linked PDMAEMA using free radical dispersion polymerization at 65 °C, 500 rpm.

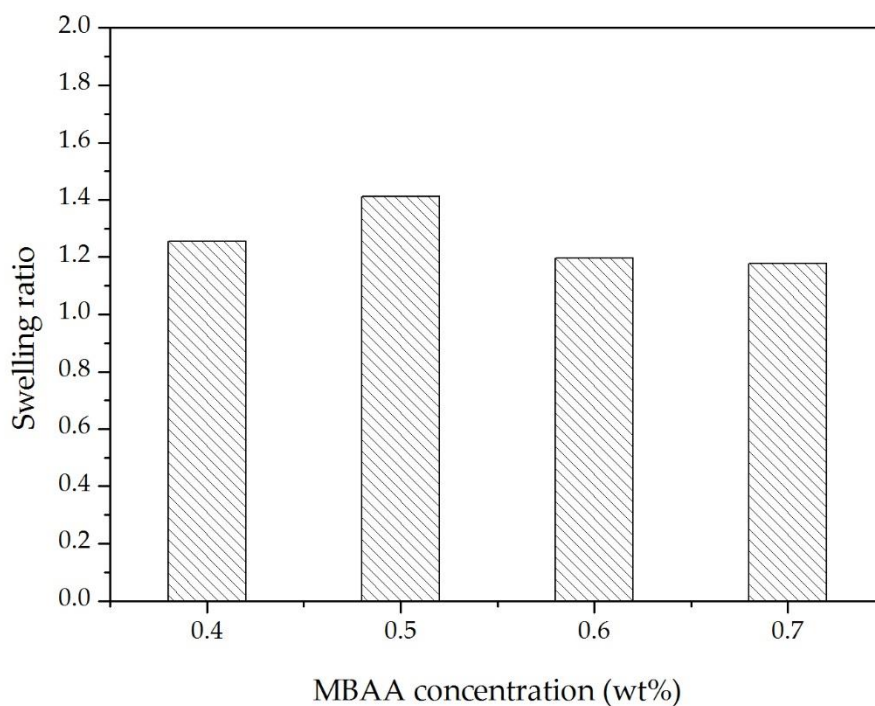


Figure 4.5. Swelling ratio of the PDMAEMA microgel particles with different cross-linker concentrations was calculated from $D_h(37\text{ }^\circ\text{C})/D_h(60\text{ }^\circ\text{C})$ at pH 7.45.

4.3.1.3 Effect of monomer concentrations

Figure 4.6. shows the effect of monomer, DMAEMA concentrations on the hydrodynamic diameters of the PDMAEMA microgel particles. The microgel dispersion that corresponded to gradual increases in DMAEMA concentration from 0.4 to 0.7 wt% were coded as M0.4, M0.5, M0.6 and M0.7, respectively. The size of the microgel particles decreased as the temperature increased from 25 to 60 °C at pH 7.45, in spite of the concentration of the DMAEMA.

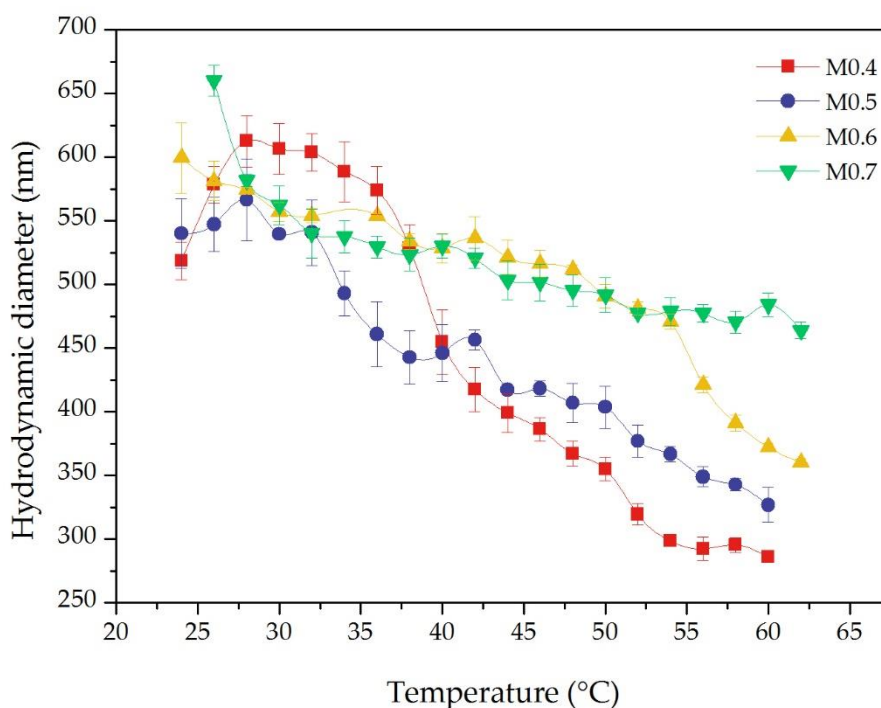


Figure 4.6. Effect of monomer concentration on the hydrodynamic diameters of the PDMAEMA microgel particles prepared with 0.5 wt% MBAA based on the weight of DMAEMA in ethanol/water mixture at a temperature ranging from 25 to 60 °C at pH 7.45. (■) 0.4 wt% of DMAEMA; (●) 0.5 wt% of DMAEMA; (▲) 0.6 wt% of DMAEMA; and (▼) 0.7 wt% of DMAEMA.

Upon increasing the DMAEMA concentration, there are two main observations: (1) the LCST for different DMAEMA concentrations were relatively similar, at approximately 30 °C, at pH 7.45. However, the LCST for M0.6 and M0.7 were rather unclear, as the curves appeared to signal a combination of slow and sharp reductions as the temperature increased; (2) the trends of the hydrodynamic diameter of the microgel particles did not significantly change as compared to the effect of cross-linker concentrations.

The outcome of the LCST was rather unexpected, as it has been reported that the LCST is readily modified by increasing the concentration or molar mass of either a hydrophilic or a hydrophobic monomer. The higher hydrophilic groups promote higher hydrogen bonding interactions, resulting in a higher transition temperature [200]. In this case, DMAEMA is a hydrophilic monomer, so as the monomer concentrations increases, the LCST should have resulted in an increase in transition temperature. The result

suggests that the interval range of the monomer concentration could be too low; as a result, the change in the LCST is insignificant.

Moreover, there was no evidence that lower monomer concentrations yielded smaller particle dimensions [117,198]. Nevertheless, at higher DMAEMA concentrations, for M0.6 and M0.7, the overall hydrodynamic diameter of the microgel particles was larger than for M0.4 and M0.5. This observation is attributed to the existing DMAEMA monomers, which were capable of cross-linking with themselves and forming larger microgel particles, which resulted from a prolonged nucleation and eventually caused aggregation. This is in agreement with findings elsewhere in the literature [96].

In general, higher DMAEMA concentrations resulted in increasing the yields of the microgel particles, signifying higher levels of hydrogen bonding between the microgel particles and solvent. Therefore, a higher swelling ratio resulted. Nevertheless, due to the cationic characteristics of PDMAEMA, the microgel particles are only capable of swelling in acidic conditions. Consequently, at pH 7.45, the interactions of the water and polymer molecules were unfavourable, resulting in a reduction in the swelling ratio as the monomer concentration increased, as shown in Figure 4.7.

In summary, it is interesting to see that the LCST did not shift as the monomer concentration increased, which could be attributed to an insignificant increase in the molar mass between the monomer and cross-linker. The determination of the monomer concentration is crucial for preventing self-cross-linked particles and aggregation. In order to examine the stability of the microgel dispersion for bulk production, M0.5 was chosen for the following experiments.

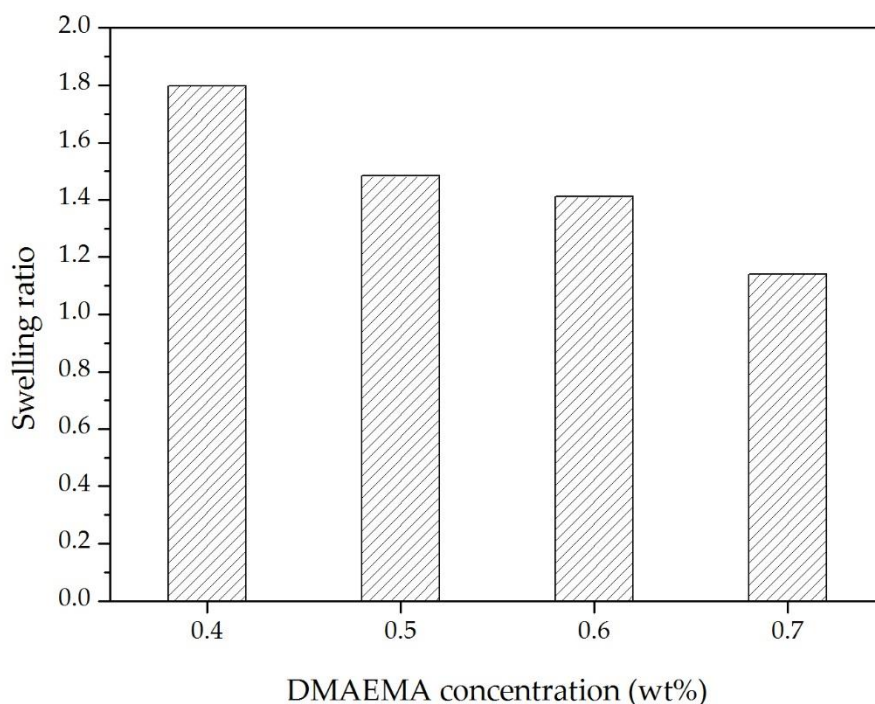


Figure 4.7. Swelling ratio of the PDMAEMA microgel particles with different monomer concentrations was calculated from $D_h(37\text{ }^\circ\text{C})/D_h(60\text{ }^\circ\text{C})$ at pH 7.45.

4.3.2 Effect of ethanol on the zeta potential of PDMAEMA microgel dispersions

Aside from the main components of the reaction mixture, the monomer and cross-linker, ethanol was added into the reaction mixture to increase the medium's polarity. The addition of ethanol improves the solubility of DMAEMA and provides better stability for microgel formation during the polymerisation process [96,111]. Therefore, it is crucial to determine the zeta potential when it comes to dispersion stability. The zeta potential of pH- and temperature-responsiveness of the PDMAEMA microgel dispersions are compared. Figure 4.8. shows that the zeta potential with respect to the temperature-responsiveness of the microgel dispersion was linear, and ranged from 25 to 60 °C, whereas the zeta potential values decreased as the pH-responsiveness of the microgel dispersion increased from 4 to 10, which is typical for cationic polymers [205].

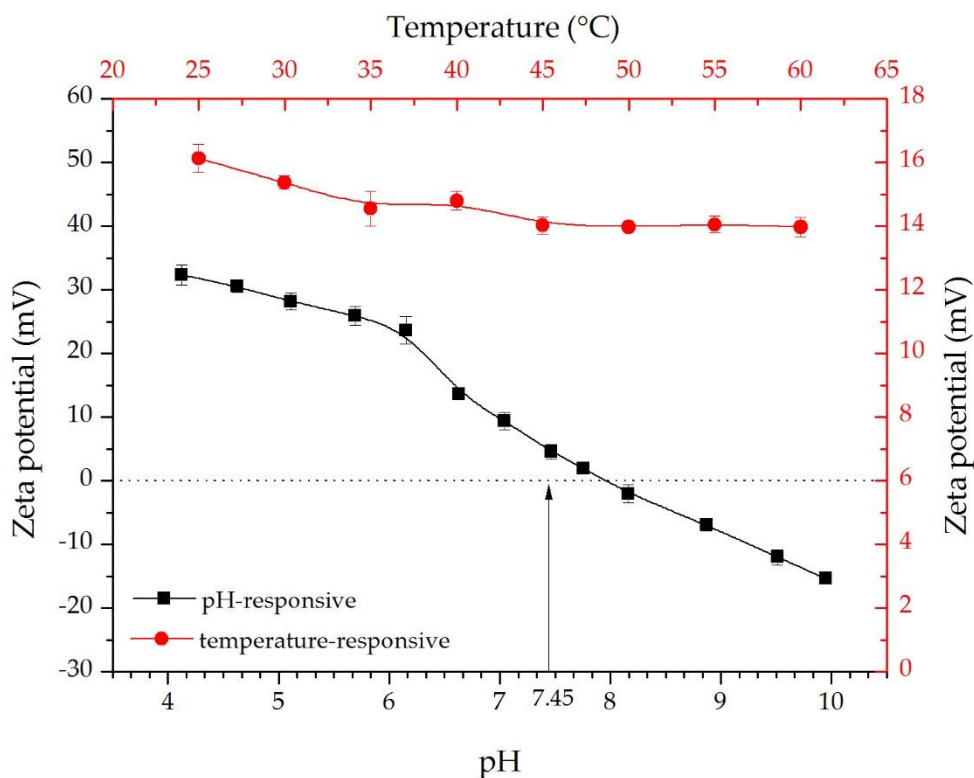


Figure 4.8. Zeta potential of the stimuli-responsive of the PDMAEMA microgel dispersion (M0.5) prepared with 0.5 wt% MBAA and 0.5 wt% DMAEMA in ethanol/water mixture. (■) pH-responsive of the microgel particles at 37 °C from pH 4-10; (●) Temperature-responsive of the microgel particles with a 1 to 5 ratio of ethanol to microgel dispersion, from 25 to 60 °C at pH 7.45.

The modification of the zeta potential with respect to pH-responsive is due to changes to the surface charge of the microgel particles. As mentioned in Section 2.3, the swelling behaviour of a particle depends on the protonation and deprotonation of the hydrogen bonding upon a change in pH, as illustrated in Figure 4.9. Therefore, when the dispersion gradually becomes acidic, the particles will contain more charges that are positive. When the dispersion becomes basic, the positive charges will gradually be neutralised. The dispersion becomes negative charge dominated, if the pH of the dispersion further increases [136]. Therefore, the dispersion resulted in a positive zeta potential at lower pH levels and a negative zeta potential at higher pH levels, as shown in Figure 4.8.

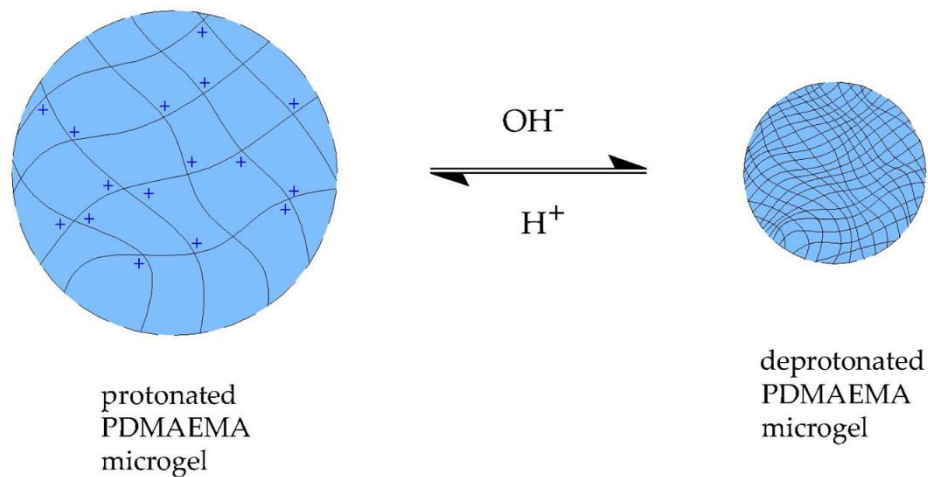


Figure 4.9. Schematic diagram of a protonated and deprotonated PDMAEMA microgel particle.

It is important to note that, at pH 7.45 (the pH of human blood), the zeta potential value approaches zero, which is known as the isoelectric point, indicating that the colloidal stability between the microgel particles is poor. The microscopic features of the microgel dispersions between pH 7.45 and 10 were compared, as shown in Figure 4.10. We can see that the zeta potential of the microgel particles, which at pH 7.45 was relatively close to the isoelectric point, were severely aggregated. On the contrary, at pH 10, the particles that possessed a higher zeta potential value repelled each other and the observed aggregation was negligible. This finding indicates that the steric stability of the microgel dispersion at pH 7.45 is weak. One possible reason for this is that the ethanol was washed out during the purification process. As a result, the diminution of the electrostatic forces between the PDMAEMA microgel particles was susceptible to aggregation in the microgel dispersion, which is barely reported.

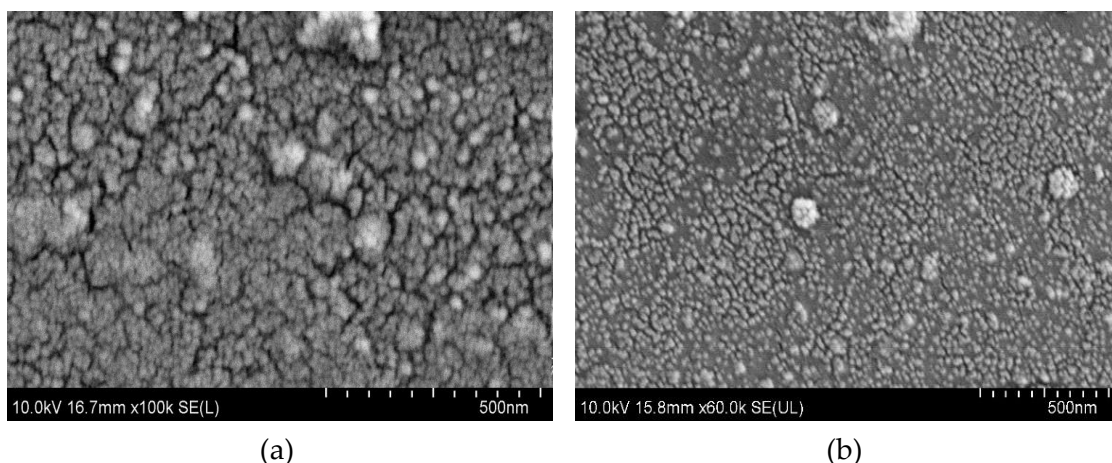


Figure 4.10. FE-SEM micrographs of PDMAEMA microgel dispersions (M0.5) at pH, (a) 7.45; (b) 10.

In order to reinforce the steric stability of the temperature-responsive microgel dispersion, the effect of ethanol on the zeta potential of the microgel dispersion was investigated. The colloidal stability of the microgel particles was first examined with no ethanol added into the microgel dispersion. Six consecutive runs were executed to obtain the zeta potential measurements, and the values fluctuated from 19 to 31 mV. The inconsistency of the measurements demonstrated that the colloidal stability of the microgel particles was highly unstable.

In order to overcome the aggregation of the dispersion overtime, ethanol was re-introduced to enhance the polarity of the dispersion. Figure 4.11. shows that the ratio of ethanol to microgel dispersion ranged from zero to 1:8 at pH 7.45. As the ethanol to microgel dispersion ratio increases from 1:1 to 1:5, the zeta potential gradually decreases, from -5.2, -13.7, -21.5, and -22.8 mV, respectively. When the ratio increases from 1:6 towards 8, the zeta potential values were comparable, due to the latter sample having a higher deviation. The results suggest that there is a limiting amount of surface charge on each particle. Incorporation of an excessive or insufficient amount of ethanol can reduce the effective charge of the particle.

According to the zeta potential data, the optimum ratio of ethanol to microgel dispersion is 1:5. The optimum ethanol ratio was then used to examine the zeta potential with respect to the temperature-responsiveness of the PDMAEMA microgel particles. With the introduction of ethanol into the dispersion, the zeta potential at pH 7.45

increased from 4.5 ± 1.3 mV to an average of 14.7 ± 0.8 mV, as shown in Figure 4.8. Moreover, the zeta potential values stayed relatively constant, indicating that the temperature-responsiveness of a microgel dispersion does not have an effect on the zeta potential. Despite the zeta potential being lower than the ideal value, 30 mV or -30 mV, the colloidal stability of the dispersion was considerably improved. This optimum ratio of ethanol to microgel dispersion was used to investigate the stability of the dispersion, which will be discussed in the later section.

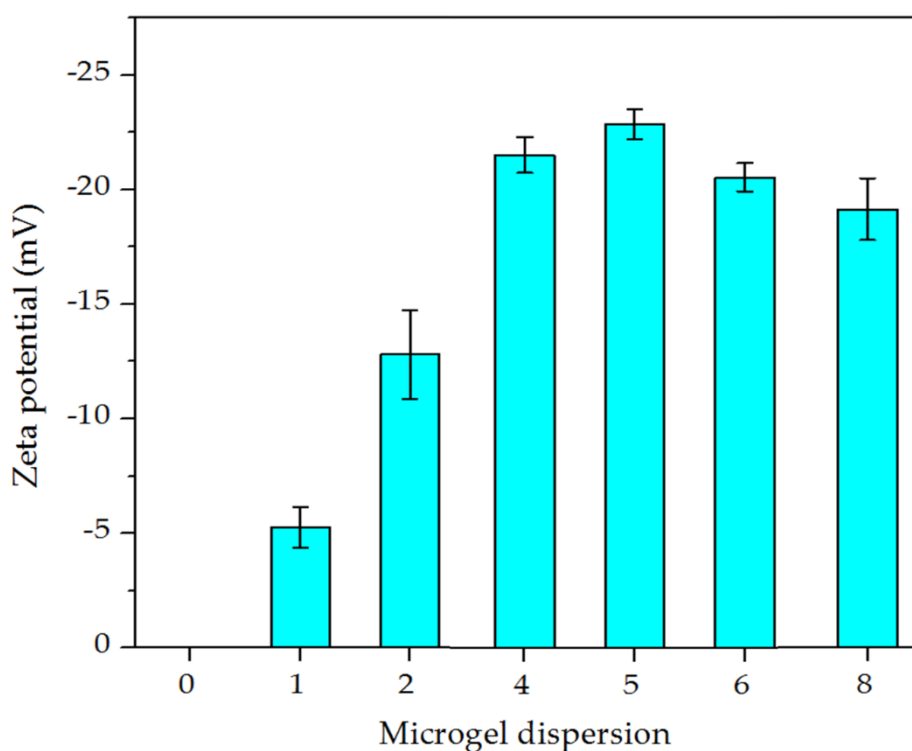


Figure 4.11. Effect of the ratios of ethanol to microgel dispersion at 37 °C, pH 7.45.

4.3.3 Dispersion stability of PDMAEMA microgel particles

The major concern after microgel synthesis is the stability of the microgel dispersion during storage for bulk production. It is crucial to examine the stability of the PDMAEMA dispersion of M0.5, hence it was monitored over a period of time: 0, 30, and 180 days.

Figure 4.12. reveals the morphology of the microgel particles that incubated in a 1:5 ethanol to microgel dispersion (M0.5-EtOH) ratio, and others without ethanol, which served as a control (M0.5-C) at 0-days of incubation. At 30-days of incubation, the majority of the M0.5-C microgel particles aggregated, forming larger and more irregular particles, as shown in Figure 4.13. (a) (ii). By the end of the 180-days incubation period, the microgel particles were 100 times greater than M0.5 at 0-days of incubation. Moreover, the regularity of the shape of the microgel particles changed significantly, as shown in Figure 4.13. (b) (ii). This outcome is attributed to an imbalance of interactions among the microgel particles themselves and the particles and solvent [127,206]. As mentioned in Section 2.5, these interactions include electrostatic forces, steric stabilisation and van der Waals forces. As PDMAEMA is a cationic microgel, at pH 7.45 the imbalance in electrostatic properties within the microgel dispersion can inevitably trigger the microgel particles to collide with each other. Consequently, they aggregate and precipitate out of the dispersion, resulting in a permanent interaction known as coagulation.

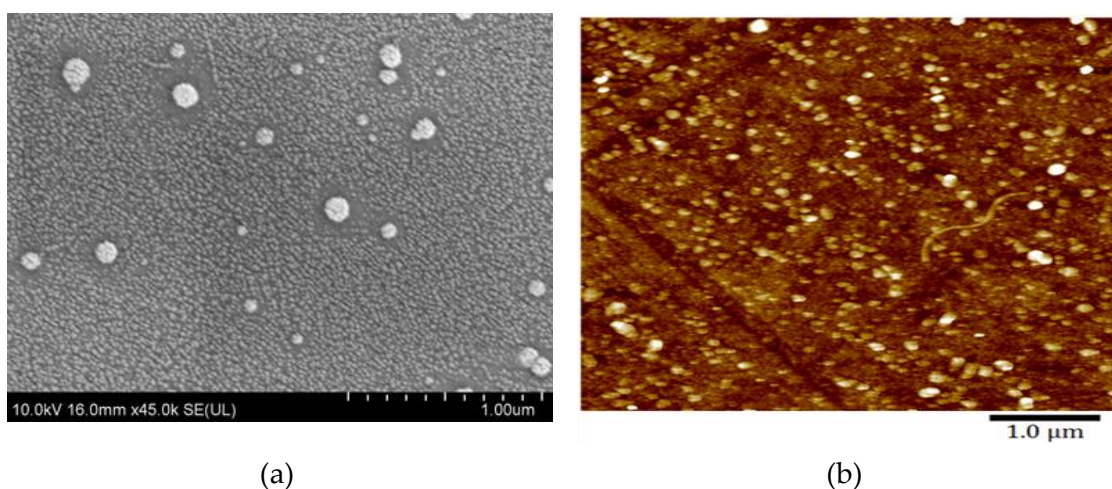


Figure 4.12. (a) FE-SEM and (b) AFM micrographs of freshly polymerised PDMAEMA microgel dispersion (M0.5) which acted as a control.

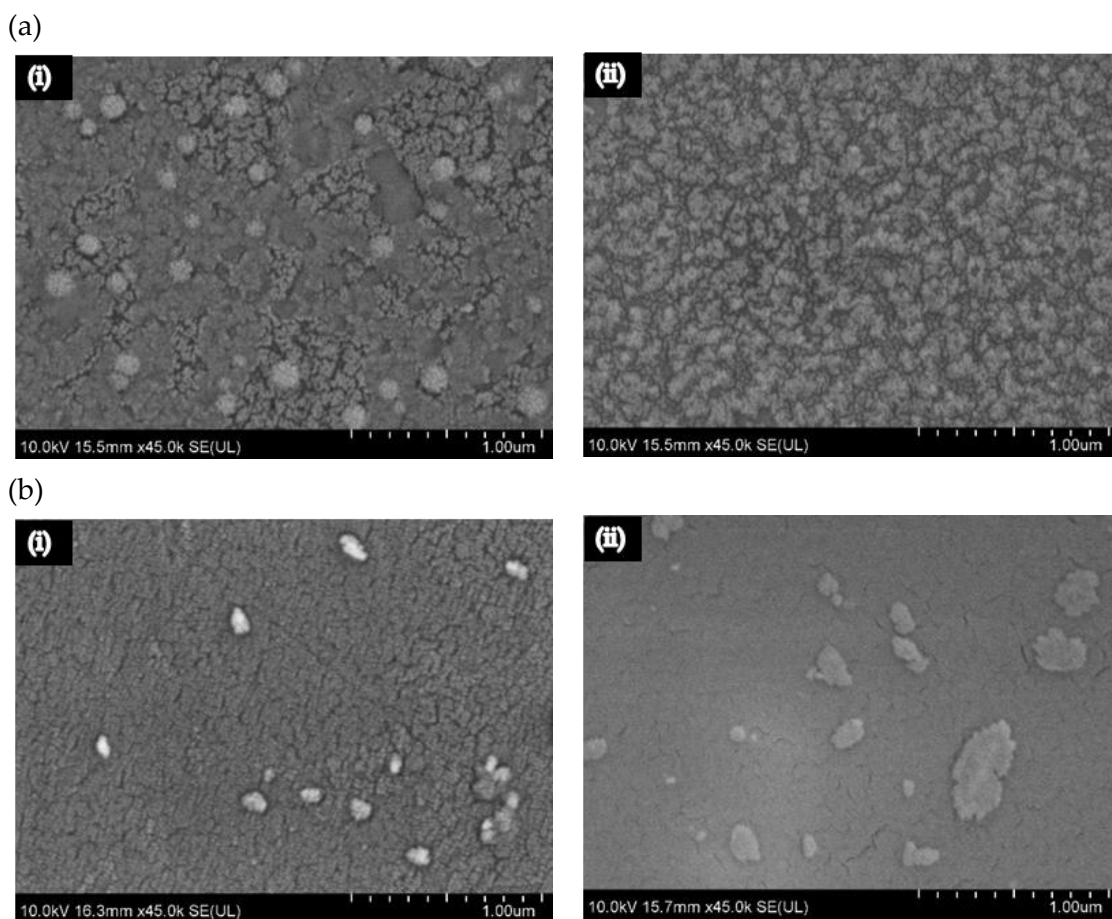


Figure 4.13. FE-SEM micrographs of PDMAEMA microgel dispersion (M0.5) incubated over a period of time (i) with (M0.5-EtOH) and (ii) without (M0.5-C) 1:5 ethanol to microgel dispersion ratio. (a) 30-days, (b) 180-days.

On the other hand, M0.5-EtOH microgel dispersion exhibits some degree of stability, although minor aggregation was observed. One possible reason would be the absence of agitation during incubation. Due to the difference in density between ethanol and water, the ethanol distribution in the microgel dispersion may become heterogeneous over a period of time. Subsequently, this leads to an imbalance in electrostatic forces occurring between the microgel particles and solvent, which eventually weakens the mutual repulsion that takes place surrounding the microgel particles.

In order to support the above statement, the hydrodynamic diameter of 180-days dispersions for both, M0.5-EtOH and M0.5-C were re-examined after constant agitation for an hour at 100 rpm. It was found that the hydrodynamic diameter of M0.5-EtOH dispersion was approximately 570 nm at 37 °C at pH 7.45, wherein the M0.5-C dispersion

was almost twice as large, as shown in Figure 4.14. These outcomes show that the interaction equilibrium within a dispersion is crucial to achieving dispersion stability. Moreover, an optimum ratio of ethanol and microgel dispersion could provide considerable stability and allow for sufficient short-term storage (of approximately 30-days), which would allow for bulk production prior to the next application.

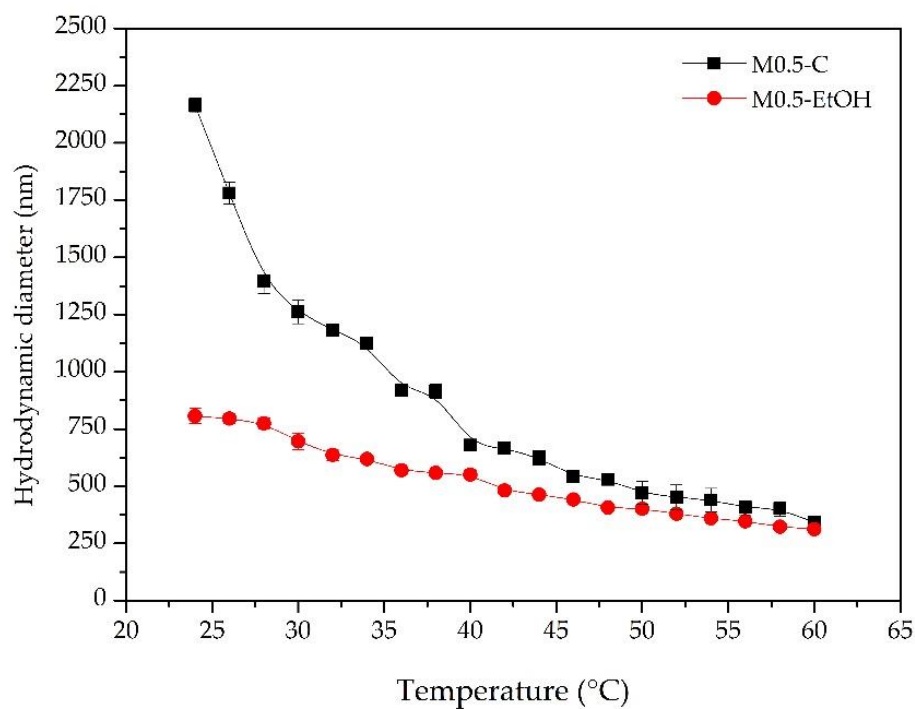


Figure 4.14. The hydrodynamic diameters of the PDMAEMA microgel particles after 180-days incubation at a temperature ranging from 25 to 60 °C at pH 7.45. (■) M0.5-C; (●) M0.5-EtOH.

4.4 Conclusion

The PDMAEMA microgel particles were synthesised by free radical polymerisation using DMAEMA as the monomer and MBAA as the cross-linker. The effect of polymerisation parameters, including steric stabilisers, cross-linkers and monomers concentration with respect to temperature-responsive behaviours were investigated. Both PVP and ethanol showed comparable steric stability, however, the addition of PVP exhibited UCST, which means it is inappropriate for use in dialysis and reprocessing. Therefore, ethanol that exhibited LCST was chosen as a stabiliser. The effect of cross-linker concentration on the microgel dispersion revealed that, with higher MBAA content, the core of the PDMAEMA microgel particles were highly cross-linked and, as a result, smaller microgel particles were formed. In addition, the optimum ethanol to microgel dispersion ratio using the zeta potential was also studied. With the addition of a 1:5 ethanol to microgel dispersion ratio, the zeta potential increased from approximately zero to 14.7 mV at pH 7.45. The morphology studies showed that the microgel dispersion that used with ethanol exhibited better stability, whereby the microgel dispersion without ethanol demonstrated a significant change in shape and size after 180-days of incubation.

Chapter 5: DEVELOPMENT OF A MICROGEL-FUNCTIONALISED HOLLOW FIBRE MEMBRANE VIA HYDROPHILIZATION BY EMBEDDING PDMAEMA MICROGEL PARTICLES ON PVDF/PSF HOLLOW FIBRE MEMBRANE

5.1 Overview

To improve the surface properties of the hollow fibre membranes, surface modification was performed to enhance the hydrophobicity of the membrane. The PVDF/PSF (S15-15) hollow fibres and PDMAEMA microgel dispersion (M0.5) that were concluded from Chapter 3 and 4, respectively were chosen as the potential blends of the substrate and microgel dispersion for the following embedment experiments.

Three different surface modification techniques were compared: dip-coating, interfacial polymerisation and a combination of dynamic adsorption and interfacial polymerisation, or, in short, dynamic-interfacial polymerisation. The modified membranes were pre-characterised using visual examination through FE-SEM to exclude unsatisfactory microgel embedment. A two-step hydrophilization was determined for microgel particle embedment. The decision was made due to the uniformity of embedment provided by dynamic adsorption and the benefits of chemically bonding two materials. The modification of the membrane, including the water contact angle, protein compatibility, and the stability of the functionalised hollow fibre membranes were methodically examined.

5.2 Experimental

5.2.1 Materials

p-Xylyene dichloride (XDC) was used as the cross-linking agent and supplied by Sigma-Aldrich, Japan. BSA with 98% purity was supplied by Merck, USA. The BSA solution was prepared by mixing a buffer solution of pH 7.45 made of sodium dihydrogen phosphate anhydrous and disodium hydrogen phosphate anhydrous from Friendemann Schmidt Chemical Pty. Ltd., Australia.

5.2.2 Fabrication of PVDF/PSF-PDMAEMA functionalised hollow fibre membranes

5.2.2.1 Preparation of PVDF/PSF hollow fibre membranes

S15-15 hollow fibre membranes were fabricated by the dry-wet spinning of a polymer/diluent weight ratio of 20/80 polymer dope solution. The weight ratio of PVDF/PSF was 100/15 and was dissolved by constant stirring in DMAc at room temperature to form a homogeneous solution. The polymer dope solution and 15 wt% DMAc/water mixture of internal coagulant were dispensed through the spinneret at a controlled volume rate using syringe pumps. The procedure was described in Section 3.2. A desired length and amount of hollow fibre membranes were air-dried at ambient temperature before any further characterisation and study. The remaining hollow fibre was kept in distilled water until use.

5.2.2.2 PDMAEMA microgel synthesis

M0.5 dispersion was synthesised with 0.5 wt% MBAA and DMAEMA in an ethanol/water mixture via free radical dispersion polymerisation. The synthesis was performed in a single step preparation that employed a conventional stirring technique. The procedure used was described in Section 4.2.2. An additional step was performed, wherein the synthesised microgel dispersion was filtered through a hydrophilic PTFE membrane filter with a 0.45 μm pore size to restrict the hydrodynamic size of the microgel particle below 500 nm. After this, a purification process was performed using the vacuum filtration technique described in Section 4.2.3.

5.2.2.3 Membrane embedment techniques

PDMAEMA-PVDF/PSF functionalised hollow fibre membranes were prepared by embedding PDMAEMA microgel particles onto the outer surface of the S15-15 membrane. The membrane was cut to a length of 5 cm. Then, both ends of the hollow fibre membrane were sealed and pre-treated by immersing them in ethanol. M0.5 dispersion was prepared using an optimal mixture of ethanol and microgel dispersion (in a 1:5 ratio, as determined in Section 4.3.2).

1. Dip-coating

S15-15 hollow fibres were dipped into 5 mL of M0.5 dispersion, which was supported with an O-ring adhered on a glass plate. The M0.5 dispersion was allowed to contact the surface of the membrane for 5 min. The coating process was repeated at least three times. The fibre was allowed to air dry before the next coating at room temperature. The resulted membrane was kept moist by placing it on pre-wetted filter paper in a petri-dish prior to characterisation.

2. Interfacial polymerisation

XDC was used as the cross-linking agent between the membrane and microgel particles. XDC was dissolved in ethanol at a pre-determined concentration. After the S15-15 membrane was pre-treated, it was placed on a glass plate, which was adhered with an O-ring. Then, S15-15 hollow fibres were immersed into the 5 mL M0.5 dispersion and the fibres were allowed to contact the membrane surface for 5 min. The coating process was repeated at least three times. The excess M0.5 dispersion was removed and the membrane was air-dried at ambient temperature, allowing a thin film to form on the surface of the membrane. Subsequently, 5 mL of the XDC-ethanol solution at 10 g/L was deposited onto the membrane, which was coated with the M0.5 dispersion for 10 min to encourage the interfacial cross-linking reaction. In order to prevent the evaporation of the ethanol during the cross-linking reaction, the reaction was performed in a closed chamber. The cross-linked membrane was then rinsed with DI water to remove any excess XDC on the membrane surface. The resulted membrane was kept moist using pre-wetted filter paper in a petri-dish prior to characterisation.

3. Dynamic-interfacial polymerisation

Membrane modules were made to facilitate the dynamic adsorption of the microgel particles, as described in Section 3.2.4, but with a 5 cm effective

length. The dynamic coating procedures adopted was an outside-in coating. Hence, the membrane module was filled with M0.5 dispersion until it reached the top of the module. Then, both orifices of the membrane module were sealed to prevent leakages. The outside-in coating was performed at a constant suction of 0.33 mL/min at ambient temperature. The flow rate of the suction was determined using the closest rate achieved prior to the membrane collapsing. The M0.5 dispersion was allowed to pass through the membrane for a certain period of time. The excess M0.5 dispersion was removed by passing DI water through the shell and lumen of the membrane. Subsequently, the XDC-ethanol solution (at 10 g/L) was injected into the membrane module, and the interfacial cross-linking reaction was performed for 10 min. In order to prevent the evaporation of ethanol during the cross-linking reaction, both orifices of the membrane module were sealed. The cross-linked membrane was then pass through with DI water at a constant flow rate to remove any excess XDC on the membrane surface until the water ran clear. The resulted membrane was kept moist using pre-wetted filter paper in a petri-dish prior to characterisation.

After the embedment process was completed, the freshly prepared functionalised membranes were subjected to 250 mL DI water and stirred at 100 rpm for 30 min to remove any uncoated microgel particles.

5.2.3 Characterisation of PVDF/PSF-PDMAEMA functionalised hollow fibre membranes

5.2.3.1 Functionalised hollow fibre membrane morphologies

The morphologies of the functionalised membrane were determined by FE-SEM and AFM, as described in Section 3.2.5.4. At least three locations were measured for each sample.

5.2.3.2 Hydrophilicity measurements

The water contact angle of the functionalised membrane surface was measured using the sessile drop method. The functionalised membranes were air-dried at ambient

temperature prior to measurements being taken. The wettability of the membrane surface was characterised using a contact angle goniometer (ramé-hart, 100-25-A). A water droplet was introduced on the surface of the membranes and the contour of the water drop was recorded. The mean water contact angle data was calculated using six measurements from different locations of the membrane surface.

5.2.3.3 Protein compatibility

The protein adsorption of the membranes was measured. Firstly, the membrane was placed in a 1.5 mL centrifuge tube with 1 mg/mL BSA in phosphate-buffered solution at pH 7.45 and incubated at 37 °C for 1 hour. The protein concentration was determined using a UV-Vis scanning spectrophotometer at a wavelength of 280 nm. The amount of adsorbed protein on the membrane surface was calculated using the following equation:

$$\text{Adsorption amount } (\mu\text{g}/\text{cm}^2) = \frac{(C_0 - C) \times V}{S} \quad \text{Eq. 5.1}$$

Where C_0 and C are the protein concentrations before and after adsorption, respectively, V is the volume, and S is the area of the membrane. The given value is the average of five different measurements, and the data were expressed as a mean \pm standard deviation (SD).

5.2.3.4 Stability of the functionalised hollow fibre membranes

Two types of stability testing on the functionalised hollow fibre membranes were conducted. First, a long-term application was assessed using pure water permeation (PWP) for ten consecutive days. Second, a backwashing treatment using ultrapure water. For the backwashing treatment, the membrane was exposed to 20 backwash cycles, each of which was at 3 bar for 1 min. The PWP was measured after every fifth backwash cycle. A schematic diagram of a PWP set-up, as previously shown in Figure 3.1.

5.3 Results and discussion

5.3.1 Effect of embedment techniques on hollow fibre membranes

In this study, the functionalised hollow fibre membranes were prepared by embedding M0.5 microgel dispersion on the outer surface of the S15-15 hollow fibre. A comparison between dip-coating, interfacial polymerisation and dynamic-interfacial polymerisation was made. The embedment technique that is selected is crucial to achieving a uniform and stable coated layer, and thus to improving the surface hydrophilicity of the membrane surface.

Figure 5.1. shows the FE-SEM micrographs of the PVDF/PSF hollow fibres embedded with PDMAEMA microgel particles with different embedment techniques, compared with the bare PVDF/PSF membrane surface. The morphological features revealed that there are no significant differences between the bare PVDF/PSF membrane surface, which represents a control, and the dip-coated membrane (after it was rinsed with DI water). Moreover, the distribution of microgel particles displayed on the membranes between dip-coating (before being rinsed with DI water) and interfacial polymerisation techniques are comparable, since similar embedment processes were performed, as shown in the inset of Figure 5.1. (b), and Figure 5.1. (c), respectively. Both membranes showed that the microgel particles were scattered and had only a limited deposit of microgel particles instead of particles that were uniformly deposited on the membrane surfaces.

Two possible reasons can explain these observations: (1) poor wettability of the hollow fibre membranes; and (2) the low density of the microgel dispersion. PVDF and PSF polymers that naturally exhibit hydrophobic behaviours had the lowest amount of hydrogen bonding interactions in the boundary layer between the PVDF/PSF membrane interface and water, thus leading to the poor wettability. Because of the repulsion of water molecules from the hydrophobic membrane is a spontaneous process [8]. Therefore, when a low-density microgel dispersion was used, the hydrophobicity of that PVDF/PSF membrane causes the hydrophilic solutes (which were dispersed in water) to concurrently repel from the membrane surfaces, resulting in limited amount of microgel

particles on the membrane surface. This indicates that the dip-coating approach is practically impossible for depositing low-density polymers. This not only failed to achieve a uniform depositing, but it also demonstrated the instability of the embedded microgel layer, which could be washed away during the operation and reprocessing. On the other hand, interfacial polymerisation showed the potential that the embedded microgel particles could sustain being rinsed under pressurised conditions. Therefore, interfacial polymerisation was used in conjunction with another adsorption approach.

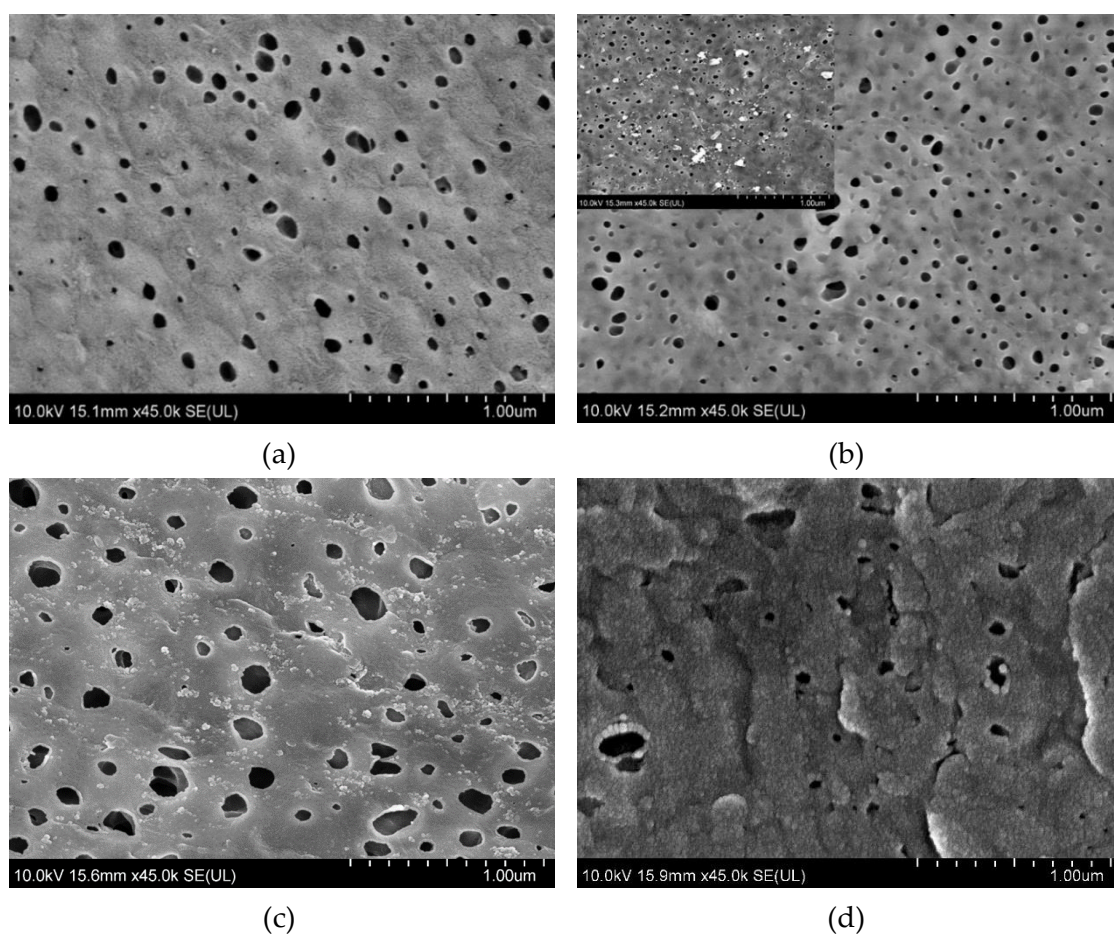


Figure 5.1. FE-SEM micrographs of the techniques applied to embed PDMAEMA microgel dispersion (M0.5) on PVDF/PSF (S15-15) hollow fibres at room temperature. 10 g/L XDC-ethanol was used to undergo interfacial polymerisation for 10 min. All membranes were rinsed with fresh DI water by stirring at 100 rpm for 30 min. (a) Uncoated-bare PVDF/PSF membrane; (b) dip-coating, inset: before rinsing; (c) interfacial polymerisation; and (d) dynamic-interfacial polymerisation.

In order to improve the distribution of the microgel particles on the membrane surface, dynamic adsorption was employed, as reported in the literature [80,89,140,141,207], whereby the microgel dispersion was filtered through the outer membrane surface into the lumen. This was followed by an interfacial polymerisation that occurred at the solid-liquid interface between PDMAEMA microgel particles and XDC solution and the membrane at room temperature. Figure 5.1. (d) shows the membrane surfaces embedded with microgel particles using the dynamic adsorption approach. It was found that, using dynamic adsorption, a uniform distribution of microgel particles on the membrane was achieved.

Nevertheless, when the pore sizes of the membrane were compared with the bare membrane, no significant changes were observed. It should be noted that the observed surface structure may differ from the structure under filtration conditions because, when using the FE-SEM observation technique, membranes have to be dried and were carried out in a vacuum environment. Therefore, AFM examination was conducted. In order to investigate the actual change in surface morphology with the embedded PDMAEMA using dynamic-interfacial polymerisation, the modified membranes were kept moist at all times (which will be discussed in Section 5.3.3).

As mentioned earlier, the interfacial polymerisation is expected to provide strong interactions, resulting in greater stability of the embedded microgel particles on the membrane, since they were chemically-bonded. The strong interaction is attributed to the formation of a cross-linked molecular network. The network is developed from quaternary ammonium salt through an alkylation reaction between the tertiary amino groups in the side chains of PDMAEMA and chloromethyl groups in the bifunctional XDC, as presented in Figure 5.2. [154,208], whereby chemical bonding between the membrane and microgel particles could be possibly accomplished using XDC cross-linking, which would lead to polar bonds being formed between the membrane and microgel particles.

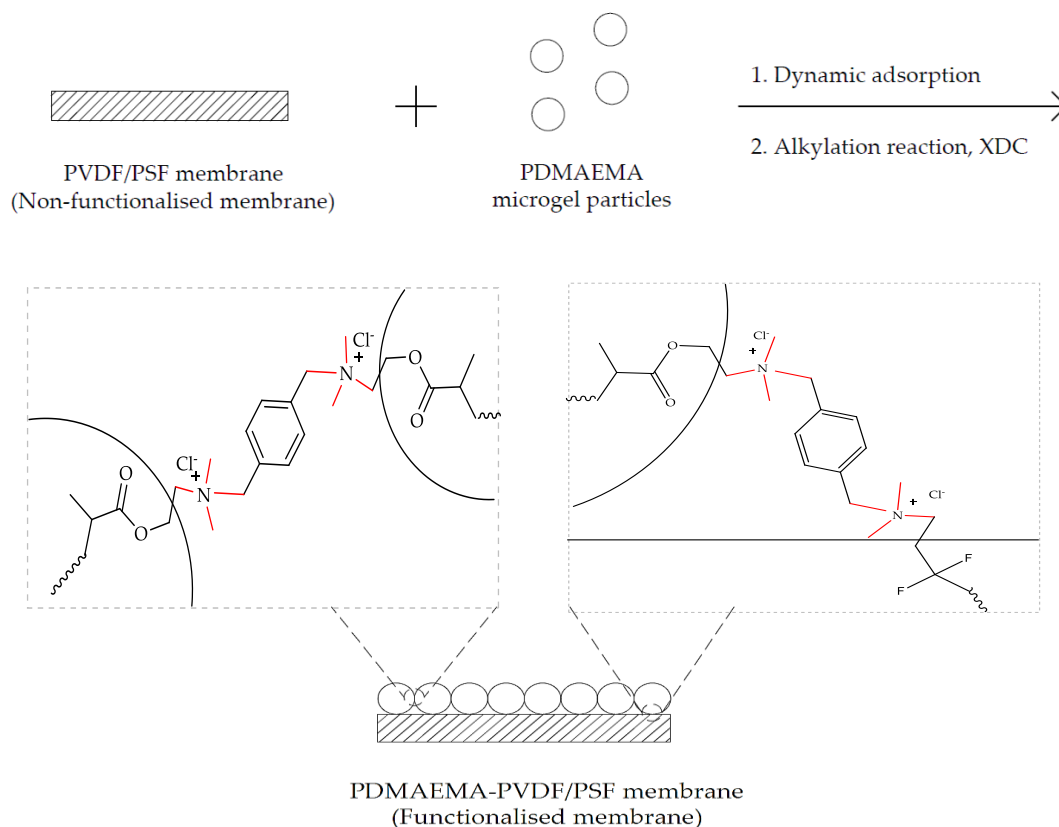


Figure 5.2. A schematic representation of the preparation of the PDMAEMA-PVDF/PSF membrane and formation of the quaternary ammonium salt (red bonds) when PDMAEMA was cross-linked with XDC.

Aside from improving the interaction between the “membrane-microgel” and “microgel-microgel”, the quaternary ammonium salt offers supplementary benefits in the context of this study. One of them is the ability to attract water, given the hygroscopic properties of the quaternary ammonium salt [209]. Another is that, as a cationic membrane surface, it has good antimicrobial properties [102,105,210]. Rawlinson, *et al.* [105] described that the way in which quaternized PDMAEMA works was similar to other cationic biocides. First, it involves direct binding to bacteria and diffuses through the cell wall. This is followed by disruption of the cytoplasmic membrane and then cell death. As a result, the embedded PDMAEMA microgel not only enhances the wettability of the membrane surface, also makes it less vulnerable to infection upon storage between clinical applications.

In summary, dip-coating, which is used as a physical adsorption approach, is inevitably a weaker embedment technique compared to those that use chemical-

bonding. The combination of dynamic adsorption and interfacial polymerisation, which referred to as dynamic-interfacial polymerisation, offers a promising approach, given that the microgel particles were uniformly distributed on the membrane surface. Therefore, further characterisations of the embedded membrane using dynamic-interfacial polymerisation were investigated. The successfully embedded membranes using microgel particles and a pure PVDF/PSF membrane will be referred to in the following discussion as functionalised and non-functionalised membranes, respectively.

5.3.2 Effect of embedment parameter on membrane permeability

In this study, this outside-in coating uses a suction approach to replicate a vacuum, but uses a lower force (indeed, one that relatively low when compared to other studies that have been reported [80,89,140,207]). One main difference with the embedment processes is that the microgel dispersion was being forced through the membrane shell to the lumen, instead of flowing through the shell side of the membrane. The use of a higher flow rate or vacuum-assisted approaches were not suitable for this study because the pores of the membrane were completely blocked. It is likely that the obstruction of the pores will cause the membrane permeability to decrease dramatically.

The effect of the embedment/coating time of the M0.5 dispersion on the membrane permeability (PWP), which was prepared at a constant suction with lower force, was examined, as shown in Figure 5.3. Upon increasing the coating time, from 0 to 30 min, the PWP gradually increased. This suggests that the membrane hydrophilicity is improved, hence the water can effortlessly pass through the membrane. When the coating time was increased to 60 min, the PWP dropped, rather than increased, indicating that the maximum microgel adsorption had been reached. A further increase in the coating time will not enhance the membrane permeability, whereby it will gradually decline. This is attributed to the increasing thickness of the coating, meaning that, in parts, the membrane pores are being concealed by the microgel particles. Similar results were reported elsewhere in the literature [141].

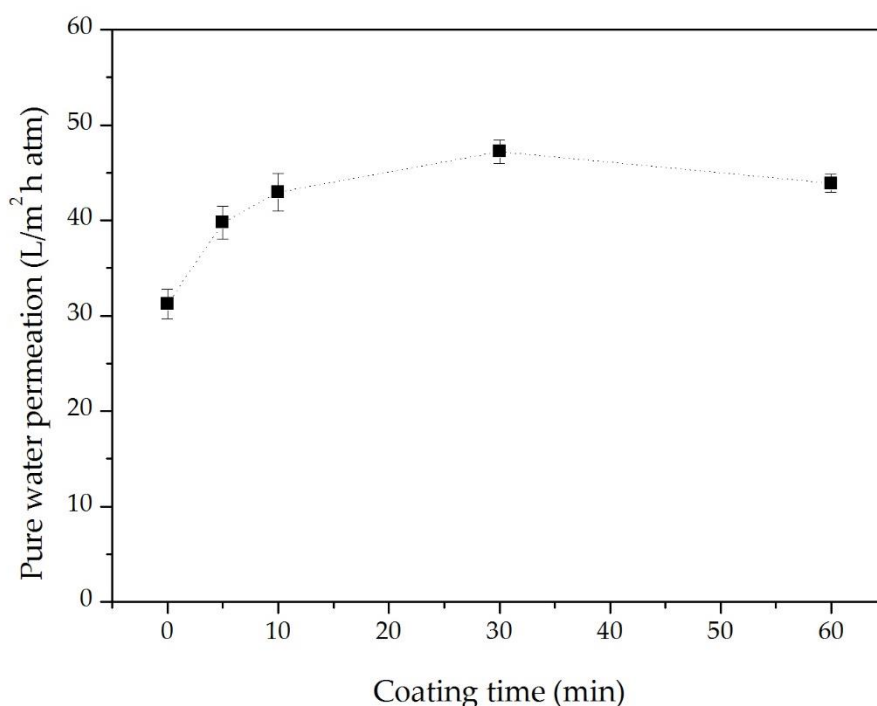


Figure 5.3. Effect of the coating time of the microgel dispersion (M0.5) on the pure water permeation of the functionalised hollow fibre prepared using dynamic-interfacial polymerization at a constant suction of 0.33 mL/min, and 10 g/L XDC for 10 min.

Figure 5.4. shows that the longer the coating time for M0.5, the more PDMAEMA microgel particles that will be adsorbed on the membrane surface. The thickness of the microgel particle layer on the membrane surface increases from approximately 70 nm to 120 nm with a coating time of 30 min and 60 min, respectively. Moreover, at 60 min of coating time, the area surrounding the pores differed significantly from the bare PVDF/PSF membrane, as shown in Figure 5.1. (a). The micrographic features verify that the embedded microgel particles were not only uniformly distributed on the membrane surface, but also improved the adsorption surrounding the pore surface. What's more, they were also transported 1-2 μm into the porous structure.

The changes in membrane permeability indicate that the coating time has reached its equilibrium at 30 min; beyond 30 min, there was little or no impact on the membrane permeability. Therefore, the subsequent examination on the functionalised membrane was prepared using an optimum coating time of 30 min.

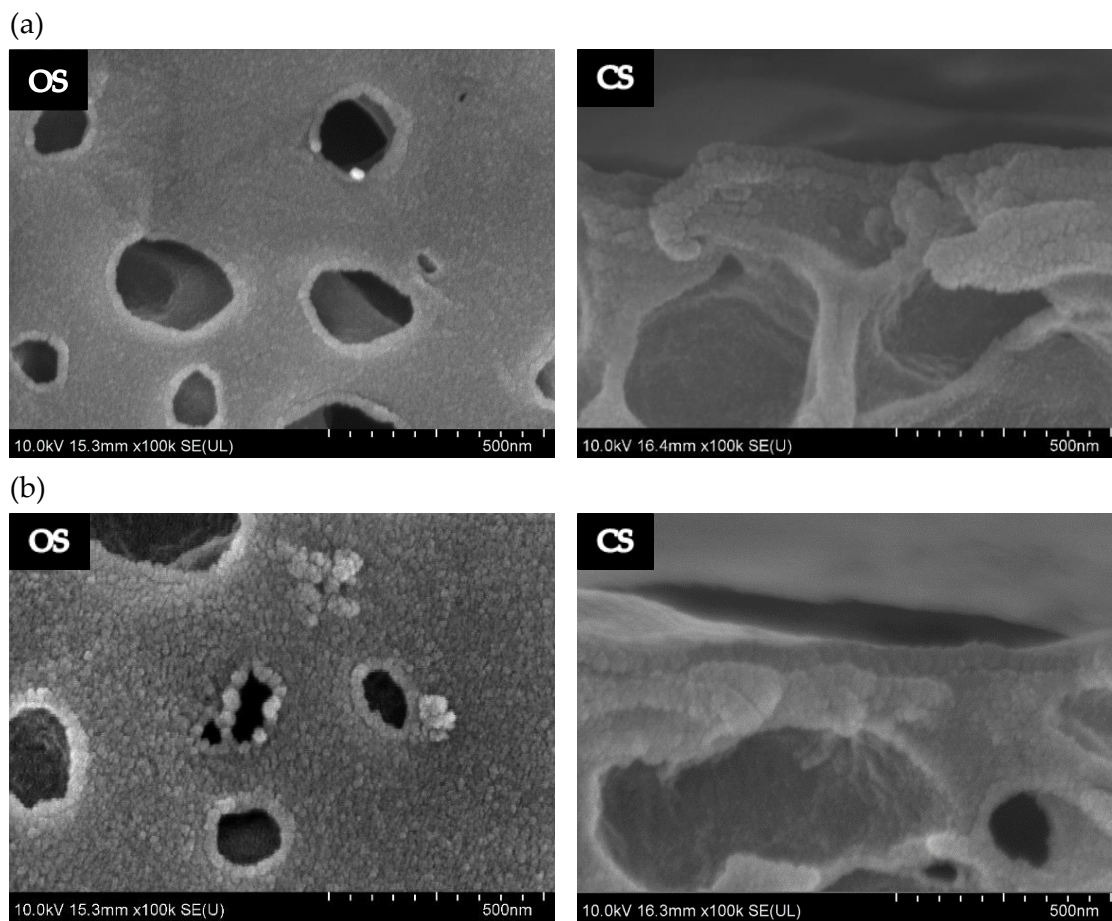


Figure 5.4. FE-SEM micrographs of the outer surface and cross-section of the functionalised hollow fibre membranes with M0.5 solution using dynamic-interfacial polymerisation. Constant suction at 0.33 mL/min for (a) 30 min; (b) 60 min. OS and CS are outer surface and cross-section, respectively.

5.3.3 Characterisation of PDMAEMA microgel layer on PVDF/PSF membrane surface

Wettability (hydrophilic or hydrophobic) can be affected by surface roughness, whereas surface roughness affects the contact angle. These inter-related properties will subsequently affect the membrane's biocompatibility, because the behaviour of the proteins on the membrane surface is dependent on the surface properties. Therefore, the surface topography, water contact angle and protein adsorption will be examined.

5.3.3.1 Surface topography and surface roughness

Figure 5.5. shows the 3-D AFM micrographs of the outer surface of the functionalised and non-functionalised S15-15 hollow fibre membranes. In the case of the non-functionalised membrane, smooth surface topography was observed, whereby the functionalised membrane exhibited a pointed spherical surface topography. Moreover, the resulted morphological features confirmed that the PDMAEMA microgel particles were uniformly distributed. The surface roughness parameters, which are expressed as R_a , R_q , and R_{max} , are tabulated in Table 5.1., which shows that the functionalised membrane has higher roughness parameters, indicating that the membrane surface is hydrophilic. High surface roughness in conjunction with a lower contact angle is the general characteristics of wettability that have been reported in literature [188,211,212]. Further confirmation of the membrane hydrophilicity is performed via water contact angle measurement, which will be discussed in the following section.

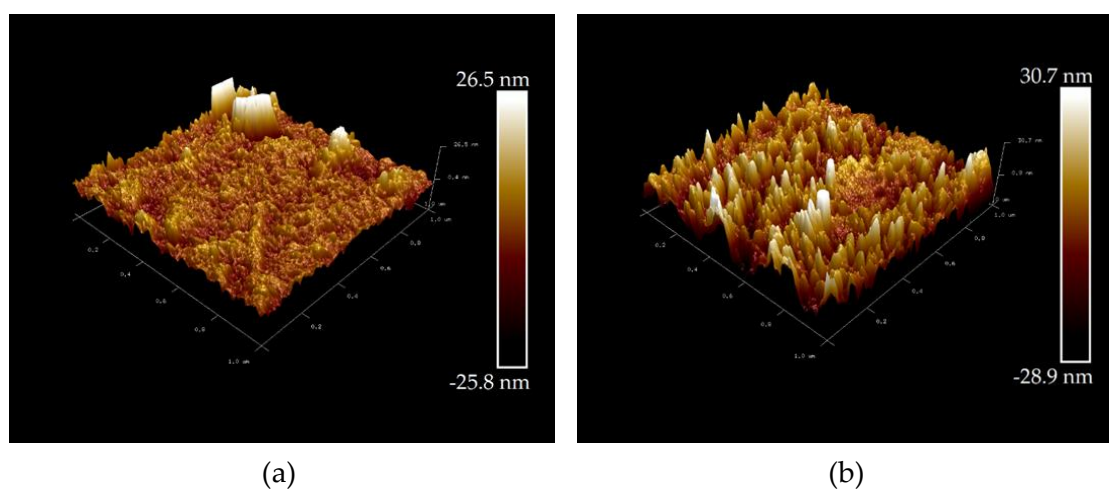


Figure 5.5. AFM micrographs of the outer surface of the S15-15 hollow fibre membranes with M0.5 dispersion using dynamic-interfacial polymerisation: (a) non-functionalised membrane; (b) functionalised membrane.

Table 5.1. Surface roughness of the non-functionalised and functionalised S15-15 hollow fibre membranes.

Membranes (S15-15)	R_a (nm)	R_q (nm)	R_{max} (nm)
Non-functionalised membrane	4.0 (± 0.82)	5.8 (± 0.64)	65.7 (± 0.91)
Functionalised membrane	6.0 (± 1.28)	8.6 (± 0.37)	84.9 (± 0.21)

Note: R_a, average roughness; R_q, root mean square roughness; R_{max}, maximum roughness distance between the highest and the lowest data points. The values in brackets are standard deviation.

5.3.3.2 Water contact angle measurement

Surface hydrophilicity is usually employed to determine the anti-fouling property of ultrafiltration membranes [213]. Aside from surface roughness, the water contact angle is also used to evaluate the surface hydrophilic and hydrophobic properties of the membranes. The terms hydrophilic and hydrophobic are defined as follows: with a given liquid, a solid is wettable when a contact angle of less than 65° occurs, and if a contact angle of greater than 65° occurs on a smooth solid, the solid is not wettable [214].

Figure 5.6. depicts the time-dependency of the water contact angles measurement on the functionalised hollow fibre and non-functionalised membranes at room temperature. The time-dependency was studied to examine the time interval between an air-dried and swollen embedded microgel layer to identify the swelling rate. At the beginning ($t = 0$ s), the water contact angle of the non-functionalised membrane was at least 26% higher than the functionalised membrane. Even with more time, the water contact angles of the non-functionalised membrane remain relatively constant (approximately 101°), whereby the contact angles for the functionalised membrane gradually decreases. When approaching 80 seconds, the contact angle achieved its equilibrium and hence ceased to continue to decrease. This outcome can be due to the water droplets gradually penetrating the microgel layers of the membrane. As a result, at least 80 seconds was required for the functionalised membrane to fully hydrate at room temperature. The time interval is important when designing the operation time required for regeneration, which will be discussed in the next chapter.

Aside from the intrinsic hydrophilicity of PDMAEMA microgel particles [210,215], it is worth noting that the quaternary ammonium salt groups that were developed between the microgel particles and XDC were also highly hydrophilic [215], as discussed in Section 5.3.1. Consequently, the results indicate that the hydrophobic surface of the PVDF/PSF membrane has effectively been modified to a hydrophilic surface through the embedment of PDMAEMA microgel particles. The functionalised membrane would expect to trigger less fouling due to improvements to the membrane after hydrophilization.

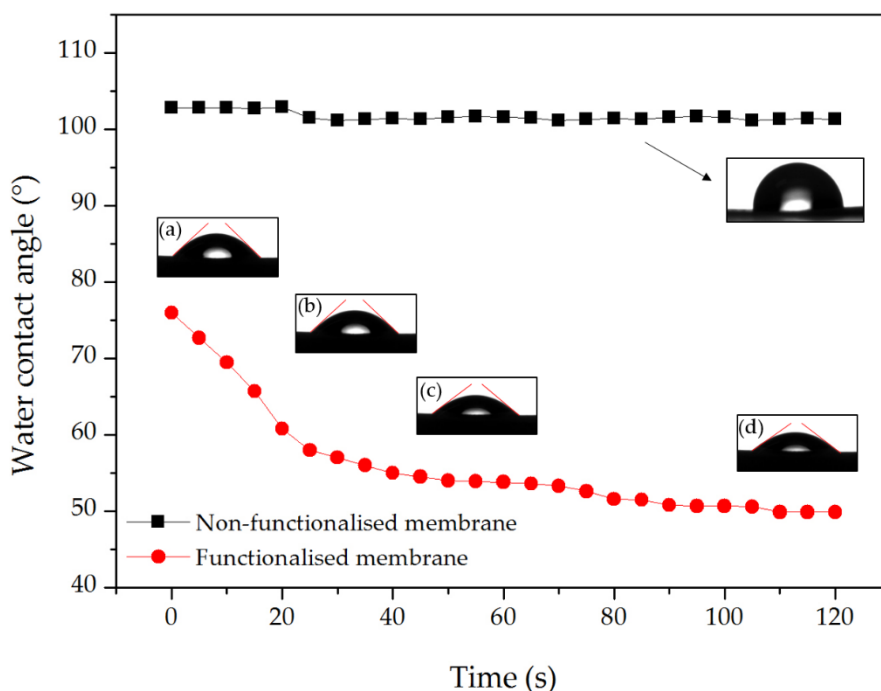


Figure 5.6. Time-dependency associated with water contact angles of the non-functionalised and functionalised hollow fibre membrane at room temperature. The inset images show the water contact angle of the functionalised membrane at different angles: (a) 75°; (b) 70°; (c) 61°; (d) 53°.

5.3.3.3 Protein compatibility of the functionalised hollow fibre membranes

The amount of protein adsorption is one of the essential characteristics of the biocompatibility of materials contacting blood. The protein adsorption of the membrane triggers clot formation and can decrease the membrane permeability over time [214,216]. A decline in the permeability eventually decreases the efficiency of the dialysis and increases the difficulty of reprocessing. In order to determine the membrane biocompatibility of the functionalised and non-functionalised membrane versus proteins, the membranes were incubated in BSA solution at 37 °C for 1 hour in a static state.

Figure 5.7. shows the amount of BSA adsorbed on the membranes. There is a significant reduction in the amount of protein adsorption on the functionalised membrane as compared to the non-functionalised membrane, which is $52.34 \pm 2.97 \mu\text{g}/\text{cm}^2$ and $24.41 \pm 3.71 \mu\text{g}/\text{cm}^2$, respectively. Table 5.2. lists protein adsorption comparison between the current work and the references. It shows that the functionalised hollow fibre membranes have greater protein adsorption than other published works. It is worth noting that both data were obtained after a rinsing process, which was not performed in the current work.

Table 5.2. Protein adsorption compared with references.

Membrane type	Additives	BSA adsorption ($\mu\text{g}/\text{cm}^2$)	Reference
PVDF/PSF	PDMAEMA	24.4	
PSF	7 – 15 wt% MPC ^a	1.0 – 0.25	[216]
PES	2 – 8 wt% HMPU ^b	4.4 – 6.5	[217]

Note: MPC represents 2-methacryloyloxyethyl phosphorylcholine, and HMPU represents heparin-mimicking polyurethane.

^a Rinsed five times with phosphate-buffered solution.

^b Rinsed slightly with a phosphate-buffered solution and three times in double-distilled water.

The higher protein adsorption of the non-functionalised membrane is expected. This outcome is postulated from the water contact angle measurement illustrated in Figure 5.6. Generally, hydrophobic surfaces have a higher tendency to adsorb larger

amount of proteins than hydrophilic surfaces. Herrwerth, *et al.* [218] reported that a material such as oligoether self-assembled monolayers, which is internally hydrophilic and has terminal groups that are also hydrophilic are the key aspects in protein resistance. This phenomenon is due to the fact that the hydrophilic surface is strongly bound with water molecules, thus forming a physical water barrier, which is harder to dislodge by the adsorbing proteins [214]. On the contrary, water molecules from the hydrophobic surface are more easily dislodged by a protein, resulting in protein adsorption and subsequently membrane fouling.

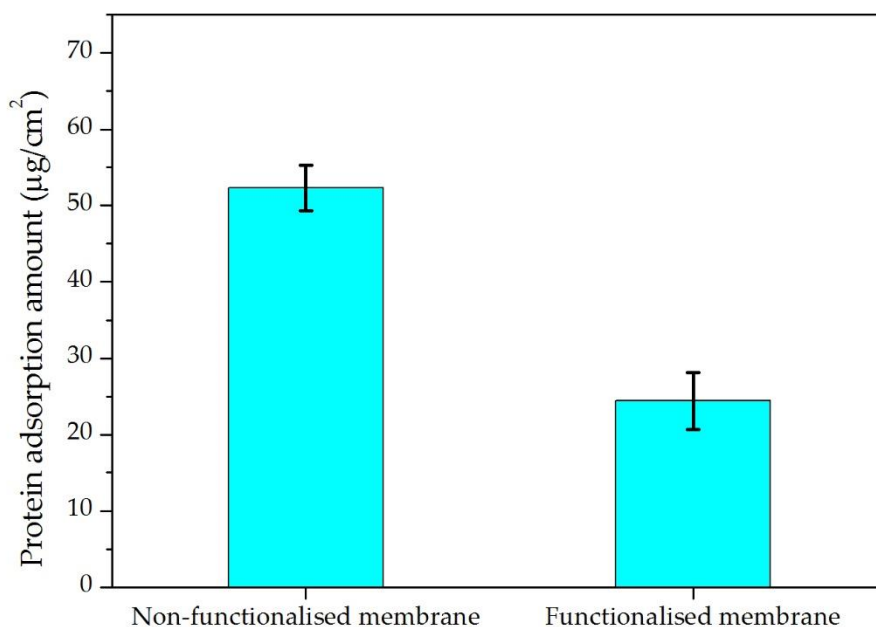


Figure 5.7. The amount of BSA adsorption on the non-functionalised and functionalised membranes determined using UV-Vis scanning at a wavelength of 280 nm. BSA solution with 1 mg/mL BSA in phosphate-buffered solution at pH 7.4 and incubated at 37 °C for 1 hour. Values were expressed as mean \pm SD, n = 5.

It is worth noting that at pH 7, BSA molecules are negatively charged [219,220], whereas the PDMAEMA microgel particles are positively charged [96,221]. Electrostatic interaction occurs between the BSA and PDMAEMA, which results in the functionalised membrane having proteins adsorbed. Nevertheless, the interaction is relatively weak due to the hydrophilic improvement of the membrane surface, where the BSA molecules

can be desorbed by rinsing the membrane with fresh DI water, as demonstrated in Figure 5.8. Similar results were also reported in the literature [214,222,223]. This phenomenon has been described by Hayashi, *et al.* [222], who concluded that, when structured water molecules form among hydrophilic constituents, which act as a physical barrier for the water molecules, water-mediated repulsion takes place at the surface. Consequently, the proteins are adsorbed loosely on a hydrophilic surface, resulting in protein resistance, which would subsequently prevent the biological responses that ultimately lead to the clot formation.

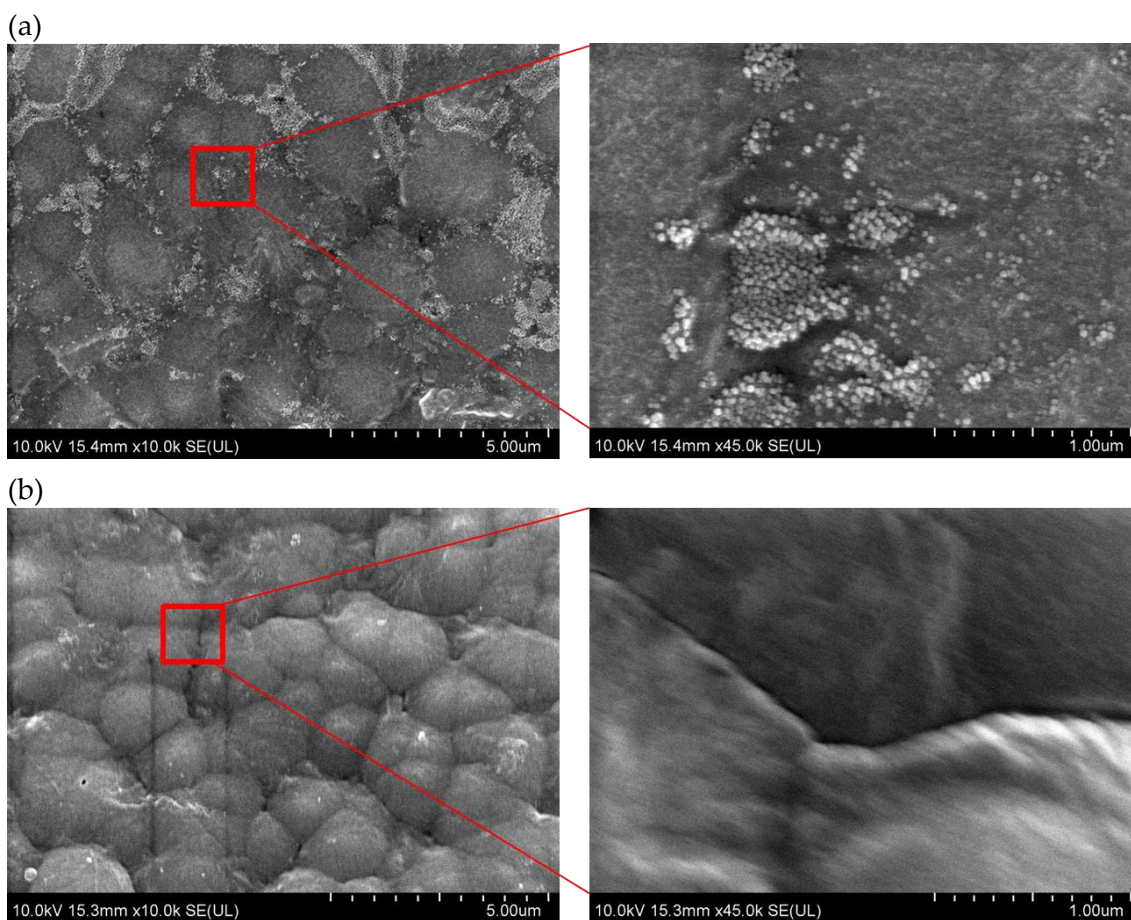


Figure 5.8. FE-SEM micrographs of the outer surface of a hollow fibre membrane coated with 1 g/L BSA in phosphate-buffered solution at pH 7.4 and incubated at 37 °C for 1 hour. All membranes were rinsed with fresh DI water. (a) Non-functionalised membrane; (b) functionalised membrane.

5.3.3.5 Stability of the functionalised hollow fibre membranes

It is important to inspect the stability of the functionalised membrane to determine the immovability of the microgel particles after chemical bonding between the “membrane-microgel” and “microgel-microgel” took place using interfacial polymerisation. The stability of the functionalised membrane is investigated with respect to long-term applications and the backwashing treatment versus membrane permeability.

Evaluation of the long-term performance of the functionalised membranes was accomplished using a standard filtration experiment with ultrapure water over ten days. Figure 5.9. shows no noticeable fluctuation in the permeability throughout the duration of the experiment. The PWP remained at approximately 46 ± 1.7 L/m² h atm. However, from day 8 onwards, a slight decrease in the PWP was observed. This unexpected reduction could be attributed to a minor blockage caused by debris within the functionalised membrane. Therefore, backwashing in conjunction with permeability testing was later performed.

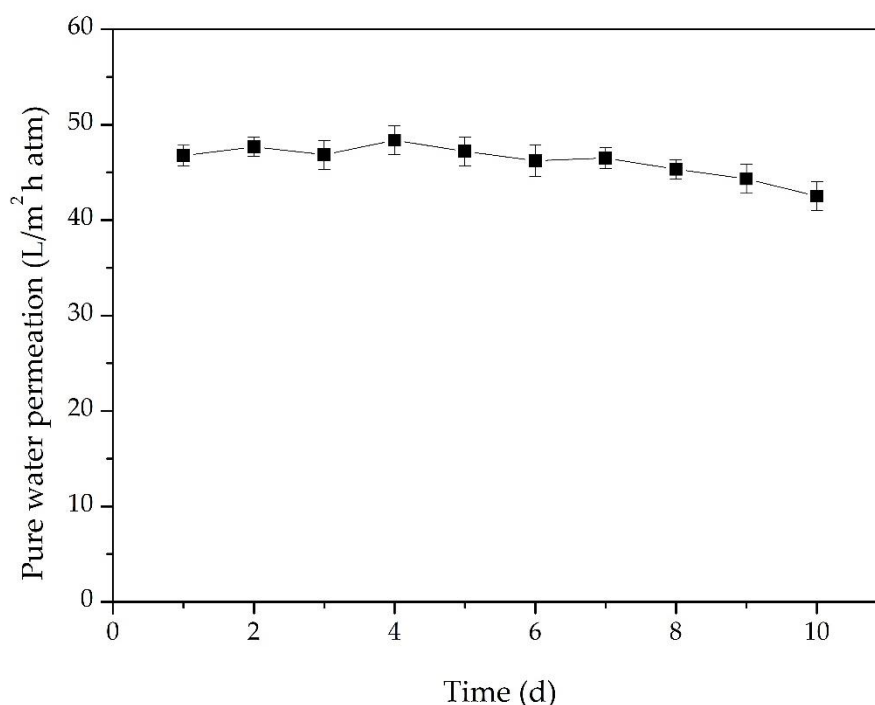


Figure 5.9. Pure water permeation of a functionalised hollow fibre membrane using dynamic-interfacial polymerization over a period of 10 days at room temperature.

The mechanical stability of the functionalised membrane was determined using backwashing, as shown in Figure 5.10. The permeability of the functionalised membrane was measured after every fifth backwash. The results show that the permeability of the functionalised membrane did not significantly change throughout the 20 backwash cycles, each of which was pressurised at 3 bar. The detection of microgel particles loss in the permeate was performed using TOC. The permeate and control (ultrapure water) exhibited similar TOC concentrations. This outcome demonstrated that the minor drop in PWP discussed previously from day 8 onwards was negligible. According to these results, it can be concluded that the functionalised membrane that was embedded with PDMAEMA microgel particles through a two-step hydrophilization using dynamic adsorption and interfacial polymerisation was reasonably stable and repeatable.

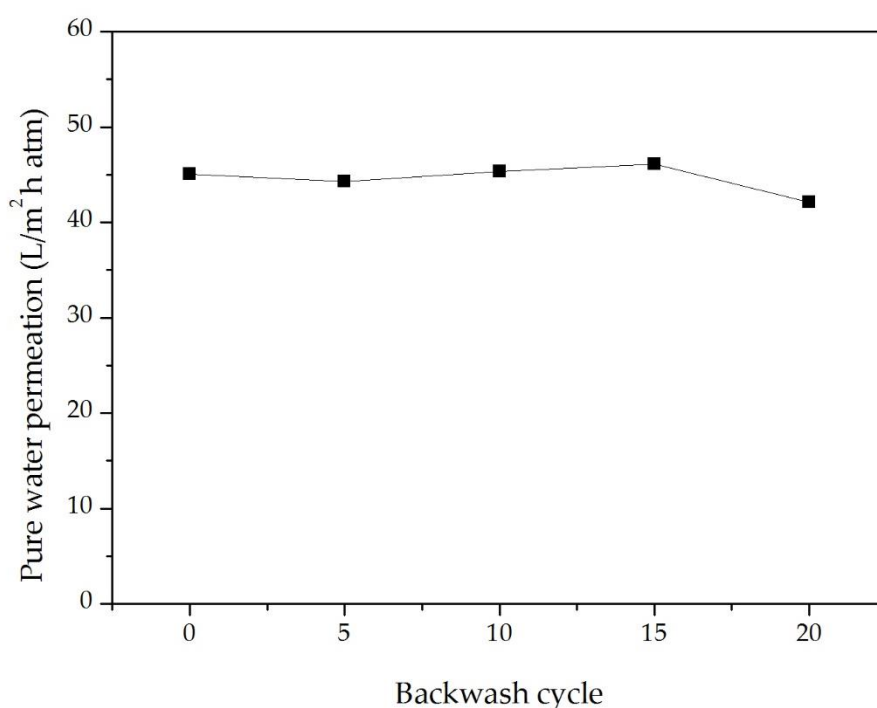


Figure 5.10. Stability of a functionalised hollow fibre using dynamic-interfacial polymerization for backwash cycles against pure water permeation conducted at 3 bar each for 1 min at room temperature.

5.4 Conclusion

The PVDF/PSF hollow fibre membrane was successfully functionalised with PDMAEMA microgel particles using the outside-in approach and dynamic-interfacial polymerisation. Physical adsorption using dip-coating was not ideal because synthesised microgel particles have a low density, which results in uneven distribution. Preliminary results demonstrated that chemical bonding between the membrane and microgel is required for more permanent embedment. The functionalised membrane exhibited two excellent improvements. First, the hydrophobic surface of the PVDF/PSF membrane was effectively modified to form a hydrophilic surface, which subsequently improved the membrane's permeability. Second, a decrease in protein adsorption on the functionalised membrane. Despite the weak electrostatic interactions between the positively charged membrane surface and negatively charged BSA molecules, the protein adsorption was notably lower than with the non-functionalised membrane. Furthermore, the functionalised membrane shows outstanding stability with respect to multiple permeability testing and backwashing.

Chapter 6: MEMBRANE PERMEABILITY AND REGENERATION OF MICROGEL-FUNCTIONALISED HOLLOW FIBRE MEMBRANES FOR DIALYSIS

6.1 Overview

The microgel-functionalised hollow fibres were created through hydrophilization using dynamic-interfacial polymerisation as described in Chapter 5. The aim of this chapter is to evaluate the regeneration of microgel-functionalised hollow fibre by performing a series of filtration experiments. The filtration experiments include determining the PWP and MWCO measurements, and protein rejection behaviours. Initially, pure water permeation was determined, followed by hemofiltration using a blood model solution. The blood model solution was comprised of BSA and a PEG with an average molecular weight of 12,000 Da. The functionalised membranes exhibit good hemofiltration performance, experience minimal fouling and have a protein retention flux of over 80%. After the hemofiltration tests, a cleaning process was undertaken as the final stage. A cleaning process that uses an external induced-stimulus (temperature) is proposed. AFM was used to examine the surface topographies of the membrane before and after cleaning.

6.2 Experimental

6.2.1 Membrane module preparation for filtration experiments

The membrane module was prepared, and is described in Section 3.2.4. The pre-treated membrane (S15-15) was immersed in DI water for 24 hours to remove glycerol and then rinsed with ethanol. Next, each module was prepared by sealing a fibre into a stainless-steel tube with a length of 22 cm. The effective length of the fibre in the stainless-steel module was 20 cm. The hollow fibre module was mounted on a permeation rig.

6.2.2 Preparation of PDMAEMA-PVDF/PSF functionalised hollow fibre membranes

PDMAEMA-PVDF/PSF functionalised hollow fibre membranes were prepared by coating PDMAEMA (M0.5) microgel particles onto the outer surface of an S15-15 membrane via dynamic adsorption polymerisation as described in Section 5.2.2.3. M0.5 was prepared with the optimal ratio of 1:5 ethanol to microgel dispersion, as determined in Section 4.3.2.

The coating procedure used was the outside-in procedure described in Chapter 5. Thus, the membrane module was filled with M0.5 dispersion and then both orifices of the module were sealed. The outside-in coating was performed at a constant suction of 0.33 mL/min at ambient temperature when the microgel particles were at swollen state. The M0.5 dispersion was allowed to pass through the membrane for 30 min. The excess M0.5 dispersion was removed by passing DI water inside-out of the membrane. Subsequently, the XDC-ethanol solution at 10 g/L was injected into the membrane module and an interfacial cross-linking reaction was performed for 10 min. In order to prevent the evaporation of ethanol during the cross-linking reaction, both orifices of the membrane module were sealed. The cross-linked membrane was then passed through with DI water to remove any excess XDC on the membrane surface until the water ran clear. The resulting module was kept moist by being immersed the module in DI water before characterisation.

6.2.3 Characterisation of functionalised hollow fibre membranes

6.2.3.1 Ultrafiltration experiments

Ultrafiltration experiments with aqueous feed solutions were used to investigate the membrane performance. The focus was on PWP, MWCO measurements, and protein rejection experiments. The measurements for the PWP and MWCO of the PDMAEMA-PVDF/PSF functionalised membranes were conducted independently, as described in Section 3.2.5.5. A schematic diagram of a PWP set-up, as shown previously in Figure 3.1.

The prepared hollow fibre membranes were hydrophobic, which increased the difficulty of measuring the pure water permeation. Therefore, the prepared membranes

were pre-wetted with pure water for at least 30 min at a transmembrane pressure (TMP) of 2.0 bar prior to collecting the permeated water. Filtration experiments were conducted at constant flow rate at 100 mL/min into the shell side of the fibres using TMP of 0.8 bar and a room temperature of $24\text{ }^{\circ}\text{C} \pm 2\text{ }^{\circ}\text{C}$. The lumen flow rate was 15 mL/min. The pressure regulator was manually controlled while manipulating the flow rate to obtain the desired TMP. The solute transport experiment was conducted using PEG and PEO feed solutions at various molecular weights. According to the solute rejection data, the membrane properties such as MWCO measurements and solute diameters were calculated using the Stokes-Einstein equation described in Section 3.2.5.5.

6.2.3.2 Hemofiltration tests using a blood model solution

A blood model solution composed of 1 g/L BSA and a PEG with an average molecular weight of 12,000 Da was adopted from Yang, *et al.* [5]. PEG is added to adjust its final viscosity to 2.9 cP, thus mimicking real blood viscosity. The final PEG composition is 6.14 wt% to achieve the closest viscosity of the real blood. The addition of 12,000 Da PEG is intended to mimic β_2 -microglobulin, the largest toxin molecule to be removed from the blood. The final pH of the blood model solution was adjusted to 7.40 ± 0.05 using the phosphate-buffered solution. The model solution was pumped into the selective surface, which was the shell side of the fibres, as described in Section 3.2.5.5. The experiment was conducted at a constant flow rate of 100 mL/min into the shell side of the fibre and TMP at 0.8 bar. The lumen flow rate was 15 mL/min. The temperature of the reservoir and the membrane module was maintained at $37\text{ }^{\circ}\text{C}$ using a water bath and heating tape, as shown in Figure 6.1. At intervals of 0.5 hours, the feed and permeate samples were collected to determine the concentrations, whereby the retentate and permeate solutions were recycled back to the reservoir and permeate tank (manually), respectively. The BSA concentrations in the feed and permeate solutions are measured using a UV-Vis scanning spectrophotometer at a wavelength of 280 nm. Rejection of BSA was calculated using Eq. 3.5. The feed and permeate were determined by TOC measurements.

The characterisation of hemofiltration to a particular solute was expressed as the sieving coefficient (SC_0),

$$SC_0 = \frac{C_p}{C_b} \quad \text{Eq. 6.1}$$

Which is the ratio of the solute concentration (C_p) in the permeate relative to the blood model solution (C_b).

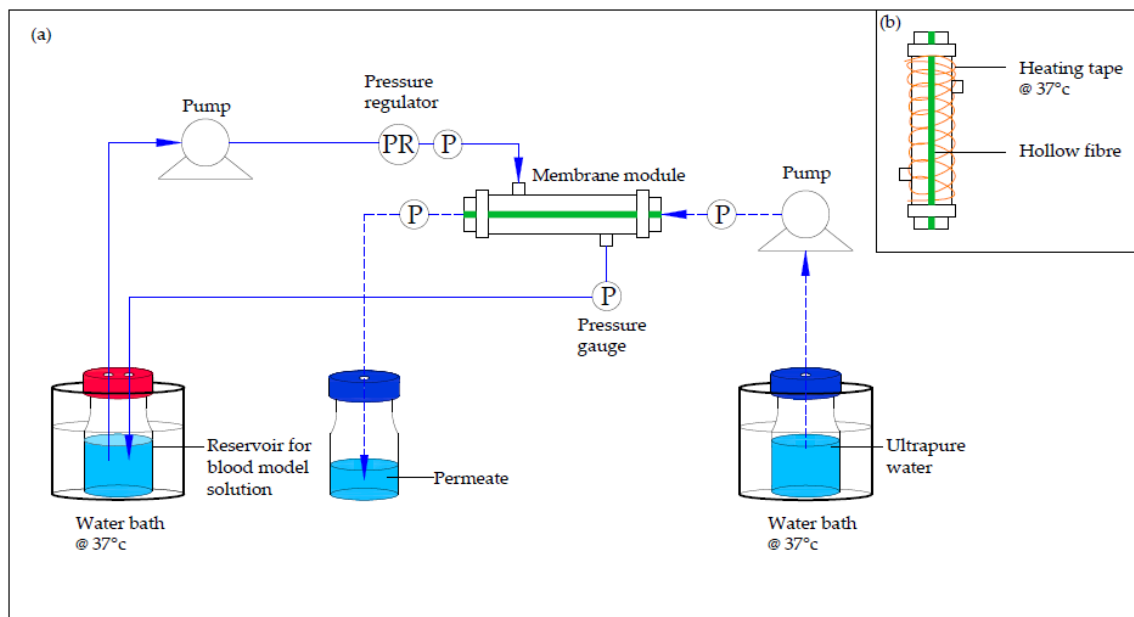


Figure 6.1. A schematic diagram of a hemofiltration experiment using blood model solution at 37 °C. (a) Standard permeation rig; (b) Membrane module with heating tape attached to maintain the temperature of the experiments.

6.2.3.3 Membrane cleaning tests

After 4 hours of the hemofiltration test, the blood model solution was replaced with ultrapure water and recirculated in the membrane module for 10 min to remove any particles deposited loosely on the membrane surface. Then, the temperature of the ultrapure water was increased to 60 °C. The temperature of the ultrapure water and membrane module were maintained at 60 ± 2 °C using a water bath and heating tape. The heated ultrapure water was pumped at 100 mL/min through both the selective surface and lumen. The TMP was at 0.8 bar. A schematic diagram of the regeneration process is shown in Figure 6.2. Similarly, the feed and permeate samples were collected at intervals (every 10 min) to measure the BSA and TOC concentrations until the

composition of the samples was equivalent to the TOC concentration of the ultrapure water. The cleaning process was completed approximately 30 min and an extra 10 min was performed to confirm the clearance of the solutes. The functionalised membrane morphologies before and after the cleaning tests were performed using AFM.

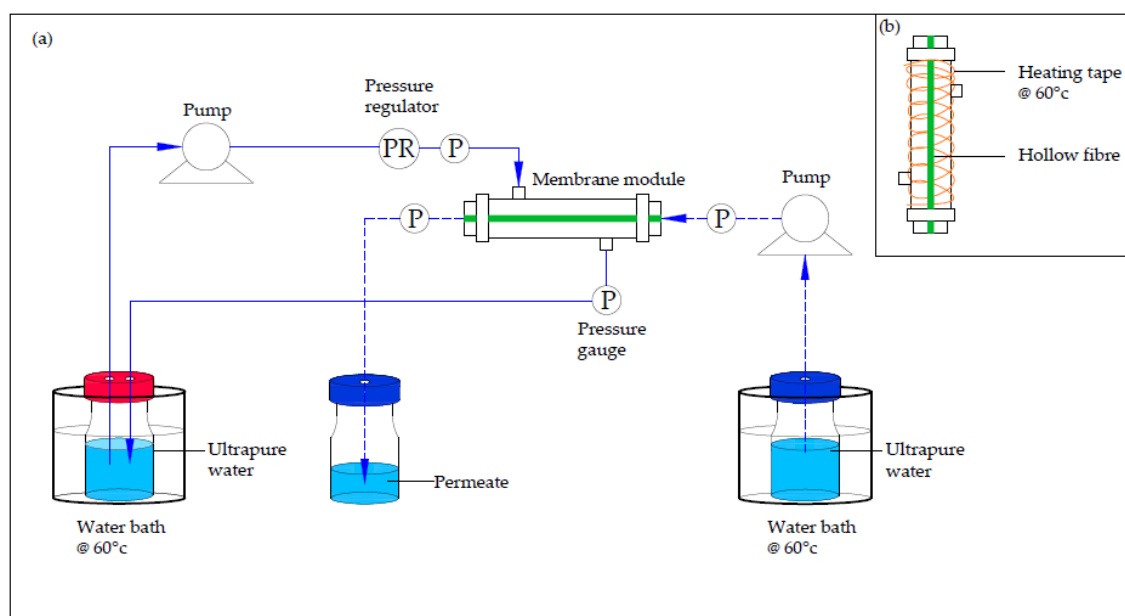


Figure 6.2. A schematic diagram of a regeneration experiment using ultrapure water at 60 °C. (a) Standard permeation rig; (b) Membrane module with heating tape attached to maintain the temperature of the experiments.

6.2.3.4 AFM characterisation of the functionalised hollow fibre membranes

Morphological examination of the regenerated membranes before and after regeneration was conducted at the outer surface of the membranes, as described in Section 3.2.5.4. At least three locations were measured for each sample.

6.3 Results and discussion

6.3.1 Pure water permeability and molecular weight cut-off measurements

Membrane permeability and MWCO measurements are important characteristics in the dialysis process. This is because they determine the overall membrane performance, which is related to the solute permeability of the membrane, including uremic toxin clearance and albumin loss. In the following discussion, the non-functionalised and functionalised membrane were coded as S15-15-Bef and S15-15-Aft, respectively.

The pure water permeation and solute rejection tests on the S15-15 hollow fibre membranes are summarised in Table 6.2 (in the interest of data comparison, table was tabulated in Section 6.3.3.). We can see that the overall performance of S15-15-Aft is higher than S15-15-Bef. This can be attributed to changes in the interaction between the modified hydrophilic membrane surface and water molecules. As mentioned in Section 5.3.3.3, the hydrophilic surface of S15-15-Aft would attract water molecules, forming structured water molecules, and thus increase the water channels within the membrane. On the other hand, the hydrophobic chains of the S15-15-Bef would extend into the water, creating repulsive forces, hence any resulting attraction between hydrogen bonds and water molecules is prohibited. Consequently, this phenomenon leads to higher water resistance on the hydrophobic membrane surface and higher PWP on the hydrophilic membrane surface. Similar outcomes were reported elsewhere in literature [224].

From the ST data, the pore size, pore size distribution, and MWCO measurements of the S15-15-Bef and S15-15-Aft membranes were determined and are presented in Table 6.3 (in the interest of data comparison, table was tabulated in Section 6.3.3.). We can see that the mean pore size and MWCO measurements of S15-15-Aft decreases. This indicates that the embedded microgel particles were swollen at 37 °C, resulting in a decrease in pore dimension and thus higher solute rejection, as observed for S15-15-Aft. The reduction of these parameters, particularly MWCO (63,000 Da), is promising if the goal is to prevent albumin loss (human serum albumin, MW: 67,000 Da). Therefore, according to this outcome, later in the hemofiltration testing, it can be speculated that the resulted pore size distribution of S15-15-Aft would result in better protein retention performance.

6.3.2 Hemofiltration tests

Figure 6.3. depicts the membrane performance of S15-15-Aft using a blood model solution over 4 hours hemofiltration. The BSA retention of S15-15-Aft increased slightly between from 0 and 1.5 hours and after which it became relatively constant until the end of the fourth hour. The resulted BSA retention is surprisingly high and constant, despite possessing layers of quaternized PDMAEMA on the membrane surface, which is positively charged.

As discussed in Section 5.3.3.3, the positively charged membrane surface is predicted to interact with negatively charged BSA molecules. The electrostatic interaction that occurs between BSA molecules and the membrane surface should have triggered protein adsorption, and eventually results in aggregation and thus a decline in BSA retention. However, it remains constant. This phenomenon suggests that there is a maximum number of BSA molecules that can interact with the membrane surface. Once the electrostatic interactions reach an equilibrium, the charges on the membrane surface become neutral. As a result, it resembles a zwitterionic membrane surface, which prevents further interaction with BSA molecules. The neutrality of the membrane surfaces has been shown to enhance the protein resistance and inhibit platelet adhesion [81,210], and the inhibition of platelet adhesion on the membrane surface subsequently suppresses the activation of protein aggregation, which is favourable for medical settings, especially dialysis. Another possible reason for the minimal protein adsorption is the hydrophilicity of the membrane surface which, as we saw in Section 5.3.3.3, meant that it was strongly bound with a hydration layer. As a result, protein adsorption was suppressed. This finding is in agreement with previous literature [79,210,225].

The inclusion of PEG was used to mimic β_2 -microglobulin, which is one of the largest middle-sized solutes to be removed from the bloodstream. The sieving coefficient is approximately 0.3, which is unexpectedly low with respect to the mean pore size and MWCO measurements. Nevertheless, the concentration of PEG (65.4 g/L) has to be taken into account, as it was much higher than BSA (1g/L). Therefore, the resulted sieving coefficient is acceptable, since both feed and permeate were determined simultaneously

using TOC. The resulted sieving coefficients are shown in Figure 6.3. corresponded with the solute rejection data, which is approximately 45%. Furthermore, the results demonstrated that, if the effective pore size or MWCO caused by protein adsorption around membrane pores decreases, this would obstruct other larger solutes, such as BSA, but would have little or no effect on the transportation of smaller solutes across the membrane.

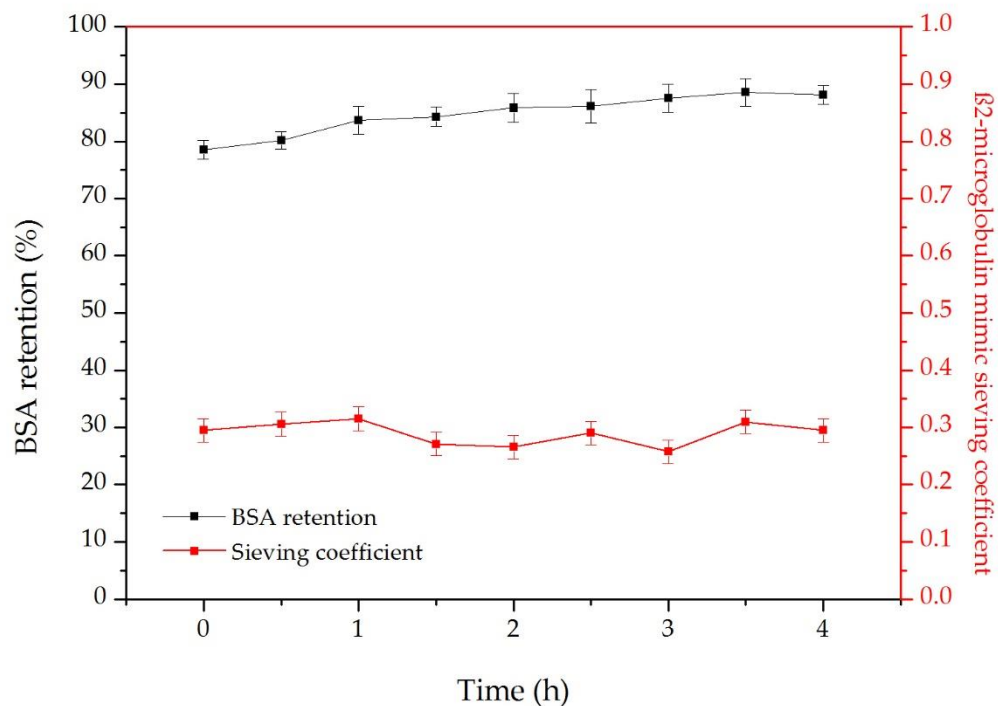


Figure 6.3. BSA rejection and PEG (12,000 Da) sieving performance for functionalised hollow fibre membrane (S15-15-Aft) during 4 hours hemofiltration tests.

The sieving coefficients of the β 2-microglobulin and BSA retention are compared with the commercial membranes as shown in Table 6.1. One of the drawbacks of the blood model solution is PEG that was used to mimic the blood viscosity and the β 2-microglobulin. Consequently, the blood model solution having a PEG concentration of 65.4 g/L, which is considerably high compared to the concentration of β 2-microglobulin for a dialysed patient ranging from 30-50 mg/L [226]. In this study, the total PEG clearance is approximately 19.6 g/L, with a sieving coefficient of about 0.3, whereas the sieving coefficient of the commercial membrane is approximately 0.7. Therefore,

reference measurements with a commercially available membrane are incompatible to be compared with the collected data.

Table 6.1. Reference measurements of the commercial membranes obtained from *in vitro* characterization.

	Base material	Blood/ dialysate flow rate (mL/min)	Treatment time (min)	Sieving coefficients		Reference
				β 2-m	alb	
F2160NR (1.5 m²)	PSF/PVP	300/500	60	0.7	<0.01	[227]
F200NR (2.0 m²)	PSF/PVP	300/500	60	0.7	<0.01	[227]
Revaclear (1.4 m²)	PAES/PVP	300/500	60	0.7	<0.01	[227]
Revaclear Max (1.8 m²)	PAES/PVP	300/500	60	0.7	<0.01	[227]
PUREMA[®] H (1.7 m²)	PES/PVP	300/500	236±11	0.72	0.001	[228]
PUREMA[®] H (1.9 m²)	PES	378±/500	229±22	0.68	0.002	[229]
Helixone[®] (1.8 m²)	PSU/PVP	300/500	236±11	0.66	0.001	[228]
Current study (0.0096 m²)	PVDF/PSF- PDMAEMA	100/15	240	0.3	0.15	

Note: PAES, Polyarylethersulfone; β 2-m, β 2-microglobulin (11,800 Da); alb, albumin (67,000 Da).

In summary, these results suggest that solute transport experiments are crucial for understanding membrane performance, as either the mean pore size or MWCO data of the membrane do not provide conclusive evidence for the membrane's overall

performance. After hemofiltration testing, the S15-15-Aft underwent reprocessing to investigate the effectiveness of the microgel-functionalised membrane.

6.3.3 Regeneration process of the functionalised hollow fibre membranes

A regeneration process was performed to examine the reusability of S15-15-Aft. The process involves hemofiltration, followed by reprocessing and a second cycle of hemofiltration. In between reprocessing, pure water permeation and solute rejection experiments were conducted. In the following discussion, the regenerated S15-15-Aft membrane was coded as S15-15-Aft-R and H1 and H2 refer to the hemofiltration tests performed before and after the reprocessing, respectively.

The effect of the temperature-responsive behaviour of PDMAEMA microgel particles on the membrane (S15-15-Aft-H1), which was subject to a hemofiltration test, was evaluated by comparing the differences in water permeation between S15-15-Aft and S15-15-Aft-R, as shown in Figure 6.4. The PWP of all samples were examined under identical conditions. The S15-15-Aft-H1 membranes were reprocessed using identical operating conditions, except for the temperature, which was heated to 60 °C. After the first hemofiltration test, we can see in Figure 6.4. that there was a minor decrease in the PWP of S15-15-Aft-H1, indicating that membrane fouling occurred, although the Reynold numbers were taken into account to ensure the feed behaviour was within a turbulent range. The morphological observations show that there is a change in S15-15-Aft-H1 membrane as compared to S15-15-Aft, which would indicate the occurrence of protein adsorption, as shown in Figure 6.5. This outcome reveals that marginal BSA molecules interacted with the quaternized PDMAEMA microgel, forming mild protein adsorption on the membrane surface.

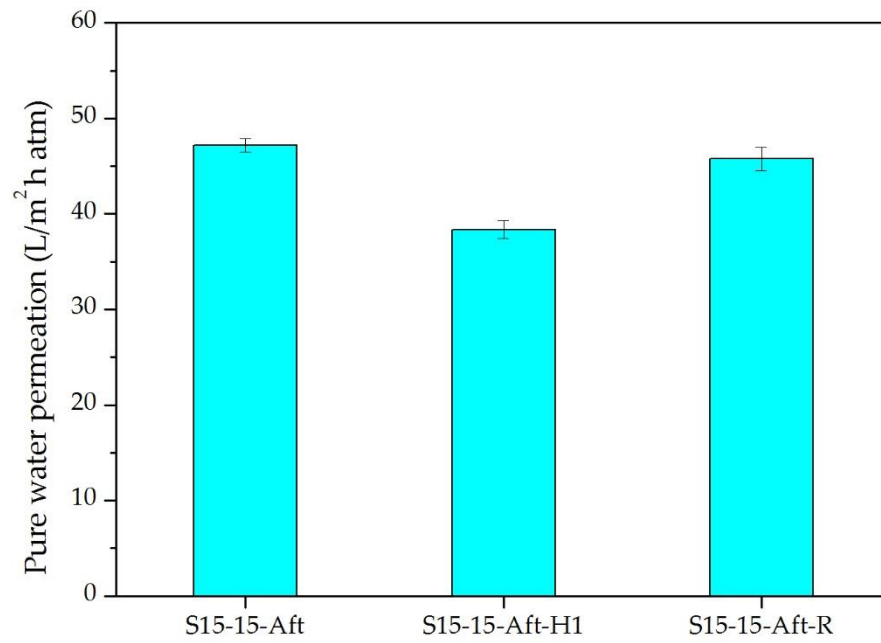


Figure 6.4. Pure water permeability of S15-15 hollow fibre membranes: S15-15-Aft refers to functionalised membrane; S15-15-Aft-H1 refers to the functionalised membrane after the first hemofiltration; S15-15-Aft-R regenerated-functionalised membrane.

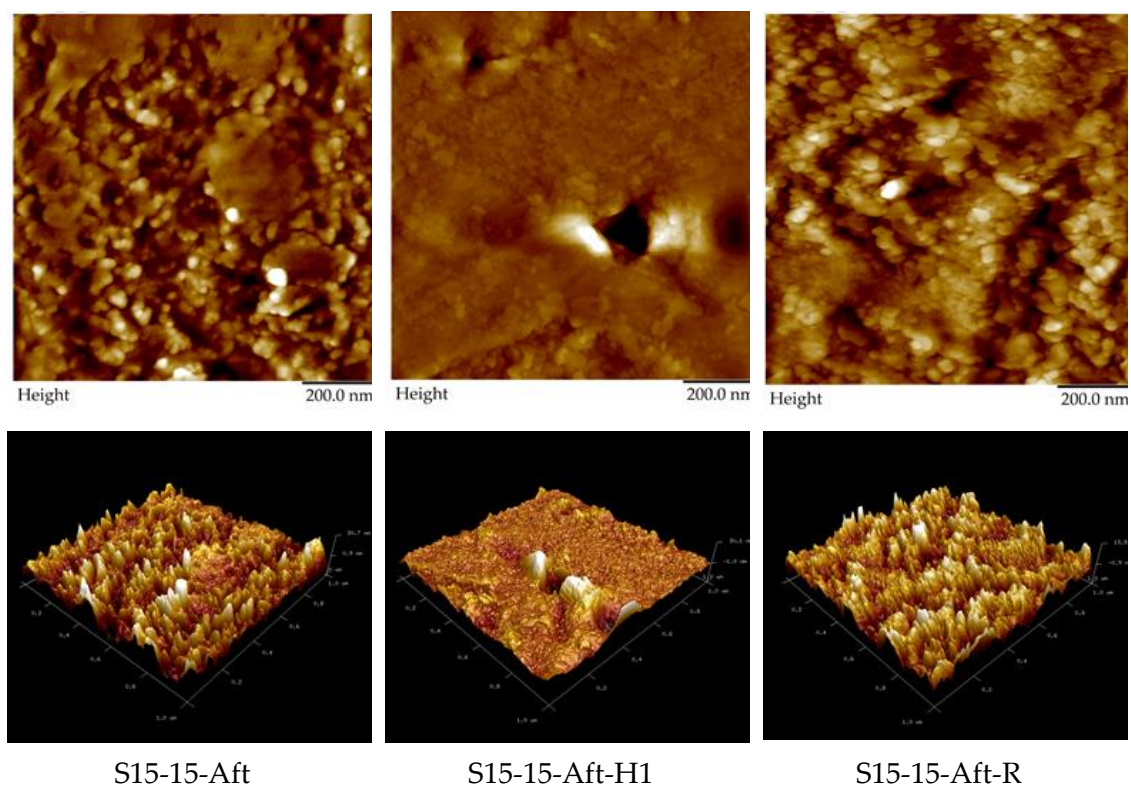


Figure 6.5. AFM micrographs of the functionalised (S15-15-Aft), after first hemofiltration (S15-15-Aft-H1), and regenerated (S15-15-Aft-R) membranes.

Later, a cleaning test using ultrapure water at 60 °C was performed on the S15-15-Aft-H1 membranes. The PWP recovery of the S15-15-Aft-H1 is satisfactory, whereby the S15-15-Aft-R membranes exhibited almost identical PWP values to those of S15-15-Aft. This indicates that a cleaning process that does not use chemical agents to remove adsorbed protein is attainable, as shown in Figure 6.5. After the cleaning test, a sequential evaluation of the modification to the mean pore size and MWCO measurements were performed. The difference of both permeation and solute rejection data between S15-15-Aft and S15-15-Aft-R is 3.5 % or less as summarised in Table 6.2 and Table 6.3. These preliminary results suggest that S15-15-Aft could have a high reusability and be promising for long-term use in clinical applications.

Table 6.2. Results of the ultrafiltration experiments of S15-15 hollow fibre membranes.

Membrane code	PWP (L/m ² h bar)	Solute separation (%)				
		PEG (Da)		BSA (Da)	PEO (Da)	
		10 000	12 000	35 000	69 000	100 000
S15-15-Bef	31.22	27.50	45.32	65.00	83.76	95.43
S15-15-Aft	47.21	35.30	49.99	85.01	89.60	98.33
S15-15-Aft-R	45.77	37.66	46.55	86.54	88.21	96.98

Note: “S15-15-Bef” and “S15-15-Aft” are the membrane codes corresponding to non-functionalised and functionalised hollow fibre membranes with M0.5 PDMAEMA microgel, respectively. S15-15-Aft-R is the regenerated-functionalised membrane after hemofiltration tests.

Table 6.3. Comparison of various parameters of S15-15 hollow fibre membranes calculated from the solute rejection experiments.

Membrane code	Mean pore size, μ_p (nm)	Standard deviation, σ_p	MWCO (Da)
S15-15-Bef	7.82	1.89	85,000
S15-15-Aft	6.68	1.89	63,000
S15-15-Aft-R	6.69	1.91	60,000

Note: MWCO refers to molecular weight cut-off, the molecular weight of the solute, 90% of which can be rejected by a membrane.

Figure 6.6. shows pore size distributions of the S15-15-Bef, S15-15-Aft, and S15-15-Aft-R membranes. The broadness of the peaks is comparable across the various membranes. The majority of the pores have a smaller range (6.68-7.82 nm) and a relatively sharp probability density function curve. However, the curves are positively skewed, indicating that the membrane surface also contains larger pores. The different pore sizes can allow for the transport of different sized BSA molecules through the membrane.

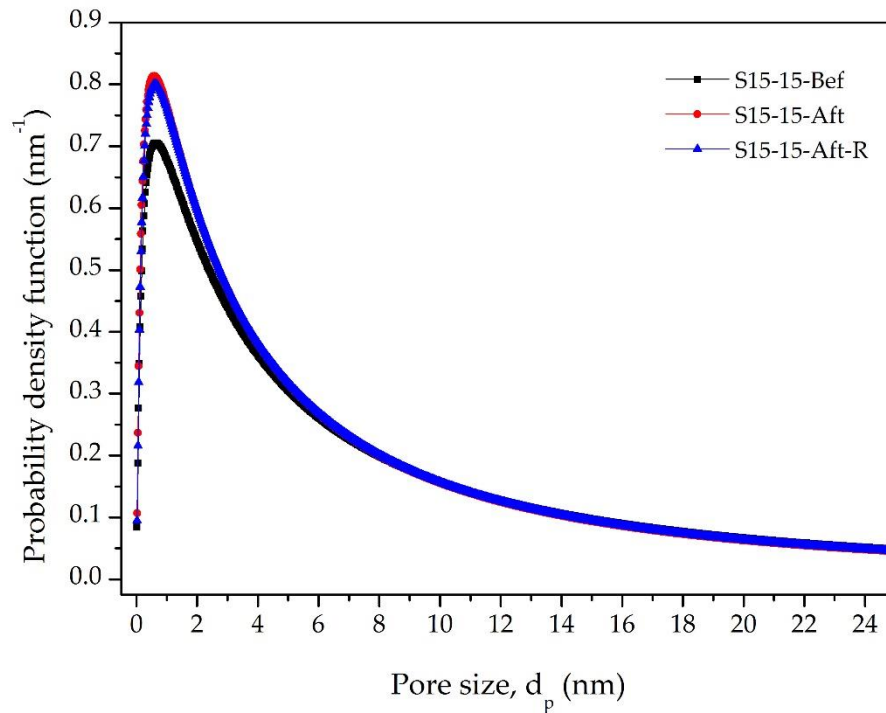


Figure 6.6. Probability density function curves of S15-15 hollow fibre membranes: (■) S15-15-Bef is a non-functionalised membrane; (●) S15-15-Aft is a functionalised membrane; (▲) S15-15-Aft-R is a regenerated-functionalised membrane after hemofiltration.

It is worth noting that the BSA molecule has an ellipsoid shape with the dimensions $4.16 \times 4.16 \times 14.09$ nm, yielding a gyration diameter of 7.28 nm [5]. According to the mean pore size of S15-15-Aft tabulated in Table 6.3., this is smaller than the gyration diameter of a BSA molecule. Although parts of the dimensions are smaller than the membrane mean pore sizes, the BSA molecule will not completely block entire cylindrical membrane pores, but rather will be subjected to mild interactions given the hydrophilic surface of the membrane. Two possible reasons can account for these assumptions: (1) the positively charged membrane surface discussed in Section 6.3.2.; the different atomic charges between the membrane surface and BSA molecules will attract each other until an equilibrium is reached. Nevertheless, (2) the electrostatic attraction is weak because the hydrophilic surface formed a physical barrier with water molecules, resulting in a water-mediated repulsion at the surface and thus preventing rigid interaction with BSA molecules. In addition, the volumetric flow rate of the blood model solution used in the membrane module was in the turbulent range, which

theoretically decreases the tendency for protein adsorption on the membrane surface. Therefore, minimal protein adsorption and fouling would occur on the membrane.

After a cycle of the hemofiltration and cleaning testing, a second round of hemofiltration was executed. The results show that the S15-15-Aft-H2 membranes attain similar BSA retention and sieving coefficients to those of H1, as shown in Figure 6.7. The coherent outcomes of the hemofiltration testing between S15-15-Aft-H1 and S15-15-Aft-H2, highlight the reusability and reliability of the functionalised membrane. The results demonstrate that the protein adsorption would reduce the large solute transportation through the membrane pores, however it will not have an effect on small or middle-sized solutes (below 12,000 Da).

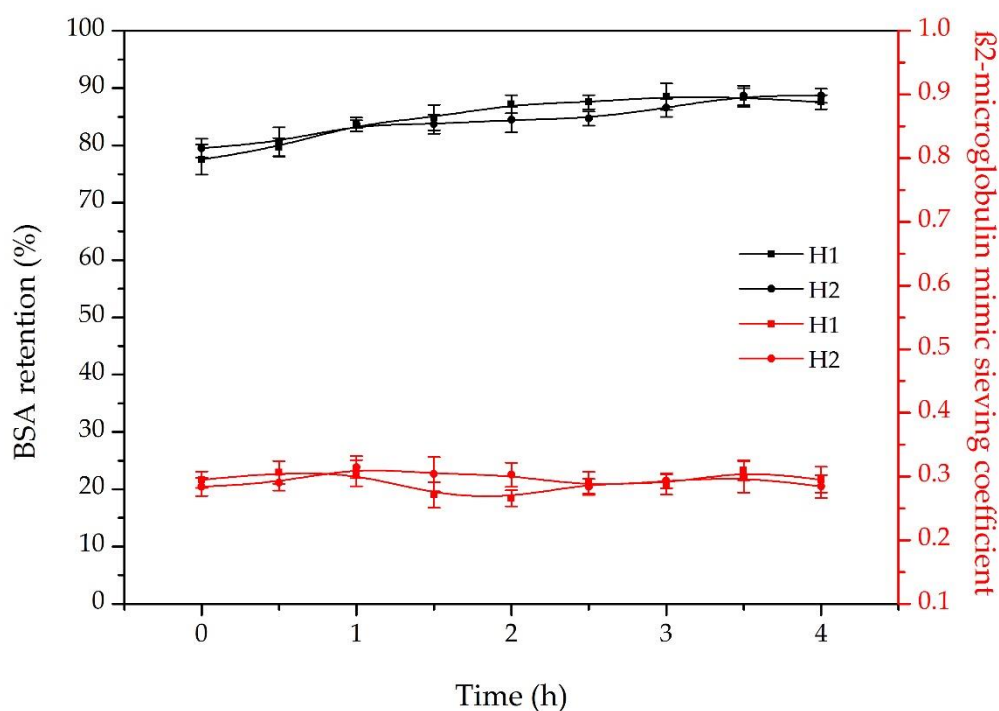


Figure 6.7. BSA rejection and PEG (12,000 Da) sieving performance before (H1) and after (H2) regeneration for functionalised hollow fibre membrane (S15-15-Aft) during 4 hours hemofiltration tests.

A schematic representation of the non-functionalised membrane and temperature-responsive microgel-functionalised membrane is proposed in Figure 6.8. A non-functionalised membrane that does not undergo hydrophilization, there higher chance that protein adsorption can occur. During hemofiltration testing, protein adsorption can

trigger a series of biological responses, resulting in severe protein caking and, eventually membrane fouling can occur by the end of the dialysis, as shown in Figure 6.8 (a) (ii). This occurrence is due to the hydrophobic interaction between the protein molecules and membrane. Therefore, during the reprocessing of the membrane, chemical cleaning agents such as bleach and peracetic acid are required to dissolve and remove the deposited proteins on the membrane, as shown in Figure 6.8. (b) (iii). Although typical dialysis membranes have a hydrophilic surface, the use of chemical agents during reprocessing was still inevitable. After several rounds of reprocessing, the harsh chemical agents will cause the hydrophilic properties of the membrane to leak out, resulting in membrane deformation.

On the contrary, a microgel-responsive functionalised membrane, during hemofiltration testing, because of the hydrophilic membrane surface, little or no protein caking is likely to occur. When the occurrence of protein adsorption is minimal, this will result in a higher removal rate of the uremic toxins than would be the case with non-functionalised membranes. Moreover, at 37 °C that is below LCST, the microgel particles swell with water molecules, and the pore dimension is controlled such that the proteins cannot pass through the membrane, resulting in high protein retention as shown in Figure 6.7. Due to the nature of the PDMAEMA microgel, which was positively charged at the physiological pH of 7.4, it attracts negatively charged biological molecules such as proteins, as illustrated in Figure 6.8. (b) (ii). Nevertheless, the high hydrophilicity of the PDMAEMA microgel particles counters the electrostatic attraction between the polymer and proteins, which is usually encountered on a hydrophobic polymer. During the reprocessing, by applying an external stimulus, such as a change in temperature (from 37 °C to 60 °C), the hydrogen bonds of polymer molecules within the microgel particles break, causing the microgel particles to shrink. As the microgel particles shrink, the adsorbed protein molecules can be released and removed from the membrane surface. The alteration of the size of the microgel particles during reprocessing induces self-cleaning using thermo-regulated microgel coating.

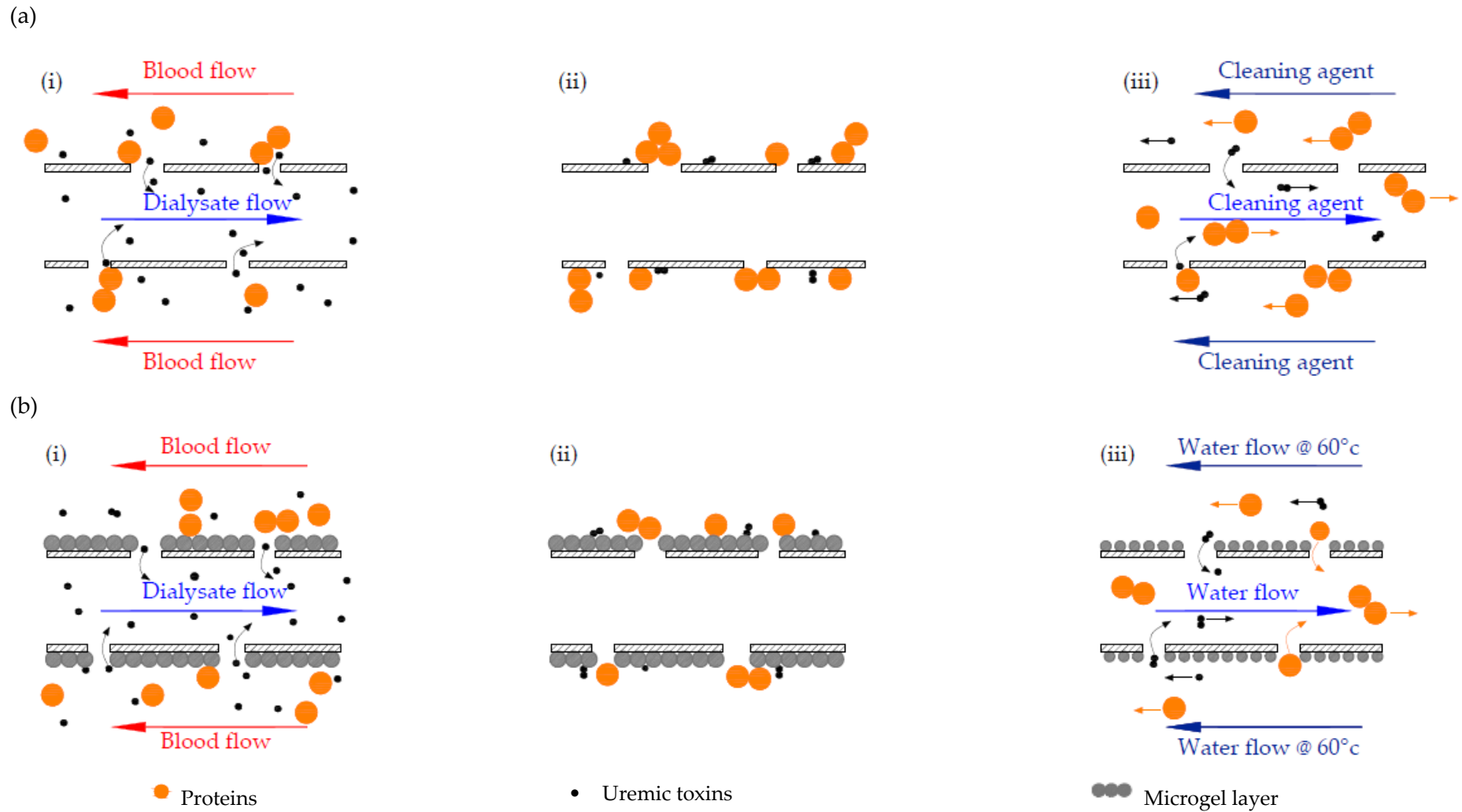


Figure 6.8. Schematic diagrams of (a) non-functionalised hollow fibre membrane and (b) microgel-responsive functionalised hollow fibre membrane (S15-15-Aft): (i) during dialysis treatment; (ii) completion of dialysis; and (iii) reprocessing–cleaning.

6.4 Conclusion

A regeneration of the microgel-functionalised hollow fibre membrane using a blood model solution was performed. The functionalised membranes exhibit good hemofiltration performance, and experience minimal fouling, with a protein retention flux above 80%. After the hemofiltration tests, a cleaning process was undertaken as the final stage. Membrane cleaning using temperature-regulated microgel particles shows that those hemofiltration tested membranes can recover to their original PWP and MWCO measurements, and protein retention flux behaviours. The cleaning approach using microgel-functionalised membranes is straightforward and efficient. The results imply that the functionalised membrane with temperature-responsive PDMAEMA microgel is potentially desirable and promising in the regeneration process. It can eliminate the application of cleaning chemicals that are usually used in conventional practice.

Chapter 7: CONCLUSION AND RECOMMENDATION FOR FUTURE RESEARCH

7.1 Conclusion

In this study, an innovative approach using temperature-responsive microgel-functionalised hollow fibre membranes was proposed to overcome the shortcomings associated with existing dialysis membranes and reprocessing. Two main issues associated with existing limitations have been addressed.

In seeking to improve the mechanical strength of the existing dialysis membrane, aside from determining the types of polymer materials, the examination of the fabrication parameters was crucial. Polymer dope composition (solid content and type of additives) and coagulant composition (nature of the solvent and relative amount of weak/strong solvent) are significant parameters that modify the resultant morphology and mechanical properties of PVDF/PSF hollow fibre membranes. The brittleness of the current dialysis membrane, PSF, was blended with PVDF to strike a balance between the ductile and brittle behaviours of both polymers. The blending was intended to improve the overall mechanical strength of hollow fibre membranes. In the process of determining the ideal ratio for membrane fabrication, several membrane characteristics need to complement the commercial dialysis membrane. These are the membrane pore size, pore size distribution and the thickness of the membrane walls, as they all have a great impact on the membrane's performance.

Synthetic polymers were used to enhance the reusability of the membranes, but the hydrophobic nature of the polymers triggered membrane fouling. Membrane hydrophilization is an essential technique to tackle the drawbacks caused by synthetic polymers. Therefore, adjustable-size (temperature-responsive) PDMAEMA microgel particles stabilised using ethanol were synthesised. The microgel dispersion stabilised using ethanol exhibited better colloidal stability, which is encouraging for mass production.

This was then used to prepare a hydrophilic and positively charged PVDF/PSF hollow fibre membrane using dynamic-interfacial polymerisation. The dynamic

adsorption provides uniform depositing. The inclusion of the interfacial polymerisation was advantageous, in that it provided for chemical-bonding between the membrane surface and microgel particles, which were shown to be stable and reproducible. The findings show an increase in protein resistance, indicating that the functionalised membrane was also effective at improving the anti-fouling properties of the PVDF/PSF hollow fibre membranes.

The regeneration of the functionalised membrane mimics dialysis and reprocessing by performing hemofiltration and cleaning tests. The findings show excellent protein retention flux without hindering the removal of middle-sized solutes. The cleaning approach adopted direct heating using ultrapure water, which offers a major advantage. This is because it allows for precise control over the changes in the size of the microgel particles during dialysis and reprocessing, which could control the pore dimension for better protein retention flux and induces self-cleaning without the use of chemical reagents, respectively.

The preparation and performance of this innovative approach were successfully undertaken in the laboratory. If this approach were to be applied in dialysis industry, it would be able to effectively reduce the costs, faced by patients, society and the environment. The anti-fouling properties of the membrane proved indispensable to the patients' health. This is because the administration of anti-coagulant is inevitable to prevent any complications during their treatments, such as blood clots. Long-term prescription of anti-coagulant causes patients to be susceptible to haemorrhage. Therefore, improvements to the anti-fouling properties of the membrane would suggest that a lower dosage of anti-coagulant is required.

It is speculated that the improved durability and reusability of the hollow fibre membranes can considerably reduce the impact on the environment. This is achieved by decreasing the amount of toxins generated during waste processing and reducing the amount of non-biodegradable waste sent to landfills. Moreover, the addition of adjustable-size additives on the membrane surface can eradicate the use of cleaning and disinfectant agents, which have a potentially devastating effect on the mucous

membrane and pulmonary functioning. Consequently, due to the reduction in costs associated with reprocessing and medical waste disposal, kidney disease treatment would become more affordable, thus decreasing global mortality.

7.2 Future recommendations

This work was a proof of concept that microgel-functionalised hollow fibre membranes are suitable for dialysis and reprocessing. Our results to date indicate that the functionalised membranes are a promising alternative to current dialysis membranes although, further work is needed to fully understand and optimise their properties. The list below offers suggestions for research that would further enhance our understanding of the use of functionalised membranes for dialysis and reprocessing:

1. The effect of the spinning parameters studied is limited, resulting in a couple of drawbacks in the PVDF/PSF hollow fibres. The relatively broad pore size distribution and large inner diameter would constrain the membrane performance and mechanical strength. Hence, in order to further optimise the membrane characteristics, extending the spinning parameters to include dope and bore fluid flow rate, air-gap distance, and coagulant composition is necessary to perfect our understanding of their use in dialysis.
2. The main challenges in synthesising PDMAEMA microgel particles is the instability of the dispersion, which prevents microgel particle aggregation. Exploring the role and potential of stabilisers can pave the way for mass production at low cost.
3. Although reasonable levels of stability were achieved, the mechanisms of the microgel embedment techniques are still poorly understood. The optimisation of the XDC in the embedment process still needs to be understood, particularly with respect to membrane permeability; for example, when it comes to the chemical quaternization reaction between PDMAEMA and XDC.

4. In addition, little or no information exists for the anti-bacterial activities, specifically those of the functionalised membrane, even in spite of the promising results for the cationic membrane. Further research in these areas would maximise the potential for these membranes being used in clinical settings.
5. In the present study, the characterisation was based on a single functionalised hollow fibre module, and the regeneration data was limited. Up-scaling by using multi-fibre modules and appropriate blood models is important if we are to better understand the overall nature of the membranes' performance.

REFERENCES

1. Luyckx, V.A.; Tonelli, M.; Stanifer, J.W. The global burden of kidney disease and the sustainable development goals. *Bull World Health Organ* **2018**, *96*, 414-422D.
2. Ismail, H.; Abdul Manaf, M.R.; Abdul Gafor, A.H.; Mohamad Zaher, Z.M.; Ibrahim, A.I.N. Economic Burden of ESRD to the Malaysian Health Care System. *Kidney International Reports* **2019**.
3. Chan, C.T.; Covic, A.; Craig, J.C.; Davenport, A.; Kasiske, B.L.; Kuhlmann, M.K.; Levin, N.W.; Li, P.K.; Locatelli, F.; Rocco, M.V.; Wheeler, D.C. Novel techniques and innovation in blood purification: a clinical update from Kidney Disease: Improving Global Outcomes. *Kidney International* **2013**, *83*, 359-371.
4. Achim, J.; Claudio, R.; John, A.K. Management of Acute Kidney Problems. Jörres, A.; Ronco, C.; Kellum, J.A., Eds. Berlin, Heidelberg: Springer Berlin Heidelberg: Berlin, Heidelberg, 2010.
5. Yang, Q.; Chung, T.S.; Weber, M. Microscopic behavior of polyvinylpyrrolidone hydrophilizing agents on phase inversion polyethersulfone hollow fiber membranes for hemofiltration. *Journal of Membrane Science* **2009**, *326*, 322-331.
6. Davenport, A. Anticoagulation for Acute Dialysis. In *Management of Acute Kidney Problems*, Jörres, A.; Ronco, C.; Kellum, J.A., Eds. Springer Berlin Heidelberg: Berlin, Heidelberg, 2010; pp 559-575.
7. Butruk-Raszeja, B.; Trzaskowski, M.; Ciach, T. Cell membrane-mimicking coating for blood-contacting polyurethanes. *Journal of biomaterials applications* **2015**, *29*, 801-812.
8. Liu, F.; Hashim, N.A.; Liu, Y.; Abed, M.R.M.; Li, K. Progress in the production and modification of PVDF membranes. *Journal of Membrane Science* **2011**, *375*, 1-27.
9. Daugirdas, J.T.; Blake, P.G.; Ing, T.S. *Handbook of Dialysis*. 5 ed.; Wolters Kluwer: Philadelphia, UNITED STATES, 2014; p 844.
10. Roy, A.; Dadhich, P.; Dhara, S.; De, S. Understanding and tuning of polymer surfaces for dialysis applications. *Polymers for Advanced Technologies* **2017**, *28*, 174-187.
11. Menon, V.; Greene, T.O.M.; Wang, X.; Pereira, A.A.; Marcovina, S.M.; Beck, G.J.; Kusek, J.W.; Collins, A.J.; Levey, A.S.; Sarnak, M.J. C-reactive protein and albumin as predictors of all-cause and cardiovascular mortality in chronic kidney disease. *Kidney International* **2005**, *68*, 766-772.
12. Boschetti-de-Fierro, A.; Beck, W.; Hildwein, H.; Krause, B.; Storr, M.; Zweigart, C. Membrane Innovation in Dialysis. *Contrib Nephrol* **2017**, *191*, 100-114.
13. Clark, W.R.; Gao, D.; Neri, M.; Ronco, C. Solute Transport in Hemodialysis: Advances and Limitations of Current Membrane Technology. *Contrib Nephrol* **2017**, *191*, 84-99.
14. Li; Liao; Tjong. Electrospun Polyvinylidene Fluoride-Based Fibrous Scaffolds with Piezoelectric Characteristics for Bone and Neural Tissue Engineering. *Nanomaterials* **2019**, *9*, 952.
15. Houis, S.; Engelhardt, E.M.; Wurm, F.; Gries, T. Application of Polyvinylidene Fluoride (PVDF) as a Biomaterial in Medical Textiles. In *Medical and Healthcare Textiles*, Anand, S.C.; Kennedy, J.F.; Mirafteb, M.; Rajendran, S., Eds. Woodhead Publishing: 2010; pp 342-352.

16. Zhang, Q.; Lu, X.; Zhang, Q.; Zhang, L.; Li, S.; Liu, S. Flux and Passage Enhancement in Hemodialysis by Incorporating Compound Additive into PVDF Polymer Matrix. **2016**, *6*, 45.
17. Zhang, Q.; Lu, X.; Zhao, L.; Liu, J.; Wu, C. Research on polyvinylidene fluoride (PVDF) hollow-fiber hemodialyzer. In *Biomedical Engineering / Biomedizinische Technik*, 2016; Vol. 61, p 309.
18. Iktzler, T.A.; Flakoll, P.J.; Parker, R.A.; Hakim, R.M. Amino acid and albumin losses during hemodialysis. *Kidney International* **1994**, *46*, 830-837.
19. Wenten, I.G.; Aryanti, P.T.P.; Khoiruddin, K.; Hakim, A.N.; Himma, N.F. Advances in Polysulfone-Based Membranes for Hemodialysis. *Journal of Membrane Science and Research* **2016**, *2*, 78-89.
20. Liu, S.; Wu, G.; Chen, X.; Zhang, X.; Yu, J.; Liu, M.; Zhang, Y.; Wang, P. Degradation Behavior In Vitro of Carbon Nanotubes (CNTs)/Poly(lactic acid) (PLA) Composite Suture. *Polymers* **2019**, *11*, 1015.
21. Zhu, L.-J.; Liu, F.; Yu, X.-M.; Gao, A.-L.; Xue, L.-X. Surface zwitterionization of hemocompatible poly(lactic acid) membranes for hemodiafiltration. **2015**, *475*, 469-479.
22. Domingues, R.C.C.; Pereira, C.C.; Borges, C.P. Morphological control and properties of poly(lactic acid) hollow fibers for biomedical applications. *Journal of Applied Polymer Science* **2017**, *134*, 45494.
23. Pavia, F.C.; La Carrubba, V.; Piccarolo, S.; Brucato, V. Polymeric scaffolds prepared via thermally induced phase separation: Tuning of structure and morphology. **2008**, *86A*, 459-466.
24. Hou, D.; Wang, J.; Sun, X.; Ji, Z.; Luan, Z. Preparation and properties of PVDF composite hollow fiber membranes for desalination through direct contact membrane distillation. *Journal of Membrane Science* **2012**, *405-406*, 185-200.
25. Cui, Z.; Hassankiadeh, N.T.; Lee, S.Y.; Lee, J.M.; Woo, K.T.; Sanguinetti, A.; Arcella, V.; Lee, Y.M.; Drioli, E. Poly(vinylidene fluoride) membrane preparation with an environmental diluent via thermally induced phase separation. *Journal of Membrane Science* **2013**, *444*, 223-236.
26. Ismail, A.F.; Mansourizadeh, A. A comparative study on the structure and performance of porous polyvinylidene fluoride and polysulfone hollow fiber membranes for CO₂ absorption. *Journal of Membrane Science* **2010**, *365*, 319-328.
27. Mackey, M.; Flandin, L.; Hiltner, A.; Baer, E. Confined crystallization of PVDF and a PVDF-TEF copolymer in nanolayered films. *Journal of Polymer Science Part B: Polymer Physics* **2011**, *49*, 1750-1761.
28. Zhu, J.; Jiang, L.; Matsuura, T. New insights into fabrication of hydrophobic/hydrophilic composite hollow fibers for direct contact membrane distillation. *Chemical Engineering Science* **2015**, *137*, 79-90.
29. Teo, A.J.T.; Mishra, A.; Park, I.; Kim, Y.-J.; Park, W.-T.; Yoon, Y.-J. Polymeric Biomaterials for Medical Implants and Devices. *ACS Biomaterials Science & Engineering* **2016**, *2*, 454-472.
30. Laroche, G.; Marois, Y.; Guidoin, R.; King, M.W.; Martin, L.; How, T.; Douville, Y. Polyvinylidene fluoride (PVDF) as a biomaterial: From polymeric raw material to monofilament vascular suture. *Journal of Biomedical Materials Research* **1995**, *29*, 1525-1536.

31. Braga, F.J.C.; Rogero, S.O.; Couto, A.A.; Marques, R.F.C.; Ribeiro, A.A.; Campos, J.S.d.C. Characterization of PVDF/HAP composites for medical applications. *Materials Research* **2007**, *10*, 247-251.
32. Sukitpaneenit, P.; Chung, T.S. Molecular elucidation of morphology and mechanical properties of PVDF hollow fiber membranes from aspects of phase inversion, crystallization and rheology. *Journal of Membrane Science* **2009**, *340*, 192-205.
33. Hassankiadeh, N.T.; Cui, Z.; Kim, J.H.; Shin, D.W.; Sanguineti, A.; Arcella, V.; Lee, Y.M.; Drioli, E. PVDF hollow fiber membranes prepared from green diluent via thermally induced phase separation: Effect of PVDF molecular weight. *Journal of Membrane Science* **2014**, *471*, 237-246.
34. Xiao, T.; Wang, P.; Yang, X.; Cai, X.; Lu, J. Fabrication and characterization of novel asymmetric polyvinylidene fluoride (PVDF) membranes by the nonsolvent thermally induced phase separation (NTIPS) method for membrane distillation applications. *Journal of Membrane Science* **2015**, *489*, 160-174.
35. Xiuli, Y.; Hongbin, C.; Xiu, W.; Yongxin, Y. Morphology and properties of hollow-fiber membrane made by PAN mixing with small amount of PVDF. *Journal of Membrane Science* **1998**, *146*, 179-184.
36. Sun, D.; Liu, M.-Q.; Guo, J.-H.; Zhang, J.-Y.; Li, B.-B.; Li, D.-Y. Preparation and characterization of PDMS-PVDF hydrophobic microporous membrane for membrane distillation. *Desalination* **2015**, *370*, 63-71.
37. Laiarinandrasana, L.; Nziakou, Y.; Halary, J. Ductile to brittle transition concept on fracture behavior of poly(vinylidene fluoride) / poly(methyl methacrylate) blends. *13th International Conference on Fracture 2013, ICF 2013* **2013**, *2*.
38. Shi, L.; Wang, R.; Cao, Y.; Feng, C.; Liang, D.T.; Tay, J.H. Fabrication of poly(vinylidene fluoride-co-hexafluoropropylene) (PVDF-HFP) asymmetric microporous hollow fiber membranes. *Journal of Membrane Science* **2007**, *305*, 215-225.
39. Teoh, M.M.; Chung, T.S. Membrane distillation with hydrophobic macrovoid-free PVDF-PTFE hollow fiber membranes. *Separation and Purification Technology* **2009**, *66*, 229-236.
40. Lalia, B.S.; Guillen-Burrieza, E.; Arafat, H.A.; Hashaikeh, R. Fabrication and characterization of polyvinylidene fluoride-co-hexafluoropropylene (PVDF-HFP) electrospun membranes for direct contact membrane distillation. *Journal of Membrane Science* **2013**, *428*, 104-115.
41. Wongchitphimon, S.; Wang, R.; Jiratananon, R.; Shi, L.; Loh, C.H. Effect of polyethylene glycol (PEG) as an additive on the fabrication of polyvinylidene fluoride-co-hexafluoropropylene (PVDF-HFP) asymmetric microporous hollow fiber membranes. *Journal of Membrane Science* **2011**, *369*, 329-338.
42. Liu, F.; Hashim, N.A.; Liu, Y.; Abed, M.R.M.; Li, K. Progress in the production and modification of PVDF membranes. *Journal of Membrane Science* **2011**, *375*, 1-27.
43. Ebnesajjad, S. 7 - Surface Preparation of Thermoplastics, Thermosets, and Elastomers. In *Handbook of Adhesives and Surface Preparation*, Ebnesajjad, S., Ed. William Andrew Publishing: Oxford, 2011; pp 107-134.
44. Crawford, R.J. CHAPTER 2 - Mechanical Behaviour of Plastics. In *Plastics Engineering (Third Edition)*, Crawford, R.J., Ed. Butterworth-Heinemann: Oxford, 1998; pp 41-167.

45. Weidhase, L.; Haussig, E.; Haussig, S.; Kaiser, T.; De Fallois, J.; Petros, S. Middle molecule clearance with high cut-off dialyzer versus high-flux dialyzer using continuous veno-venous hemodialysis with regional citrate anticoagulation: A prospective randomized controlled trial. *PLOS ONE* **2019**, *14*, e0215823.
46. Zhang, Q.; Lu, X.; Zhao, L. Preparation of Polyvinylidene Fluoride (PVDF) Hollow Fiber Hemodialysis Membranes. *Membranes* **2014**, *4*, 81-95.
47. Zhang, Q.; Lu, X.; Liu, J.; Zhao, L. Preparation and preliminary dialysis performance research of polyvinylidene fluoride hollow fiber membranes. *Membranes* **2015**, *5*, 120-135.
48. Ding, Z.; Liu, X.; Liu, Y.; Zhang, L. Enhancing the Compatibility, Hydrophilicity and Mechanical Properties of Polysulfone Ultrafiltration Membranes with Lignocellulose Nanofibrils. *Polymers* **2016**, *8*, 349.
49. Kim, K.; Lee, K.; Cho, K.; Park, C. Surface modification of polysulfone ultrafiltration membrane by oxygen plasma treatment. *Journal of Membrane Science* **2002**, *199*, 135-145.
50. Ren, J.; Wang, R.; Zhang, H.; Li, Z.; Liang, D.; Tay, J. Effect of PVDF dope rheology on the structure of hollow fiber membranes used for CO₂ capture. *Journal of Membrane Science* **2006**, *281*, 334-344.
51. Bakeri, G.; Ismail, A.F.; Shariaty-Niassar, M.; Matsuura, T. Effect of polymer concentration on the structure and performance of polyetherimide hollow fiber membranes. *Journal of Membrane Science* **2010**, *363*, 103-111.
52. Tang, Y.; Li, N.; Liu, A.; Ding, S.; Yi, C.; Liu, H. Effect of spinning conditions on the structure and performance of hydrophobic PVDF hollow fiber membranes for membrane distillation. *Desalination* **2012**, *287*, 326-339.
53. Peng, N.; Chung, T.-S.; Wang, K.Y. Macrovoid evolution and critical factors to form macrovoid-free hollow fiber membranes. *Journal of Membrane Science* **2008**, *318*, 363-372.
54. Wei, W.; Zhang, H.; Li, X.; Zhang, H.; Li, Y.; Vankelecom, I. Hydrophobic asymmetric ultrafiltration PVDF membranes: an alternative separator for VFB with excellent stability. *Physical chemistry chemical physics : PCCP* **2013**, *15*, 1766-1771.
55. Deshmukh, S.P.; Li, K. Effect of ethanol composition in water coagulation bath on morphology of PVDF hollow fibre membranes. *Journal of Membrane Science* **1998**, *150*, 75-85.
56. Young, T.-H.; Cheng, L.-P.; Lin, D.-J.; Fane, L.; Chuang, W.-Y. Mechanisms of PVDF membrane formation by immersion-precipitation in soft (1-octanol) and harsh (water) nonsolvents. *Polymer* **1999**, *40*, 5315-5323.
57. Wang, K.Y.; Chung, T.S.; Gryta, M. Hydrophobic PVDF hollow fiber membranes with narrow pore size distribution and ultra-thin skin for the fresh water production through membrane distillation. *Chemical Engineering Science* **2008**, *63*, 2587-2594.
58. Wang, D.; Li, K.; Teo, W.K. Preparation and characterization of polyvinylidene fluoride (PVDF) hollow fiber membranes. *Journal of Membrane Science* **1999**, *163*, 211-220.
59. Bonyadi, S.; Chung, T.S. Highly porous and macrovoid-free PVDF hollow fiber membranes for membrane distillation by a solvent-dope solution co-extrusion approach. *Journal of Membrane Science* **2009**, *331*, 66-74.
60. Mansourizadeh, A.; Ismail, A.F. Effect of LiCl concentration in the polymer dope on the structure and performance of hydrophobic PVDF hollow fiber membranes for CO₂ absorption. *Chemical Engineering Journal* **2010**, *165*, 980-988.

61. Chung, T.S.; Teoh, S.K.; Hu, X. Formation of ultrathin high-performance polyethersulfone hollow-fiber membranes. *Journal of membrane science* **1997**, *133*, 161-175.
62. Steen, M.L.; Hymas, L.; Havey, E.D.; Capps, N.E.; Castner, D.G.; Fisher, E.R. Low temperature plasma treatment of asymmetric polysulfone membranes for permanent hydrophilic surface modification. *Journal of Membrane Science* **2001**, *188*, 97-114.
63. Liu, F.; Tao, M.-m.; Xue, L.-x. PVDF membranes with inter-connected pores prepared via a Nat-ips process. *Desalination* **2012**, *298*, 99-105.
64. Yang, X.; Wang, R.; Shi, L.; Fane, A.G.; Debowski, M. Performance improvement of PVDF hollow fiber-based membrane distillation process. *Journal of Membrane Science* **2011**, *369*, 437-447.
65. Kajekar, A.J.; Dodamani, B.M.; Isloor, A.M.; Karim, Z.A.; Cheer, N.B.; Ismail, A.F.; Shilton, S.J. Preparation and characterization of novel PSf/PVP/PANI-nanofiber nanocomposite hollow fiber ultrafiltration membranes and their possible applications for hazardous dye rejection. *Desalination* **2015**, *365*, 117-125.
66. Simone, S.; Figoli, A.; Criscuoli, A.; Carnevale, M.C.; Rosselli, A.; Drioli, E. Preparation of hollow fibre membranes from PVDF/PVP blends and their application in VMD. *Journal of Membrane Science* **2010**, *364*, 219-232.
67. Mei, S.; Xiao, C.; Hu, X.; Shu, W. Hydrolysis modification of PVC/PAN/SiO₂ composite hollow fiber membrane. *Desalination* **2011**, *280*, 378-383.
68. Bae, T.-H.; Tak, T.-M. Effect of TiO₂ nanoparticles on fouling mitigation of ultrafiltration membranes for activated sludge filtration. *Journal of Membrane Science* **2005**, *249*, 1-8.
69. Rajabzadeh, S.; Maruyama, T.; Ohmukai, Y.; Sotani, T.; Matsuyama, H. Preparation of PVDF/PMMA blend hollow fiber membrane via thermally induced phase separation (TIPS) method. *Separation and Purification Technology* **2009**, *66*, 76-83.
70. Lin, D.-J.; Chang, C.-L.; Lee, C.-K.; Cheng, L.-P. Preparation and characterization of microporous PVDF/PMMA composite membranes by phase inversion in water/DMSO solutions. *European Polymer Journal* **2006**, *42*, 2407-2418.
71. Ma, Y.; Shi, F.; Ma, J.; Wu, M.; Zhang, J.; Gao, C. Effect of PEG additive on the morphology and performance of polysulfone ultrafiltration membranes. *Desalination* **2011**, *272*, 51-58.
72. Yu, L.-Y.; Shen, H.-M.; Xu, Z.-L. PVDF-TiO₂ composite hollow fiber ultrafiltration membranes prepared by TiO₂ sol-gel method and blending method. *Journal of Applied Polymer Science* **2009**, *113*, 1763-1772.
73. Bottino, A.; Capannelli, G.; Comite, A. Preparation and characterization of novel porous PVDF-ZrO₂ composite membranes. *Desalination* **2002**, *146*, 35-40.
74. Yu, L.-Y.; Xu, Z.-L.; Shen, H.-M.; Yang, H. Preparation and characterization of PVDF-SiO₂ composite hollow fiber UF membrane by sol-gel method. *Journal of Membrane Science* **2009**, *337*, 257-265.
75. Damodar, R.A.; You, S.J.; Chou, H.H. Study the self cleaning, antibacterial and photocatalytic properties of TiO₂ entrapped PVDF membranes. *Journal of hazardous materials* **2009**, *172*, 1321-1328.
76. Chen, S.; Li, L.; Zhao, C.; Zheng, J. Surface hydration: Principles and applications toward low-fouling/nonfouling biomaterials. *Polymer* **2010**, *51*, 5283-5293.

77. Irfan, M.; Idris, A. Overview of PES biocompatible/hemodialysis membranes: PES–blood interactions and modification techniques. *Materials Science and Engineering: C* **2015**, *56*, 574-592.
78. Susantitaphong, P.; Jaber, B.L. Chapter 11 - Methods and Complications of Dialyzer Reuse. In *Handbook of Dialysis Therapy (Fifth Edition)*, Nissenson, A.R.; Fine, R.N., Eds. Elsevier: 2017; pp 144-151.e141.
79. Nishigochi, S.; Ishigami, T.; Maruyama, T.; Hao, Y.; Ohmukai, Y.; Iwasaki, Y.; Matsuyama, H. Improvement of Antifouling Properties of Polyvinylidene Fluoride Hollow Fiber Membranes by Simple Dip Coating of Phosphorylcholine Copolymer via Hydrophobic Interactions. *Industrial & Engineering Chemistry Research* **2014**, *53*, 2491-2497.
80. Lohaus, T.; de Wit, P.; Kather, M.; Menne, D.; Benes, N.E.; Pich, A.; Wessling, M. Tunable permeability and selectivity: Heatable inorganic porous hollow fiber membrane with a thermo-responsive microgel coating. *Journal of Membrane Science* **2017**, *539*, 451-457.
81. Zhao, D.; Qiu, G.; Li, X.; Wan, C.; Lu, K.; Chung, T.-S. Zwitterions coated hollow fiber membranes with enhanced antifouling properties for osmotic power generation from municipal wastewater. *Water research* **2016**, *104*, 389-396.
82. Yue, W.-W.; Li, H.-J.; Xiang, T.; Qin, H.; Sun, S.-D.; Zhao, C.-S. Grafting of zwitterion from polysulfone membrane via surface-initiated ATRP with enhanced antifouling property and biocompatibility. *Journal of Membrane Science* **2013**, *446*, 79-91.
83. Zhang, X.; Li, C.; Hu, Y.; Liu, R.; He, L.; Fang, S. A novel temperature and pH dual-responsive hybrid hydrogel with polyhedral oligomeric silsesquioxane as crosslinker: synthesis, characterization and drug release properties. *Polymer International* **2014**, *63*, 2030-2041.
84. Li, S.K.; and D'Emanuele, A. On-off transport through a thermoresponsive hydrogel composite membrane. *Journal of Controlled Release* **2001**, *75*, 55-67.
85. Butruk, B.; Trzaskowski, M.; Ciach, T. Fabrication of biocompatible hydrogel coatings for implantable medical devices using Fenton-type reaction. *Materials science & engineering. C, Materials for biological applications* **2012**, *32*, 1601-1609.
86. Butruk-Raszeja, B.A.; Lojszczyk, I.; Ciach, T.; Koscielniak-Ziemniak, M.; Janiczak, K.; Kustos, R.; Gonsior, M. Athrombogenic hydrogel coatings for medical devices-- Examination of biological properties. *Colloids and surfaces. B, Biointerfaces* **2015**, *130*, 192-198.
87. Hennink, W.E.; van Nostrum, C.F. Novel crosslinking methods to design hydrogels. *Advanced Drug Delivery Reviews* **2012**, *64*, 223-236.
88. Maccarrone, S.; Scherzinger, C.; Holderer, O.; Lindner, P.; Sharp, M.; Richtering, W.; Richter, D. Cononsolvency Effects on the Structure and Dynamics of Microgels. *Macromolecules* **2014**, *47*, 5982-5988.
89. Menne, D.; Pitsch, F.; Wong, J.E.; Pich, A.; Wessling, M. Temperature-modulated water filtration using microgel-functionalized hollow-fiber membranes. *Angewandte Chemie* **2014**, *53*, 5706-5710.
90. Sahiner, N.; Godbey, W.T.; McPherson, G.L.; John, V.T. Microgel, nanogel and hydrogel-hydrogel semi-IPN composites for biomedical applications: synthesis and characterization. *Colloid and Polymer Science* **2006**, *284*, 1121-1129.

91. Zhang, X.Z.; Wu, D.Q.; and Chu, C.C. Effect of the crosslinking level on the properties of temperature-sensitive poly(N-isopropylacrylamide) hydrogels. *Journal of polymer science: Part B: Polymer Physics* **2003**, *41*, 582-593.
92. Boyko, V.; Pich, A.; Lu, Y.; Richter, S.; Arndt, K.-F.; Adler, H.-J.P. Thermo-sensitive poly(N-vinylcaprolactam-co-acetoacetoxyethyl methacrylate) microgels: 1—synthesis and characterization. *Polymer* **2003**, *44*, 7821-7827.
93. Schmidt, S.; Hellweg, T.; Klitzing, R.V. Packing density control in P (NIPAM-co-AAc) microgel monolayers: effect of surface charge, pH, and preparation technique. *Langmuir : the ACS journal of surfaces and colloids* **2008**, *24*, 12595-12602.
94. Xu, F.-J.; Kang, E.-T.; Neoh, K.-G. pH- and temperature-responsive hydrogels from crosslinked triblock copolymers prepared via consecutive atom transfer radical polymerizations. *Biomaterials* **2006**, *27*, 2787-2797.
95. Zhan, Y.; Gonçalves, M.; Yi, P.; Capelo, D.; Zhang, Y.; Rodrigues, J.; Liu, C.; Tomas, H.; Li, Y.; He, P. Thermo-redox-pH-triple sensitive poly(N-isopropylacrylamide-co-acrylic acid) nanogels for anticancer drug delivery. *Journal of Materials Chemistry B* **2015**, *3*, 4221-4230.
96. Hu, L.; Chu, L.Y.; Yang, M.; Wang, H.D.; Hui Niu, C. Preparation and characterization of novel cationic pH-responsive poly(N,N'-dimethylamino ethyl methacrylate) microgels. *Journal of colloid and interface science* **2007**, *311*, 110-117.
97. Wang, B.; Xu, X.D.; Wang, Z.C.; Cheng, S.X.; Zhang, X.Z.; Zhuo, R.X. Synthesis and properties of pH and temperature sensitive P(NIPAAm-co-DMAEMA) hydrogels. *Colloids and surfaces. B, Biointerfaces* **2008**, *64*, 34-41.
98. EBARA, M.; AOYAGI, T.; SAKAI, K.; OKANO, T. The incorporation of carboxylate groups into temperature-responsive poly(N-isopropylacrylamide)-based hydrogels promotes rapid gel shrinking. *Journal of Polymer Science Part A: Polymer Chemistry* **2001**, *39*, 335-342.
99. Xu, X.-D.; Zhang, X.-Z.; Cheng, S.-X.; Zhuo, R.-X.; Kennedy, J.F. A strategy to introduce the pH sensitivity to temperature sensitive PNIPAAm hydrogels without weakening the thermosensitivity. *Carbohydrate Polymers* **2007**, *68*, 416-423.
100. Plamper, F.A.; Ballauff, M.; Müller, A.H.E. Tuning the Thermoresponsiveness of Weak Polyelectrolytes by pH and Light: Lower and Upper Critical-Solution Temperature of Poly(N,N-dimethylaminoethyl methacrylate). *Journal of the American Chemical Society* **2007**, *129*, 14538-14539.
101. Yuan, W.; Zou, H.; Guo, W.; Wang, A.; Ren, J. Supramolecular amphiphilic star-branched copolymer: from LCST-UCST transition to temperature-fluorescence responses. *Journal of Materials Chemistry* **2012**, *22*, 24783.
102. La, Y.-H.; McCloskey, B.D.; Sooriyakumaran, R.; Vora, A.; Freeman, B.; Nassar, M.; Hedrick, J.; Nelson, A.; Allen, R. Bifunctional hydrogel coatings for water purification membranes: Improved fouling resistance and antimicrobial activity. *Journal of Membrane Science* **2011**, *372*, 285-291.
103. Kim, B.; Hong, D.; Chang, W.V. LCST and UCST double-phase transitions of poly(N-isopropylacrylamide-co-2-acrylamidoglycolic acid)/poly(dimethylaminoethyl methacrylate) complex. *Colloid and Polymer Science* **2015**, *293*, 699-708.
104. Yancheva, E.; Paneva, D.; Maximova, V.; Mespouille, L.; Dubois, P.; Manolova, N.; Rashkov, I. Polyelectrolyte Complexes between (Cross-linked) N-Carboxyethylchitosan

- and (Quaternized) Poly[2-(dimethylamino)ethyl methacrylate] Preparation, Characterization, and Antibacterial Properties. *Biomacromolecules* **2007**, *8*, 976-984.
105. Rawlinson, L.-A.B.; Ryan, S.a.M.; Mantovani, G.; Haddleton, D.M.; Brayden, D.J. Antibacterial Effects of Poly(2-(dimethylamino ethyl)methacrylate) against Selected Gram-Positive and Gram-Negative Bacteria. *Biomacromolecules* **2010**, *11*, 443-453.
 106. Xu, F.J.; Kang, E.T.; Neoh, K.G. pH- and temperature-responsive hydrogels from crosslinked triblock copolymers prepared via consecutive atom transfer radical polymerizations. *Biomaterials* **2006**, *27*, 2787-2797.
 107. Zhang, J.; Xie, R.; Zhang, S.-B.; Cheng, C.-J.; Ju, X.-J.; Chu, L.-Y. Rapid pH/temperature-responsive cationic hydrogels with dual stimuli-sensitive grafted side chains. *Polymer* **2009**, *50*, 2516-2525.
 108. Chen, J.; Dai, P.; Liu, M. Rapid Responsive Behaviors of the Dual Stimuli-Sensitive Poly(DEA-co-DMAEMA) Hydrogel via Comb-Type Grafted Polymerization. *International Journal of Polymeric Materials* **2012**, *61*, 177-198.
 109. Gao, C.; Liu, M.; Chen, J.; Chen, C. Physicochemical characterization and drug release properties of PDMAEMA/OSA Semi-IPN hydrogels with microporous structure. *Polymers for Advanced Technologies* **2012**, *23*, 389-397.
 110. Hertle, Y.; Hellweg, T. Thermoresponsive copolymer microgels. *Journal of Materials Chemistry B* **2013**, *1*, 5874.
 111. Emileh, A.; Vasheghani-Farahani, E.; Imani, M. Preparation and Characterization of pH-Sensitive Microgels of Poly((2-dimethylamino) ethyl methacrylate). *Macromolecular Symposia* **2007**, *255*, 1-7.
 112. Barrett, K.E.J. Dispersion polymerisation in organic media. *British Polymer Journal* **1973**, *5*, 259-271.
 113. Sudol, E.D. Dispersion Polymerization. In *Polymeric Dispersions: Principles and Applications*, Springer Science & Business Media: 2012; pp 141-153.
 114. K., H.F.; J., U. Particle nucleation in emulsion polymerization. I. A theory for homogeneous nucleation. *Journal of Polymer Science: Polymer Chemistry Edition* **1978**, *16*, 1953-1979.
 115. Butté, A.; Storti, G.; Morbidelli, M. Miniemulsion Living Free Radical Polymerization by RAFT. *Macromolecules* **2001**, *34*, 5885-5896.
 116. Liu, G.; Li, X.; Xiong, S.; Li, L.; Chu, P.K.; Yeung, K.W.K.; Wu, S.; Xu, Z. Fluorine-containing pH-responsive core/shell microgel particles: preparation, characterization, and their applications in controlled drug release. *Colloid and Polymer Science* **2012**, *290*, 349-357.
 117. Zha, L.; Hu, J.; Wang, C.; Fu, S.; Elaissari, A.; Zhang, Y. Preparation and characterization of poly (N-isopropylacrylamide-co-dimethylaminoethyl methacrylate) microgel latexes. *Colloid and Polymer Science* **2002**, *280*, 1-6.
 118. Luo, Y.; Dalton, P.D.; Shoichet, M.S. Investigating the Properties of Novel Poly(2-hydroxyethyl methacrylate-co-methyl methacrylate) Hydrogel Hollow Fiber Membrane. *Chemistry of Materials* **2001**, *13*, 4087-4093.
 119. Becer, C.R.; Hahn, S.; Fijten, M.W.M.; Thijs, H.M.L.; Hoogenboom, R.; Schubert, U.S. Libraries of methacrylic acid and oligo(ethylene glycol) methacrylate copolymers with LCST behavior. *Journal of Polymer Science Part A: Polymer Chemistry* **2008**, *46*, 7138-7147.

120. Zhang, C.; Maric, M. Synthesis of Stimuli-responsive, Water-soluble Poly[2-(dimethylamino)ethyl methacrylate/styrene] Statistical Copolymers by Nitroxide Mediated Polymerization. *Polymers* **2011**, *3*.
121. Ma, G.-H.; Nagai, M.; Omi, S. Study on preparation of monodispersed poly(styrene-co-N-dimethylaminoethyl methacrylate) composite microspheres by SPG (Shirasu Porous Glass) emulsification technique. **2001**, *79*, 2408-2424.
122. Orakdogan, N. Novel responsive poly(N,N-dimethylaminoethyl methacrylate) gel beads: preparation, mechanical properties and pH-dependent swelling behavior. *Journal of Polymer Research* **2012**, *19*.
123. Orakdogan, N. pH-responsive swelling behavior, elasticity and molecular characteristics of poly(N,N-dimethylaminoethyl methacrylate) gels at various initial monomer concentrations. *Polymer Bulletin* **2011**, *67*, 1347-1366.
124. Yuk, S.H.; Cho, S.H.; Lee, S.H. pH/Temperature-Responsive Polymer Composed of Poly((N,N-dimethylamino)ethyl methacrylate-co-ethylacrylamide). *Macromolecules* **1997**, *30*, 6856-6859.
125. Goganian, A.M.; Arsalani, N.; Khaksar Khiabani, H.; Zakerhamidi, M.S. Microwave promoted synthesis of smart superporous poly (dimethylaminoethyl methacrylate-co-acrylamide) hydrogels and study of Kamlet-Abboud-Taft polarity functions for obtained materials. *Journal of Polymer Research* **2014**, *21*.
126. Ni, H.; Kawaguchi, H.; Endo, T. Preparation of Amphoteric Microgels of Poly(acrylamide/methacrylic acid/dimethylamino ethylene methacrylate) with a Novel pH-Volume Transition. *Macromolecules* **2007**, *40*.
127. Thorne, J.B.; Vine, G.J.; Snowden, M.J. Microgel applications and commercial considerations. *Colloid and Polymer Science* **2011**, *289*, 625-646.
128. Hamzah, Y.B.; Hashim, S.; Rahman, W.A.W.A. Synthesis of polymeric nano/microgels: a review. *Journal of Polymer Research* **2017**, *24*, 134.
129. Lee, T.B.; No, K.T.; Cho, S.H.; Kim, S.S.; Seo, J.K.; Lee, J.H.; Yuk, S.H. Polymeric nanosphere formed from temperature-responsive polymer composed of (N,N-dimethylamino)ethyl methacrylate and ethyl acrylamide. *Journal of Polymer Science Part B: Polymer Physics* **2001**, *39*, 594-600.
130. Tejamaya, M.; Römer, I.; Merrifield, R.C.; Lead, J.R. Stability of Citrate, PVP, and PEG Coated Silver Nanoparticles in Ecotoxicology Media. *Environmental science & technology* **2012**, *46*, 7011-7017.
131. Tolaymat, T.M.; El Badawy, A.M.; Genaidy, A.; Scheckel, K.G.; Luxton, T.P.; Suidan, M. An evidence-based environmental perspective of manufactured silver nanoparticle in syntheses and applications: A systematic review and critical appraisal of peer-reviewed scientific papers. *Science of The Total Environment* **2010**, *408*, 999-1006.
132. Riley, T.; Govender, T.; Stolnik, S.; Xiong, C.D.; Garnett, M.C.; Illum, L.; Davis, S.S. Colloidal stability and drug incorporation aspects of micellar-like PLA-PEG nanoparticles. *Colloids and Surfaces B: Biointerfaces* **1999**, *16*, 147-159.
133. Zhao, C.; Yuan, G.; Han, C.C. Stabilization, Aggregation, and Gelation of Microsphere Induced by Thermosensitive Microgel. *Macromolecules* **2012**, *45*, 9468-9474.
134. Wang, D.; Dimonie, V.L.; Sudol, E.D.; El-Aasser, M.S. Effect of PVP in dispersion and seeded dispersion polymerizations. *Journal of Applied Polymer Science* **2002**, *84*, 2721-2732.

135. Moore, J.; Cerasoli, E. Particle Light Scattering Methods and Applications. In *Encyclopedia of Spectroscopy and Spectrometry*, 3rd ed.; John C. Lindon; Tranter, G.E.; Koppelaar, D.W., Eds. Elsevier Science: 2017; pp Pages 543-553.
136. Zetasizer Nano Series User Manual MANO485. In *Zeta potential theory*, Malvern Instruments Ltd.: United Kingdom, 2013; p 250.
137. Fang, W.; Shi, L.; Wang, R. Interfacially polymerized composite nanofiltration hollow fiber membranes for low-pressure water softening. *Journal of Membrane Science* **2013**, *430*, 129-139.
138. Li, X.-L.; Zhu, L.-P.; Xu, Y.-Y.; Yi, Z.; Zhu, B.-K. A novel positively charged nanofiltration membrane prepared from N,N-dimethylaminoethyl methacrylate by quaternization cross-linking. *Journal of Membrane Science* **2011**, *374*, 33-42.
139. Peeva, P.D.; Million, N.; Ulbricht, M. Factors affecting the sieving behavior of anti-fouling thin-layer cross-linked hydrogel polyethersulfone composite ultrafiltration membranes. *Journal of Membrane Science* **2012**, *390-391*, 99-112.
140. Menne, D.; Üzüüm, C.; Koppelman, A.; Wong, J.E.; Foeken, C.v.; Borre, F.; Dähne, L.; Laakso, T.; Pihlajamäki, A.; Wessling, M. Regenerable polymer/ceramic hybrid nanofiltration membrane based on polyelectrolyte assembly by layer-by-layer technique. *Journal of Membrane Science* **2016**, *520*, 924-932.
141. Menne, D.; Kamp, J.; Erik Wong, J.; Wessling, M. Precise tuning of salt retention of backwashable polyelectrolyte multilayer hollow fiber nanofiltration membranes. *Journal of Membrane Science* **2016**, *499*, 396-405.
142. Kochan, J.; Wintgens, T.; Wong, J.E.; Melin, T. Properties of polyethersulfone ultrafiltration membranes modified by polyelectrolytes. *Desalination* **2010**, *250*, 1008-1010.
143. He, T.; Frank, M.; Mulder, M.H.V.; Wessling, M. Preparation and characterization of nanofiltration membranes by coating polyethersulfone hollow fibers with sulfonated poly(ether ether ketone) (SPEEK). *Journal of Membrane Science* **2008**, *307*, 62-72.
144. Chanachai, A.; Meksup, K.; Jiratananon, R. Coating of hydrophobic hollow fiber PVDF membrane with chitosan for protection against wetting and flavor loss in osmotic distillation process. *Separation and Purification Technology* **2010**, *72*, 217-224.
145. Zhang, G.; Gu, W.; Ji, S.; Liu, Z.; Peng, Y.; Wang, Z. Preparation of polyelectrolyte multilayer membranes by dynamic layer-by-layer process for pervaporation separation of alcohol/water mixtures. *Journal of Membrane Science* **2006**, *280*, 727-733.
146. Wei, X.; Wang, R.; Li, Z.; Fane, A. Development of a novel electrophoresis-UV grafting technique to modify PES UF membranes used for NOM removal. *Journal of Membrane Science* **2006**, *273*, 47-57.
147. Jeong, B.-H.; Hoek, E.M.V.; Yan, Y.; Subramani, A.; Huang, X.; Hurwitz, G.; Ghosh, A.K.; Jawor, A. Interfacial polymerization of thin film nanocomposites: A new concept for reverse osmosis membranes. *Journal of Membrane Science* **2007**, *294*, 1-7.
148. Chou, S.; Wang, R.; Shi, L.; She, Q.; Tang, C.; Fane, A.G. Thin-film composite hollow fiber membranes for pressure retarded osmosis (PRO) process with high power density. *Journal of Membrane Science* **2012**, *389*, 25-33.
149. Ismail, A.F.; Padaki, M.; Hilal, N.; Matsuura, T.; Lau, W.J. Thin film composite membrane – Recent development and future potential. *Desalination* **2015**, *356*, 140-148.

150. Sun, S.P.; Hatton, T.A.; Chan, S.Y.; Chung, T.-S. Novel thin-film composite nanofiltration hollow fiber membranes with double repulsion for effective removal of emerging organic matters from water. *Journal of Membrane Science* **2012**, *401-402*, 152-162.
151. Song, Y.; Fan, J.-B.; Wang, S. Recent progress in interfacial polymerization. *Materials Chemistry Frontiers* **2017**, *1*, 1028-1040.
152. Wang, K.Y.; Chung, T.-S.; Amy, G. Developing thin-film-composite forward osmosis membranes on the PES/SPSf substrate through interfacial polymerization. *AIChE Journal* **2012**, *58*, 770-781.
153. Zhao, Y.; Qiu, C.; Li, X.; Vararattanavech, A.; Shen, W.; Torres, J.; Hélix-Nielsen, C.; Wang, R.; Hu, X.; Fane, A.G.; Tang, C.Y. Synthesis of robust and high-performance aquaporin-based biomimetic membranes by interfacial polymerization-membrane preparation and RO performance characterization. *Journal of Membrane Science* **2012**, *423-424*, 422-428.
154. Du, R.; Feng, X.; Chakma, A. Poly(N,N-dimethylaminoethyl methacrylate)/polysulfone composite membranes for gas separations. *Journal of Membrane Science* **2006**, *279*, 76-85.
155. Cheng, Q.; Cui, Z.; Li, J.; Qin, S.; Yan, F.; Li, J. Preparation and performance of polymer electrolyte based on poly(vinylidene fluoride)/polysulfone blend membrane via thermally induced phase separation process for lithium ion battery. *Journal of Power Sources* **2014**, *266*, 401-413.
156. Yang, Q.; Chung, T.S.; Santoso, Y.E. Tailoring pore size and pore size distribution of kidney dialysis hollow fiber membranes via dual-bath coagulation approach. *Journal of Membrane Science* **2007**, *290*, 153-163.
157. Bottino, A.; Capannelli, G.; Munari, S.; Turturro, A. High performance ultrafiltration membranes cast from LiCl doped solutions. *Desalination* **1988**, *68*, 167-177.
158. Tomaszewska, M. Preparation and properties of flat-sheet membranes from poly(vinylidene fluoride) for membrane distillation. *Desalination* **1996**, *104*, 1-11.
159. Wang, D.; Li, K.; Teo, W.K. Porous PVDF asymmetric hollow fiber membranes prepared with the use of small molecular additives. *Journal of Membrane Science* **2000**, *178*, 13-23.
160. Zhang, P.-Y.; Yang, H.; Xu, Z.-L.; Wei, Y.-M.; Guo, J.-L.; Chen, D.-G. Characterization and preparation of poly(vinylidene fluoride) (PVDF) microporous membranes with interconnected bicontinuous structures via non-solvent induced phase separation (NIPS). *Journal of Polymer Research* **2013**, *20*.
161. Edwie, F.; Teoh, M.M.; Chung, T.S. Effects of additives on dual-layer hydrophobic-hydrophilic PVDF hollow fiber membranes for membrane distillation and continuous performance. *Chemical Engineering Science* **2012**, *68*, 567-578.
162. Van De Witte, P.; Dijkstra, P.J.; Van Den Berg, J.W.A.; Feijen, J. Phase separation processes in polymer solutions in relation to membrane formation. *Journal of Membrane Science* **1996**, *117*, 1-31.
163. Lloyd, D.R.; Kim, S.S.; Kinzer, K.E. Microporous membrane formation via thermally-induced phase separation. II. Liquid-liquid phase separation. *Journal of Membrane Science* **1991**, *64*, 1-11.
164. Lloyd, D.R.; Kinzer, K.E.; Tseng, H.S. Microporous membrane formation via thermally induced phase separation. I. Solid-liquid phase separation. *Journal of Membrane Science* **1990**, *52*, 239-261.

165. Lin, D.-J.; Chang, C.-L.; Huang, F.-M.; Cheng, L.-P. Effect of salt additive on the formation of microporous poly(vinylidene fluoride) membranes by phase inversion from LiClO₄/Water/DMF/PVDF system. *Polymer* **2003**, *44*, 413-422.
166. Sukitpaneenit, P.; Ong, Y.K.; Chung, T.-S. PVDF Hollow-Fiber Membrane Formation and Production. In *Membrane Fabrication*, Hilal, N.; Ismail, A.F.; Wright, C., Eds. CRC Press: 2015; pp 216-241.
167. Zisman, W.A. Relation of the Equilibrium Contact Angle to Liquid and Solid Constitution. In *Contact Angle, Wettability, and Adhesion*, Fowkes, F.M., Ed. AMERICAN CHEMICAL SOCIETY: 1964; Vol. 43, pp 1-51.
168. Ren, J.; Chung, T.-S.; Li, D.; Wang, R.; Liu, Y. Development of asymmetric 6FDA-2,6 DAT hollow fiber membranes for CO₂/CH₄ separation: 1. The influence of dope composition and rheology on membrane morphology and separation performance. *Journal of Membrane Science* **2002**, *207*, 227-240.
169. Wang, X.; Zhang, L.; Sun, D.; An, Q.; Chen, H. Formation mechanism and crystallization of poly(vinylidene fluoride) membrane via immersion precipitation method. *Desalination* **2009**, *236*, 170-178.
170. Liu, F.; Abed, M.R.M.; Li, K. Preparation and characterization of poly(vinylidene fluoride) (PVDF) based ultrafiltration membranes using nano γ -Al₂O₃. *Journal of Membrane Science* **2011**, *366*, 97-103.
171. Bajpai, O.P.; Panja, S.; Chattopadhyay, S.; Setua, D.K. Process–structure–property relationships in nanocomposites based on piezoelectric-polymer matrix and magnetic nanoparticles. **2015**, 255-278.
172. Schick, C. Differential scanning calorimetry (DSC) of semicrystalline polymers. *Analytical and bioanalytical chemistry* **2009**, *395*, 1589-1611.
173. Groeninckx, G.; Harrats, C.; Vanneste, M.; Everaert, V. Crystallization, Micro- and Nano-structure, and Melting Behavior of Polymer Blends. In *Polymer Blends Handbook*, 2nd ed. ed.; Utracki, L.A.; Wilkie, C.A., Eds. Dordrecht: Springer Netherlands: Dordrecht, 2014; Vol. 1, pp 291-446.
174. Ng, C.W.A.; MacKnight, W.J. Ionomeric Blends of Poly(ethyl acrylate-co-4-vinylpyridine) with Metal-Neutralized Sulfonated Poly(ethylene terephthalate). 4. Effects of Counterions. *Macromolecules* **1996**, *29*, 2421-2429.
175. Naffakh, M.; Marco, C.; Ellis, G. Non-Isothermal Cold-Crystallization Behavior and Kinetics of Poly(l-Lactic Acid)/WS₂ Inorganic Nanotube Nanocomposites. *Polymers* **2015**, *7*, 2175-2189.
176. Zhong, G.; Su, R.; Zhang, L.; Wang, K.; Li, Z.; Fong, H.; Zhu, L. Evolution of nanodroplets and fractionated crystallization in thermally annealed electrospun blend fibers of poly(vinylidene fluoride) and polysulfone. *Polymer* **2012**, *53*, 4472-4480.
177. Müller, A.J.; Balsamo, V.; Arnal, M.L.; Jakob, T.; Schmalz, H.; Abetz, V. Homogeneous Nucleation and Fractionated Crystallization in Block Copolymers. *Macromolecules* **2002**, *35*, 3048-3058.
178. Frensch, H.; Jungnickel, B.-J. Some novel crystallization kinetic peculiarities in finely dispersing polymer blends. *Colloid and Polymer Science* **1989**, *267*, 16-27.
179. Lv, Z.; Yang, Y.; Wu, R.; Tong, Y. Design and properties of a novel nucleating agent for isotactic polypropylene. *Materials & Design* **2012**, *37*, 73-78.

180. Lin, Y.; Chen, H.; Chan, C.-M.; Wu, J. Nucleating effect of calcium stearate coated CaCO₃ nanoparticles on polypropylene. *Journal of colloid and interface science* **2011**, *354*, 570-576.
181. Ji, G.-L.; Zhu, B.-K.; Cui, Z.-Y.; Zhang, C.-F.; Xu, Y.-Y. PVDF porous matrix with controlled microstructure prepared by TIPS process as polymer electrolyte for lithium ion battery. *Polymer* **2007**, *48*, 6415-6425.
182. Sakai, K. Dialysis membranes for blood purification. *Front Med Biol Eng* **2000**, *10*, 117-129.
183. Brydson, J.A. *Plastics materials*. 7th ed. ed.; Oxford Boston : Butterworth-Heinemann: Oxford Boston, 1999.
184. 19 - Fracture toughness properties of aerospace materials. In *Introduction to Aerospace Materials*, Mouritz, A.P., Ed. Woodhead Publishing: 2012; pp 454-468.
185. Ofsthun, N.J.; Karoor, S.; Suzuki, M. Hemodialysis Membranes. In *Advanced Membrane Technology and Applications*, Norman N. Li; Anthony G. Fane; Ho, W.S.W., Eds. American Institute of Chemical Engineers: 2008; pp 519-539.
186. Barton, A.F.M. *CRC handbook of solubility parameters and other cohesion parameters*. 2nd ed. ed.; Boca Raton : CRC Press: Boca Raton, 1991.
187. Goriainov, V.; Cook, R.; M. Latham, J.; G. Dunlop, D.; Oreffo, R.O.C. Bone and metal: An orthopaedic perspective on osseointegration of metals. *Acta biomaterialia* **2014**, *10*, 4043-4057.
188. Rosales-Leal, J.I.; Rodríguez-Valverde, M.A.; Mazzaglia, G.; Ramón-Torregrosa, P.J.; Díaz-Rodríguez, L.; García-Martínez, O.; Vallecillo-Capilla, M.; Ruiz, C.; Cabrerizo-Vílchez, M.A. Effect of roughness, wettability and morphology of engineered titanium surfaces on osteoblast-like cell adhesion. *Colloids and Surfaces A: Physicochemical and Engineering Aspects* **2010**, *365*, 222-229.
189. Kubiak, K.J.; Wilson, M.C.T.; Mathia, T.G.; Carval, P. Wettability versus roughness of engineering surfaces. *Wear* **2011**, *271*, 523-528.
190. Gadelmawla, E.S.; Koura, M.M.; Maksoud, T.M.A.; Elewa, I.M.; Soliman, H.H. Roughness parameters. *Journal of Materials Processing Technology* **2002**, *123*, 133-145.
191. Mariani, A.; Nuvoli, D.; Alzari, V.; Pini, M. Phosphonium-Based Ionic Liquids as a New Class of Radical Initiators and Their Use in Gas-Free Frontal Polymerization. *Macromolecules* **2008**, *41*, 5191-5196.
192. Chen, G.; Liu, J.; Yang, Y.; Zhang, L.; Wu, M.; Ni, H. Preparation of pH-sensitive nanoparticles of poly (methacrylic acid) (PMAA)/poly (vinyl pyrrolidone) (PVP) by ATRP-template miniemulsion polymerization in the aqueous solution. *Colloid and Polymer Science* **2015**, *293*, 2035-2044.
193. Si, R.; Zhang, Y.-W.; You, L.-P.; Yan, C.-H. Self-Organized Monolayer of Nanosized Ceria Colloids Stabilized by Poly(vinylpyrrolidone). *The Journal of Physical Chemistry B* **2006**, *110*, 5994-6000.
194. Kao, C.-Y.; Lo, T.-C.; Lee, W.-C. Influence of polyvinylpyrrolidone on the hydrophobic properties of partially porous poly(styrene-divinylbenzene) particles for biological applications. *Journal of Applied Polymer Science* **2003**, *87*, 1818-1824.
195. Koczur, K.M.; Mourdikoudis, S.; Polavarapu, L.; Skrabalak, S.E. Polyvinylpyrrolidone (PVP) in nanoparticle synthesis. *Dalton Transactions* **2015**, *44*, 17883-17905.

196. Jiang, Y.N.; Mo, H.Y.; Yu, D.G. Electrospun drug-loaded core-sheath PVP/zein nanofibers for biphasic drug release. *Int J Pharm* **2012**, *438*, 232-239.
197. Lopérgolo, L.C.; Lugão, A.B.; Catalani, L.H. Direct UV photocrosslinking of poly(N-vinyl-2-pyrrolidone) (PVP) to produce hydrogels. *Polymer* **2003**, *44*, 6217-6222.
198. Sanson, N.; Rieger, J. Synthesis of nanogels/microgels by conventional and controlled radical crosslinking copolymerization. **2010**, *1*, 965.
199. Pelton, R. Temperature-sensitive aqueous microgels. *Advances in colloid and interface science* **2000**, *85*, 1-33.
200. Roy, D.; Brooks, W.L.A.; Sumerlin, B.S. New directions in thermoresponsive polymers. *Chemical Society Reviews* **2013**, *42*, 7214-7243.
201. Saunders, B.R.; Laajam, N.; Daly, E.; Teow, S.; Hu, X.; Stepto, R. Microgels: From responsive polymer colloids to biomaterials. *Advances in colloid and interface science* **2009**, *147-148*, 251-262.
202. Liu, F.; Urban, M.W. Dual Temperature and pH Responsiveness of Poly(2-(N,N-dimethylamino)ethyl methacrylate-co-n-butyl acrylate) Colloidal Dispersions and Their Films. *Macromolecules* **2008**, *41*, 6531-6539.
203. Duracher, D.; Elaïssari, A.; Pichot, C. Characterization of cross-linked poly(N - isopropylmethacrylamide) microgel latexes. *Colloid & Polymer Science* **1999**, *277*, 905-913.
204. Guillermo, A.; Cohen Addad, J.P.; Bazile, J.P.; Duracher, D.; Elaïssari, A.; Pichot, C. NMR investigations into heterogeneous structures of thermosensitive microgel particles. *Journal of Polymer Science Part B: Polymer Physics* **2000**, *38*, 889-898.
205. Koetting, M.C.; Peters, J.T.; Steichen, S.D.; Peppas, N.A. Stimulus-responsive hydrogels: Theory, modern advances, and applications. *Materials science & engineering. R, Reports : a review journal* **2015**, *93*, 1-49.
206. Islam, A.M.; Chowdhry, B.Z.; Snowden, M.J. Heteroaggregation in colloidal dispersions. *Advances in colloid and interface science* **1995**, *62*, 109-136.
207. Zhang, Q.; Wang, Z.; Lei, L.; Tang, J.; Wang, J.; Zhu, S. CO₂-Switchable Membranes Prepared by Immobilization of CO₂-Breathing Microgels. *ACS applied materials & interfaces* **2017**, *9*, 44146-44151.
208. Du, R.; Chakma, A.; Feng, X. Interfacially formed poly(N,N-dimethylaminoethyl methacrylate)/polysulfone composite membranes for CO₂/N₂ separation. *Journal of Membrane Science* **2007**, *290*, 19-28.
209. Roy Choudhury, A.K. 10 - Antistatic and soil-release finishes. In *Principles of Textile Finishing*, Roy Choudhury, A.K., Ed. Woodhead Publishing: 2017; pp 285-318.
210. Zhao, Y.-F.; Zhu, L.-P.; Jiang, J.-H.; Yi, Z.; Zhu, B.-K.; Xu, Y.-Y. Enhancing the Antifouling and Antimicrobial Properties of Poly(ether sulfone) Membranes by Surface Quaternization from a Reactive Poly(ether sulfone) Based Copolymer Additive. *Industrial & Engineering Chemistry Research* **2014**, *53*, 13952-13962.
211. Elias, C.N.; Oshida, Y.; Lima, J.H.C.; Muller, C.A. Relationship between surface properties (roughness, wettability and morphology) of titanium and dental implant removal torque. *Journal of the Mechanical Behavior of Biomedical Materials* **2008**, *1*, 234-242.

212. Huang, F.L.; Wang, Q.Q.; Wei, Q.F.; Gao, W.D.; Shou, H.Y.; Jiang, S.D. Dynamic wettability and contact angles of poly(vinylidene fluoride) nanofiber membranes grafted with acrylic acid. *Express Polymer Letters* **2010**, *4*, 551-558.
213. Yu, L.; Zhang, Y.; Zhang, B.; Liu, J.; Zhang, H.; Song, C. Preparation and characterization of HPEI-GO/PES ultrafiltration membrane with antifouling and antibacterial properties. *Journal of Membrane Science* **2013**, *447*, 452-462.
214. Xu, L.-C.; Bauer, J.W.; Siedlecki, C.A. Proteins, platelets, and blood coagulation at biomaterial interfaces. *Colloids and Surfaces B: Biointerfaces* **2014**, *124*, 49-68.
215. Zhao, H.-Y.; Cao, Y.-M.; Ding, X.-L.; Zhou, M.-Q.; Yuan, Q. Poly(N,N-dimethylaminoethyl methacrylate)-poly(ethylene oxide) copolymer membranes for selective separation of CO₂. *Journal of Membrane Science* **2008**, *310*, 365-373.
216. Ishihara, K.; Hasegawa, T.; Watanabe, J.; Iwasaki, Y. Protein Adsorption-Resistant Hollow Fibers for Blood Purification. *Artificial organs* **2002**, *26*, 1014-1019.
217. Ma, L.; Su, B.; Cheng, C.; Yin, Z.; Qin, H.; Zhao, J.; Sun, S.; Zhao, C. Toward highly blood compatible hemodialysis membranes via blending with heparin-mimicking polyurethane: Study in vitro and in vivo. *Journal of Membrane Science* **2014**, *470*, 90-101.
218. Herrwerth, S.; Eck, W.; Reinhardt, S.; Grunze, M. Factors that Determine the Protein Resistance of Oligoether Self-Assembled Monolayers – Internal Hydrophilicity, Terminal Hydrophilicity, and Lateral Packing Density. *Journal of the American Chemical Society* **2003**, *125*, 9359-9366.
219. Hashino, M.; Hiram, K.; Ishigami, T.; Ohmukai, Y.; Maruyama, T.; Kubota, N.; Matsuyama, H. Effect of kinds of membrane materials on membrane fouling with BSA. *Journal of Membrane Science* **2011**, *384*, 157-165.
220. Song, Y.; Zhang, T.; Song, X.; Zhang, L.; Zhang, C.; Xing, J.; Liang, X.-J. Polycations with excellent gene transfection ability based on PVP-g-PDMAEMA with random coil and micelle structures as non-viral gene vectors. *Journal of Materials Chemistry B* **2015**, *3*, 911-918.
221. Cerda-Cristerna, B.I.; Flores, H.; Pozos-Guillen, A.; Perez, E.; Sevrin, C.; Grandfils, C. Hemocompatibility assessment of poly(2-dimethylamino ethylmethacrylate) (PDMAEMA)-based polymers. *Journal of controlled release : official journal of the Controlled Release Society* **2011**, *153*, 269-277.
222. Hayashi, T.; Tanaka, Y.; Koide, Y.; Tanaka, M.; Hara, M. Mechanism underlying bioinertness of self-assembled monolayers of oligo(ethyleneglycol)-terminated alkanethiols on gold: protein adsorption, platelet adhesion, and surface forces. *Physical Chemistry Chemical Physics* **2012**, *14*, 10196-10206.
223. Agnihotri, A.; Siedlecki, C.A. Time-Dependent Conformational Changes in Fibrinogen Measured by Atomic Force Microscopy. *Langmuir : the ACS journal of surfaces and colloids* **2004**, *20*, 8846-8852.
224. Sun, S.P.; Chung, T.S. Outer-selective pressure-retarded osmosis hollow fiber membranes from vacuum-assisted interfacial polymerization for osmotic power generation. *Environmental science & technology* **2013**, *47*, 13167-13174.
225. Rajabzadeh, S.; Sano, R.; Ishigami, T.; Kakihana, Y.; Ohmukai, Y.; Matsuyama, H. Preparation of hydrophilic vinyl chloride copolymer hollow fiber membranes with antifouling properties. *Applied Surface Science* **2015**, *324*, 718-724.

226. Dasgupta, A.; Wahed, A. Chapter 13 - Tumor Markers. In *Clinical Chemistry, Immunology and Laboratory Quality Control*, Dasgupta, A.; Wahed, A., Eds. Elsevier: San Diego, 2014; pp 229-247.
227. Misra, M.; Moore, H. A clinical study comparing the basic performance and blood compatibility characteristics of Nipro ELISIO-H®, Gambro Polyflux Revaclear®, and Fresenius Optiflux® dialyzers. *Hemodialysis International* **2018**, 22, S15-S23.
228. Krieter, D.H.; Morgenroth, A.; Barasinski, A.; Lemke, H.-D.; Schuster, O.; von Harten, B.; Wanner, C. Effects of a polyelectrolyte additive on the selective dialysis membrane permeability for low-molecular-weight proteins. *Nephrology Dialysis Transplantation* **2006**, 22, 491-499.
229. Krieter, D.H.; Hackl, A.; Rodriguez, A.; Chenine, L.; Moragues, H.L.; Lemke, H.-D.; Wanner, C.; Canaud, B. Protein-bound uraemic toxin removal in haemodialysis and post-dilution haemodiafiltration. *Nephrology Dialysis Transplantation* **2009**, 25, 212-218.